Autoignition of Hydrocarbons in Relation to Engine Knock

by

Caroline Mohamed BSc.

submitted in accordance with the requirements for the degree of PhD.

The University of Leeds
School of Chemistry

October 1997

The candidate confirms that the work submitted is her own and that appropriate credit has been given where reference has been made to the work of others.

ABSTRACT

A single piston Rapid Compression Machine (RCM) has been used to investigate the autoignition of hydrocarbons under conditions of temperature and pressure similar to those which occur in the end-gas of a spark-ignition engine under knocking conditions.

Extents of reactant consumption have been measured during the course of autoignition following rapid compression of hydrocarbon-air mixtures. Evidence for the occurrence of low temperature oxidation during the compression stroke has been found and its effect on the overall ignition delay has been determined by numerical methods. The influence of diethylamine on this reactivity during compression and on the overall ignition delay has been investigated experimentally. The amine was shown to exert an inhibiting influence on the low temperature oxidation of n-heptane and n-pentane.

Measurements of autoignition delays have been made over a range of compressed gas temperatures for different hydrocarbons (C_4-C_8). The results illustrate the relationship between autoignition delay and octane rating and the effect of molecular structure on the reactivity of hydrocarbons in an RCM. In general, as the Research Octane Number (RON) increases the duration of the ignition delay following compression to 900 K increases, however, a quantitative correlation of the two could not be made.

Spatial imaging techniques (schlieren imaging, image intensified Charge Coupled Device (CCD)), used in the investigation of the spatial development of autoignition in the RCM, confirm the existence of spatial temperature inhomogeneities within the combustion chamber during the post-compression period. These imaging techniques have also been used in the study of spark-ignition and "knock" in the RCM.

The ignition of methane in the RCM has been studied. The experimental results suggest that the presence of higher alkanes (ethane, propane and n-butane) or carbonaceous particles enhances the initiation of ignition of methane-oxygen mixtures. The effects of pressure and temperature on this behaviour have been explored experimentally.

Publications and Conference Presentations

"Extents of alkane combustion during rapid compression leading to single and two-stage ignition", A.Cox, J.F.Griffiths, C.Mohamed, H.J.Curran, W.J.Pitz, C.K.Westbrook *26th International Symposium on Combustion*, The Combustion Institute. Pittsburgh, (1996) p 2685.

"Experimental and numerical studies of oxidation chemistry and spontaneous ignition phenomena", J.F.Griffiths and C.Mohamed Chapter 6 in *Comprehensive Chemical Kinetics*, series ed. G.Hancock, Elsevier, Amsterdam, 1996, in press.

"Spontaneous ignition delays as a diagnostic of the propensity of alkanes to cause engine knock", J.F.Griffiths, P.Halford-Maw and C.Mohamed, *Combustion and Flame*, 1997, in press.

"Suppression of reaction during rapid compression and its effect on ignition delay", C.Mohamed, *Combustion and Flame*, 1997, in press.

"The relationship between autoignition delay in a rapid compression machine and research octane number", C.Mohamed, J.F.Griffiths and P.A.Halford-Maw
"Schlieren imaging of autoignition in a rapid compression machine", C.Mohamed, J.F.Griffiths, J.Pan and C.G.W.Sheppard, *Joint meeting of the British, Spanish, Swedish and Portuguese Sections of the Combustion Institute*, Funchal, Madeira, 1-4 April 1996.

"Kinetic modelling of hydrocarbon autoignition at low and intermediate temperatures in a rapid compression machine", H.J.Curran, J.F.Griffiths, C.Mohamed, W.J.Pitz and C.K.Westbrook, *Third Symposium on Numerical Modelling*, Heidelberg,1996.

"Chemical kinetic modelling of hydrocarbon oxidation", C.Mohamed, J.F.Griffiths, H.J.Curran, C.K.Westbrook, *14th International Gas Kinetics Symposium*, Leeds, 7-12 September 1996.

"Schlieren imaging of hydrocarbon autoignition in a Rapid Compression Machine", C.Mohamed, J.F.Griffiths, J.Pan and C.G.W.Sheppard, *Institute of Physics, Combustion Physics Group: Current Research in Combustion Physics, Gas Research Centre*, Loughborough, 10 September 1997.

ACKNOWLEDGEMENTS

My sincerest thanks go first and foremost to Prof. J. F. Griffiths for his supervision and guidance throughout this research programme. I am extremely grateful for all the support and encouragement he has given me over the last three years and for his unfailing energy and enthusiasm for combustion research.

I would also like to acknowledge EPSRC and The Associated Octel Company Ltd. (Jonathan Evans) for financial support

Over the last three years several undergraduate project students have contributed good quality research to this thesis. I am grateful for their hard work and perseverance: Adam Cox, Simon Cole and Siu Kwan Wo. I would also like to acknowledge the technical expertise and assistance of Iain Clarke of The Associated Octel Company Ltd., Jinfeng Pan, Chris Hildyard, Henry Curran, and John Clarkson. Thanks also to Barry Johnson for proof-reading and valuable comments.

I would like to thank all the technical staff of the School of Chemistry at Leeds University and would particularly like to acknowledge David Fogarty and Bernard Frere (GC and GC-MS) for their help, and also Peter Halford-Maw for the provision of data capture software and assistance with electronic and electrical instrumentation.

My time spent in Leeds has been extremely enjoyable and memorable, for this my thanks go to all my friends and colleagues, past and present. In particular, Jon and Sophie for keeping in touch over the years and subsidising our too infrequent reunions, and my house-mates and dear friends, Jo and Mark, "good luck for the future and keep in touch".

Thank you to Mike, for tolerating and comforting me throughout a very difficult and trying time and for your unfailing optimism and reassurance (not forgetting that good luck cuddle).

And thank you to Dave, for all the support and encouragement over the years. Your patience and understanding and your sound advice helped me to get where I am today.

Finally, to my family. Thanks to my Father, for all the encouragement and advice (not to mention financial support) throughout my academic career, and to my 3 sisters Sherene, Jacqueline and Joyce, for their guidance and understanding and for setting the high standards to which I endeavour to aspire.

Dedicated to and in
loving memory
of my mother

CONTENTS

FIGURES

TABLES

GLOSSARY OF TERMS AND ABBREVIATIONS

ϕ	equivalence ratio
γ	polytropic ratio (C_p/C_v)
τ (also, τ_T, t_i, t_{ign})	ignition delay
A/D	analogue/digital
ASTM	American Society for Testing and Materials
atdc	after top dead centre
bdc	bottom dead centre
btdc	before top dead centre
BS	British Standards
c.i.	compression-ignition
CCD	Charge Coupled Device
ccds	combustion chamber deposits
CCR	Critical Compression Ratio
CFD	Computational Fluid Dynamics
CFR	Co-operative Fuels Research
C_p	molar heat capacity at constant pressure
CR	Compression Ratio
C_v	molar heat capacity at constant volume
fps	frames per second
GC	gas chromatography
GC-MS	gas chromatography - mass spectrometry
HAPs	Hazardous Air Pollutants

MON	Motor Octane Number
NMA	N-methylaniline
ntc	negative temperature coefficient
pc	personal computer
p_c	compressed gas pressure
p_f	final pressure
p_i	initial pressure
PMT	Photomultiplier Tube
PRF	Primary Reference Fuel
RCM	Rapid Compression Machine
RON	Research Octane Number
rpm	revolutions per minute
s.i.	spark-ignition
T_{ad}	adiabatic compressed gas temperature (from CR)
T_{ad}'	adiabatic compressed gas temperature (from p_c)
T_c	average compressed gas temperature
TIC	Total Ion Current
tdc	top dead centre
T_i	initial temperature
V_c	compressed gas volume
V_f	final volume
V_i	initial volume
VOCs	Volatile Organic Compounds

Chapter 1

Introduction

1 INTRODUCTION

The work described in this thesis is an exploration of the combustion of hydrocarbons leading to spontaneous ignition (or autoignition) under conditions which relate to the performance of gasoline in spark-ignition (s.i.) engines. The experiments reported have been carried out in a rapid compression machine. The detailed aims and purpose are discussed in Section 1.6 and the apparatus is described in Chapter 2. A background to the present understanding and social attitudes towards engine performance is presented in the first part of this introduction, followed by an overview of hydrocarbon oxidation chemistry and some of its consequences. Brief reviews of experimental and numerical approaches to the study of hydrocarbon autoignition in relation to engine knock are provided in Sections 1.4 and 1.5 respectively.

1.1 A general perspective of combustion in engines

Most modern texts attribute the invention of the internal combustion (i.c.) engine to Nicolaus A. Otto and Rudolph Diesel in the late 19th Century. However, the true birth of the internal combustion engine dates back to 1509 and is accredited to Leonardo da Vinci [1]. Hidden amongst an enormous wealth of Leonardo's manuscripts, occupying just a small corner of a page of random jottings, was a description of the fundamental principle of the internal combustion engine, described as the "fire engine" on the basis of the first words of the note, "In order to raise a body with fire".

The subsequent developments of these early ideas by engineers and finally by Otto and Diesel in Germany, between 1867 and 1918, culminated in a feasible method of utilising the energy released from fuel combustion to provide mechanical power. The invention of the s.i. engine by Otto in 1876 [2] and the subsequent invention of the compression-ignition (c.i.) engine by Diesel in 1892 [3], were amongst the greatest inventions of the 19th century and had an enormous impact on society, industry and the economy. Motorised vehicles introduced the exciting prospect of freedom and

independence. More than 100 years later, the praise and acclaim for the internal combustion engine is gradually being superseded by scorn and contempt, now conjuring images of filthy, harmful pollutant emissions and long-term environmental damage. However, despite the deleterious environmental effects of their exhaust gas emissions, motor vehicles remain the most convenient and comfortable means of land transport currently favoured by the vast majority of modern society. The demand placed on the scientist and the engineer is to head the progression to cleaner and more economical alternatives and to offer an acceptable solution to the problems.

As a consequence of the increasing global demand for energy, the threat of depleted hydrocarbon resources is becoming more imminent. Energy consumption in the UK alone has increased by approximately 70 % since 1990. The concern for long-term availability of petroleum and the increasing awareness of the political issues surrounding the oil industry, exemplified in the Oil Crisis of the 1970s (when the crude petroleum price rose rapidly to several times its previous cost), has encouraged the search for alternatives to gasoline and diesel.

Substantial investments of time and resources have been made into research in the areas of fuel technology and engine design since the early 20th century. The most significant progress has continued to lie in the improved design of s.i. and diesel engines as opposed to the development of economically viable alternatives to gasoline as a fuel. Particular emphasis has been placed on the reduction of emissions and improved fuel economy and efficiency, e.g., lean burn engines, gasoline reformulation and detergent additives.

One of the predominant drawbacks of the s.i. engine is the low efficiency (approximately 17 % of the fuel is converted into useful energy). This can be enhanced by increasing the volumetric compression ratio of the engine. However this can result in the occurrence of "knock" in the engine. The term "knock" (or "pinking") refers to the characteristic "tinny rattle" which emanates from the engine cylinders as a result of the irregular pressure waves propagating back and forth in the cylinders at an acoustic frequency (> 15 kHz). It is now commonly accepted that engine knock is a physical

consequence of the occurrence of hydrocarbon autoignition in the unburned end-gas ahead of the spark-ignited flame [4]. Aside from the objectionable noise which can be heard from outside the engine, persistent knocking combustion can cause severe long term physical damage to the piston crown, cylinder head and piston seals [5]. Maly recently reviewed the current status of spark-ignition engine combustion research [6], addressing the main features including engine knock and engine modelling. The research and development requirements for engines of the future were also identified.

After almost a decade of attempts to modify the Clean Air Act of 1970, on October 27 1990 the U.S. Senate gave final approval to amendments which would significantly strengthen and broaden the federal governments regulation of air pollution. The main highlights of the 1990 Clean Air Act that President Bush signed into law in November 1990 were related to, urban smog reduction; reduced emissions of hazardous air pollutants (HAPs); protection of stratospheric ozone; increased control and reduction of pollution from motor vehicles; and cleaner burning, alternative fuels. In order to combat the growing problem of urban air pollution due to increased traffic in the cities and towns, new government legislation states that all cars manufactured after 1990 must be fitted with a catalytic converter and run on unleaded petrol. It is speculated that by the year 2000, at least 80 % of all vehicles on the roads will be fitted with a catalytic converter. The result, a significant reduction in pollution, in particular urban ozone, which results from reaction of volatile organic compounds (VOCs) with nitrogen oxides in the atmosphere, both major pollutants from spark-ignition engines.

The main pollutant emissions from internal combustion engines are unburned hydrocarbons (VOCs), oxides of nitrogen (NO_x), carbon monoxide and particulates. It is estimated that motor vehicles are responsible for 40-45 % of VOCs and 45 % of total NO_x emissions. The Clean Air Act of 1990, stipulates that tailpipe emissions of hydrocarbons and NO_x must be reduced by 40 % and 60 % respectively in all new cars by 1996. In addition to this, all new cars must have pollution control equipment with a lifetime of 10 years, beginning in 1998. In 1996, automobile manufacturers had to begin producing at least 150,000 experimental cars and light trucks a year for a

California pilot program designed to launch alternative-fuel vehicles. The production level increases to 300,000 annually in 1999.

Car manufacturers are becoming increasingly aware of the demands of motorists in the 1990s and the regulations set by governing bodies on "cleaner burning" engines and fuels. Endeavouring to meet these requirements, highly competitive automotive and petroleum industries have developed. The two main problems which need to be combated are the fuel economy (or efficiency of the engine) and the pollutant emissions. The use of piezoelectric audio sensors in the engine cylinders coupled to an electronic spark timing control system allows the engine to operate at the maximum compression ratio before knock occurs, i.e. at the knock limit. This is effectively a self-regulating, automated, control system ensuring that spark-ignition engines operate at the maximum level of efficiency and power whilst avoiding the problem of audible knock outside the engine so both consumer and manufacturer are satisfied. Figure 1.1 is an artistic impression of such of system.

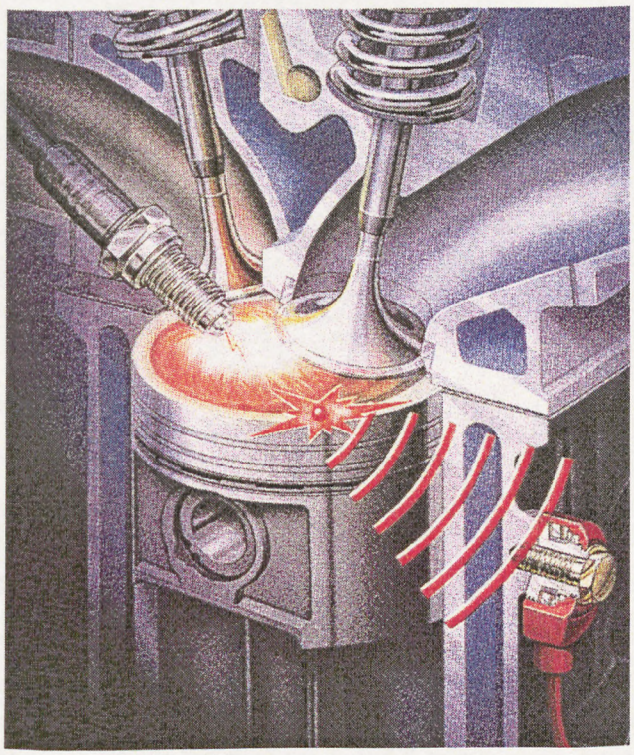

Figure 1.1 In-cylinder detection and control of engine knock (published with permission from BMW (GB) Ltd.).

In October 1996, Nissan announced the introduction of their all-new electric vehicle (EV) to the California market in early 1998. The new Nissan EV will be powered by a lithium-ion battery with an exceptionally long lifetime. In line with the developments of leading-edge technology in electric vehicle design, the Chrysler car company claims that by the year 2005 they will have developed a prototype electric car which runs on petrol. Using a Platinum catalyst and an on-board fuel processor to break down the petrol into hydrogen and water, a fuel cell will use the hydrogen gas to produce electricity to power the car. Daimler-Benz forecast that their sales of electric vehicles in the year 2005 will be in the region of 100,000.

If the occurrence of knock in the s.i. engine can be avoided or reduced then the maximum efficiency and power attainable can be increased. Over the last 70 or so years, petroleum companies have been developing a new reformulated gasoline (rfg) with a new blend of components for higher resistance to knock (see Section 1.36) and reduced tailpipe emissions [7]. Prior to rfg, when the major fuel components were alkanes, spark-ignition engines were commonly operated in the compression ratio range 8:1 - 9:1. With the new rfg containing increased proportions of octane boosters (see Section 1.3.6) such as alkenes, aromatics, oxygenates and branched alkanes, compression ratios of up to 11:1 are attainable.

A large proportion of the research and development in this area of combustion science has been performed or sponsored by motor companies, petroleum organisations, and fuel additive companies. In addition, the contributions of combustion science and technology research in academic and government research institutes to the understanding of the complex fundamental phenomena which underlie this costly and irritating problem also effect the advances in engine design and fuel technology [8]. A thorough scientific understanding of the physical and chemical processes which lead to hydrocarbon autoignition in the end-gas is one of the primary objectives in reducing and ultimately eliminating the problem of engine knock and its consequent limitations on progress in engine technology.

Under controlled conditions, autoignition can be a very useful tool, providing the energy for the power stroke of the diesel engine cycle [5]. It can also be extremely damaging and a severe nuisance, such as in the case of engine knock occurrence in s.i. engines. Spontaneous ignition (or autoignition) is the sudden inflammation of a gaseous charge when exposed to a particular temperature and pressure, in the absence of an external stimulus, (such as an electric spark or friction). The phenomenon of autoignition can present a serious hazard and was considered during enquiry as a possible cause of the disaster on the Piper Alpha oil platform in 1988. Wherever fuels are contained in large amounts at high temperatures in the presence of an oxidising atmosphere there is the potential for a hazardous situation, due to their combustible properties. Standard tests can be performed to determine the "conditions of safe operation", or to define the hazard presented by different fuels under specific conditions. The test procedures may be those of the American Society for Testing and Materials (ASTM), or British Standards (BS) or those set by the EEC. The control parameters of pressure, temperature, vessel size and fuel-air composition for various hydrocarbons and other organic compounds have been studied extensively and a substantial amount of useful information has been compiled [9].

The present study is focused primarily on the occurrence of autoignition of hydrocarbon-air mixtures in relation to engine knock in s.i. engines. Chapter 8 describes a study of methane ignition and the influence of higher hydrocarbons and particulates, in which the potential for sensitisation is explored. Although there may be some relevance to industrial combustion hazards, this investigation is not so far removed from the discussion of engine knock. With the recent introduction of natural gas-fuelled vehicles onto the market [10], the autoignition of methane and the effect of particulates, or combustion chamber deposits (ccds), has some relevance to combustion in engines.

A Rapid Compression Machine (RCM) has been used to investigate hydrocarbon autoignition under conditions comparable with those in the end-gas of a spark-ignition engine under knocking conditions. The general purpose of the study was to develop an improved understanding of the chemical and physical processes giving rise to the

fundamental combustion phenomenon of autoignition, which ultimately results in the occurrence of engine knock in spark-ignition engines.

1.2 Autoignition and Engine Knock

The autoignition characteristics of hydrocarbons have been of interest to scientists and engineers for many decades. The predominant interest presently relates to combustion in reciprocating engines and the occurrence of engine knock in s.i. engines. The four-stroke Otto cycle of the spark-ignition engine comprises induction, compression, power and exhaust strokes. The induction and exhaust strokes involve the intake of fuel-air and outlet of burned or partially oxidised gases respectively. The compression stroke is rapid enough to be virtually adiabatic and raises the pressure and temperature of the fuel-air mixture. Spark-ignition occurs before the piston reaches the end of its compression stroke, referred to as top dead centre (tdc). The spark-ignited flame expands and propagates across the volume of the combustion chamber, providing the force for the power stroke of the engine cycle. Under normal, non-knocking, conditions the end-gases are consumed by the flame front before they can autoignite. However, the expanding spark-ignited flame instils an additional compression and heating effect on the end-gas (the unburned gas most remote to the spark plug) and the spontaneous ignition of hydrocarbon-air mixtures can occur at these high temperatures and pressures in localised regions. If the end-gas reacts rapidly enough, it can ignite prior to the arrival of the flame front. The occurrence of autoignition and the time it takes to develop (the ignition delay) in the end-gas depends on the temperature, pressure, composition and nature of the fuel. Figure 1.1 is an illustration of the occurrence of engine knock in a spark-ignition engine cylinder.

The events can be imagined as a "race" between the time for complete consumption of reactants by the propagating spark-ignited flame and the time it takes for autoignition to occur in the end-gas (the ignition delay). Fuels with longer ignition delays are more likely to survive the additional compression and heating by the expanding spark-ignited flame without the occurrence of autoignition in the end-gas than fuels with short

ignition delays. Evidently, the occurrence of autoignition in the end-gas could be beneficial, providing a method of removing unburned hydrocarbons from the combustion chamber which would otherwise be a pollutant component of the tailpipe emissions.

The efficiency (ratio of useful work done to the energy input) and power of spark-ignition engines is enhanced by operating at higher compression ratios, however, the compression ratio (CR) is limited to a critical value at which engine knock occurs, the critical compression ratio (CCR). The CCR for incipient knock is a measure of the tendency of a fuel to undergo knocking combustion in a spark-ignition engine. Experimental studies of the relationship between fuel structure and the ease of spontaneous ignition have received considerable attention from engineers through the characterisation of knock ratings of fuels in research engines. Such studies began in the 1920s, however the study reported by Lovell [11] illustrates with remarkable clarity the way in which the isomeric structure of pure components relates to engine-knock resistance, measured by critical compression ratio (CCR) (Figure 1.2). Both the autoignition temperature and the onset of engine knock depend upon the ease of low temperature oxidation as discussed in Section 1.3.

The tendency of a fuel to knock in a spark-ignition engine is measured on a scale of octane rating. The most common octane ratings are research octane number (RON) and motor octane number (MON). The research octane number (RON) is the percentage of i-octane in a mixture of n-heptane and i-octane which has the same tendency to cause knock as the test fuel in a CFR (Co-operative Fuel Research) engine under standard operating conditions (600 rpm; 2.5 ms compression; fuel-air for maximum knock; full load; variable CR). The two fuels chosen as reference fuels for the octane rating scale, the primary reference fuels (PRFs), are n-heptane (RON 0) and i-octane (RON 100). These two fuels were chosen on account of their distinctly different chemical reactivity during oxidation and similar physical properties such as vapour pressure and viscosity. The use of two fuels with similar physical properties is important if the physical characteristics of the mixture are to remain unchanged.

The first kinetic and mechanistic link of knock rating to fuel structure can be attributed to Walsh [12]. Working from a set of qualitative rules, Walsh suggested that the knock resistance of a fuel decreases as the chain length increases, and increases as CH_2 groups are replaced by CH and H atoms are replaced by CH_3 groups. It has been suggested that octane number depends on the rate of OH production through isomerisation reactions [13] and on factors influencing the rate of isomerisation such as the molecular size and structure [14]. Cartlidge and Tipper noted that the increased tendency to knock is related to an increased tendency of the fuel to form hydroperoxides [15].

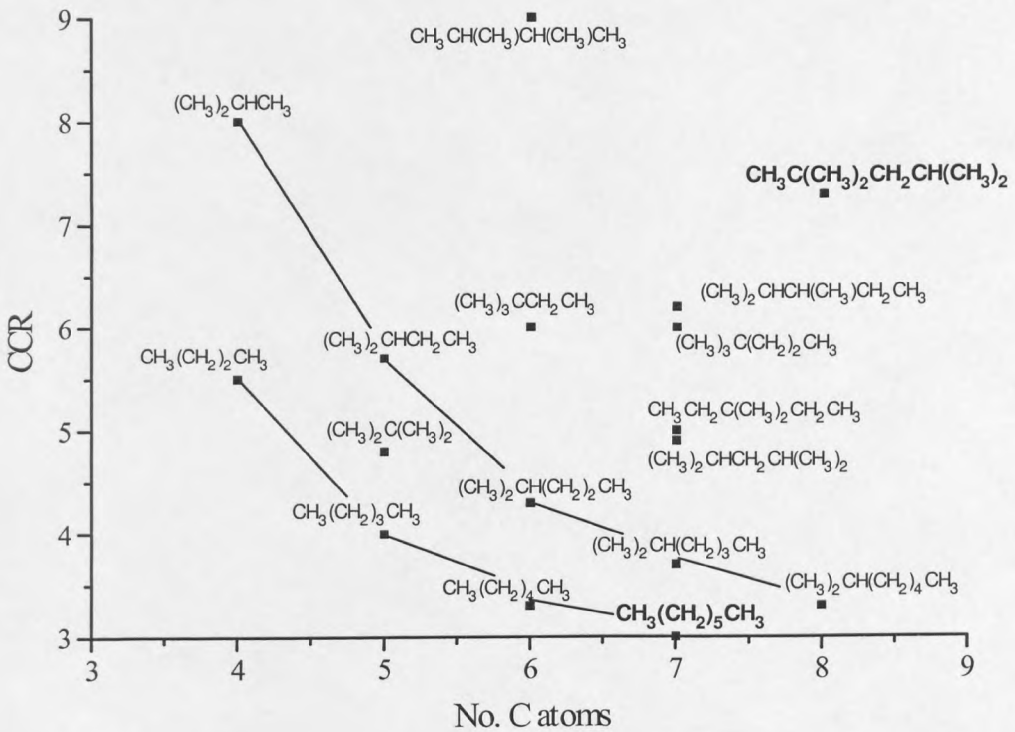

Figure 1.2 Effect of molecular structure on critical compression ratio (CCR) (600 rpm GM engine; Air 340 K; Jacket 450 K; Spark for Max. Power; Mixture Ratio for Max. Knock) [11]. Lines adjoin the members of a homologous series of hydrocarbons, i.e. n-alkanes and 2-methylalkanes.

Affleck and Fish [16] compared the phenomena of flame propagation and spontaneous ignition in an attempt to resolve the problem of the origin of engine knock. Pressure change measurements, emission spectroscopy and product analysis led to the conclusion

that the smooth propagation of a spark-ignited flame leads discontinuously to a rapid spontaneous phenomenon which consumes the remainder of the charge and shows properties typical of knock. This is in accord with the opinion that engine knock is a spontaneous explosion of the end-gas.

1.3 The Chemistry of Autoignition

Autoignition represents a parametric sensitivity of a system and is defined as the sudden inflammation of a gaseous charge at a critical condition of pressure, temperature and mixture composition. Autoignition is a physico-chemical phenomenon which occurs as a result of thermal feedback and chain-branching, resulting in an auto-acceleration of the overall reaction rate. The chemical energy of the hydrocarbon is transformed primarily into heat energy and a relatively small proportion of light energy.

The oxidation of hydrocarbons and related compounds is a complex process involving many intermediate compounds, which, ideally, leads to the final products of combustion, CO_2 and H_2O. The process of oxidation is known to develop through a radical chain mechanism. An important manifestation of this mechanism is chain branching which renders the process capable of self-acceleration, augmented by the exothermicity of reaction, which occurs at both low and high temperatures. The mechanism of autoignition was first described in terms of thermal explosion theory where autoignition occurs as a consequence of a greater rate of chemical heat release compared with heat losses from the system [17]. At a similar date autoignition was also described as a chain-branching explosion [18], in which the reaction of one active species results in the formation of two or more active species, each of which is able to propagate the reaction chain. It is now generally accepted that autoignition is a chain-thermal explosion [19] resulting from a combination of chemical and thermal processes.

The autoignition and associated features of organic gases and vapours are a consequence of their exothermic oxidation chemistry, but the way in which events unfold is determined by the physical environment within which reaction takes place. The

autocatalytic action required for a thermal explosion can arise from the self-heating produced by exothermic reactions because the rates of chemical reactions increase dramatically as the temperature increases. The occurrence of an explosion is therefore related to the net heat release or loss from the reacting system. If the rate of heat release due to reaction exceeds the rate of heat loss due to conduction, convection or radiation, then the system experiences a thermal runaway and subsequent ignition.

1.3.1 The overall mechanism of low temperature hydrocarbon oxidation

Historically, the underlying theme in the interpretation of the low temperature oxidation of hydrocarbons has been the formation of a molecular intermediate of limited stability which acts as a chain-branching agent [20]. As the temperature is increased the rate of decomposition of the chain-branching agent is enhanced, but also there are competing non-branching processes which are increasingly favoured at the higher temperatures. The successful competition of these non-branching processes results in a reduction in the overall reaction rate as the temperature is raised (negative temperature coefficient) (Section 1.3.4).

The majority of alkanes follow a similar mechanism of oxidation in the low to intermediate temperature regime (600-1000 K) outlined below using the generalised terminology for an alkane (RH), alkyl radical (R), propagating free radicals, hydroxyl, OH and hydroperoxy, HO_2, (represented as X), molecular oxygenated species, AO and BO, etc.. The individual reaction steps are discussed in further detail in Section 1.3.2.

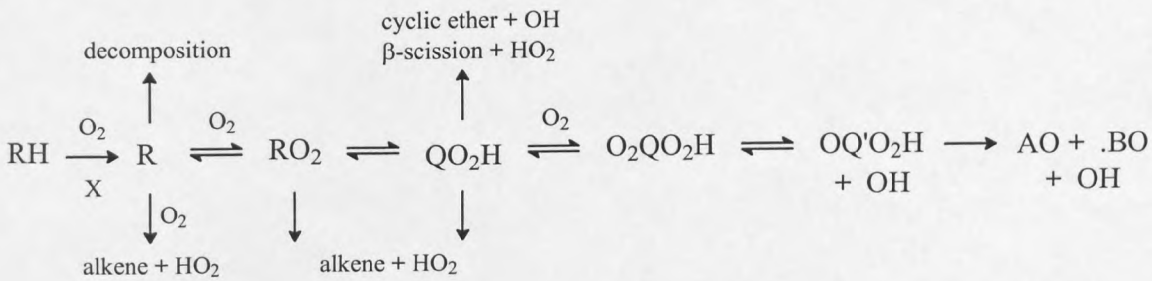

For the oxidation of an alkane, initiation may be by molecular oxygen, hydroxyl radical or hydroperoxy radical (1).

(1) $RH + O_2/OH/HO_2 \rightarrow R + HO_2/H_2O/H_2O_2$

The rate of H-atom abstraction by OH species varies according to the type of C-H bond being broken in the parent alkane. In general, secondary and tertiary C-H bonds are more easily broken than primary C-H bonds (Table 1.1). Molecular oxygen then associates with the alkyl radical to form an alkylperoxy radical.

Table 1.1 Rate constant parameters for H-atom abstraction from the fuel at primary, secondary and tertiary C-H sites (A values given per C-H)[21].

Reaction (1)	Primary		Secondary		Tertiary	
	A /cm^3 mol^{-1} s^{-1}	E /kJ mol^{-1}	A /cm^3 mol^{-1} s^{-1}	E /kJ mol^{-1}	A /cm^3 mol^{-1} s^{-1}	E /kJ mol^{-1}
OH + RH	6.1×10^{11}	6.9	1.4×10^{12}	3.6	1.25×10^{12}	-0.8
HO_2 + RH	4.9×10^{10}	62.5	4.9×10^{10}	52.6	4.9×10^{10}	41.5

Since the early 1960s the key to the thermokinetic switch in the low to intermediate temperature regime has been recognised to involve the alkyl/alkylperoxy radical equilibrium,

(2) $R + O_2 \rightleftharpoons RO_2$

in which the alkyl moiety, R takes whatever forms are appropriate as a result of H atom abstraction from the fuel molecule. Consequently, differences in behaviour emerge from different isomeric structures within a hydrocarbon series [22]. This is a fast, reversible reaction, with a reasonable exothermicity associated with the forward reaction (~ 40 kJ mol^{-1}). The energetics of the forward and reverse reactions determine the oxidation pathway and also whether an essentially branching or non-branching route is followed.

The forward reaction has a negligible energy barrier to reaction, due to the free radical site and the unpaired electrons on the oxygen. Therefore the association of these two

molecules is favoured at low temperatures. At low temperatures $[RO_2]/[R] > 1$ and slow, degenerately branched chain oxidation occurs. As the temperature increases the higher activation energy dissociation of alkylperoxy becomes favoured at $[RO_2]/[R] < 1$. The shift in the equilibrium toward the dissociation of RO_2 can be followed by H-atom abstraction by molecular oxygen to form the conjugate alkene and hydroperoxy radical,

(3) $\quad R + O_2 \rightarrow \text{alkene} + HO_2 .$

In this intermediate temperature region the predominant propagating free radical is the hydroperoxy radical which tends to abstract a further H-atom to form hydrogen peroxide, H_2O_2.

The temperature at which $[RO_2]/[R] = 1$ is known as the *ceiling temperature* and is dependent on the structure of the alkyl radicals and on the partial pressure of oxygen. The ceiling temperature represents the temperature at which the oxidation mechanism shifts from vigorous chain-branching and exothermic, OH propagation to non-branching and virtually thermoneutral, HO_2 propagation.

For the equilibrium $R + O_2 \rightleftharpoons RO_2$,

$$K_c = \frac{k_f}{k_r} = \frac{A_f \exp^{(-(E_a)_f/RT)}}{A_r \exp^{(-(E_a)_r/RT)}}$$

and $(E_a)_f \approx 0$

$\therefore$

$$K_c = \frac{k_f}{k_r} = \frac{A_f}{A_r \exp^{(-(E_a)_r/RT)}} = \frac{A_r \exp^{((E_a)_r/RT)}}{A_f} \qquad 1.1$$

Since the forward reaction incurs a negligible energy barrier ($E_a \approx 0$), as T increases K_c decreases and k_r increases, i.e. as the temperature of the system increases the reverse reaction is kinetically favoured. The temperature sensitivity of this equilibrium is not

identical for all alkyl radicals, thus different low temperature reactivities of hydrocarbons exist. Table 1.2 gives the rate parameters for the $R + O_2 \rightleftharpoons RO_2$ equilibrium, for primary, secondary and tertiary alkyl radicals [23]. The negative temperature coefficient is discussed further in Sections 1.3.3 and 1.3.4.

Table 1.2 Rate parameters for $R + O_2 \rightleftharpoons RO_2$ [23].

Reaction (2)	A / s^{-1} or cm^3 molecule s^{-1}	(E/R) / K
$R_1 + O_2 \rightarrow R_1O_2$	9.0×10^{-12}	0
$R_1O_2 \rightarrow R_1 + O_2$	7.6×10^{16}	16358
$R_2 + O_2 \rightarrow R_2O_2$	9.0×10^{-12}	0
$R_2O_2 \rightarrow R_2 + O_2$	6.0×10^{15}	17080
$R_3 + O_2 \rightarrow R_3O_2$	9.0×10^{-12}	0
$R_3O_2 \rightarrow R_3 + O_2$	2.8×10^{15}	15625

1.3.2 Further reactions of alkylperoxy radicals

Low temperature chain-branching and the first stage of a two-stage ignition arises from the further reactions of RO_2. Current interpretations of the chain-thermal interactions leading to cool flames and spontaneous ignition differ from those invoked formerly, insofar that the simplistic concept of a critical concentration of a molecular intermediate being reached before ignition can occur, is not a requirement. The subtle balance achieved between branching and non-branching reactions in a changing temperature environment is sufficient to give rise to the complex, non-isothermal combustion phenomena that result from the exothermic oxidation of hydrocarbons.

Within the overall oxidation mechanism of a hydrocarbon in air there are four main types of reaction, these are, initiation, propagation, branching and termination. Initiation involves the formation of an active species from the molecular reactants, which can

propagate the reaction chain. Propagation reactions involve the reaction of an active species with a stable molecule to form another active species. Branching reactions are central to the occurrence of spontaneous ignition and they involve the reaction of one active species with a molecule to form two or more active species, each of which can then propagate another reaction chain. Termination reactions remove the active species from the system, either by reaction with another species or by wall reaction.

At low temperatures (<650 K) reactions of RO_2 are mainly intermolecular H-atom abstraction by the parent alkane molecule to form an alkylhydroperoxy radical and another alkyl radical,

(4) $RH + RO_2 \rightarrow R + ROOH.$

The weak O-O bond can break to form an alkoxy radical and OH, this is the degenerate branching route. In general, external H-atom abstraction, or intermolecular abstraction, results in chain branching whereas internal H-atom abstraction, or intramolecular abstraction, results in chain propagation.

At intermediate temperatures internal isomerisation by intramolecular H-atom abstraction is possible,

(5) $RO_2 \rightleftharpoons QOOH,$

QOOH is also an alkylhydroperoxy radical with a weak O-O bond, it is a very reactive species which decomposes in one of two modes, dependent on the location of the free radical and -OOH sites, to give an oxygenated molecular intermediate and a free radical. Alternatively, a further addition of molecular oxygen can occur at the free radical site to form a diperoxy species (O_2QOOH). This can then undergo an internal isomerisation and H-atom abstraction to form a ketohydroperoxide (OQ'OOH), which is now recognised as the main kinetic chain-branching agent in the low temperature oxidation of hydrocarbons. This pathway to chain-branching oxidation is discussed in further detail in Chapter 4.

1.3.3 Negative temperature coefficient under isothermal conditions

The majority of chemical systems, complex or otherwise, exhibit a monotonic increase in reaction rate as the temperature is increased, i.e. can be characterised by an Arrhenius temperature dependence of the reaction rate constant. However, the majority of n-alkanes exhibit a negative temperature dependence, or negative temperature coefficient (ntc) [24,25], of the overall rate of oxidation within the approximate temperature range 750-850 K. Hence, as the temperature of the system is increased in this range, the rate of reaction decreases. The kinetic origin of this negative temperature coefficient (ntc) lies in the shift in the R/RO_2 equilibrium at the ceiling temperature and the associated transition from low temperature degenerate branching to non-branching oxidation. The ntc represents a transition in the oxidation chemistry as a result of the thermokinetic switch.

The ntc was first observed by Pease during studies of the oxidation of propane and n-butane using both flow and static systems [26]. This phenomenon holds significant importance in determining the global characteristics of the non-isothermal oxidation of alkanes. The complexity of the combustion of hydrocarbons emerges as a result of the interaction of thermal feedback and chemical autocatalysis. An important consequence of the ntc is a complex dependence of the ignition delay on initial or control temperature. The two-stage development of ignition during hydrocarbon oxidation from temperatures below about 750 K also arises from the kinetic interactions which give rise to the ntc of reaction rate, coupled to thermal feedback.

As the temperature of the system exceeds about 850 K then chain-branching again predominates due to the dissociation of hydrogen peroxide (6) and a chain-thermal explosion follows.

(6) $H_2O_2 + M \rightleftharpoons 2OH + M$

The kinetic foundation of the negative temperature coefficient of the reaction rate can be summarised as follows:-

a) At low temperatures the formation of RO_2 is favoured and the oxidation proceeds via the formation of alkylhydroperoxides and diperoxy species. Autocatalysis occurs through degenerate chain-branching and the mechanism is propagated mainly by OH.

b) As the temperature increases the fraction of alkylperoxy radicals formed decreases and the formation of the conjugate alkene occurs more favourably, propagation is mainly by HO_2.

c) as the temperature exceeds 750 K there is an increase in reactivity through the further reaction of molecular intermediates and the increased rate of decomposition of H_2O_2 which promotes autocatalysis.

1.3.4 Non-isothermal oxidation, the role of the ntc, two-stage ignition and cool flames

In a non-isothermal system thermal feedback, as a result of exothermic reaction, can cause the reactant temperature to increase. At low temperatures (<650 K) degenerate chain-branching occurs and propagation is predominantly by OH radicals. Hydroxyl radicals are very reactive and their propagation reactions are significantly exothermic so the system begins to self-heat. As the temperature of the system increases the multiplication of reaction chains becomes curtailed by the displacement from branching to non-branching modes, as described above. The main propagating radical is then HO_2. This is less reactive than OH and therefore the propagation rate falls as the transition occurs. However, HO_2 propagation reactions leading to H_2O_2 formation are virtually thermoneutral and so the overall heat release rate is reduced. Also, below about 850 K, the rate of hydrogen peroxide decomposition to OH radicals is relatively slow and so does not promote autocatalysis readily. Hydrogen peroxide can accumulate in the system, and will decompose at an increasing rate as the temperature rises beyond 900 K. Chain branching processes are controlled by two different mechanisms in these two distinct temperature regimes, which depend on the nature of the intermediate species formed in the combustion process (i.e. alkylhydroperoxy at low temperature and hydrogen peroxide at higher temperature). In non-isothermal conditions this transition

is manifest as a two-stage ignition. An early, weak ignition (or "cool flame"), where the OH/RO_2 radical activity dominates, is followed by a later and much stronger second stage ignition, driven by the H_2O_2 decomposition and, subsequently, chain-branching reactions involving H and O [27].

Cool flames were first observed by Davy in 1815 and were investigated further by Perkin in 1888 [28] by dropping liquid diethyl ether onto a bath of hot sand. More recent studies have illustrated the relatively low burning velocities of cool flames (0.05 - 0.1 m s^{-1}, compared with normal flame speed of 0.4 m s^{-1}). Typical temperature increases associated with cool flame propagation are in the range 50 - 200 K, hence the term "cool flame".

Cool flames are characterised by a faint blue luminescence which originates from an electronically excited state of formaldehyde (~340 kJ mol^{-1}) formed in the chemiluminescent reactions (7) and (8), [29, 30].

(7) $CH_3O + OH \rightarrow CH_2O^* + H_2O$; $\Delta H°_{298} = -296.4$ kJ mol^{-1}

(8) $CH_3O + CH_3O \rightarrow CH_2O^* + CH_3OH$; $\Delta H°_{298} = -278.5$ kJ mol^{-1}

where the enthalpies refer to the production of ground state formaldehyde. [a]

It is possible to see this very weak, pale blue light by eye in a darkened laboratory when it is isolated in a cool flame reaction, as opposed to a two-stage ignition. In two-stage ignition the emission is indicative of the free radical concentrations in the first stage of the ignition. In some combustion systems there is a further complexity of behaviour at conditions between the cool flame region and the ignition boundary, termed multiple stage ignitions [31].

The light output which accompanies the final stage of two-stage ignition is considerably more intense. It is characteristic of the emission from premixed flames of hydrocarbons and arises predominantly from chemiluminescent reactions, mainly giving electronically excited CH*, C_2*, CO_2* and OH* [32].

[a] for further discussion of the spectroscopy of cool flames see ref. 32.

1.3.5 Structure dependent reactivity

The structure dependent reactivity of hydrocarbons in the low to intermediate temperature oxidation arises as a result of the structure dependent rate of the reactions

(5) $RO_2 \rightleftharpoons QOOH$

and

(9) $O_2QOOH \rightleftharpoons OQ'OOH + OH$

Several alternatives for this reaction (5) exist for a given hydrocarbon, the relative importance in the overall chain-branching mechanism being determined by the steric hindrance and energetics of the reaction. The rate is influenced by the bond strength of the C-H bond which is broken, by the ring strain energy of the transition state and also by the number of C-H bonds of a particular type available for fission (the degeneracy).

Consider, for example, the pentylperoxy radical with the peroxy group at the second carbon. The most energetically favoured and hence the fastest internal H-atom abstraction reaction, is the (1,5s) transition involving the breakage of a secondary C-H bond via a relatively stable, 6-membered ring transition state.

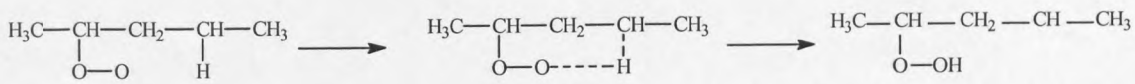

The observed difference in reactivity of the two primary reference fuels, n-heptane and i-octane (2,2,4-trimethylpentane) [33-36], can be explained in terms of the relative ease of internal isomerisation via H-atom abstraction for n-heptane when compared with i-octane, which exhibits very little reaction at temperatures below 850 K. The evidence lies in the different molecular structures and the possible reaction pathways for

(5) $RO_2 \rightleftharpoons QOOH$.

Normal-heptane has four possible isomers of RO_2 and 18 different possible structures of QOOH. Iso-octane also has 4 different isomers of RO_2 but only 14 QOOH isomers. For the i-octane RO_2 radical there are no readily abstractable H atoms which do not incur a significant ring strain in the transition state or the breakage of the relatively strong primary C-H bond. Therefore the rates of these reactions are slow compared with those for n-heptane, which has a long linear chain of secondary C-H bonds available and can undergo the energetically favourable (1,5s) isomerisation reaction. The formation of the six-membered cyclic transition state is energetically favoured ($E_{a\ (5)}$ = 109 kJ mol^{-1} for the R_sO_2 1,5s transition) due to the absence of steric interaction of internal rotors.

The effect of molecular structure of hydrocarbons on reactivity has been studied extensively [12,13-14,37]. The following conclusions can be made:-

a) the reactivity decreases as the number of side chains replacing $-CH_2-$ increases
b) the presence of unsaturated bonds in the molecule reduces its reactivity
c) cyclic alkanes show a lower reactivity than linear or branched chain alkanes
d) aromatic compounds show a very low reactivity compared with aliphatic alkanes

The highly branched alkanes offer a much higher proportion of primary C-H bonds with a corresponding higher bond energy, therefore rendering them more difficult to abstract and the rate of abstraction slower compared with the secondary and tertiary C-H bonds. The high degree of branching and compact structure of a molecule such as i-octane prevents many possible modes of internal isomerisation.

Aromatic hydrocarbons such as toluene exhibit no low temperature oxidation via R/RO_2 equilibrium and RO_2 isomerisation and the rate of oxidation is very slow. This is due to the formation of a relatively inert free radical, stabilised by the delocalisation of electrons within the π-electron system of the aromatic ring (10). Increasing the charge density of the aromatic ring also has the effect of reducing reactivity and ease of autoignition and can be facilitated by the addition of substituent methyl groups onto the

aromatic ring. Allylic radicals illustrate a similar resonance stabilisation due to delocalisation of electrons (11). (X = propagating free radical, e.g. OH or HO_2).

(10)

(11)

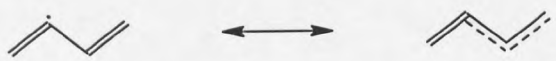

1.3.6 Gasoline, antiknocks and octane boosters

The structure dependent reactivity of hydrocarbons, described above, accounts for the relatively high knock resistance incurred by the incorporation of high proportions of aromatics, alkenes and branched alkanes in a gasoline, such as in standard unleaded gasoline. Current unleaded petrol contains approximately 40 % by volume of aromatics. In contrast, leaded 4 star fuel contains only a very small proportion of toluene, but does contain ~12 % non-1-ene which has a relatively low knock resistance. There is also a lower proportion of branched alkane structures than in unleaded gasoline. The resultant potentially low knock rating of 4 star leaded petrol is counteracted by the presence of a trace amount (~150 ppm) of antiknock agent, tetraethyl lead (TEL), $Pb(C_2H_5)_4$.

An effective antiknock agent is one which results in a large increase in CCR for only a small concentration of additive. Antiknocks can act by chain-termination or by removal of chain-propagating free radicals. Midgely and Boyd of General Motors first discovered the potential of lead alkyls as antiknock additives in 1919 [38,39]. They

became commercially available as a gasoline additive in the US in 1923. TEL acts by destroying free radicals and therefore prevents the development of chain-branching reactions in the end-gas. The lead alkyl is oxidised in the combustion chamber to lead oxide, forming a fine dispersion of PbO particles in the hot gas. These small particles provide a large surface area for the destruction of reactive radical intermediates and thus inhibit spontaneous ignition development. The lead alkyl itself can only affect the second stage of ignition, by radical-radical recombination. TEL was successfully used as a knock suppressant for many years before its harmful effect on health and poisoning effect on exhaust catalysts required its elimination from emission-controlled vehicles in the 1970s.

As a result of the removal of lead alkyls from gasoline, there has been a move toward the search for alternative antiknocks, such as the "ashless" antiknocks [40,41]. Ashless antiknocks, such as amines and phenols, contain no metal and tend to be much less effective than the metal alkyls and carbonyls. They are generally liquid phase inhibitors which react with the active radicals in the combustion chamber, such as OH and HO_2, to form inert radicals. One example is N-methylaniline (NMA) which reacts with OH to form a resonance-stabilised free radical (12) (similar electron delocalisation as with toluene (10)), which, because of its low energy, cannot react to regenerate active propagating free radicals, but it may undergo radical recombination reactions. To date, no ashless antiknocks have proved sufficiently cost effective to be made commercially available.

(12)

NMA

An alternative method of increasing knock resistance is the inclusion of "octane boosters" in the fuel blend. These are generally oxygenates such as ethanol, methyl-t-

butyl ether (MTBE) or ethyl-t-butyl ether (ETBE) and may be found at up to 15 % by volume proportions in unleaded gasoline. These components are included to an increasing extent because, not only do they enhance octane rating, but they also add an oxygen content to the fuel which ultimately helps to reduce the proportions of carbon monoxide and unburned hydrocarbons in the engine exhaust emissions.

1.4 Experimental studies of Hydrocarbon Autoignition

Experimental investigations of hydrocarbon autoignition are an obvious and invaluable means of enhancing understanding of this physico-chemical phenomenon. They yield a panoply of information relating to the detailed mechanism of hydrocarbon oxidation, the relative reactivity of different hydrocarbons, and the effect of external control parameters on the reactivity of a system, e.g. pressure, temperature, composition. All of this information can be used either in the direct assessment of the combustion characteristics of a system or to validate detailed chemical kinetic models which can then be used to predict behaviour in combustion systems. Practical solutions to combustion problems are also sought via controlled experimental studies of the fundamental scientific features.

This section is concerned with experimental observations and measurements and the valuable information gleaned from them. The importance and usefulness of experimental observations and measurements in the provision of detailed information pertaining to combustion systems will become evident in the description of the different methods and the results which have been obtained. The demand for experimental measurements in the validation of detailed chemical kinetic reaction mechanisms is also escalating.

The main experimental techniques that have been used to study physical and chemical aspects of hydrocarbon oxidation, especially at temperatures below 1000 K will be described. Measurements of ignition delays hold great significance in the studies relating to engine knock, therefore a description of the ignition delay parameter and its

measurement in different devices will be given. A more detailed, comprehensive review of the experimental studies of hydrocarbon oxidation from the 1960s to 1996 can be found elsewhere [20,42].

A detailed analysis of rapid compression machines is given in Chapter 2, with a brief summary of the devices currently in use around the world.

Closed, constant volume reaction vessels

Experiments in closed, constant volume vessels involve admission of reactants to an evacuated vessel. The vessel is maintained at constant temperature in an electrically heated oven so that an experiment is performed at a given initial reactant pressure (p) and vessel temperature (T_a). The reaction vessels used in studies at pressures below one atmosphere are normally made from Pyrex glass. Optical access within the visible transmission range also presents no problem with glass vessels. Metal vessels (normally stainless steel) are required for experiments performed at pressures at or above atmospheric.

For any interpretation of kinetic parameters from chemical measurements of exothermic elementary reactions it is essential that the reaction be performed under isothermal conditions so that the reactor temperature itself is the control parameter. However, low temperature hydrocarbon oxidation is sufficiently exothermic that there must be an accompanying temperature change in closed vessels, which can be very large when cool flames occur ($\Delta T > 100$ K). The quantitative evidence for changes of mechanism cannot be distinguished if no temperature record is obtained simultaneously. Chemical analyses made in non-isothermal conditions must also be interpreted with caution if the system is not well-stirred so that a uniform temperature is maintained throughout the reactants [43-46].

Flow systems

Flow systems in use may be classified as heated laminar tubes, or plug flow tube reactors (PFTRs), and burners, or heated turbulent flow reactors and well-stirred reactors, or continuous stirred-tank reactors (CSTRs).

The simplest flow systems, namely laminar flow tubes operated at atmospheric pressure, were used in some of the earliest chemical studies of hydrocarbon oxidation [26,47-48]. Premixed gaseous fuel and air flowed through a heated tube and the products were collected at the outflow under stationary state conditions. Product compositions were analysed and extents of reaction deduced.

CSTRs and turbulent flow reactors have been operated mainly at pressures from 0.1 to 1 MPa, with residence times varying from several seconds to less than 100 ms at the highest operating pressures. Studies of the combustion of hydrogen [49], carbon monoxide [50] and acetaldehyde [51, 52] at sub-atmospheric pressure have also been reported. In most cases the reactants are mixed after metering and pre-heating, and then flow through the reactor at constant pressure and flow rate. The reactor temperature may be held constant, or it may be varied continuously or in a stepped manner, in order to probe the modes of behaviour for a given fuel-oxidant composition over the temperature range.

A well-mixed condition can be established in the CSTR by either a mechanical stirrer [53,54] or jet mixing of the gases [55-57]. A turbulent flow reactor, at Princeton University, has been operated at atmospheric pressure over many years to give information on the detailed chemistry of hydrocarbon oxidation in the temperature range 1000-1200K. Aromatic compounds as well as alkanes and alkenes have been investigated, [58-66]. A turbulent, high pressure, flow reactor has been developed by Koert et al. [67] for studies throughout the temperature range from 600 to 1000 K and at pressures up to 1.5 MPa.

Heated, flat flame burners have also been used for the stabilisation of cool flame and two-stage ignitions. These systems were pioneered by Agnew et al. [68], and a definitive study of the spatially resolved chemistry of diethyl ether combustion has been reported [69]. Ballinger and Ryason [70] have described this type of burner in detail and have reported the relative behaviour of some n-alkanes, PRF fuel mixtures, and the effect of anti-knock additives.

Shock tubes

The combustion of hydrocarbons covers a wide temperature range (600-2500 K), so it is essential that kinetic data of many elementary reactions be obtained over a similar range. Elementary reaction rate data can be derived from flame studies [71], but another source of data at high temperatures is through study of reactions behind a shock wave under controlled experimental conditions in a shock tube.

A high temperature and pressure is rapidly attained in a shock heated gas, governed ideally by the pressure ratio across the shock front and the ratio of heat capacities of the gases [72-74]. The discontinuity means that a reactant gas is raised virtually discontinuously to the shocked gas temperature, T_o. The time interval available before a rapid cooling occurs, 10 - 1000 μs, is kinetically significant at high temperatures. Heat losses are negligible over this reaction time interval. These are ideal circumstances in which quantitative kinetic measurements may be made.

A plane shock wave is produced in a long, closed tube by the sudden bursting of a diaphragm (e.g. aluminium foil, mylar) which separates one gas at high pressure, the driver gas, from another at low pressure, the test gas. The contact surface is at the interface between the driver gas and the test gas. It moves rapidly along the tube but only at a subsonic velocity as opposed to the supersonic velocity of the shock front. The driver gas at the contact surface is cold, and so when it envelopes the test gas, any high temperature reactions are quenched instantly. The reaction time is represented by the interval between the arrival of the incident shock front and the arrival of the contact surface. Its duration is determined by the point in the tube at which the kinetic

measurements are being made. The rarefaction fan, which is driven back into the driver gas, is an expansion wave and it has a divergent character because the velocity of its "tail" is governed by gas that has already been cooled by the rarefaction head.

Typically the shocked gas temperatures for kinetic studies [75] or ignition delay times [75,76] fall in the range 1500 - 2500 K. The near discontinuity in temperature that is achieved when the shock passes through the reactants gives a very well defined start to the reaction, from which an ignition delay can be well-characterised. Extremely high pressures are attainable in shock tubes and conditions are close to those in engines. However, if the development of reaction is relatively slow, with ignition delays of several milliseconds, there can be appreciable heat losses during the induction period which complicates the interpretation of the behaviour [77].

Cadman [78] studied ignition delays of toluene behind a reflected shock in the shocked gas temperature range above 1000 K. Liquid fuel droplets were injected into the shock tube in these experiments. It is likely that their complete evaporation occurred during the interval between passage of the incident and reflected shocks.

Motored engines

Many combustion scientists have exploited motored engines for the study of partial combustion of fuel-air mixtures. Invariably a single cylinder CFR engine is used, driven by an electric motor but there is no spark-ignition. Although the fuel-air mixture does not experience the additional compression of the flame or consumption by it, the charge does undergo compression and heating, which may lead to spontaneous combustion. This is one way in which end-gas autoignition can be investigated and the technique can be used to study the unburned hydrocarbons. Supplementary sampling devices are often used in conjunction with motored engines so that the intermediate stages of the processes may be examined. These could involve a rapid sampling system [79, 80], which snatches a small amount of the charge while the overall process continues, probe sampling [81,82], or exhaust gas analysis [83-86].

The motored engine is a chemical reactor in which the period for reaction is governed by the engine speed. The conditions under which reaction occurs are governed by the compression ratio which, linked to the inlet temperature and pressure, controls the highest temperature and pressure. Whilst there may be some difficulty in defining very precisely the temperature history of the reactants, comparative chemical measurements can be made by variations of engine speed, inlet temperature and pressure. Leppard has adopted this approach to useful effect [85,86]. The exhaust gas is analysed from a number of motored cycles so that cycle-to-cycle variations are averaged.

These studies have contributed significantly not only to the better understanding of the mechanisms of hydrocarbon oxidation but also to a bridging of the gap between the interpretation of reactions investigated in more conventional chemical systems, and the reactions of hydrocarbon fuels in s.i. engines.

Ignition delays

The time taken for spontaneous ignition to develop, the ignition delay, is important in many applications, and it is also important to know how the ignition delay is affected by changes in pressure, temperature and composition. These data are relevant to combustion in reciprocating engines. Many complications are associated with measurements in engines themselves. Therefore, the understanding and interpretation of spontaneous ignition is best approached in more simple devices. Low pressure closed vessels and flow reactors can, and have been used, but engine operating conditions are more closely represented by rapid compression machine, shock tube or motored engine studies.

If ignition delays measured in different devices under the same conditions are brought together it becomes clear that there are incompatibilities that cannot be attributed to differences in composition or pressure. In rapid compression machines the discrepancies between different sets of results may arise from different rates of compression [87], which can affect the rate of heat transfer in the early stage of the post compression interval as a result of the extent of gas motion that is created by the piston

motion [88,89]. Ignition delays become longer as the heat loss rates are increased, and there may be a failure of spontaneous ignition to occur in the limit of very high heat loss rates. Differences in behaviour can also arise because, with a slow compression of very reactive fuels in air, quite significant extents of reaction can occur during the final stages of the compression stroke. Much less reaction would occur during the shorter interval available in the final stage of a compression at a higher rate [88]. This is not usually a problem for fuels of low reactivity.

The last point is of practical significance because spontaneous oxidation of the fuel-air charge admitted to the cylinders of a s.i. engine can occur during the compression stroke, which is a preliminary to the eventual autoignition of the end-gas. Thus there are attributes of the application of rapid compression machines to spontaneous ignition studies which relate to combustion engines, especially with regard to an understanding of the development of end-gas combustion in association with engine knock. The typical initial temperature and pressure ranges of interest in studies of ignition delay related to engine combustion are 600 - 1000 K and 1.0 - 3.0 MPa (10 - 30 atm). The ignition delay and how it is affected by the compressed gas (or shocked gas) temperature and pressure is related to the type of oxidation processes that can occur within these ranges of conditions.

The value of experimental observations and measurements in the study of hydrocarbon oxidation is clear. However, the complexities and inconsistencies which can arise are also apparent. Experimental investigations are both time-consuming and costly. Therefore, alternative, cost-effective methods of understanding, assessing and providing practical solutions to combustion problems are sought. The most promising way forward appears to be in the use of numerical modelling techniques to predict the behaviour of a system. However, the requirement for experimental validation and the provision of accurate elementary reaction rate data remains essential. The progression and development of numerical methods and the current status is discussed below (Section 1.5).

1.5 Numerical Modelling approaches to Hydrocarbon Autoignition and Engine Knock

Kinetic understanding via numerical modelling provides the power to gain quantitative insight into kinetic interactions at the elementary reaction level, which govern the global behaviour, so one is able to predict the performance of complex fuel mixtures. The establishment of a detailed kinetic model also provides an opportunity for the numerical prediction of the behaviour of a chemical system under conditions that may not be accessible by experimental means. However, large-scale models with many variables may require considerable computer resource for their implementation. Computation in a spatial domain, for which partial differential expressions are appropriate, becomes considerably demanding. There are also many important fluid mechanical considerations in reactive systems, the detailed kinetic representation of the chemistry for which would be highly desirable, but which cannot yet be computed economically. In such circumstances there is a need for reduced or simplified kinetic models. Comprehensive reaction mechanisms extended over a wide range of conditions with their inclusion of all the detailed sub-mechanisms involved in the oxidation of hydrocarbons are valuable. Not only do comprehensive kinetic models constitute a starting point of the formal mathematical methods for reduction to simplified schemes, but also they may be used as analytical tools against which the performance of reduced models may be tested. Prior to the advent of comprehensive and reduced kinetic models, simple skeleton schemes also provided important analytical insights into the nature of hydrocarbon oxidation in the low to intermediate temperature regime.

Skeleton schemes

Skeleton schemes are analytical methods which have been adopted for the prediction of isothermal and non-isothermal oscillatory reaction and the negative temperature coefficient. They represent the minimum kinetic criteria appropriate to particular experimental features. In 1965 Yang and Gray [90] introduced a formal kinetic scheme for hydrocarbon combustion, which coupled chain-branching and thermal feedback. This provided a thermokinetic model which could account for spontaneous ignition and

oscillatory cool flames, associated with an overall negative temperature dependence of reaction rate. The kinetic structure is as follows:

F	→	X	initiation	(i)
X	→	inert	termination 1	(t_1)
X	→	2X	branching	(b)
X	→	inert	termination 2	(t_2)

where X is a reactive intermediate and F is the primary reactant (or parent fuel). The mechanism requires that $E_{t1} < E_b < E_{t2}$, this being the only requirement which ensures an overall negative temperature dependence of reaction rate within a limited temperature range.

The mass and energy conservation equations are given by,

$$\frac{dx}{dt} = k_i - (k_{t1} + k_{t2} - k_b)x \qquad 1.2$$

$$C_v \frac{dT}{dt} = k_i q_i + (k_{t1} q_{t1} + k_{t2} q_{t2} + k_b q_b)\, x - \chi(T - T_o) \qquad 1.3$$

where x is the concentration of the intermediate X, q is the exothermicity of a reaction, C_v is the volumetric heat capacity, χ is the Newtonian heat transfer coefficient and ($T-T_o$) is the temperature difference between the reactants (T) and the vessel wall (T_o).

The successful interpretation of cool flames, two-stage ignition and the ntc, is encapsulated in the interaction between branching and non-branching reactions, which in turn is controlled by the relative activation energies and coupled to thermal feedback.

Further developments of the Gray and Yang model have followed which enable the prediction of multiple stage ignitions [91] observed in acetaldehyde, propane and butane oxidation systems. Also, more recently, a simple kinetic structure derived from the Gray and Yang model has been used in the interpretation of the onset of autoignition

and the occurrence of knock in engines [92]. Similarly, Bradley et al. [93] have included a high temperature initiation step, which performs a function in the promotion of chain branching in the high temperature, second stage of autoignition.

Between 1971 and 1977, employees of Shell Research and Technology Centre developed a thermokinetic interpretation of hydrocarbon combustion, referred to as the "Shell" model [94]. Simulations of ignition delays measured in an RCM and p-T ignition boundaries supported the suitability of the structure of the model, i.e. a simple representation of alkane oxidation. In contrast to earlier skeleton kinetic schemes, the inclusion of several propagation reactions and the formation of molecular oxygenated products and intermediates was made. Also, the exclusion of high temperature branching reactions was made, with consequent difficulties in the simulation of the second stage development of autoignition.

Reduced kinetic models

Thermokinetic models compute the chemical reaction rate and the associated enthalpy change in order to predict the overall behaviour of a system under a given set of control parameters. A reduced kinetic model represents the oxidation of a single component fuel by a sequence of kinetic steps identified with elementary reactions which are known to be associated with the oxidation of that compound. The temporal evolution of a chemical reaction is derived numerically from the simultaneous integration of a set of differential equations, each representing the concentration of a species in the system.

The underlying low temperature, kinetic structure of alkane oxidation to which reduced kinetic schemes relate has been represented by Morley [95]. Both the Cox and Cole [96] and the Hu and Keck [97] models were developments of the Shell model which included more explicit representations of the elementary reactions appropriate to the low temperature oxidation of alkanes.

Recent developments in the understanding of the elementary reactions associated with alkane oxidation, e.g. $R + O_2 \rightleftharpoons RO_2$ and $RO_2 \rightleftharpoons QOOH$, have led to a unified approach

to alkane oxidation modelling based on the specific type of alkyl radical, i.e. primary, secondary or tertiary [98].

Comprehensive chemical kinetic models

Present day detailed, comprehensive models include all relevant chemical reactions for the oxidation of hydrocarbons in the temperature range 500 - 2500 K [99]. The construction of a comprehensive kinetic model to represent the oxidation of a hydrocarbon, incorporating the "best" available kinetic parameters, permits a quantitative link to be forged between detailed chemical measurements and the interpretation of the underlying kinetics and mechanism of the combustion system. If the model yields a satisfactory quantitative representation of the observed chemistry, which requires exhaustive tests over as wide ranges of experimental conditions as possible, then the model is ready for application in a number of different ways. These may have essentially chemical purposes, such as the prediction of a product yield in a chemical process, but often the aim is to predict other sorts of behaviour, such as the possibility of spontaneous ignition, ignition delay times, or more complex phenomena such as engine knock.

There has been very substantial progress in the United States and Western Europe to construct comprehensive kinetic models to represent hydrocarbon combustion over wide temperature and pressure ranges [100-102]. There have also been advances in large scale numerical modelling in Russia [103]. The present position is that comprehensive kinetic models exist for the combustion of alkanes, certainly up to i-octane with some exploration towards the components of kerosene and diesel fuels [104]. The temperature range for the intended application of existing models is approximately 600 - 2600 K. The largest kinetic schemes now run to many thousands of elementary steps, but their origins were more modest.

Until about 1985 the emphasis remained on high temperature combustion and flame properties. That is the detailed models were confined to temperatures above about 1000 K. There has been some progress towards an understanding of the reaction

mechanisms of benzene and toluene at temperatures above 1000 K, supported by experimental studies [105].

The inclusion of reactions to represent the "low temperature" chemistry in a detailed model for n-butane oxidation at high pressures, that is appropriate to temperatures down to about 600 K began in 1986 [106]. At the present time, models which include around 500 species and more than 2000 reversible reactions to represent alkane isomers up to heptane are in use [101], and still larger schemes are under development [102].

Applications of comprehensive kinetic models

The only specific application of a comprehensive kinetic model that appears to have been reported so far is the comparison of predicted times of ignition for selected alkanes with the research octane number (RON) measured in a CFR engine [13,102]. The calculations were based on the variable volume numerical model matched to a motored engine pressure history from a primary reference fuel mixture corresponding to RON 90 in a stoichiometric proportion with air ($\phi = 1.0$). The time to ignition was determined from bottom dead centre (bdc), or the start of the compression stroke in the simulated engine cycle to the maximum rate of temperature change in autoignition.

The duration of the compression stroke in the calculated times corresponded to approximately 50 ms, signifying that autoignition occurred after top dead centre, as observed experimentally. The choice of bdc as the initial condition is essential to permit the development of spontaneous combustion during the course of the compression stroke as the gas pressure and temperature increase. This definition of the time for ignition differs from that given by, (i) the admission of reactants to a hot, closed reaction vessel, (ii) the end of compression in an RCM, or (iii) the passage of a shock through the reactants in a shock tube. It is not easy to rationalise these times for ignition with the research octane number for each fuel. Moreover, isomers of similar structure that exhibit a similar RON do not show a similar degree of correspondence in the calculated ignition delay.

Numerical studies have yielded a clearer insight into the kinetic structures that are involved in the complex thermokinetic interactions leading to spontaneous ignition. There is no doubt that numerical modelling has played a very important part in combustion research in the last twenty years [107]. Numerical approaches have enhanced the link between the formal understanding of the elementary foundations and the interpretation of hydrocarbon ignition.

However, the ability to compute complex reaction details can not preclude the necessity for basic experimental studies of chemical kinetics and for experimental validation of reaction mechanisms. Fundamental experimental measurements of rate constants are an essential requirement of any detailed chemical kinetic model, but can themselves incur a significant error during extrapolation to high pressures. Detailed numerical models applied to the simulation of combustion systems over more than one dimension are extremely time consuming and costly. Solutions to this problem require an enormous research effort in themselves. Of the possible remedies, perhaps one of the most promising is the reduction of model complexity using "lumping" procedures [108], where the kinetic and thermochemical data are derived from a composite of parameters on the basis of some prescribed procedure such as steady state analysis, applied to certain elementary species in the chemical kinetics. The alternative option is to await the evolution of more powerful (and expensive) computing resources.

1.6 Aims and Objectives

The aim of this research programme was to use the Rapid Compression Machine (RCM) to study the autoignition characteristics of hydrocarbon-air mixtures under conditions of temperature and pressure similar to those which occur in the end-gas of a spark-ignition engine under knocking conditions. Using measurements of spontaneous ignition delays extracted from measured pressure-time profiles, chemical analysis of extents of reactant consumption and visual imaging techniques, the overall understanding of hydrocarbon autoignition in relation to engine knock has been advanced and prompts further

investigations into this interesting and complex phenomenon. The main research objectives are outlined as follows:-

i. Measure extents of fuel consumption during compression and ignition for selected hydrocarbons in the RCM.
ii. Quantify the effect of alkylamines on the ignition delay of hydrocarbons in the RCM.
iii. Examine the effect of the molecular structure of hydrocarbons on their reactivity in terms of ignition delay.
iv. Determine the relationship between ignition delay measured in an RCM and the Research Octane Number.
v. Seek experimental evidence which supports the numerically predicted spatial temperature inhomogeneities within the combustion chamber of the RCM during the post-compression period.
vi. Use visual imaging techniques to study and record the evolution of single and two-stage ignition in the RCM.
vii. Reproduce and characterise the knock-like characteristics of a spark-ignition engine in the RCM.
viii. Determine the influence of particulates and higher alkanes on the ignition of methane-oxygen mixtures in the RCM.

Chapter 6 addresses the issues relating to numerical modelling of hydrocarbon autoignition in the RCM and provides a general discussion of numerical modelling as a tool to understanding engine knock. In Chapter 7 an overall summary of the results presented in Chapters 3-5 will be given and the main conclusions outlined. A brief overview of each chapter of experimental results (Chapters 3-5 and 8) is given overleaf.

Reactivity during compression and the role of additives (Chapter 3)

The objective was to measure directly the extent of reactant consumption during compression and ignition for n-heptane, n-pentane and a PRF 60 mixture in stoichiometric proportion in air ($\phi = 1.0$) and for a lean i-octane-air mixture ($\phi = 0.6$).

The method employed was quenching of the reaction by rapid adiabatic expansion and gas chromatographic analysis of the combustion chamber contents.

Using the light output record as an indicator of the first stage (or "cool flame") of autoignition, the influence of an aliphatic amine on the reactivity during compression and the overall ignition delay was quantified.

Ignition delays and their relation to octane rating (Chapter 4)

Global combustion phenomena including cool flames, 2-stage ignition and the negative temperature coefficient (ntc) have been studied for various hydrocarbons in stoichiometric proportion in air ($\phi = 1.0$). Extensive measurements of ignition delays of a range of hydrocarbons (C_4-C_8) over the accessible temperature range in the rapid compression machine have been made. Inherent in the ignition delay measurements was a study of the effect of molecular structure on the reactivity of the fuel. This subsequently led to an investigation of the relationship between the autoignition delay and the knock tendency of a fuel. It is commonly accepted that the occurrence of knock in spark-ignition engines is a consequence of autoignition in the end-gas. Therefore the aim was to determine the relationship between the ignition delay of a hydrocarbon in air as measured in the RCM and the research octane number (RON) as measured in a CFR engine under standard operating conditions. The behaviour of some of the single component hydrocarbons in the RCM has been well documented [88]. An additional aim of this study was to compare the ignition delays of hydrocarbons of known RON with those of the corresponding mixtures of the primary reference fuels (PRFs) in the RCM. A supplementary investigation of the influence of equivalence ratio ($\phi = 0.5$-2.0) on ignition delay was carried out for n-pentane in air. Also, a diesel injection pump and nozzle was used in the study of the autoignition of n-heptane following direct liquid spray injection into adiabatically compressed air.

Autoignition centres and knock features in the RCM (Chapter 5)

The aim of this study was to seek experimental evidence in support of the numerical prediction that spatial temperature inhomogeneities exist within the combustion chamber of the RCM during the post-compression period and that autoignition centres may originate in the cooler regions of the combustion chamber. Using schlieren imaging and an image intensified charge-coupled device (CCD) camera, planar 2-dimensional images of the evolution of autoignition in the rapid compression machine for different fuels under different conditions of compressed gas temperature have been obtained.

In addition to this, a spark-plug was incorporated into the side wall of the combustion chamber to allow knock-like characteristics to be reproduced and imaged in the RCM and to quantify the knock intensity using well-established mathematical methods. The intensity of knock at different compressed gas temperatures for a given fuel was studied.

Ignition of methane in the RCM (Chapter 8)

The aim was to determine the influence of higher alkanes and particulates on the ignition characteristics of methane-oxygen mixtures in the RCM. These results are presented after the main discussion chapter of the thesis (Chapter 6) because it was felt that the investigation of methane ignition in the RCM was a digression from the overall theme of Chapters 3-5. The results of the experimental study of the ignition of methane-oxygen mixtures in the RCM will be discussed in Section 8.4.

Chapter 2

The Rapid Compression Machine and its operation

2 THE RAPID COMPRESSION MACHINE AND ITS OPERATION

2.1 The general principles of adiabatic compression

Rapid compression is accompanied by heating, the extent of which depends on the ratio of specific heats, γ (C_p/C_v), of the test gas and on the volumetric compression ratio (CR). The fundamental objective of a Rapid Compression Machine (RCM) is to heat a test gas as rapidly as possible to a high temperature and pressure with negligible heat and mass loss. The apparatus can be used to simulate the compression stroke of a single engine cycle, allowing autoignition phenomena to be studied in a more ideal, constant and controllable environment than in a reciprocating engine. An ideal RCM isentropically compresses the reactants virtually instantaneously, such that no reaction or heat loss occurs during the compression stroke. Since only the test gas is heated and not the vessel walls (assuming complete adiabaticity) then wall reactions are avoided and essentially homogeneous reaction occurs. Even if some heat transfer to the walls occurs, the effect on the wall temperature is negligible because the thermal mass of the combustion chamber walls is considerably greater than that of the reacting gas.

Figure 2.1 is a schematic representation of a rapid compression experiment. The piston travels in one continuous stroke to constant volume with no reciprocation. Calculation of the final temperature employs an iterative calculation in which the compression is considered to occur incrementally, e.g., $p_1,V_1 \rightarrow p_2,V_2 \rightarrow p_3,V_3 \rightarrow p_4,V_4$ (Section 2.4 and Appendix A).

An ideal adiabatic compression from an initial volume, V_i, and pressure, p_i, to a constant final volume, V_f, and compressed gas pressure, p_f, occurs according to the relationship,

$$pV^{\gamma} = \text{constant}, \qquad (2.1)$$

where γ is the polytropic ratio, the ratio of specific heat capacities, C_p/C_v, and, for all except the monatomic gases, is temperature dependent.

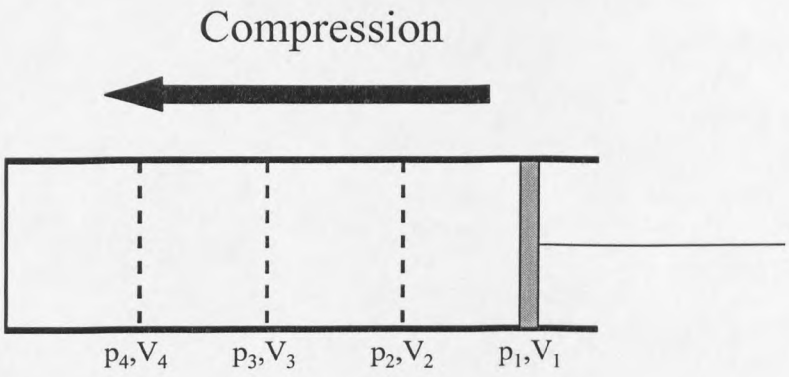

Figure 2.1 Schematic representation of rapid compression experiment.

For a multi-component mixture (i components) the molar heat capacity is a mole fraction (x_i) average of the pure components, i.e.

$$C_p = \Sigma\ x_i\ C_{pi} \tag{2.2}$$

$$C_v = \Sigma\ x_i\ C_{vi} \tag{2.3}$$

From Eq. 2.1, for an incremental change in conditions from p_1,V_1 to p_2, V_2 :-

$$p_1 V_1^{\gamma} = p_2 V_2^{\gamma} \tag{2.4}$$

rearranging this and since V_1/V_2 is the volumetric compression ratio (CR),

$$\frac{p_2}{p_1} = \left(\frac{V_1}{V_2}\right)^{\gamma} = CR^{\gamma} \tag{2.5}$$

Assuming ideal gas behaviour one can substitute for pressure to obtain an expression for the temperature, T_2, in terms of volume and γ,

for an ideal gas,

$$pV = nRT. \tag{2.6}$$

Assuming isentropic compression, pV = RT and R is the universal gas constant (8.314 J mol^{-1} K^{-1}) therefore,

$$\frac{T_2}{T_1}\frac{V_1}{V_2} = \left(\frac{V_1}{V_2}\right)^{\gamma} \tag{2.7}$$

which rearranges to

$$\frac{T_2}{T_1} = \left(\frac{V_1}{V_2}\right)^{\gamma-1} = CR^{\gamma-1}. \tag{2.8}$$

Substituting for volume in Eq. 2.5

$$\frac{p_2}{p_1} = \left(\frac{T_1}{T_2}\right)^{\gamma}\left(\frac{p_2}{p_1}\right)^{\gamma} \tag{2.9}$$

which rearranges to,

$$\frac{T_2}{T_1} = \left(\frac{p_2}{p_1}\right)^{\frac{\gamma-1}{\gamma}} \tag{2.10}$$

The calculated value, T_2, is then used in the next iteration of the calculation as the initial temperature for the step change 2 → 3 and a value of T_3 is calculated. This procedure is repeated until the final temperature at position 4 (end of compression stroke) is calculated. In the present work the calculation incurred 200 iterations. At each step the value of γ is readjusted for the new initial temperature conditions of the increment, thus accounting for the polynomial temperature dependence of heat capacity. With sufficient iterations this calculation is an excellent approximation of the analytical expression (Eq. 2.11) discussed below.

Assuming ideal gas behaviour and rapid isentropic compression of reactants, we can write an expression for the adiabatically compressed core gas temperature, T_{ad}'. Using the equation of state for an ideal, adiabatic, isentropic compression, the measured pressures at the start and end of compression, p_i and p_c, the heat capacities of the

mixture components, and taking into account the temperature dependence of γ, the relationship is,

$$\int_{T_i}^{T_{ad}'} \frac{\gamma}{\gamma - 1} d \ln T = \ln\left(\frac{p_c}{p_i}\right) \tag{2.11}$$

Where T_i is the temperature of the combustion chamber wall, measured by a chromel/alumel thermocouple situated in the wall of the combustion chamber.

Assuming a fixed volumetric compression ratio, CR, and initial temperature, T_i, the ideal adiabatic compressed gas temperature can be calculated using the relationship,

$$T_{ad} = T_i (CR)^{\gamma-1} \tag{2.12}$$

The effect of increasing the polytropic ratio (γ) on the adiabatic core gas temperature is much greater than the effect of increasing the compression ratio. A 10 % increase in CR from 10 to 11:1 results in only a 3 % increase in T_{ad}, whereas a 10 % increase in the polytropic ratio from 1.30 to 1.43 results in a 37 % increase in T_{ad}. The significance of the two expressions for compressed gas temperature, T_{ad}' or T_{ad}, (Eqs. 2.11 and 2.12 respectively) is discussed in Section 2.4.

2.2 Rapid Compression Machines

The method of adiabatic compression to study combustion processes, originally suggested by Nernst, was first put into practice by Falk in 1906 [109] during experiments to follow the spontaneous ignition of homogeneous combustible mixtures and to determine the practicability of the method of adiabatic compression in the quantitative determination of ignition temperatures. A similar method was also employed by Dixon et al. [110-111] in the study of the adiabatic compression and ignition of gaseous flammable mixtures. The application of RCMs in the experimental investigation of hydrocarbon combustion following adiabatic compression has progressed considerably since then and remains an extremely valuable technique.

In their most familiar role, RCMs comprise a mechanically driven piston which is used to compress a gaseous charge in a combustion chamber to a closed, constant volume. That is, there is no reciprocation as in a piston engine. The compression occurs sufficiently rapidly to induce heating of the gaseous charge, commonly in the range 500 - 1000 K according to the mechanical compression ratio and the ratio of heat capacities of the gaseous mixture. High pressures can be achieved (0.5 - 5 MPa) with a typical compression ratio of about 10:1. Such devices enable measurements to be made under conditions close to those of the end-gas in reciprocating engines, but without a number of the experimental complications that may arise in an engine as a result of the opening and closing of valves or the expansion caused by the piston during its down-stroke. The charge is fuel and air, the fuel being either premixed as a vapour in oxygen and other diluting gases, which is a further simplification, or injected as liquid droplets. Rapid compression machines have been used also for other types of kinetic studies [112] or to investigate the gas motion and turbulence that are set up by the piston motion [113], and to measure the heat transfer rates from moving gases in a combustion chamber [114].

RCMs are not without technical difficulty, nor are the data obtained easy to interpret quantitatively. Amongst the major technical problems associated with the operation of an RCM is the ability to attain a sufficiently fast compression, yet arrest the motion of the solid piston without vibration or bounce. The early developments and applications of rapid compression machines have been reviewed by Jost [115], Sokolik [116] and Martinengo [117]. The earliest recorded application of an RCM to spontaneous ignition studies appears to be that of Falk in 1906 [118], which was a gravity driven machine. Rapid compression machines have also been used for many years in the former Soviet Union [116,118].

The earliest Rapid Compression Machines comprised a vertical cylinder with a piston driven by the impact of a falling weight. The second generation of RCM made provision for the piston to be stopped and maintained in its final position. Since the late 1930s a third generation of RCMs has evolved, driven by compressed gas with the ability to achieve compression times of less than 20 ms and a capacity to operate at

higher compression ratios. A summary of the rapid compression machines presently in use around the world can be found in Table 2.1.

Table 2.1 A comparison of rapid compression machines currently in use and their characteristics.

RCM	General Description	CR	Piston Speed / m s^{-1}	p_i / atm	p_c / atm	Compression stroke / cm	Ref.
Shell	twin opposed piston	7-10 :1	38	0.3-3	6-60	19 (x 2)	119
Leeds	single horizontal piston	11:1	10	0.3	7-10	22	120
MIT	single adjustable, vertical piston	19:1 (max.)	5-10	~1	10-100	11	121
Lille	right-angled driver piston driven by cam	10:1	20-60	1.8	3-16	19.9	122
Tokyo	bursting of cellophane diaphragm to initiate compression	12.2:1	7	1	<50	7	123
Toyota	electrically-driven compression and expansion	11.0:1	5	1	>20	7.5	124

No single design or mode of operation has dominated the field. A compressed air-driven piston is generally favoured to achieve high piston speeds, ranging from about 5 to 15 m s^{-1}. Park and Keck [121] have shown that piston speeds of about 10 m s^{-1} are optimal for near adiabatic compression without inducing vigorous gas motion, and the creation of a roll-up vortex in the corner between the moving piston crown and cylinder wall. Flow visualisation techniques were used to observe the vortex motion at the

interface of the piston face and cylinder wall and both the vortex size and stability have been determined [113]. The experiments illustrate the formation of a toroidal vortex at the intersection of the piston face and the cylinder wall as the wall moves towards the piston and a transition from stable to unstable or turbulent flow as the piston velocity increases. A similar corner vortex formation has been found in spark-ignition engines [125]. CFD computation coupled to the simulation of autoignition in an RCM has verified the formation of a flow vortex and the resulting non-uniformity of temperature and species concentration in the combustion chamber [126]. This exemplifies one of the disadvantages of RCM studies, i.e. the difficulty in the characterisation of the reacting mixtures and, ultimately, difficulties in the results of ignition delay measurements obtained from different RCMs under the same nominal conditions. An ideal RCM would create a fully mixed reactant core, either by vigorous turbulent mixing or by the suppression of the generation of the boundary layer. An alternative is to suppress the vortex formation whilst keeping the laminar reacting core gases intact. This has been achieved in a recent modification to the RCM at MIT [127], involving the design of a piston crevice which "swallows" the thermal boundary layer along the wall, resulting in improved definition of the core conditions.

A hydraulic control for both compression and expansion of the charge, at piston speeds below 5 m s^{-1}, has been adopted by workers at the Toyota Research Laboratories [124]. At Shell Research Centre, Affleck and Thomas [119] adopted the innovative, double opposed piston action in order to minimise the piston stroke while maintaining a high compression ratio. Additional advantages of this design were believed to be the creation of a plane of aerodynamic symmetry of the compressed charge and reduced gas motion in the centre of the chamber. However there is restricted optical access in a machine of this design. This apparatus has been applied to the extensive study of alkane combustion by Fish and co-workers [41,94,119,128-132] throughout the late 1960s and into the 1970s and now resides with the Simmie research group in Galway, Ireland. The design and construction of the RCM at Leeds University, used by Griffiths and co-workers [133], evolved from that of the Shell rapid compression machine but incorporating one single horizontal compressing piston.

Most modern RCMs operate with the compressing piston directly in line with the driving piston. There are two pistons in the RCM at Lille which are connected by a cam [122, 134-136]. The driving piston is perpendicular to the driven piston in the combustion chamber. Compression within the combustion chamber results from motion of the driving piston away from the axis of the connection. The speed of the driving piston and the profile of the connecting cam control the rate of compression. The cam profile also ensures the anchoring of the compression piston at the end of its travel. There is scope to control the "profile" of the piston motion with this design, and also measurement of the piston speed is very easy. However, the piston speeds that can be attained during compression are limited by the mechanical stresses imposed.

Amongst the main parameters of interest in rapid compression studies are the temperature and pressure that are reached at the end of compression. Pressure measurements are made by fast response pressure transducers (>10 kHz), and ignition delay times are measured from the pressure-time profiles. The measurements of pressure may be supplemented by the detection of light output through windows, and by chemical analysis at intermediate stages of reaction by rapid expansion and quenching methods [130,133-135].

Although piston motion may be rapid, a “perfect” adiabatic compression is not always possible since heat losses are inevitable in some RCMs. Heat losses to the chamber wall and boundary layer development as a result of the gas motion generated by the piston are the main causes of departures from ideality. Nevertheless, gas at the core of the compressed charge may be regarded to have experienced an adiabatic compression, assuming heat losses are confined to the boundary layer.

Since the state of the gas at the end of compression is a function of the RCM and its operating conditions, the quantitative characteristics of ignition, such as the duration of the ignition delay under given conditions, are specific to a particular machine. The qualitative structure, such as the occurrence of two-stage ignition and the existence of a region of negative temperature dependence of ignition delay, are common features of corresponding experiments performed in different machines.

2.3 The Leeds Rapid Compression Machine

The Leeds RCM, illustrated photographically in Figure 2.2, is a single horizontal piston machine, driven by compressed air. It is approximately 1.5 m long and a similar height. The machine consists of 4 main parts: the combustion chamber (A) (electrically heated stainless steel cylinder and block); the hydraulic chamber (B); the driver and compressing piston assembly (C); and the compressed air driver tank (D). The combustion chamber corresponds to the stainless steel cylinder with a volume of 339 cm^3. After the compression stroke the combustion chamber volume is 29 cm^3 (bore diameter 45 mm; chamber depth 18 mm). The piston is also made of stainless steel and fitted with Teflon seals to avoid surface scratching. Piston motion is controlled by the displacement of hydraulic fluid and is held in the firing position against a driver gas pressure (~1.0 MPa) by hydraulic fluid at high pressure (~2.0 MPa).

One advantage of the RCM lies in its adaptability for use in different types of investigations. For example chemical analysis by the quenching method, schlieren imaging experiments, spark-ignition and fuel injection. Specific details of these experimental systems and the necessary modifications to the RCM and the electronic control will be provided in the relevant chapters.

2.3.1 Design

The Leeds RCM was constructed on the same design principles as the double opposed piston RCM at Shell Research Centre, but utilising only one compressing piston. Figure 2.3 is a schematic diagram of the Leeds RCM illustrating the main features of the design.

The pressure and temperature do not vary linearly with increasing compression ratio because it is an adiabatic compression not an isothermal compression. Therefore wall condensation could occur for certain low vapour pressure hydrocarbons if the walls were not preheated, i.e. increasing the pressure, but not a sufficiently high temperature to avoid condensation of fuel vapour on cylinder walls. This is a limitation set by the

critical temperature and pressure conditions of the gaseous charge and represents one of the reasons for preheating the cylinder and chamber walls. In addition to this, increasing T_i increases the final compressed gas temperature T_{ad}.

The initial criterion in designing a Rapid Compression apparatus is the strength and durability of the combustion chamber, it must be capable of withstanding intense pressure in the region of 5.0 MPa during ignition. Also, the shape and diameter of the combustion chamber are important, if heat losses to the vessel walls are to be minimal then the surface area/volume ratio should be as small as possible.

The piston motion from rest, through acceleration to the maximum speed and finally coming to rest at top dead centre, is also an important consideration. During the last stages of compression the test gas mixture is already at sufficiently high temperature for the overall reaction rate to begin increasing, therefore this stage must be passed through as rapidly as possible. Equally important is the deceleration of the piston from its maximum velocity to zero within the shortest distance possible. The kinetic energy of the compressing piston must be removed irreversibly if the piston is not to rebound. The transfer of momentum to a heavy mass results in rapid piston stopping. This incurs the destruction or transfer of the kinetic energy of the piston. In the Leeds RCM the piston motion is controlled by hydraulic fluid pressure. The piston is stopped in the last 0.5 cm of the compression stroke by fluid damping and then comes to rest against a clash ring. Assuming pressures in excess of ~3.0 MPa are not achieved during the subsequent events then the piston is held in position by the driving pressure (~1.0 MPa) behind it.

In common with the Shell twin opposed piston RCM, the piston is driven by compressed gas pressure which is applied to the driver piston on the side most remote to the test gas. The trailing piston which passes through the driver gas chamber controls the piston motion. This control of piston motion involves the start of piston motion, the control of speed throughout the compression stroke and stopping the piston at the end of compression. These functions are largely performed by the hydraulic fluid system.

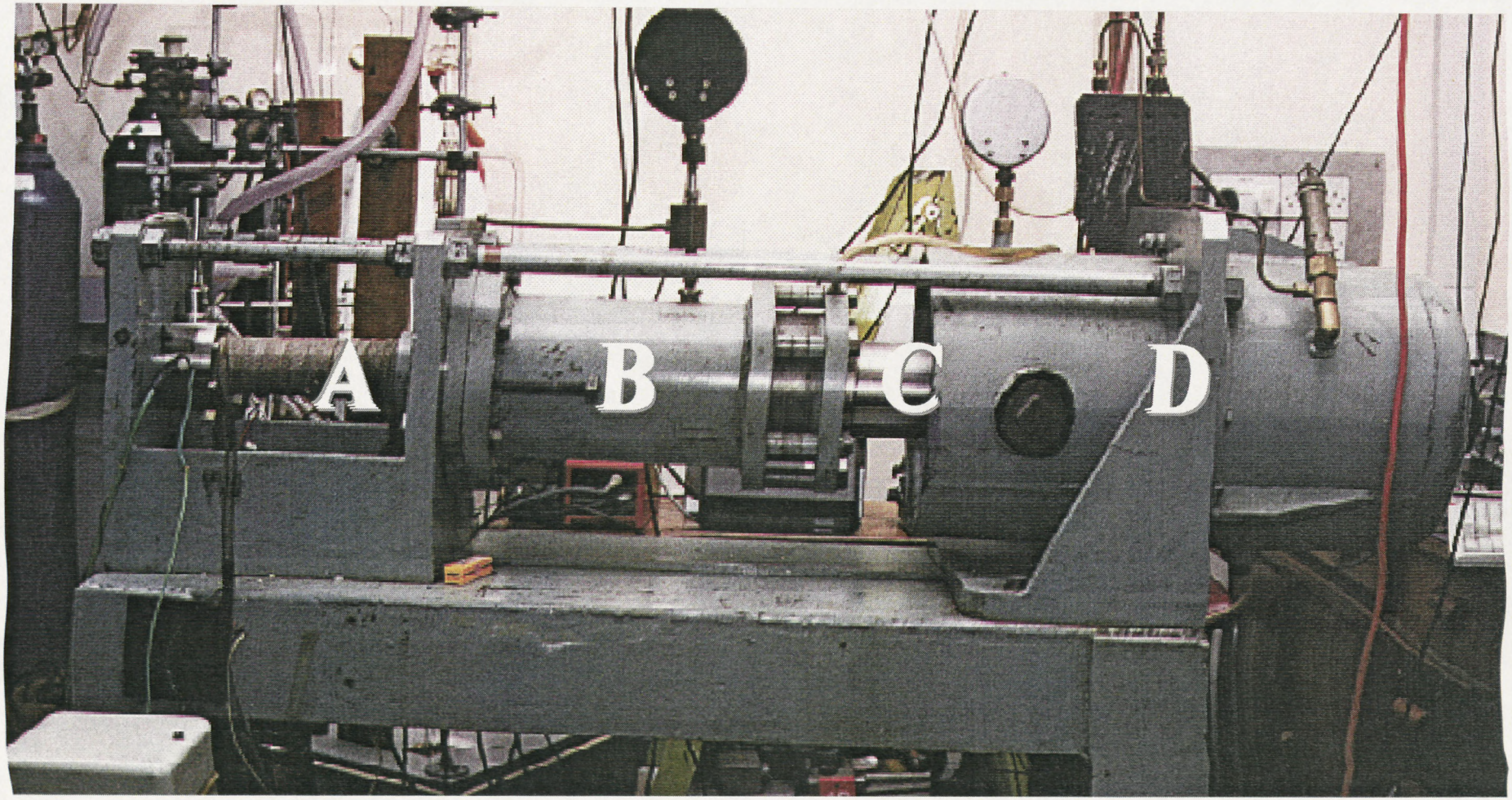

Figure 2.2 Photograph of the Leeds RCM. Main features of apparatus are marked with letters A - D. A- combustion chamber; B - hydraulic chamber; C - driver and compressing piston assembly; and D - compressed air driver tank;. (1 cm ≈ 0.1 m).

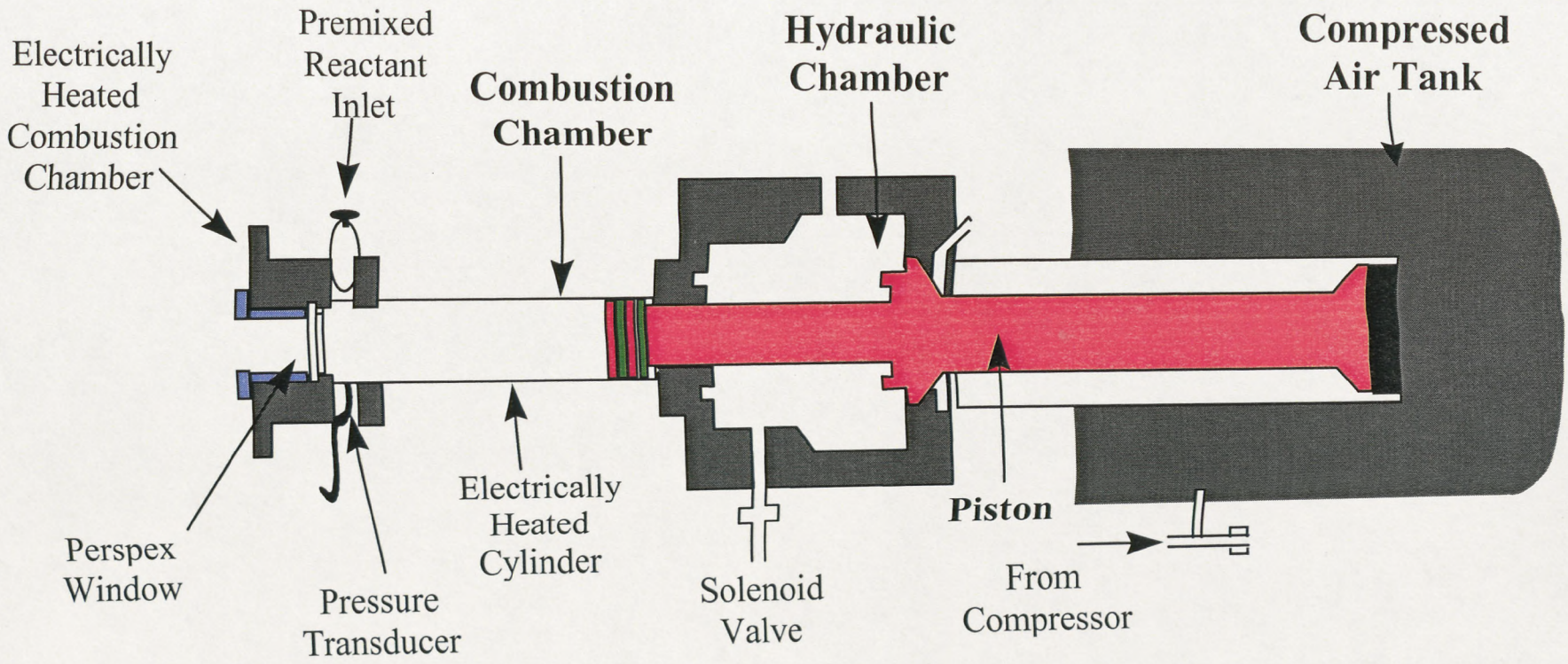

Figure 2.3 Schematic diagram of the Leeds Rapid Compression Machine

The piston is held in the firing position by a retaining force (hydraulic pressure) which opposes the driving pressure force. The pressurised liquid exerts a force in all directions forcing the piston assembly against the hydraulic lock seal. Release of this hydraulic pressure by venting a small volume of liquid results in the full driving force becoming immediately available. Air is forced out of the void volume when the hydraulic lock seal is broken. With the driving piston no longer in balance, the piston assembly accelerates. The subsequent control of piston speed throughout the compression stroke is also controlled by the displacement of hydraulic fluid. The driving force behind the piston must be sufficient at the end of the stroke to contain the pressure developed in the reaction chamber without any rebound of the piston.

The design of the piston stopping method incurs a compromise of performance and durability with ease of use. The most rapid method is by momentum transfer as used by Jost [115], attaining a deceleration of 2×10^6 m s^{-2} (0.1 mm in 10 μs) for an approach velocity of 20 m s^{-1}. The Leeds RCM uses a similar method of stopping piston motion as that employed by Affleck and Thomas [119], where the pressure generated in the hydraulic fluid acts as a transfer of kinetic energy. The small volume of fluid trapped by the slotting of the stop ring in the stop groove becomes compressed. The precise clearance measurement results in the progressive venting of the fluid at a rate which gives uniform deceleration within the last 0.5 cm of the compression stroke. In the final stages, the deceleration force and the piston velocity tend to zero and the final arrest of the piston occurs without any piston bounce (or rebound).

2.3.2 Operation

Hydrocarbon gases or vapours (analytical or research grade) were mixed with "air" comprising 21 % oxygen and a 79 % composite of inert components (nitrogen, argon, carbon dioxide). The proportions of the inert gases were varied to alter the overall heat capacity of each mixture and hence the ratio C_p/C_v (γ). A range of compressed gas temperatures (650 - 1000 K) could be achieved with a fixed compression ratio of the machine (CR = 11.00(± 0.15) :1). This small variation in CR results from variations in the final position of the piston as the operating conditions are changed. The adiabatic

pressure increase is 57 times the initial pressure for a monatomic gas and 30 times for a diatomic gas. Correspondingly, the maximum possible temperatures are 1485 K and 789 K respectively, if the gas is compressed from room temperature.

The premixed fuel-air mixtures were transferred at an initial pressure of 0.033 MPa from a storage reservoir to the evacuated (≤ 1 mmHg) combustion chamber. The wall temperature was controlled by an electrical heater within the range 320-350 (±1) K. The piston was held in the firing position by a hydraulic pressure of 2.0 MPa, the compressed air tank was charged to a pressure of 1.0 MPa and the reactants admitted to the evacuated combustion chamber. With the combustion chamber inlet valve closed the computer was used to trigger the opening of a solenoid valve which released the hydraulic retaining pressure. The piston travels forward at an average speed of 10.6 m s^{-1} (Appendix B) under the influence of the compressed air driving force. The compression stroke duration is 22 (±1) ms (Appendix C). The speed of the piston is controlled by the displacement of hydraulic oil and the piston decelerates rapidly in the last 0.5 cm of the compression stroke and is stopped by a clash ring at the end of the compression. The piston is then maintained in that position by the pressure of compressed air behind it.

Once the solenoid has been triggered by the computer to open the valve the data capture begins after a short initial delay (~100 ms). This is to ensure that the required data is captured within the limited time "window" (200 ms) for data capture. A pressure record and a light output record is obtained in the majority of experiments, as illustrated for the two-stage autoignition of n-pentane in Figure 2.4. The computer captures one data point every 0.2 ms (sampling frequency, 5 kHz) for a 200 ms duration.

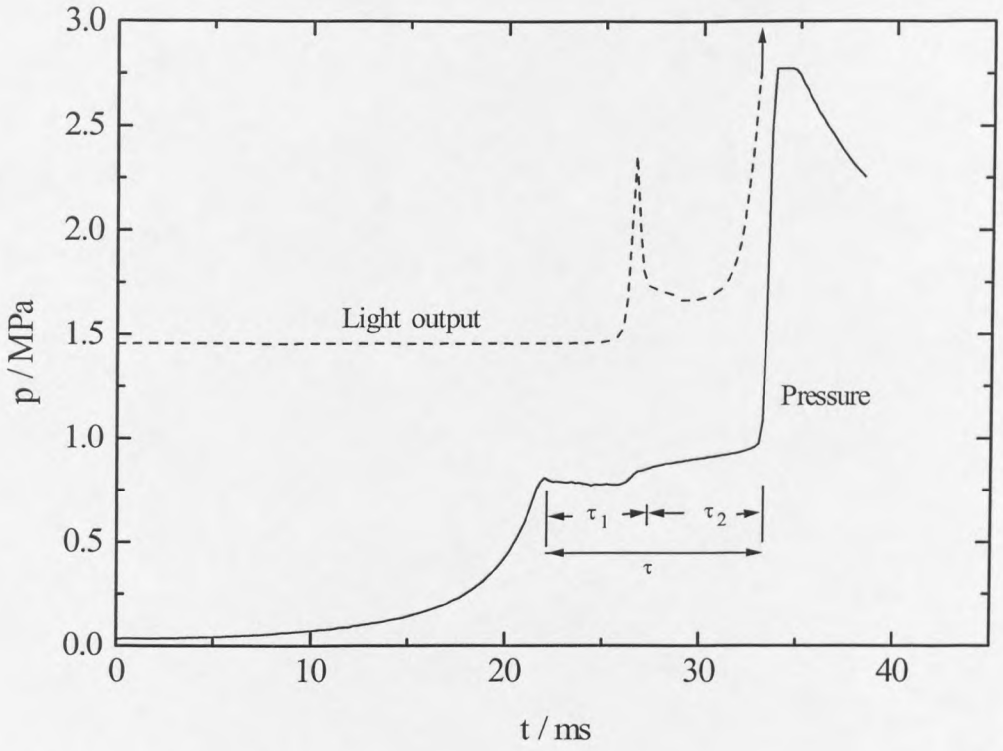

Figure 2.4 The two-stage autoignition of n-pentane-air following rapid compression to 744 K. Pressure (—) and light output (...) records.

Pressure changes within the combustion chamber are measured using a pressure transducer (Kistler 601A, natural frequency 130 kHz, sensitivity 15.8 pCb/atm, maximum pressure 750 atm) situated in the side wall of the chamber. The charge generated in the transducer as a result of the applied pressure is converted to a low impedance voltage signal by a Kistler Charge Amplifier. Total light emission intensity is measured using a photomultiplier tube (THORN EMI 9924B) positioned at the transparent, Perspex end-window. Each analogue signal is relayed, via one of six channels of an A/D converter, to the computer data capture program and can be displayed as temporal pressure and light output profiles.

The compressed gas pressure and the time at which it is achieved are derived from the pressure record by using a cursor to move along the computer-plotted pressure-time curve to locate the end of compression. Ignition is characterised by the maximum rate

of pressure increase and an intense light output and the ignition delay is defined as the time difference between the end of compression and the maximum rate of pressure rise during ignition. These and the common features of a two-stage ignition are illustrated for n-pentane in Figure 2.4 above. It is also possible to define the ignition delay as the time from the end of compression to the maximum light output during autoignition, this was not considered as definitive as the pressure method because the sensitivity of the PMT was such that it was readily saturated during autoignition.

2.3.3 Limitations and non-idealities

The initial pressure, and consequently the final pressure following compression, are limited by the pressure of the driver gas, which in turn is limited by the maximum stress due to high pressure which the pipes, valves and compressed air chamber can endure. In the majority of the experiments performed in this study the operating initial pressure was 0.033 MPa, approximately a third of the initial pressure normally encountered in spark-ignition engines. Towards the end of this project a modification to the RCM was commissioned, which will allow higher driver pressures and hence higher initial pressures (0.1-0.2 MPa) in the combustion chamber . Design changes incurred during this modification include replacement of all brass valves and fittings with stainless steel, a new compressed air tank which can safely withstand pressures of approximately 2.8 MPa and also a direct high pressure inlet system, i.e. direct inlet from nitrogen cylinder to driver gas chamber. A high pressure inlet of reactants is also required, this could be achieved using a high pressure reservoir tank for the mixing of reactants as opposed to the Pyrex vacuum system used for sub-atmospheric initial pressures.

The temperature of the combustion chamber (T_i) is limited to approximately 343 K, this is a consequence of the reduced durability of the Teflon piston seals and other seals at high temperatures. Thus, there is a limit to the extent of control on compressed gas temperatures which can be achieved by varying the initial temperature.

Compression at the piston speeds used in the Leeds machine has been shown previously to be virtually adiabatic [88]. Therefore, assumptions of adiabaticity of the system and

spatial uniformity of temperature and concentration (in the numerical modelling) during the compression stroke are very satisfactory. However, spatial temperature variations develop within the combustion chamber during the post-compression period as a result of heat transfer to the combustion chamber walls. The heat loss rates are highest just after compression ceases because the residual gas motion is greatest at this stage [121]. Thereafter the rate of heat loss decreases as the gas motion decays.

The gas motion ahead of the piston forms a roll-up vortex [113] and heat losses to the walls are particularly significant in the first few milliseconds after the end of compression. Following the first 9 milliseconds of the post-compression period, the vigorous gas motion decays and the pressure-time profile follows a Newtonian cooling curve. The effects of a net heat release and a net heat loss on the pressure profile are illustrated in Figure 2.5. This allows a comparison of the behaviour of a reactive fuel-air mixture (n-pentane-air) following rapid compression, with that of an unreactive gaseous charge (N_2) under similar conditions of temperature and pressure.

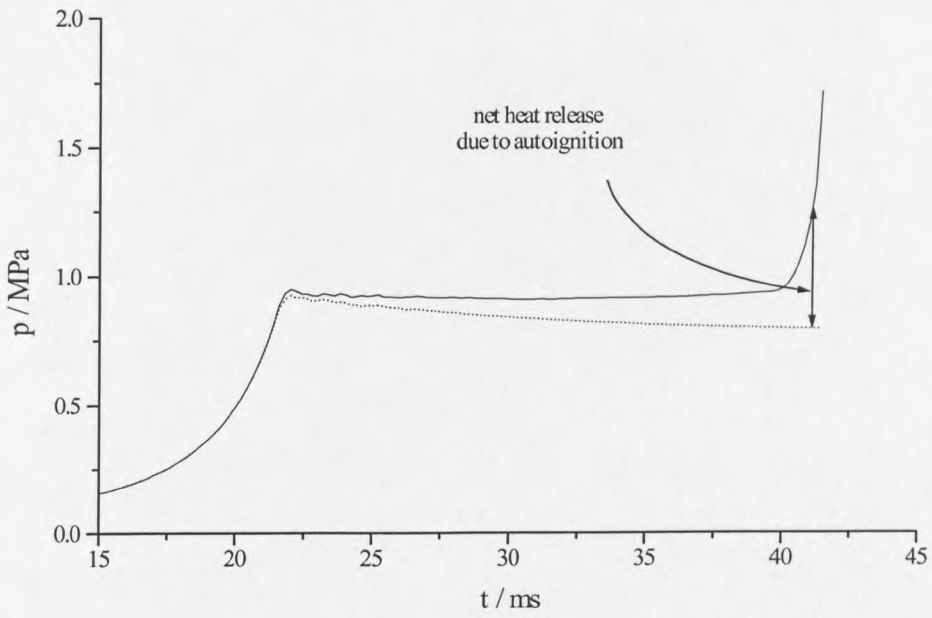

Figure 2.5 Pressure time profiles for autoignition of n-pentane-air (—) and for an inert gas (N_2) (...) following compression to ~ 850 K.

The piston begins moving at t = 0, the speed of travel is relatively slow at first but, as the momentum increases, the compression speed increases, achieving a maximum at approximately 20 ms after the start. The piston reaches the end of the compression stroke at 22 ms and remains in position. Thereafter, the events evolve in a closed constant volume at high temperature and pressure. Therefore, any increase or decrease in pressure is a result of either, a net heat release or, a net heat loss respectively. The reaction stoichiometry can also affect the pressure in the chamber during the post-compression period but this has negligible influence during these experiments due to the dilution with inert gases. For the example shown in Fig. 2.5, both gaseous charges achieve a comparable pressure and temperature at the end of compression, the distinctions are as follows:

- unreactive:

  Just after the end of compression the pressure begins to fall due to heat losses to the chamber walls.

- reactive:

  The pressure fall just after compression is also a consequence of heat losses to the chamber walls, however, the pressure profile always lies above the unreactive profile implying a net heat release. Any departure from the unreactive experimental result is a result of a net heat release due to exothermic chemical reaction as indicated on the diagram for the onset of autoignition.

The post-compression cooling of the gases in the combustion chamber results in a cooler boundary layer adjacent to the chamber wall, piston crown and the internal surface of the Perspex window. The existence of this cooler boundary layer implies that there is not a uniform temperature throughout the chamber and therefore the rate of reaction may vary in different regions according to the Arrhenius parameters (Chapter 5). For example, a compression to 850 K, following heat losses from the compressed gases to the chamber walls, may force the overall reaction rate within that vicinity into the temperature region of the ntc and cool flame activity.

There is a slight recoil of the machine when the piston is fired due to the rapid momentum transfer, this was exemplified in the schlieren images (Fig. 2.6 and Section 5.3). Frames 2, 3, 6 and 7 illustrate a partial loss of image due to a movement of the machine and a slight loss of alignment of the optical axis in the experimental set-up.

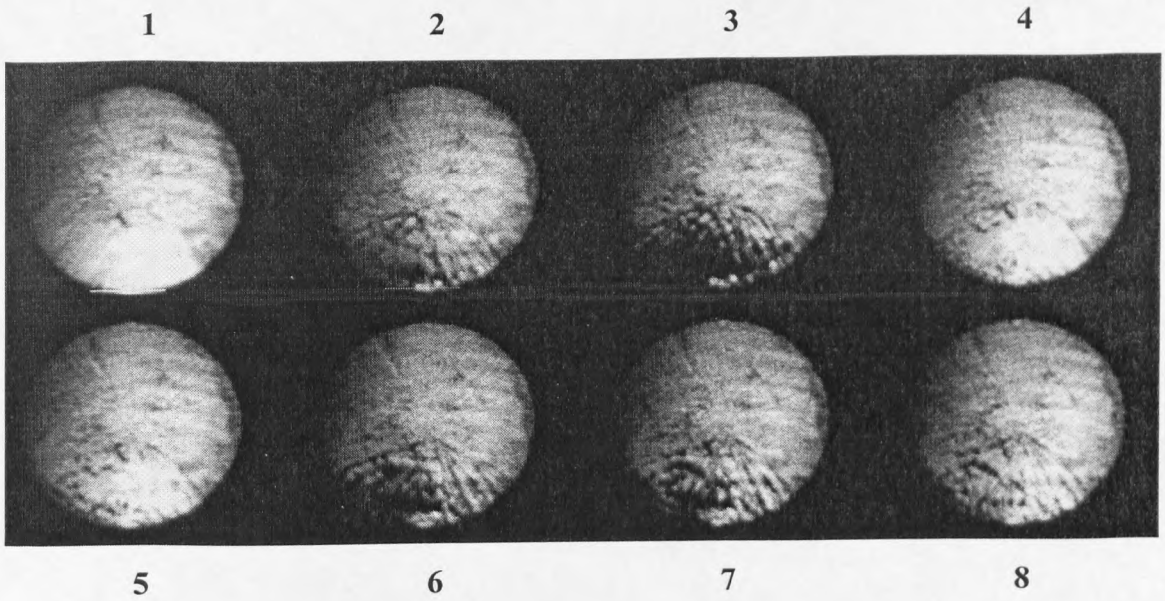

Figure 2.6 Schlieren image sequence illustrating loss of image due to movement of RCM on firing. Successive images obtained at 0.2 ms intervals (frames read left to right downward, framing rate 5000 fps). Frame 1 corresponds to the end of compression.

In a given set of experiments to measure ignition delays, at increasing compressed gas temperature, the CR decreased. This is an effect of the piston not quite reaching the end of the compression stroke because of the higher pressure achieved inside the chamber towards the end of compression.

2.4 Assessment of compressed gas temperature

In most, but not all, circumstances the core gas temperature, T_{ad}', is the natural reference temperature for the compressed gas because in most circumstances the highest

temperature at the end of compression is responsible for the development of spontaneous ignition in the shortest time [113,121]. When the compression heats the reactants to temperatures that correspond to the region of ntc for that particular mixture, combustion may be initiated in the cooler boundary layer region. That is, gases which, at the end of compression, are colder than those in the adiabatic core control the duration of the ignition delay. This was demonstrated by Schreiber et al. [89, 137-139] by the simulation of alkane combustion, using various reduced kinetic schemes, in computational fluid dynamic calculations.

The core gas temperature is derived from the measured pressure ratio as described in Section 2.1., The expression for an isentropic compression over the range $T_i \rightarrow T_{ad}$' and $p_i \rightarrow p_c$, which takes into account the temperature dependence of the heat capacities, is

$$\int_{T_i}^{T_{ad}'} \frac{\gamma}{\gamma - 1} \, d \ln T = \int_{p_i}^{p_c} d \ln p \qquad (2.13)$$

where γ is the ratio of the heat capacities (C_p/C_v) of the reactant mixture.

If heat losses during compression are only slight then the bulk of the compressed gas will be at the core gas temperature. However, if heat losses during compression are very significant, e.g. for a slow compression, then a rather smaller fraction of the compressed charge will be at the core temperature. The extent to which heat losses during compression cause departures from the adiabatic ideal, may be assessed from a comparison of T_{ad}' (2.13) with the temperature (T_{ad}) which is predicted on an ideal volumetric basis (2.14) from a knowledge of the dimensions of the RCM [88]. That is

$$\int_{T_i}^{T_{ad}} \frac{1}{(\gamma - 1)} \, d \ln T = \int_{V_i}^{V_c} d \ln V \qquad (2.14)$$

where V_i and V_c are the initial and final volumes of the combustion chamber respectively and from which $CR = V_i/V_c$.

In addition to the non-ideality presented by heat losses, the compressed gas temperature calculated by (2.13) does not represent an appropriate reference temperature when the fuel-air mixture is so reactive that exothermic oxidation begins during the compression stroke. The pressure reached at the end of compression does not then arise solely form p-V work, and application of a thermodynamic relationship (2.13) based on the measured pressure is not valid. The ideal gas equation may be applied to the system in these circumstances, the compressibility factor of the gas being assumed to be unity, this gives only a spatially averaged compressed gas temperature, T_c, where

$$\frac{T_c}{T_i} = \frac{p_c V_c}{p_i V_i} \tag{2.15}$$

or,

$$T_c = T_i \frac{p_c}{p_i (CR)} \tag{2.16}$$

This parameter representing the temperature at the end of compression is the average compression temperature T_c, derived from the ideal gas law applied to initial and final compression conditions. This is the only relationship of the three mentioned that is applicable to reactive and unreactive compression stroke conditions.

If there is little or no change in the number of moles of material as a result of reaction an average gas temperature may also be interpreted during the post-compression period from the instantaneous pressure by use of Eq. (2.15). Experiments are normally performed under relatively dilute conditions (~80 % inert gas) and, in general, the number of moles of product and reactant are approximately equal during the "slow oxidation" of hydrocarbons. Equation (2.13) is the most satisfactory reference temperature for the compressed gas but it is not valid in all circumstances. The application of equations (2.13)-(2.15) has been tested by Griffiths et al. [88].

In summary, the ideal adiabatic compression temperature is given by the equation,

$$T_{ad} = T_i (CR)^{\gamma-1} \tag{2.12}$$

where CR is the mechanical compression ratio (V_i/V_c) and γ is the ratio of heat capacities of the reactant mixture (C_p/C_v). For all, except the monatomic gases, C_p varies with temperature, thus, the heat capacities are expressed as temperature dependent polynomials ($C_p = a + bT + cT^2.....$).

Since departures from ideality may occur during the compression as a result of heat losses and boundary layer effects, a more accurate reference for the adiabatic temperature, T_{ad}', is regarded as that associated with the core gas within the combustion chamber. This adiabatic core gas temperature, T_{ad}' is derived from the measured pressures at the start and end of compression, p_i and p_c, such that

$$T_{ad}' = T_i \, (p_c/p_i)^{\gamma-1/\gamma} \tag{2.17}$$

The extent to which the experimentally measured p_c/p_i differs from the compression ratio (V_i/V_c) raised to the power (γ-1) is a quantitative measure of the extent of departure from ideal adiabatic compression.

In practice, taking into account the temperature dependence of γ, the temperatures T_{ad} and T_{ad}' are derived by an iterative calculation, which give a good approximation to the equations,

$$\int_{T_i}^{T_{ad}} \frac{1}{(\gamma - 1)} \, d \ln T = \ln\left(\frac{V_i}{V_c}\right) \tag{2.18}$$

$$\int_{T_i}^{T_{ad}'} \frac{\gamma}{\gamma - 1} \, d \ln T = \ln\left(\frac{p_c}{p_i}\right) \tag{2.19}$$

The compression is considered to occur incrementally and the value of γ taken to be that at the average temperature at each increment, as described in Appendix A.

A FORTRAN program (Predict 3, Appendix A(i)) has been compiled which allows the prediction of the end of compression temperatures and a final value of γ for a given

mixture at known initial temperature and pressure, given a value for the compression ratio, i.e. Equation (2.18).

Predict 4 (Appendix A(ii)) is a similar FORTRAN program which also uses best fit C_p data to calculate the end of compression temperatures from the measured compressed gas pressure and calculates γ by an iterative procedure with respect to the compression stroke, i.e. takes into account the change in p/T at intervals throughout the stroke of the piston (200 iterations), i.e. Eq. 2.19.

The average temperature within the combustion chamber at any time during the post-compression period, $T_{(t)}$, where the system is at constant volume, can be deduced from the conditions of temperature and pressure at the end of compression. Assuming negligible change in number of moles of reactants and using the ideal gas relationship, the equation is

$$T_{(t)} = T_c \, (p_c/p_{(t)}) \qquad (2.20)$$

The temperature at any time throughout the compression stroke can be calculated using Eq. 2.19, assuming ideal, adiabatic, isentropic compression.

Chapter 3

Reactivity in compression and the role of additives

3 REACTIVITY IN COMPRESSION AND THE ROLE OF ADDITIVES

3.1 Introduction

This chapter describes direct experimental measurements of the extents of fuel consumption during single and two-stage ignition of hydrocarbons in the RCM (3.2). An investigation into the effect of diethylamine on ignition delay is also presented in this chapter (Section 3.3). This study of the effect of additives on ignition delay is included here because the interpretation of the results relates to the measured extents of fuel consumption during the first stage of two-stage ignition.

A description of the experimental sampling device and analytical techniques employed is given in Section 3.2.1. In Section 3.2.2 the experimental results are presented and finally, in Section 3.2.3, the significance of the results obtained and the conclusions reached will be discussed. These experimental measurements have been used to validate a recently modified comprehensive chemical kinetic model of hydrocarbon oxidation [140], this will be described in more detail in Chapter 6.

The experimental results described in Section 3.2.2 illustrate the reactivity of hydrocarbons during the compression stroke of the Leeds RCM. Normal-heptane exhibits significant reactivity during compression to high temperatures, whereas n-pentane undergoes negligible reaction during compression. This "pre-reaction" can have a significant effect on the duration of the ignition delay as demonstrated by numerical methods [141]. The experimental investigation into the effect of diethylamine on the extent of reaction that can occur during compression and on the overall ignition delay will be described in Section 3.3.

3.2 Reactivity during compression

For the temperatures which are achieved during compression in RCMs (and engines), autoignition often occurs in two stages. This will be described in Chapter 4. At sufficiently high temperatures, the ignition occurs in a single stage governed by the high temperature branching mechanism. However, for some highly reactive fuels, the two-stage characteristic may persist in the higher temperature regime because the first stage chemistry is fast enough to occur in the final stages of compression when the piston is slowing down. The purpose of the work described in this chapter is to show, by direct experimental measurement, the extent to which this occurs and how it is governed by the reactivity of the fuel and the pressure and temperature to which the reactant mixture is compressed.

Previous studies in the Leeds RCM [88] have shown from pressure-time records that during the combustion of n-heptane and n-hexane following compression to temperatures above 750 K, sufficiently rapid exothermic reaction can occur during the final stages of piston motion such that the gas temperature is enhanced beyond that which would normally be achieved as a result of adiabatic compression alone. This arises when the first (or cool flame) stage of two-stage ignition coincides with the end of the compression stroke. These earlier studies also indicate that negligible oxidation occurs during the compression when a less reactive fuel such as n-butane is used.

In addition to the quantitative measurements of extent of fuel consumption during the development of spontaneous ignition, with particular emphasis on reactivity during the compression, the presence of molecular intermediates in the combustion system has also been measured qualitatively.

3.2.1 Experimental

The principles of rapid compression and the experimental method have been described in detail in Chapter 2. For the measurement of fuel consumption, experiments were performed within two compressed gas temperature ranges, 720-750 K and 845-875 K.

Premixed gaseous fuel-air mixtures prepared in stoichiometric proportion ($\phi = 1.0$) were stored in a Pyrex glass vacuum line, transferred at an initial pressure of 0.033 MPa to the combustion chamber and then compressed into a cylindrical combustion chamber by a pneumatically driven piston. The compression stroke duration is 22 ms. The compressed gas density was 131 mol m^{-3} in all experiments.

Pressure-time data during the compression and throughout the post-compression period were measured by a pressure transducer and recorded digitally on a pc at a sampling rate of 200 μs per point via an A/D converter, for a total duration of 200 ms. In selected experiments chemiluminescent emission accompanying reaction was measured by a photomultiplier, however these measurements were not possible during the experiments to measure extents of fuel consumption due to the replacement of the end-window with the rapid sampling device.

Rapid Sampling Device

The technique of adiabatic expansion was used to quench the reaction and enable measurements of the reactant concentration at intermediate stages. The reaction was quenched by the bursting of a diaphragm (99 % purity Aluminium, 0.1 mm thickness) in the end wall of the combustion chamber, which formed the cylinder head. This was followed by the rapid expansion (and therefore cooling) of the reactant mixture into a hemispherical expansion chamber (1.5 dm^3) (Figure 3.1). The time at which the diaphragm was burst was controlled by a time-delayed signal generated at a threshold pressure during the compression stroke. This signal was used to actuate an electromagnetically-driven needle. The electromechanical delay incurred in the movement of the bursting needle was approximately 9 ms [133]. The quenched reaction mixture in the expansion chamber represented the reactant composition in the combustion chamber at the time of burst of the diaphragm. The technique for rapid quenching of reaction in an RCM followed by chemical analysis was pioneered by Martinengo et al. [142] in their determination of the time dependence of reactant, intermediate and product concentrations during the autoignition of hydrocarbons.

Increasing the pressure differential across the diaphragm increases the strength of the rarefaction wave and provides a greater rate of cooling during the expansion. The time for expansion into the expansion chamber was less than 0.5 ms for a 50 % decrease in pressure, thus a sufficiently high rate of cooling and adiabatic expansion was achieved. However, the higher pressure differential across the diaphragm also increases the shock strength and the reflected shock wave can induce further reaction in the previously quenched gaseous reaction mixture. The rapid sampling device used in these experiments is a comparable design to that originally employed by Roblee [143]. The design features of the hemispherical expansion chamber are such as to obtain high cooling rates and avoid shock heating by reflected shock waves. The large surface area concave end of the expansion chamber diverges and therefore weakens the reflected shock. In addition to this, the narrow tube at a 45° angle to the axis of the combustion chamber, discourages ideal shock propagation. The overall performance of the rapid sampling device used in the present study was examined exclusively by Beeley [133] during studies of the decomposition of alkylnitrates in the RCM.

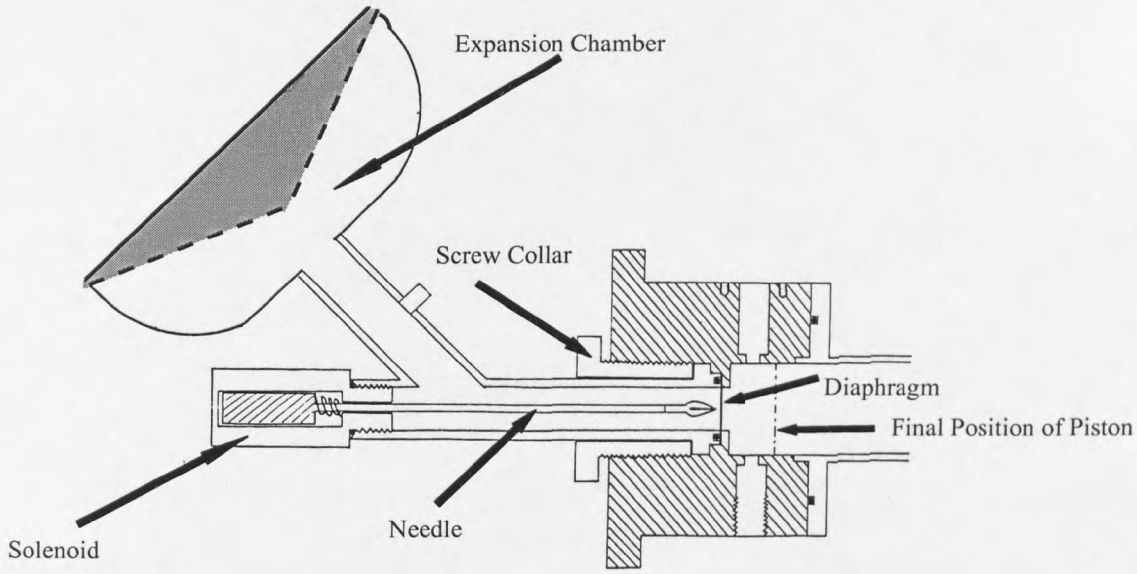

Figure 3.1 Schematic diagram of the Rapid Sampling Device.

With the diaphragm in place, in these experiments, the calculated compression ratios were less than those normally achieved under similar conditions without an Al diaphragm in place. This was due to a slight bowing out of the Aluminium diaphragm during the compression, providing a slightly larger volume at the end of compression than in normal operation, therefore resulting in a lower CR. Since the compressed gas temperature is calculated from measured values of p_c, p_i and γ, the slight inconsistency in volumetric compression ratio does not have a significant consequence on the results.

The condensable quenched reaction mixture was evacuated through a liquid nitrogen cooled U-tube coupled to the vacuum line. In order to obtain a time dependent profile of the reactant concentration, experiments were performed under similar compression conditions but the reaction was quenched at different times throughout the post-compression period. The results for each set of experimental conditions were obtained from a number of separate gaseous reactant mixtures prepared to the same composition. In order to standardise the extents of reaction in a series of experiments the sealed cold trap was allowed to warm to room temperature and a standard volume of n-butane injected into the trap via a septum cap. The results of successive experiments were normalised to a given n-butane peak area in the chromatogram.

Chemical Analysis

After complete mixing, a sample (1 ml or 0.1 ml, GC or GC-MS respectively) was withdrawn from the trap via a syringe and injected into the analytical system. Two methods of chemical analysis were employed in this study. The quantitative analysis of reactant concentration was performed using capillary column gas chromatography (GC), the qualitative analysis of intermediate species employed gas chromatography coupled to mass spectrometry (GC-MS).

For the GC analysis the gaseous mixture was separated by gas chromatography (Carlo-Erba) on a fused silica, BP-1-coated, capillary column (12 m x 0.33 mm) (SGE), in an isothermal oven (50 °C). The mixture components were separated in order of increasing boiling point. A quantitative analysis was obtained by integration of peak areas of the

individual components, this being proportional to the concentration of the component. The proportions (%) of the fuel remaining in each experiment were obtained from the determination of the peak area of the primary fuel relative to the n-butane peak. This result was then normalised to a constant peak area representing the n-butane signal. Extents of reaction (%) were measured relative to the amount of reactant measured following compression under non-reactive conditions. The non-reactive conditions could be achieved either by the compression of a fuel-inert gas mixture, prepared in the necessary proportions to achieve a similar compressed gas temperature, or by bursting the diaphragm and sampling at a time where reaction was unlikely to have commenced, i.e. > 5 ms before the end of compression where T < 500 K.

In selected experiments intermediate and product species were identified by gas chromatography - mass spectrometry (GC-MS) by the on-column injection of a 0.1 cm^3 sample into the GC-MS (Carlo-Erba) system. The oven temperature was programmed to increase steadily from 330 K to 500 K over 38 minutes, following an initial 5 minute period of isothermal operation at 330 K. The chromatography column used was a Chrompak fused silica, Poraplot Q-coated capillary column (0.32 mm x 25 m). Compounds eluted from the column were then transferred to a mass-spectrometer, where electron impact was used to produce a mass/charge fragmentation pattern characteristic of the compound. The compounds could be identified by one of three methods. The most common method of identification of compounds following GC-MS is by comparison of the mass spectrum with a library of known mass spectra to determine the nearest fit. A more tedious and time-consuming method is to identify all the fragments from the spectrum and elucidate the structure of the compound. Also, because similar conditions were employed in the chromatographic separation, the chromatographic peaks could be compared to those of earlier work by Minetti et al. on the oxidation of n-heptane in an RCM [136]. Although this is less precise, it proved to be a very useful method, particularly for the aliphatic hydrocarbons as it is very difficult to distinguish their similar fragmentation patterns.

3.2.2 Results

Combustion at T_c = 720-750 K

Figures 3.2 and 3.3 illustrate the measured pressure and fractional extent of fuel consumption (%) with time during the two-stage autoignition of n-C_5H_{12} and n-C_7H_{16} respectively. The pressure records begin 2 ms before the end of the compression stroke (t = 20 ms) and continue throughout the post-compression period and the development of ignition. The pressure record shown in Figure 3.2 also includes the sharp fall in pressure associated with the bursting of the diaphragm The rate of the pressure decrease illustrates the rate of expansion of the reactant mixture into the hemispherical dump tank. Note, the pressure did not reach the maximum which would normally be attained during ignition (>3.0 MPa) under these conditions. This is because the maximum attainable pressure is limited by the natural bursting pressure of the aluminium diaphragm (~ 1.8 MPa).

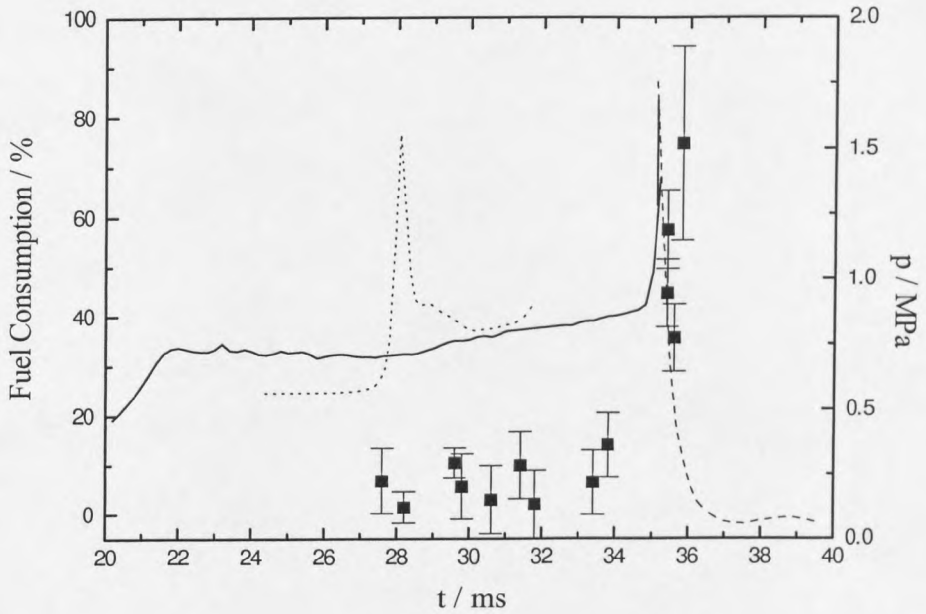

Figure 3.2 Extent of consumption (%) of n-C_5H_{12} (■) during autoignition following compression to T_c = 750 (±5) K. Pressure ((—) and (----)) and light output (...) profiles are also shown for a representative case.

Both fuels exhibited two-stage ignition following rapid compression to temperatures in the range 720-750 K, as illustrated by the rising pressure record and by the accompanying chemiluminescent emission due to cool flame activity (dotted line). There was negligible consumption of either fuel during the compression to these temperatures. However, during the post-compression period where the first and second stages of autoignition develop, 40 (±10) % of the n-C_7H_{16} had reacted by the end of the first stage (cool flame), whereas less than 15 % of the n-C_5H_{12} had been consumed after the first stage of autoignition under similar compressed gas conditions. During the development of the second stage of autoignition, both fuels exhibited a significantly rapid acceleration in the rate of fuel consumption and approximately 80 % had been consumed at the highest quenching pressure (1.7 MPa). The error bars represent variations in results from multiple gas analyses of each sample collected. The discrepancies of experimental results in Figures 3.2 and 3.3 which seem to imply that there is a lower extent of conversion at a later time during the development of the hot

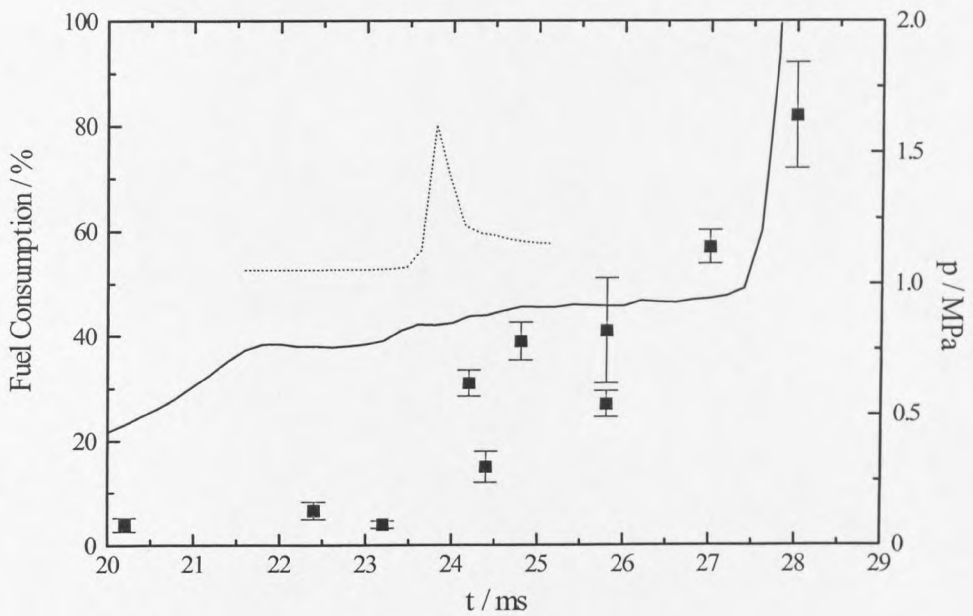

Figure 3.3 Extent of consumption (%) of n-C_7H_{16} (■) during autoignition following compression to T_c = 750 (±5) K. The combustion chamber pressure (—) and light output (...) records are also shown.

stage of ignition, arise from the small variations in ignition delay from one experiment to another. The peak in the light emission profile accompanying the first stage of autoignition is uncalibrated in these figures. However, in reality, the light emission due to cool flame activity during the two-stage autoignition of n-heptane is qualitatively more intense than that for n-pentane autoignition.

Combustion at T_c = 845-875 K

The experimental reactant consumption profiles and pressure-time records for the combustion of n-C_5H_{12} and n-C_7H_{16} are shown in Figures 3.4 and 3.5 respectively. The autoignition of n-pentane following compression to 853 (±4) K developed in a single stage. There was no measured reactant consumption before the end of compression and the extent of fuel consumption increased smoothly (and slowly at first) throughout the post-compression period to almost 100 % conversion at the highest quenching pressure (1.8 MPa).

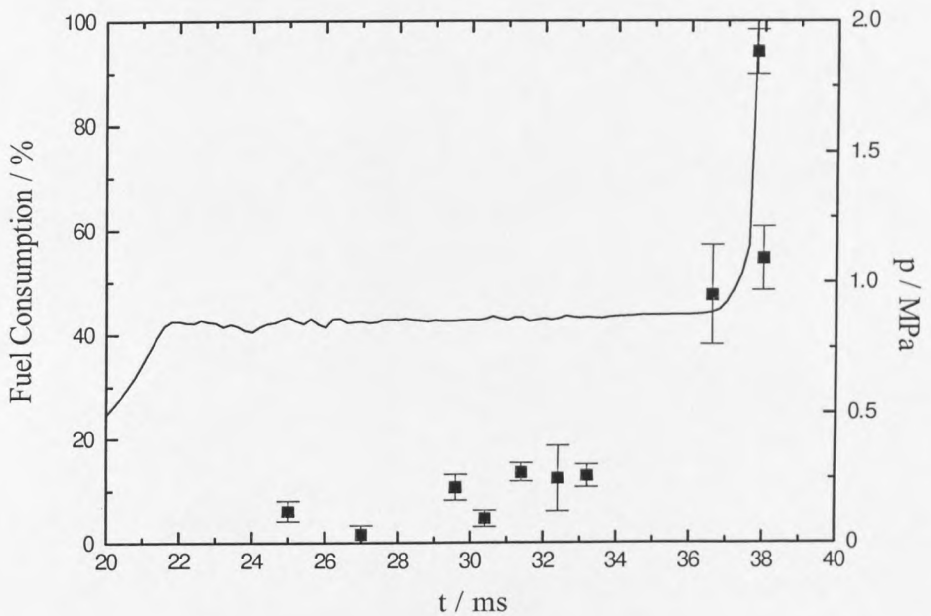

Figure 3.4 Extent of consumption of n-C_5H_{12} (■) during autoignition following compression to T_c = 853 (±4) K. The pressure-time profile (—) is given but the light output record has been omitted because there was no significant light emission due to first stage reaction.

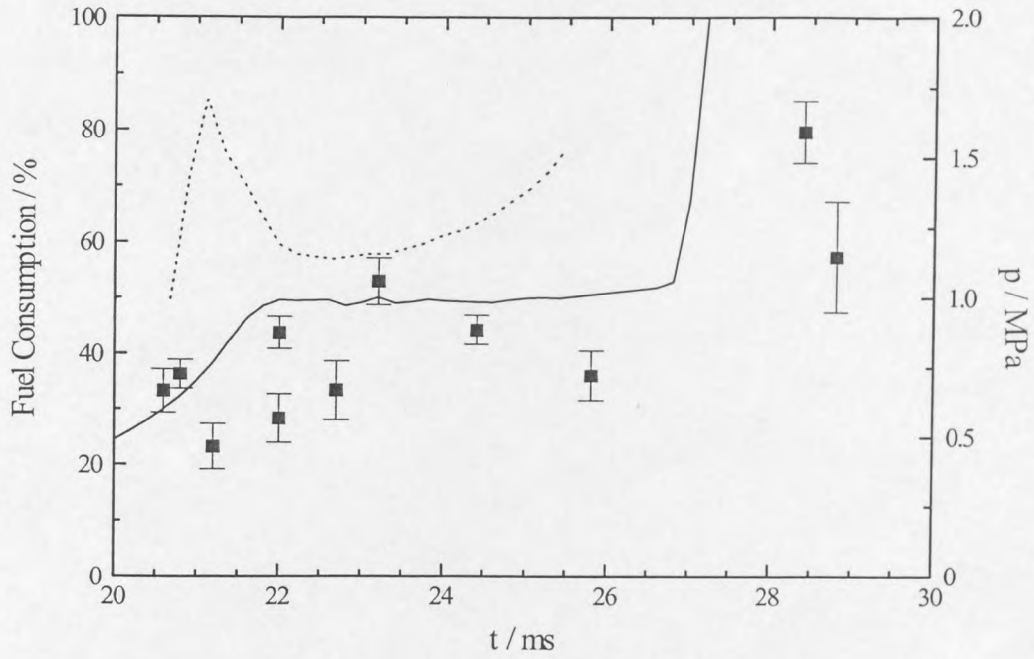

Figure 3.5 Extent of consumption of n-C_7H_{16} (■) during autoignition following compression to T_c = 870 (±5) K and the accompanying cool flame light emission (...). The combustion chamber pressure (—) is also shown. A significant amount of reactant has been consumed before the piston stops (22 ms).

The pressure record for the combustion of n-heptane at T_c = 870 (±5) K is characteristic of a single stage development of autoignition. However, the reactant consumption profile illustrates a significant extent of reactant consumption before the piston reaches the end of its travel. Reactant consumption began more than 1 ms before the end of compression and 40 (±5) % of the n-C_7H_{16} had been consumed by top dead centre. As illustrated by the accompanying light output record, this reaction was associated with the first stage (or cool flame) chemistry.

The experimental results obtained from ignition of the binary mixture 0.6 i-C_8H_{18} + 0.4 n-C_7H_{16} (PRF 60) at a compressed gas temperature of 864 (±4) K are shown in Figure 3.6. Interpretation of events from the pressure record in the post-compression period is of a single stage ignition (total ignition delay, τ = 32 (±2) ms). However, the

consumption of both reactants began while the piston was still moving and there was a weak cool flame emission before the end of compression. A greater percentage of n-C_7H_{16} (45 (±5) %) than i-C_8H_{18} (37 (±5) %) had reacted by the end of the compression. Very little of either fuel was consumed further during the post-compression period until the rapid acceleration in reaction rate and rate of fuel consumption in the final stage of ignition. There was no appreciable distinction between the behaviour of the two fuels in this stage.

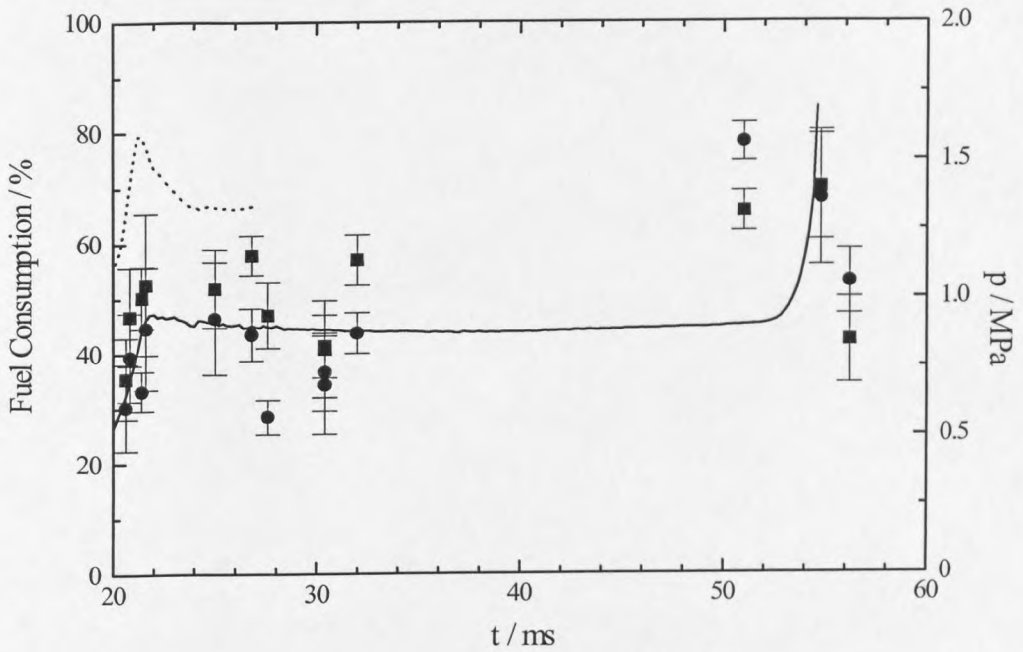

Figure 3.6 Extent of consumption (%) of n-C_7H_{16} (■) and i-C_8H_{18} (●) in a PRF 60 mixture during autoignition following rapid compression to T_c = 864 (±4) K. A significant proportion of both reactants has been consumed before the piston stops and there is accompanying cool flame light emission (…).

Experimental measurements have also been made of the proportion of i-C_8H_{18} consumed in a reactive mixture containing only the i-octane component (i.e. i-C_8H_{18} at ϕ = 0.6) but of similar overall heat capacity to the PRF 60 mixture. Ignition of this mixture did not occur following compression to 860 (±5) K, but nevertheless approximately 20 % of the reactant had been consumed before the end of the

compression stroke, with a gradual increase to 30 % during the 10 ms post-compression interval (Figure 3.7).

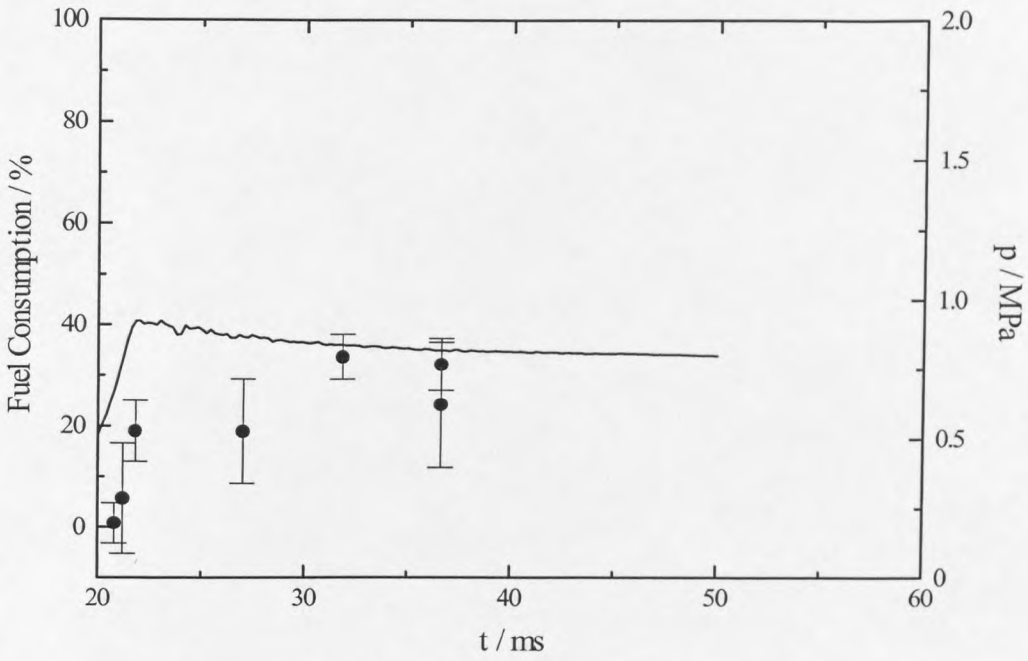

Figure 3.7 Extent of consumption (%) of i-C_8H_{18} (●) at ϕ = 0.6 following rapid compression to T_c = 860 (±5) K. Ignition did not occur and there was negligible light emission accompanying the reaction.

Intermediate species identification

The analytical technique of GC-MS has enabled the identification of a number of molecular intermediate species which are formed during the autoignition of n-heptane and PRF 60 (ϕ = 1.0) following rapid compression to T_c ~ 750 and 850 K. A quantitative analysis of these species was not possible with the available methods because the detector response has a limited range of linearity before it becomes saturated and does not give an accurate measure of concentration. The integrated peak area is proportional to species concentration which in turn is proportional to the total ion current (TIC), only up to a saturation limit. The results of the GC-MS analysis for n-heptane autoignition at 720 K and 850 K and PRF 60 at 875 K are shown in Figures 3.8, 3.9 and 3.10 respectively. In order to increase the intensity of the peaks for several

of the low concentration components of the original chromatogram, it was necessary to expand regions of the chromatogram (b and c).

The gas-chromatographic peaks identified by mass-spectrometry, by comparing the mass spectrum with standards in a library or by comparison with previous analytical measurements by Minetti et al. [136], are listed in Table 3.1. The results clearly illustrate that reactions involving alkyl and alkylperoxy radicals occur during the first stage of ignition but that the interactions are very complex, resulting in the formation of a variety of molecular intermediates.

Table 3.1 Intermediate molecular species identified by GC-MS for the autoignition of n-heptane-air and a PRF 60 mixture in air during the first stage of autoignition. Peak numbers refer to Figures 3.8-3.10.

Peak	Retention time / min	Species
1	8.04	propene
2	16.43	but-1-ene
3	16.58	1,4-butadiene
4	17.31	n-butane
5	21.04	(unidentified)
6	21.43	propenal
7	22.31	propanal
8	24.04	acetone
9	28.04	pent-1-ene
10	28.23	butanal
11	28.47	butanone
12	30.25	hex-1-ene
13	30.55	2-butenal
14	31.33	2-methyl,3-ethyloxiran
15	33.15	4,4-dimethylpent-2-ene
16	34.03	2,4-dimethylpent-2-ene
17	34.23	2,4-dimethylpent-1-ene
18	35.55	hept-2-ene
19	36.23	n-heptane
20	38.09	2,2,4-trimethylpentane

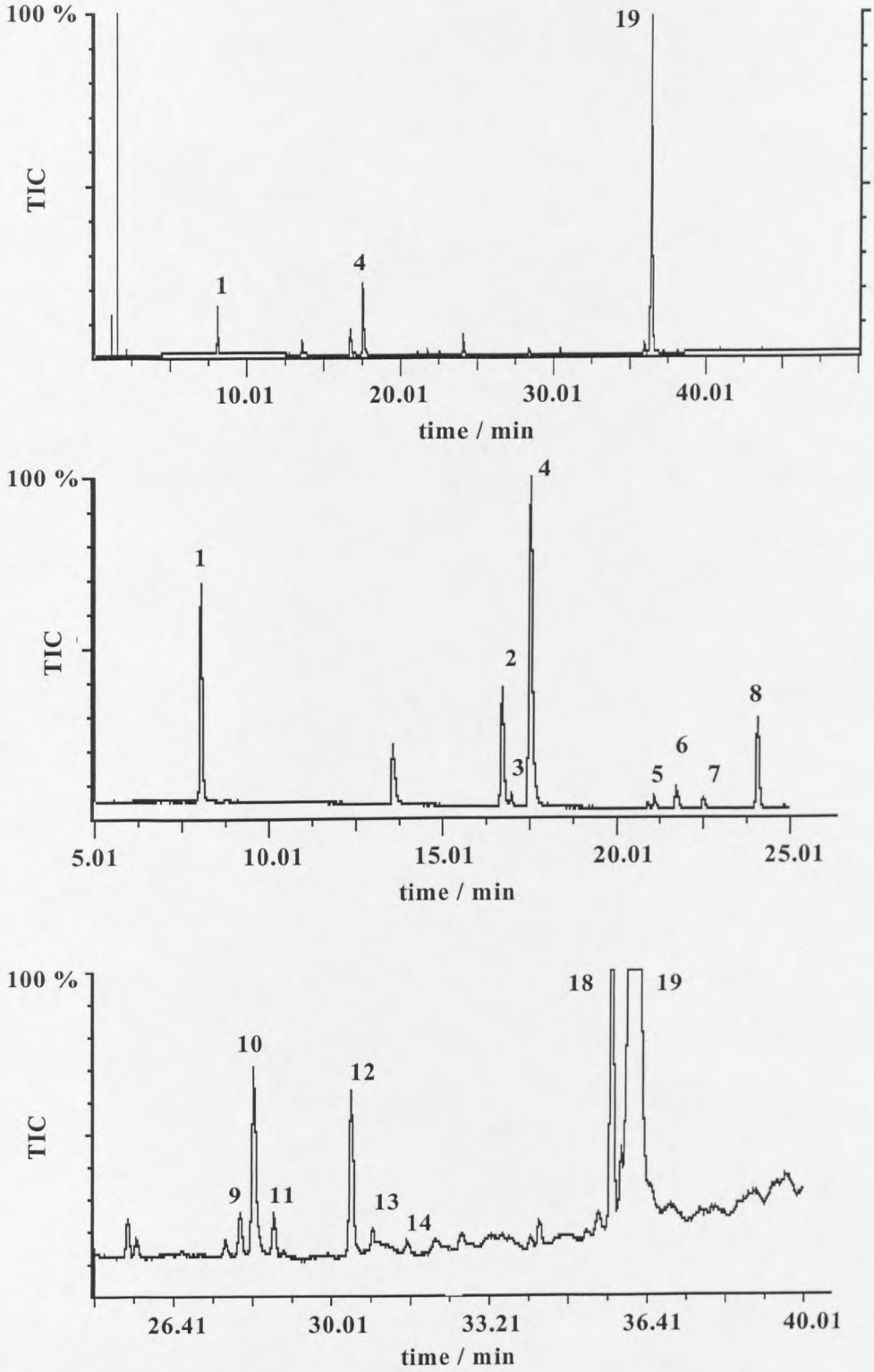

Figure 3.8(a)GC-MS chromatogram for n-heptane-air autoignition following rapid compression to T_c = 720 K, reaction quenched 3.8 ms atdc, during cool flame (or first stage) of ignition (b)Chromatogram expanded over the range 5 to 25 minutes (c)Chromatogram expanded over the range 25 to 40 minutes.

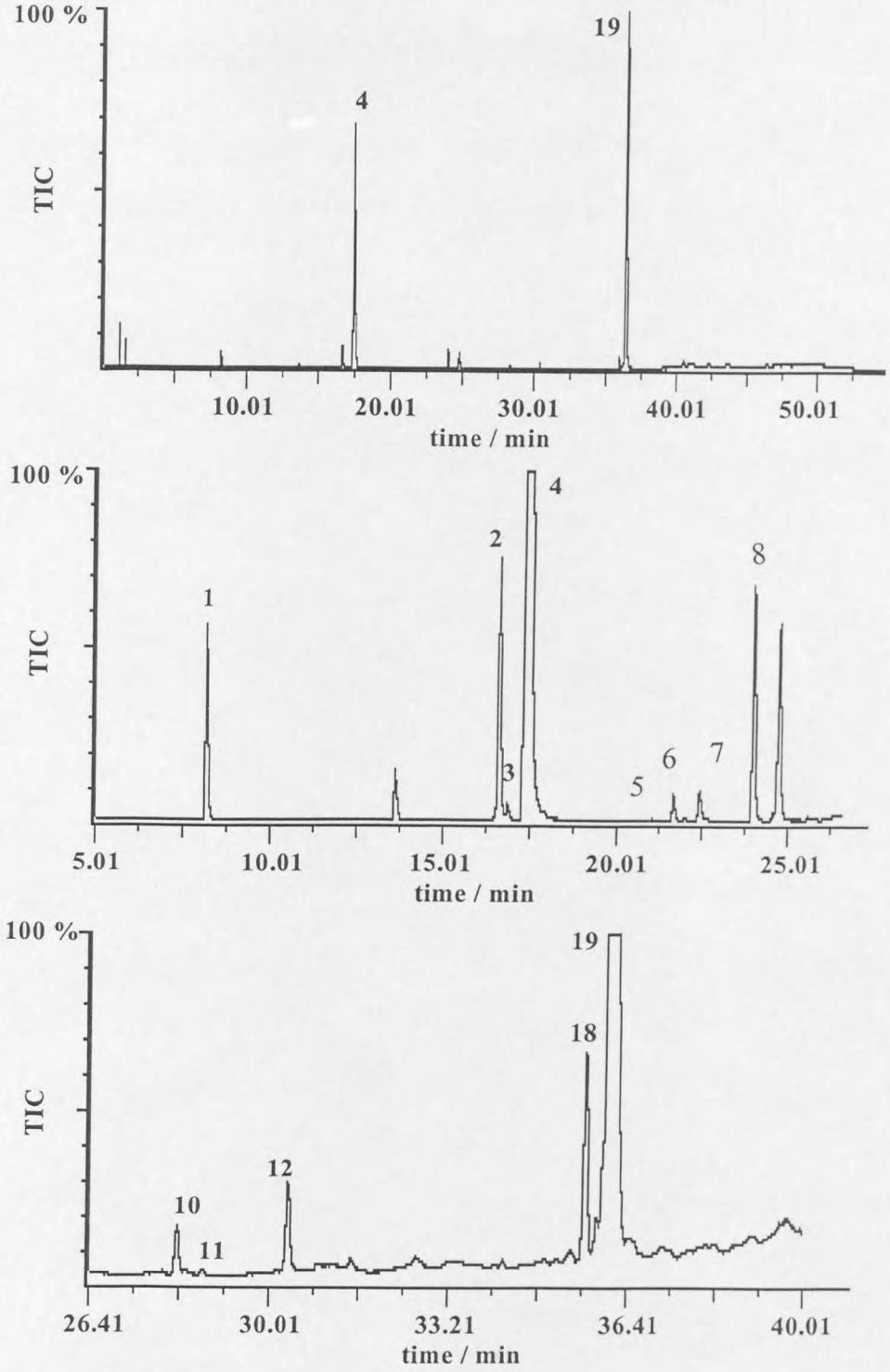

Figure 3.9(a)GC-MS chromatogram for n-heptane-air autoignition following rapid compression to T_c = 850 K, reaction quenched at tdc, during cool flame (or first stage) of ignition (b)Chromatogram expanded over the range 5 to 25 minutes (c)Chromatogram expanded over the range 25 to 40 minutes.

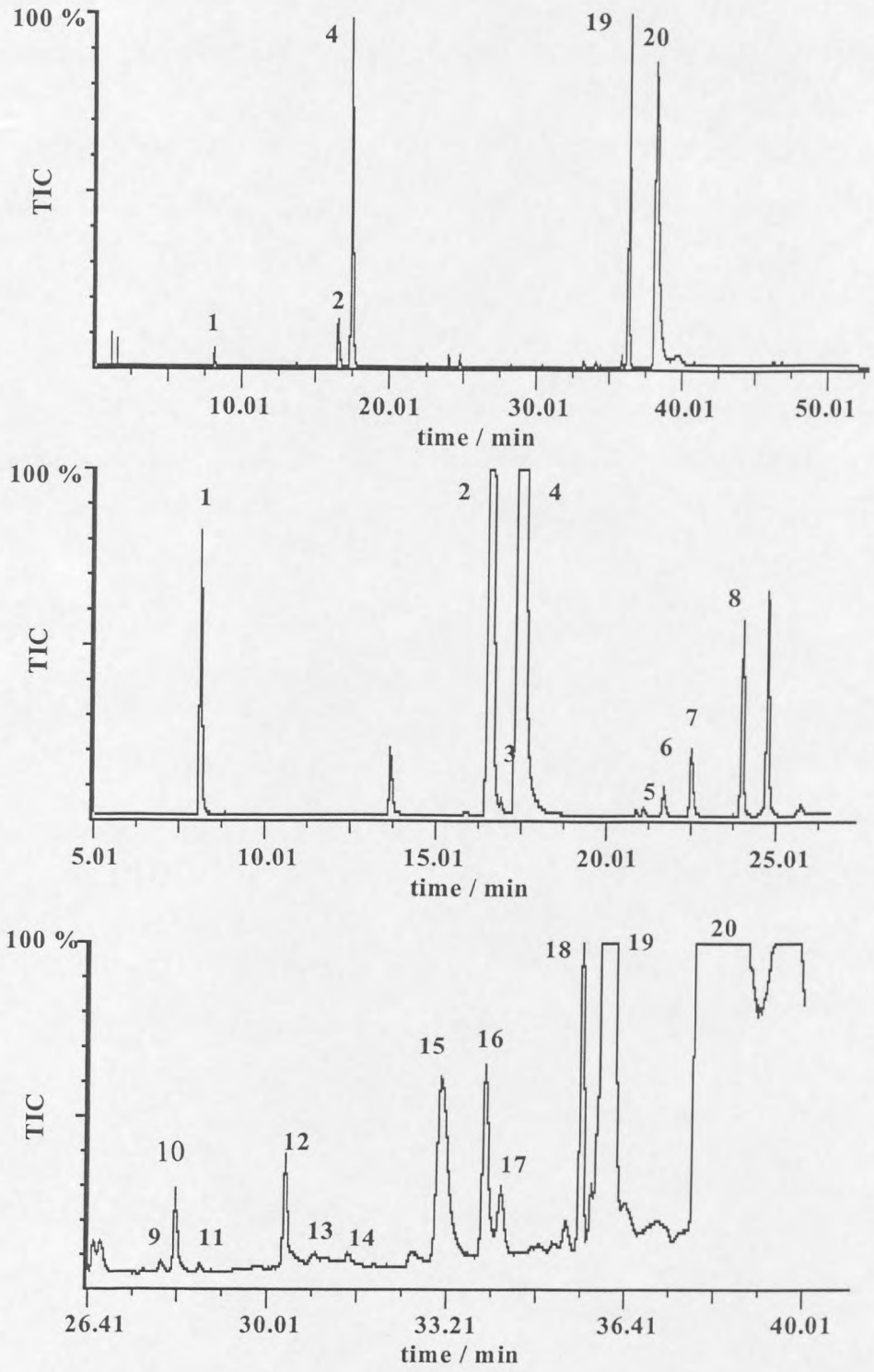

Figure 3.10(a)GC-MS chromatogram for PRF 60-air autoignition following rapid compression to T_c = 875 K, reaction quenched at tdc, during cool flame (or first stage) of ignition (b)Chromatogram expanded over the range 5 to 25 minutes (c)Chromatogram expanded over the range 25 to 40 minutes.

3.2.3 Summary and Conclusions

Reaction during compression

Reaction of n-heptane during compression results in a discrepancy in the determination of p_c and a value which differs from that which would be obtained by adiabatic compression alone, because the end of the compression stroke becomes obscured by the pressure rise due to the first stage of ignition which coincides with the end of compression. This ultimately leads to a discrepancy in the calculated compressed gas temperature, T_{ad}', and is most significant in the range 780-830 K. To avoid this ambiguity in determining the pressure at the end of the compression stroke it would be valuable to have a method of following the piston motion accurately. The Shell RCM used by Affleck et al. [16,119,128,129] employs a sophisticated method for the measurement of piston position during compression, using an optical probe and the light reflected by bright reflecting bands on the piston bore on to a photoelectric cell. In the present study, the start of piston travel has been monitored using the rapid release of air at the start of piston movement to deflect a thin strip of paper between the two arms of a photoelectric diode (Appendix C). This technique allows the end of the compression stroke to be defined in situations where the pressure increase due to first stage reaction at or near the end of compression appears to be an extension of the effect due to the compression.

It was found that when n-heptane was the fuel, temperatures at the end of compression below about 750 K and above 850 K were experimentally accessible, but there was an interval between 750 K and 850 K which was essentially inaccessible, regardless of the argon/nitrogen content of the reactant mixture. The implication is that the onset of the first stage of ignition is very rapid once the mixture temperature reaches 750 K, so any mixture that reaches this temperature during compression will react and the temperature will rapidly increase to 850 K. The effect of reaction during compression ceases once the compressed gas temperature exceeds about 900 K because, for n-heptane, this represents the top of the ntc region, i.e. the temperature at which there is a switch to second stage, high temperature oxidation chemistry. Also, the low temperatures

associated with the first stage reactions are passed through at a much faster rate on the steep pressure rise of the compression profile so there is insufficient time available for reactions to occur during the compression stroke.

Figure 3.11 overleaf illustrates the manifestation of reaction during compression in the pressure-time profile for n-heptane autoignition following compression to 880 K. The departure of the pressure profile of the reactive mixture from that of the inert mixture begins at 21 ms and escalates during the last millisecond of the compression where the piston is coming to a stop. This is because the n-heptane fuel exhibits sufficiently vigorous first stage reactivity for it to occur during the time available in the last stages of compression.

A very small extent of reaction in compression can result in shorter ignition delays than those which would result from adiabatic compression alone. The effect of reaction during the compression stroke is two-fold, there is a thermal effect and a chemical effect. The first stage oxidation chemistry is chain-branching and exothermic. The net heat release to the surroundings raises the temperature of the system resulting in a greater average compressed gas temperature than that resulting from adiabatic compression alone. The first stage of a two-stage ignition also involves the formation of partially oxygenated molecular intermediates, such as aldehydes, which are significantly more reactive than the parent fuel. The overall consequence of these effects is a sensitisation (or "pre-conditioning) of the fuel-air charge and the subsequent time for the second stage of ignition to evolve is reduced, i.e. the overall ignition delay, measured as the time from the end of compression to the maximum rate of pressure increase during ignition, is reduced. In experiments where no light emission occurred before the end of compression this does not necessarily imply that there was no reaction during the compression stroke. Even a small amount of fuel consumed in low temperature oxidation reactions can have a preconditioning effect and result in shorter overall ignition delays.

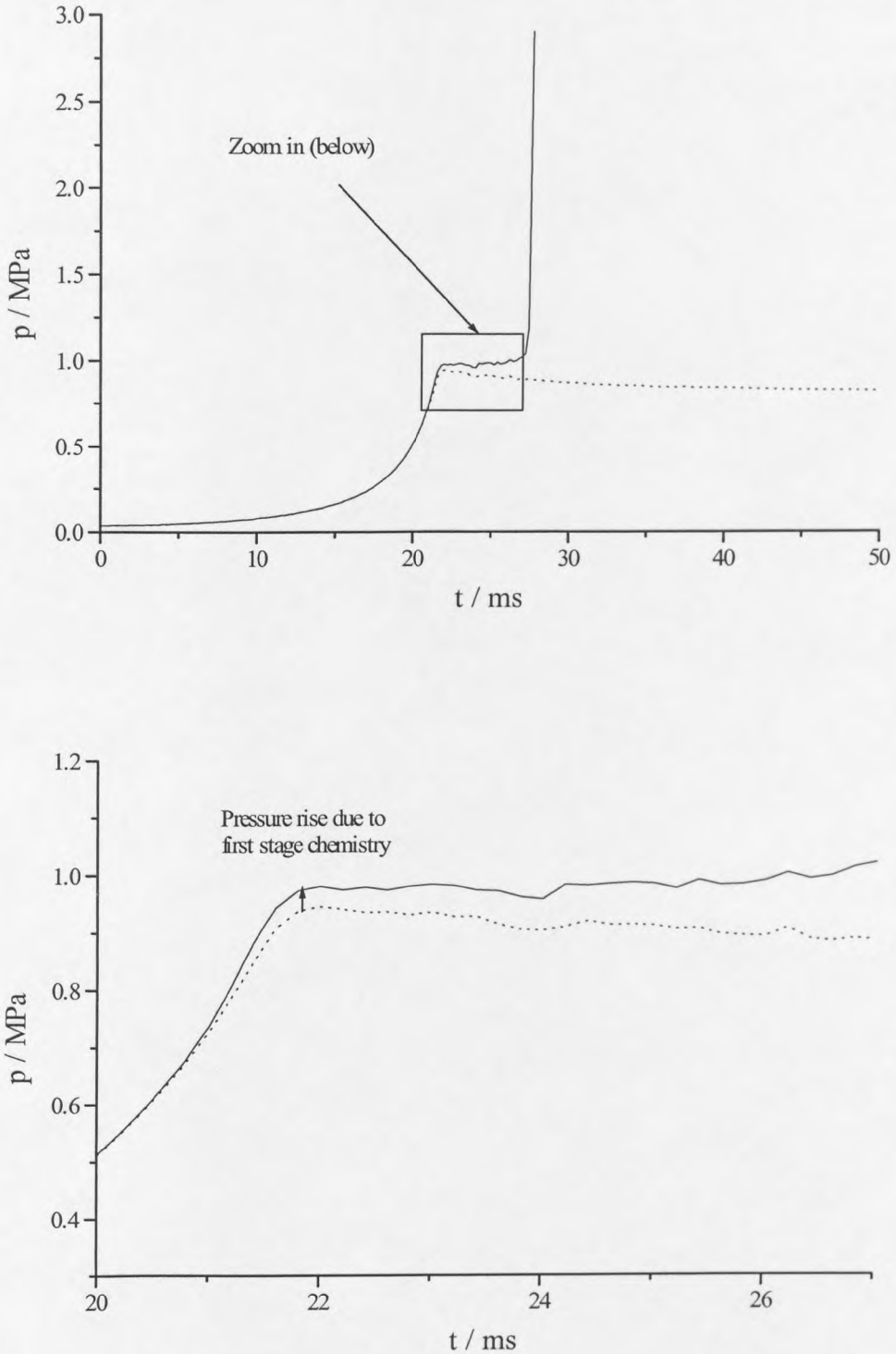

Figure 3.11 Effect of exothermic first stage reaction on the pressure profile for n-heptane autoignition at T_c = 880 K (n-heptane-air (—); n-heptane-inert (...)).

The quantitative effect of reaction during compression on the measured ignition delay can be determined by comparing the ignition delays obtained from RCM experiments with those from a shock tube or a closed constant volume reactor under the same conditions of pressure and temperature. Alternatively, numerical modelling can be used to simulate the experiment but "switch off" the chemistry during compression. The results of this type of investigation will be described in full detail in Chapter 6.

Ignition delays determined in shock tube experiments do not provide a valid comparison with rapid compression and engine studies because there is no time available for reaction during compression. Shock tubes give a definite measure of the ignition delay in the absence of pre-reactions, the instantaneous pressure change means reaction can only begin after passage of the shock front. The rapid compression experiment provides a more satisfactory comparison with engine combustion, allowing for both reaction during the compression stroke and heat losses during the post-compression period.

Ignition delay and the effect of reaction during compression

The ignition delay of a hydrocarbon in an RCM is commonly defined as the time from the end of compression to the attainment of the maximum rate of pressure rise during ignition [16,36]. It is a manifestation of the overall rate of reaction of the fuel-air mixture under the conditions of temperature and pressure achieved on completion of the compression stroke. The typical compression time of rapid compression machines (10-60 ms) allows the more reactive fuels sufficient time to undergo low temperature oxidation reactions even during the late stages of compression when the gases are at a sufficiently high temperature and pressure. The contrasting behaviour of n-heptane and n-pentane shown in Figs. 3.4 and 3.5 illustrates this point. The experimental investigation of the ignition delay variation with compressed gas temperature for several different hydrocarbons will be described in Chapter 4.

The consequence of reaction occurring in the compression stroke is that an ignition delay, defined from the end of compression, is different from that which would be obtained from the same gas mixture if it were raised instantaneously to the same

pressure and temperature. This implies that ignition delays measured in RCMs are unique to a particular apparatus, even at the same gas temperature and density. These factors, although often disregarded, contribute some difficulties to making quantitative comparisons between results from different experimental systems. Nevertheless, they also encapsulate the characteristics which prevail within reciprocating engines themselves, notably that spontaneous reaction may have started even while the charge is being compressed in the cylinder.

3.3 The Role of Additives

The likelihood of autoignition in spark-ignition engines is dependent on the time for the spark-ignited flame to engulf the contents of the combustion chamber relative to the autoignition delay of the unburned end-gas. In order to increase the octane rating of gasoline, antiknock additives are sought which will result in a lengthening of the overall ignition delay of a multi-component fuel, hence reducing the likelihood of end-gas autoignition.

The RCM provides a valuable method of causing autoignition under conditions of temperature and pressure comparable with those in the end-gas of a spark-ignition engine (i.e., T ~ 900 K and p > 10 atm) [144]. The nature of the experiment, involving the compression of premixed gaseous fuel and air by a piston in a cylinder to a constant volume, causes the reactive charge to experience a temperature and pressure history similar to that in spark-ignition engines. However, whilst the lack of reciprocation in the RCM is a useful simplification of events, it does not allow for the build up of reactive intermediates as residuals in the combustion chamber during successive cycles, as in motored engine studies [145].

The previous section illustrates that significant low temperature oxidation can occur during the late stages of the compression stroke if a reactive fuel is compressed to a sufficiently high temperature and pressure. The summary (Section 3.2.3) describes the chemical and thermal effect of reaction during compression on the overall ignition delay. Evidently, if sufficient pre-conditioning has occurred during the compression then the measured ignition delay will be considerably shorter than that which would occur if the extent of reaction during compression had been suppressed or inhibited. The aim of the work described in this section was to demonstrate the effect of suppression of this low temperature chemistry by diethylamine on the extent of reaction that can occur during the compression stroke and on the overall ignition delay.

The retarding effect of amines on the low temperature oxidation of organic compounds is well established [40,41,146] and believed to proceed via a mechanism involving the

production of a relatively stable radical which is unable to propagate the reaction chain to autoignition. Early studies in a closed vessel at atmospheric pressure have illustrated that, of the aliphatic amines, secondary amines are the most effective inhibitors of autoignition [147] This represents one of the reasons for the choice of diethylamine in this investigation. Diethylamine also has particular experimental advantages over other aliphatic and aromatic amines due to its comparatively high vapour pressure at room temperature (~100 mm Hg). The aim of the present study was to determine how this secondary aliphatic amine effects the ignition of n-pentane and n-heptane in the Leeds RCM.

3.3.1 Experimental

The RCM has been used to investigate the effect of diethylamine (5 mol%) on the autoignition of n-heptane and n-pentane in stoichiometric proportion in air ($\phi = 1.0$). Autoignition delays were measured at compressed gas temperatures and pressures in the range 650-1000 K and 9-11 atm respectively. In addition to the pressure-time data obtained, the total light output from the chamber was also recorded as a function of time using a PMT positioned at the end-window.

The diethylamine used was of analytical grade (98 (±1) %) and the proportion used in each gaseous mixture was 5.0 (±0.5) mol% of the fuel. Premixed gaseous reactants stored in Pyrex glass storage bulbs (5 dm^3) were admitted to the combustion chamber ($T_i = 323$ (±1) K) at an initial pressure of 0.033 MPa then compressed by a pneumatically driven piston, the compression stroke taking 22 (±1) ms. The compressed gas density was 131.0 (±1.8) mol m^{-3} in all experiments in this study. This is approximately half of the compressed gas density that would normally be encountered in a s.i. engine.

The ignition delay (τ) was determined from the pressure record, defined as the time from the end of compression to the maximum rate of pressure increase during ignition. Two-stage autoignition is characterised by a cool flame of relatively weak light intensity which precedes the hot stage of ignition. The first stage duration (τ_1) is defined as the

time from the end of compression to the maximum in the light output due to cool flame emission, also coinciding with the point of inflexion on the pressure profile. The second stage duration (τ_2) is the subsequent interval to the hot stage ($\tau_1 + \tau_2 = \tau$). These features of a two-stage ignition following rapid compression are illustrated by the pressure and light output records for the combustion of n-pentane in the RCM shown in Chapter 2 (Fig 2.4).

The methods for calculating the gas temperature at the end of compression have been described in Chapter 2. In the present study, it was prudent to calculate the compressed gas temperature from the ideal gas law, assuming a fixed compression ratio, i.e.

$$T_c = T_i \frac{p_c}{p_i(CR)} \tag{2.16}$$

3.3.2 Results

Ignition delays and the effect of diethylamine

(a) n-Heptane

Reaction of n-heptane occurring in the late stages of compression has been measured experimentally and confirmed in numerical simulations [141]. All or part of this reaction occurs during the course of compression when the gas temperature is above about 750 K. Evidence for the occurrence of the first (cool flame) stage before the end of compression is provided by the light output record. Where significant reaction has occurred before the end of the compression stroke, it is necessary to calculate the end of compression temperature (T_c) using the ideal gas law. Therefore, one can obtain an appropriate value for T_c which accounts for the augmentation of the gas temperature due to exothermic low temperature oxidation reactions during the compression.

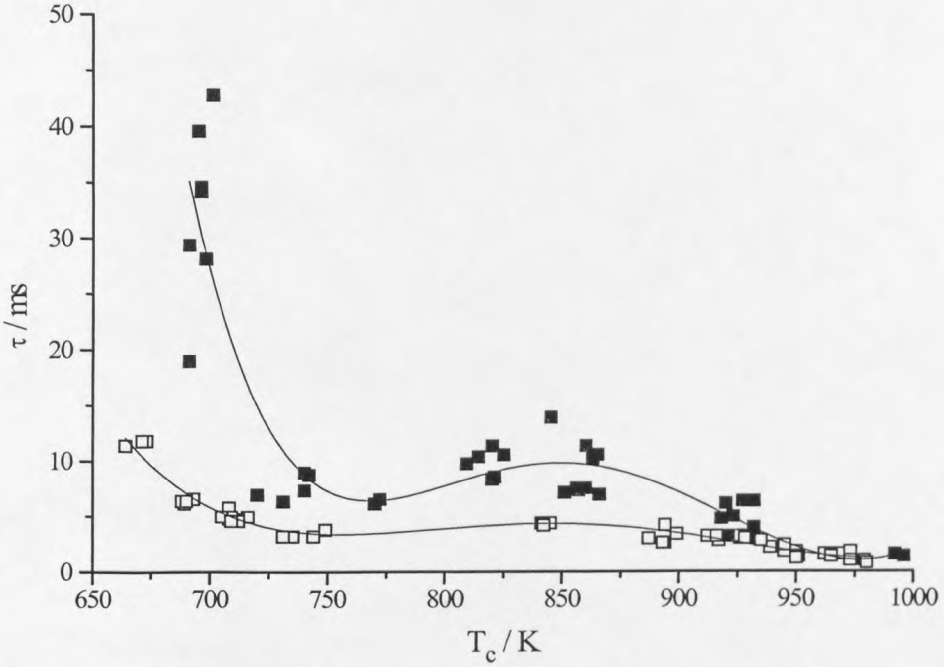

Figure 3.12 Comparison of the ignition delay (τ) over the compressed gas temperature range T_c = 650-1000 K for n-heptane (□) and n-heptane with diethylamine added as 5 mol% of the fuel (■). (This method of representing ignition delay dependence on temperature is discussed fully in the next chapter).

Figure 3.12 illustrates the effect of diethylamine (5.0 (±0.5) mol% of the fuel) on the duration of the ignition delay (τ) for n-heptane in the range T_c = 650 - 1000 K. The diethylamine causes a lengthening of autoignition delay at all compressed gas temperatures investigated below 950 K. The scatter of experimental data about the best fit curve is believed to be a consequence of difficulties of reproducibility in the preparation of each fuel-air-diethylamine mixture. (The absolute vapour pressures of diethylamine being generated were < 5 mm Hg). Nevertheless, additional experiments were performed to confirm this sensitivity to amine concentration. The results showed that greater increases in τ occurred as the proportion of diethylamine was raised in the range 0-7.5 mol% (Table 3.1) and the extent of this sensitivity was also affected by the compressed gas temperature.

Table 3.2 Effect of proportion of diethylamine (mol% of fuel) on the ignition delay of n-heptane in air in the RCM following compression to ~ 800 K. ($\Delta\tau$ = τ with amine - τ without amine).

Proportion of diethylamine / mol% of fuel	T_{ad} / K	T_c / K	τ / ms	ΔT (=T_c - T_{ad}) / K	$\Delta\tau$ / ms
0	802	901	2.6	99	
2.5	802	870	4.8	68	+ 2.2
0	788	887	3.0	99	
5.0	788	860	7.6	72	+ 4.6
0	802	937	1.8	135	
7.5	802	846	9.2	44	+ 7.4

A comparison of pressure and light output profiles versus time is shown in Figure 3.13 for n-heptane alone (a) and n-heptane with 5 mol% diethylamine added (b). Both mixtures were prepared to a similar overall molar heat capacity to achieve a temperature of 850(±5) K following rapid compression. Although the cool flame occurred during compression for both mixtures, the light intensity was reduced in the presence of diethylamine and also a lower pressure was achieved at the end of compression. The lower compressed gas pressure, in the presence of diethylamine, signifies that a lower compressed gas temperature was reached as a result of a smaller extent of n-heptane oxidation during compression. Both the reduced temperature enhancement and the lower extent of "chemical pre-conditioning", caused by the diminished extent of n-heptane oxidation, contribute to the longer ignition delay.

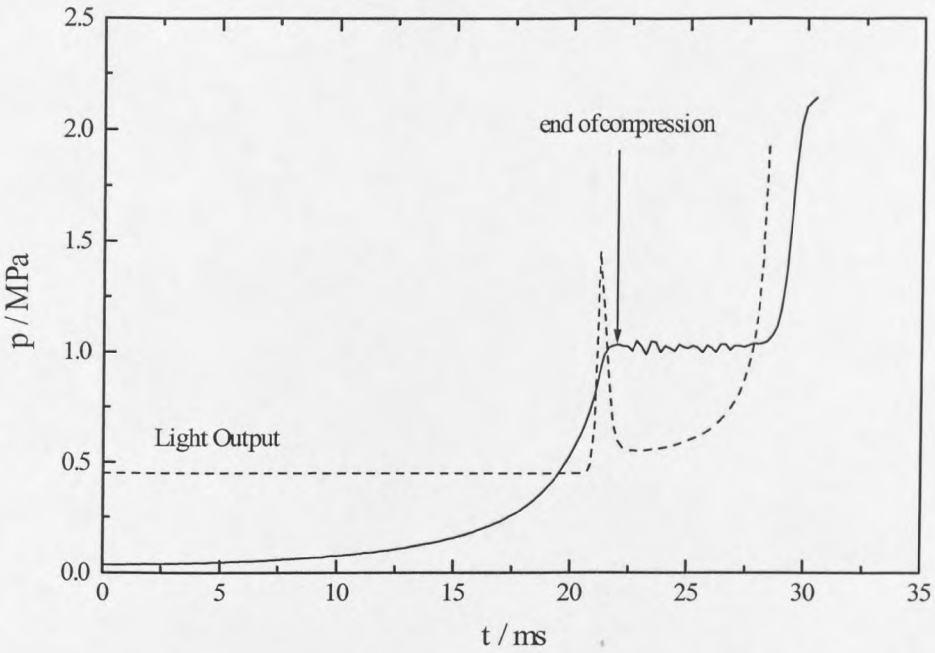

Figure 3.13(a) Pressure (—) and light output (---) records for n-heptane autoignition following compression to 850 K in the RCM.

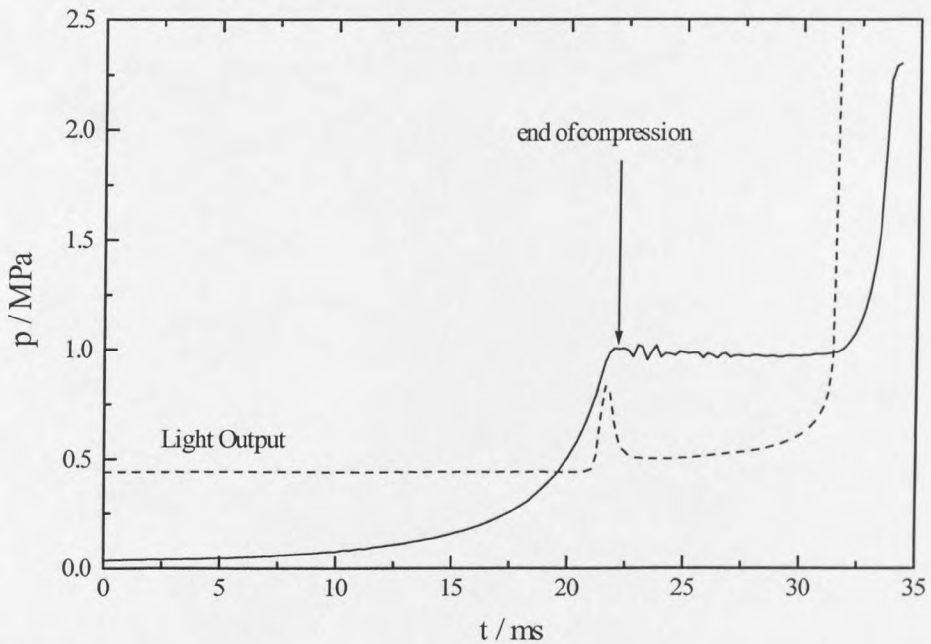

Figure 3.13(b) Pressure (—) and light output (---)records for n-heptane + 5 mol% diethylamine autoignition following compression to 850 K.

(b) n-Pentane

The contrasting response of the ignition delay of n-pentane due to the presence of diethylamine can be seen from Figure 3.14. Addition of diethylamine results in longer ignition delays in the temperature range 700 - 800 K, but with decreasing effectiveness as the compressed gas temperature is raised further. As T_c = 850 K is approached, there is a crossover of the two curves and by 900 K there is a reduction in τ of about 50 % in the presence of diethylamine.

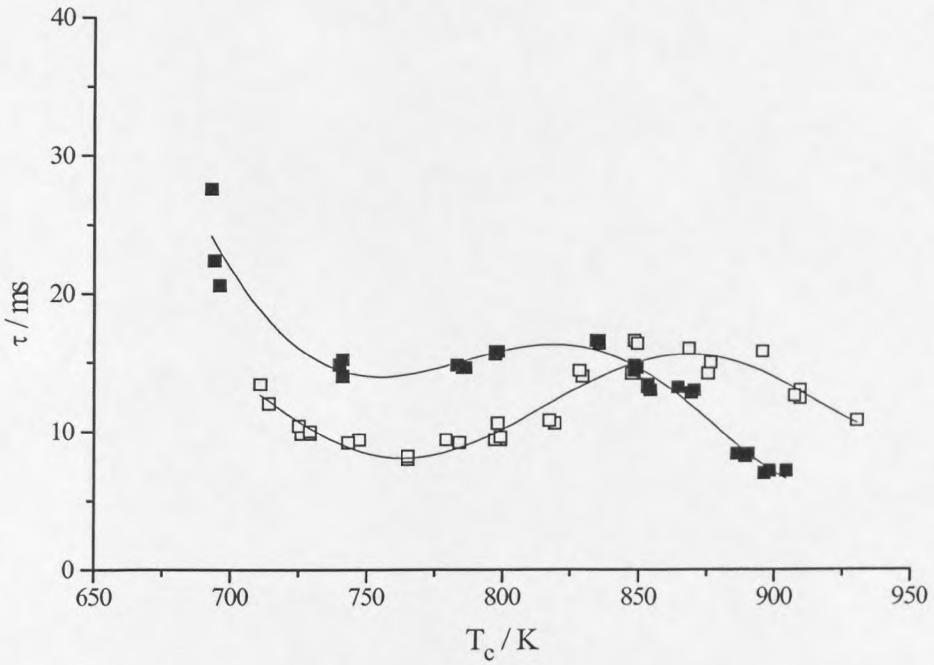

Figure 3.14 Comparison of ignition delay (τ) variation with compressed gas temperature (T_c) for n-pentane (□) and n-pentane + 5 mol% diethylamine (■).

The pressure-time profiles and light output records for two-stage autoignition of n-pentane mixtures compressed to 740 K shown in Figure 3.15 are in marked contrast to those of n-heptane (Fig 3.13). There is a considerable increase in the duration of τ_1 in the post-compression period which is caused by the addition of diethylamine. However, rather like n-heptane, there is also a reduction of light intensity and rate of pressure change at the first (cool flame) stage. These features were observed throughout the range 650 $<T_c<$ 850 K, where two-stage ignition occurs.

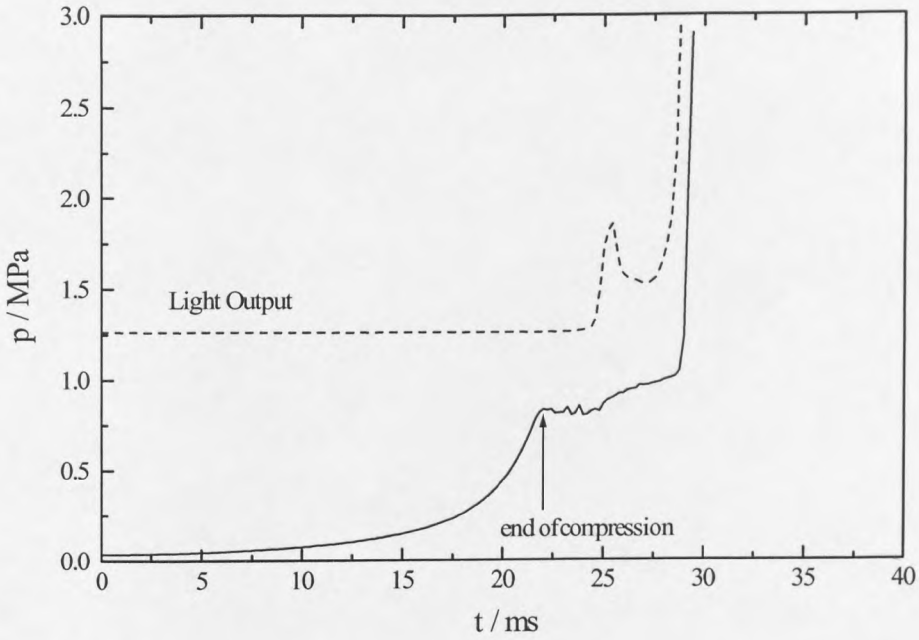

Figure 3.15(a) Pressure and light output records for two-stage autoignition of n-pentane following compression to 740 K.

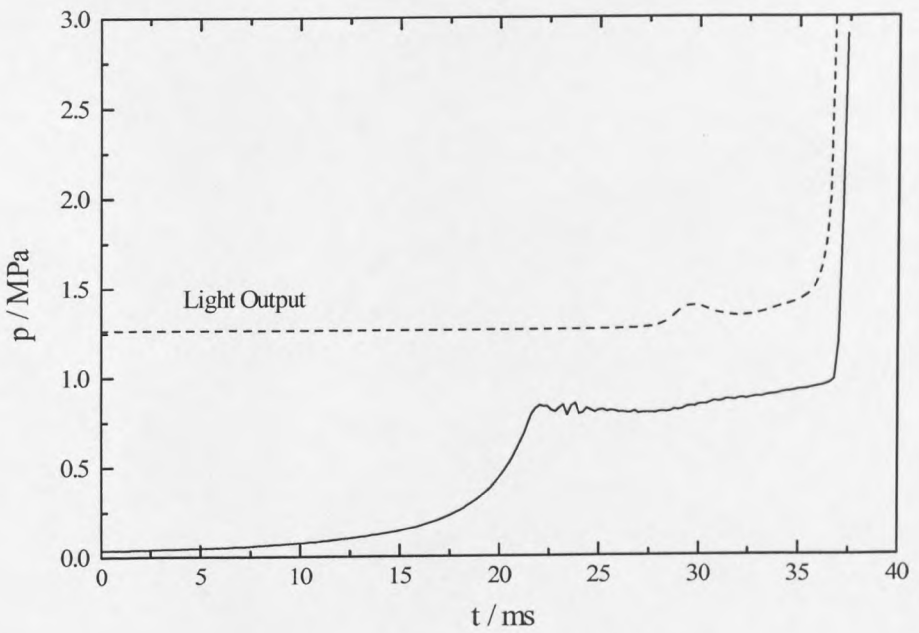

Figure 3.15(b) Pressure and light output records for two-stage autoignition of n-pentane + 5 mol% diethylamine following compression to 740 K.

3.3.3 Summary and Conclusions

The chemical effect of diethylamine

Any modification of the chemistry which suppresses chain branching in the low temperature regime is capable of reducing the extent of reaction that can occur during the compression stroke. Previous experiments in the RCM have shown that there is always some possibility of first stage chemistry with n-heptane [141] on which diethylamine may have a retarding influence. For n-pentane there is a compressed gas temperature above which no low temperature chemistry occurs, so the retarding effect of the amine is no longer possible.

The present results show that the addition of diethylamine to n-heptane can suppress reaction during compression to the extent that the heat release rate due to exothermic oxidation is appreciably less than that for n-heptane alone. However, in the proportions used here, diethylamine does not completely inhibit reactions, so that weak, cool flame reactions still occur during compression. The effect on the overall ignition delay is both thermal and chemical in origin. The retarded first stage reaction results in a smaller concentration of reactive intermediates as well as giving a lower gas temperature at the end of compression, both of which control the development of the second stage. The intermediates include partially oxidised molecular products, such as aldehydes, cyclic ethers and peroxides, as well as radical species. The free radical activity is confirmed by the weak light emission from the cool flame, characteristic of excited formaldehyde formed in chemiluminescent reactions. Since all of the post-compression chemistry is "second stage" chemistry, the measured ignition delay is increased by the effect of diethylamine throughout the compressed gas temperature range from 700 K.

There is a related effect on the chemistry of n-pentane oxidation , but because all of the reaction occurs in the post-compression period, there is a lengthening of the ignition delay when the (retarded) first stage chemistry has a controlling effect. As shown earlier, from $T_c > 850$ K there is no prospect of first stage (cool flame) chemistry. The influence then exerted by diethylamine appears to be a promoting effect on the high

temperature reactions. This is shown by the reduction of τ at $T_c > 850$ K. This promoting influence of diethylamine on autoignition was also observed by Cullis et al. [148] for the combustion of n-heptane in a closed vessel at atmospheric pressure.

Diethylamine retards the first stage of the two-stage ignition of n-heptane and n-pentane, causing a reduction in both the pressure rise and the light intensity associated with the first (cool flame) stage. A longer duration of the second stage of ignition is measured. Consequently, an increase in ignition delay was observed for n-heptane throughout the temperature range 650-950 K, for which first stage reactions persist in the compression stroke at temperatures above 850 K. The ignition delay of n-pentane is increased in the range 650-850 K by the addition of diethylamine but is decreased at compressed gas temperatures greater than 850 K. The possible mechanisms of the inhibition of first stage autoignition chemistry and promotion of second stage autoignition chemistry by diethylamine are outlined below.

Although the details of the chemical role of amines as additives in controlling the development of spontaneous ignition are not yet understood, that the retarding effect is associated with low temperature chemistry involving alkylperoxy and alkyldiperoxy species is clear.

The mechanism of inhibition of first-stage autoignition chemistry and promotion of high temperature chemistry cannot be directly elucidated from the present experimental study. A more detailed analysis including numerical modelling techniques and species measurements is required for this purpose. However, based on the present and previous studies of the effects of amines on low temperature oxidation, the following suggestions are made.

The switch to the high temperature branch of the chemistry is completed when the equilibrium

(2) $\quad R + O_2 \rightleftharpoons RO_2$

is displaced far to the left hand side. The propagation is then driven by the decomposition of alkyl radicals (R) but HO_2 is probably the main propagating species (at least at $750 < T > 850$ K) through reactions of the kind

(3) $R + O_2 \rightarrow \text{alkene} + HO_2$.

Thus the retarding effect of diethylamine could be related to its interference with the formation of the diperoxy species, i.e., interference with propagation by competing with oxygen for free radicals, e.g.,

(13) $R + (C_2H_5)_2NH \rightarrow RH + (C_2H_5)_2N$.

In the closed vessel studies of secondary amines as autoignition inhibitors by Cullis and Waddington [147], it was suggested that the favoured point of attack by molecular oxygen and free radicals was at the secondary ($-CH_2-$) site. However, the retarding effect of aliphatic amines must be related to the presence of the nitrogen since other aliphatic compounds do not show similar inhibitory characteristics. Numerical modelling could be usefully applied to confirm this.

Cullis et al. [148] later attributed the retarding role of amines to the labile abstraction of an H atom to produce a relatively unreactive free radical, e.g.

(14) $RO_2 + (C_2H_5)_2NH \rightarrow ROOH + (C_2H_5)_2N$.

The bond strength of N-H is 360 kJ mol^{-1}, which is considerably lower than that of primary (410 kJ mol^{-1}) or secondary (397 kJ mol^{-1}) C-H bonds. Indicating the favourable competition by diethylamine for RO_2. Waddington [149] regarded there to be a similar role of amines in the inhibition of diethyl ether/oxygen flames. The inhibitory nature of the $(C_2H_5)_2N$, or equivalent radicals, from secondary amines was not disclosed by either group of workers.

By contrast, the promoting effect of diethylamine (at $T_c > 850$ K for n-pentane) is connected with an augmentation of the reaction rate when radical concentrations are (at first) very low and HO_2 is predominant as a propagating species. A promoting role can be envisaged in circumstances where HO_2 is a key propagating species because the formation of H_2O_2 via

(15) $HO_2 + (C_2H_5)_2NH \rightarrow H_2O_2 + (C_2H_5)_2N$

becomes quite strongly favoured. This may lead to chain branching at higher temperatures ($T > 850$ K) at which the decomposition of hydrogen peroxide

(6) $H_2O_2 + M \rightarrow 2OH + M$

then becomes favourable.

It is unlikely that diethylamine would find favour as an antiknock in gasoline, nor would it be used in such high proportions. Nevertheless, these results show the strengths and weaknesses of such compounds in this role and under what circumstances they may be most effective.

Chapter 4

Ignition delays and their relation to octane rating

4 IGNITION DELAYS AND THEIR RELATION TO OCTANE RATING

The purpose of the first part of this chapter (Sections 4.1 - 4.4) is to present and discuss experimental results which illustrate the different reactivity of hydrocarbons (C_4-C_8) during autoignition in an RCM, and to investigate the relationship between ignition delay and research octane number (RON). The ignition delay as a function of compressed gas temperature, T_c, for single component hydrocarbons of known RON was compared with the primary reference fuel mixtures (PRFs), n-heptane and i-octane (or 2,2,4-trimethylpentane) of similar RON. The study of the autoignition of hydrocarbons in an RCM is relevant to progress in understanding the behaviour of a multi-component gasoline in a spark-ignition engine as illustrated in Chapter 3.

In Section 4.5 the experimental investigation of the effect of fuel:air equivalence ratio on ignition delay following rapid compression will be described. Section 4.6 is concerned with the autoignition of hydrocarbons following direct injection of a liquid spray into the combustion chamber. These results facilitate a broader understanding of the autoignition of hydrocarbons in a s.i. engine - the dependence on mixture composition and the effect of the physical environment, and also have significance with respect to diesel engine combustion.

4.1 Ignition delays and Octane Rating

Ignition delays were measured across the accessible compressed gas temperature range in the RCM and the ignition delay at $T_c = 900$ K for the PRF mixtures and for the single component fuels was correlated with their RON. Emerging from this study is the investigation of the effect of molecular structure on the autoignition characteristics of hydrocarbons in the RCM and on their relative reactivities. In general, these results corroborate previous postulates regarding the influence of molecular structure on autoignition delay [12].

4.1.1 Background

Engine knock has historically been considered to be a consequence of either acceleration of the spark-ignited flame front or the occurrence of autoignition in the end-gas [16]. However, it is now commonly accepted that engine knock occurs as a result of autoignition in the unburned end-gas and can be closely correlated to the autoignition of a narrow region of unburned end-gas ahead of the spark-ignited flame. Engine studies have shown that the occurrence of autoignition does not inevitably result in the occurrence of knocking combustion, but where knock does occur, autoignition centres are always evident in the end-gas [4].

Octane rating

The tendency of a fuel to cause knock in a spark-ignition engine is measured on the scale of octane rating (RON or MON). The determination of RON is performed in a single cylinder research engine, under relatively mild conditions where "low temperature chemistry" most likely applies. A Co-operative Fuels Research (CFR) engine is run under prescribed operating conditions, i.e. 600 rpm, full load, fuel:air for maximum power, spark advance (i.e. the crank angle preceding tdc at which the spark is initiated) for maximum power. The critical compression ratio (CCR) is determined as the compression ratio at which engine knock becomes just audible under these conditions. The RON value is found by comparison of the CCR for the test mixture with that for standard PRF mixtures, and the research octane number is defined as the percentage by volume of i-octane in a mixture of n-heptane and i-octane which has the same CCR as that at which knock is caused by the test fuel. The RON scale is defined from 0 to 100, the CCR for n-heptane being designated 0 and the CCR for pure i-octane being designated 100.

Structure related reactivity and knock tendency

The comprehensive report by Lovell [11] in 1949 is distinguished amongst experimental studies of structure related reactivity and knock tendency by the extent of its scope and

clarity in which the structures of single-component hydrocarbons were shown to relate to their engine-knock resistance. The increasing resistance to engine knock was recorded as an increasing CCR in a CFR engine (Figure 1.2).

The first kinetic and mechanistic link between chemical structure and knock rating was made by Walsh [12], who suggested a set of qualitative rules for the structure dependent reactivity of hydrocarbons, as described in Chapter 1. The relative locations of the p-T_a ignition boundaries for different hydrocarbons in oxygen, measured in closed vessels at low pressures, also appear to be related to their ease of engine knock. In their RCM studies of the autoignition of hydrocarbons in air at high temperature and pressure, Fish and co-workers [128] confirmed that these processes were likely to be driven by the same degenerate chain-branching mechanism [12]. It has, however, been argued that the relative knock characteristic of a compound is not necessarily a property of the compound but depends upon the engine conditions under which the comparison with other fuels is made [11]. This emphasises the difficulties which can arise when comparing experimental results obtained using different experimental systems.

The foundation for a kinetic link between the ease of autoignition of alkanes and the propensity to cause engine knock lies in the overall structure of the hydrocarbon oxidation mechanism (see Chapter 1). It is generally accepted that the internal isomerisation reactions of RO_2 radicals play a vital role in the propagation steps of autoignition.

Walsh recognised that the ease of RO_2 isomerisations to the hydroperoxyalkyl species, QOOH, was closely related to the size of the transition state ring structure, which in turn is related to the molecular fuel structure [12]. This constitutes a qualitative relationship between autoignition and engine knock. A quantitative interpretation has been developed based on a calculated chain-branching rate parameter derived from the alkane structure [95]. The rate of formation of the kinetic chain-branching agent, ketohydroperoxide, was correlated with the blending research octane number and a good linear relationship between the two was found to exist. This verified that the low

temperature hydrocarbon oxidation mechanism could provide a possible explanation for the autoignition behaviour of hydrocarbons in an engine test.

Since the processes of knock and autoignition hold the same chemical origin [12], knock ratings of fuels may be explained in terms of the chemical reactions which result in autoignition of the end-gas in spark-ignition engines. Westbrook et al. [13], amongst others, have argued that autoignition is possible if the ignition delay of the reactants at the temperature of the end-gas is less than the time taken for the unburned fuel to be totally consumed by the spark-ignited flame. In recent numerical studies [13,102] the time of ignition of a range of alkane isomers, taken from bdc in a simulated motored engine cycle, has been calculated. The conclusion was that a satisfactory correlation of ignition time from bdc with RON exists. The results presented in this chapter do not support this claim in a quantitative way.

Autoignition delays measured in an RCM, or similar experimental device such as a shock tube or flow tube, are global quantities and their interpretation in terms of chemical reactions is not superficial. In an RCM the total ignition delay of a fuel-air mixture is a manifestation of the overall rate of reaction at the end of compression conditions of temperature, pressure and concentration. Ignition delay measurements have been widely applied in the validation of numerical modelling predictions but also provide a valuable indication of the overall rate of reaction at a given condition of temperature, pressure and concentration.

The first attempt to correlate ignition delays observed in an RCM with results from an engine study was by Livengood and Wu in 1955 [150], using an empirically derived relationship between ignition delay measured in an RCM and the overall reaction rate at the onset of knock. The primary difference in the experimental rapid compression device and engine test studies lies in the inherent reciprocation of firing and motored engines as opposed to the single shot to constant volume in the RCM. However, from their experiments in motored and firing engines and the RCM, Livengood and Wu were able to show that the agreement between predicted and measured times of occurrence of

autoignition following compression for n-heptane and a PRF 55 blend was satisfactory (Figure 4.1).

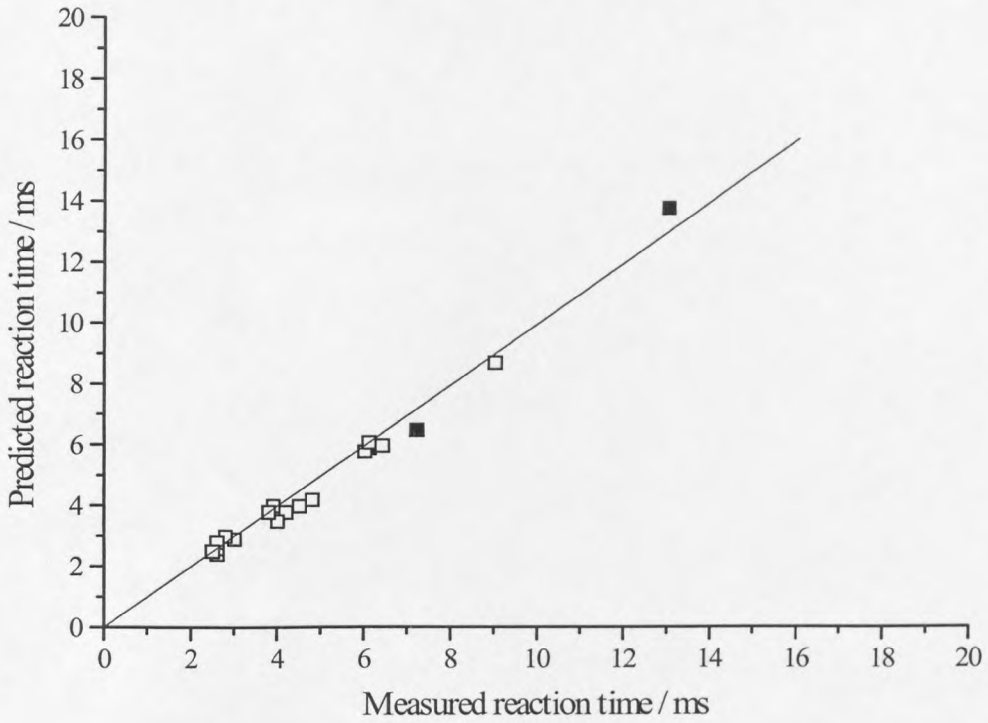

Figure 4.1 Correlation of predicted and measured time of autoignition or knock for n-heptane and PRF 55, from results of motored (■) and firing (□) engine tests [150] for various engine speeds, CR and spark advance.

It has been suggested that the alk-1-enes may provide a more satisfactory correlation with the PRFs than n-alkanes [151]. It is generally accepted that for a n-alkane with x number of carbon atoms, the alkene with x + 1 carbon atoms and double bond at position 1 has a very similar octane rating [11]. It has also been argued that it is more appropriate to regard alkanes as "abnormal" due to the existence of a negative temperature coefficient (ntc) of the reaction rate and ignition delay, compared with alkenes which exhibit a negligible ntc of ignition delay. The results described in this chapter give some support for this argument (Figure 4.10).

4.2 Experimental

The apparatus and experimental procedure have been described in detail in Chapter 2. The gaseous fuel vapour was premixed with "air" in stoichiometric proportion ($\phi = 1.0$). Gaseous reactants stored in Pyrex glass storage bulbs (5 dm^3) were admitted to the combustion chamber ($T_i = 323$ (± 1) K) at an initial pressure of 33.3 kPa then compressed to a constant volume by a pneumatically driven piston. The compressed gas density was 136 (± 1) mol m^{-3} in all experiments in this study.

Pressure-time data during the compression and throughout the post-compression period were measured and chemiluminescent emission accompanying reaction was detected by a photomultiplier tube positioned at the Perspex end-window of the chamber and recorded digitally on a pc.

The adiabatic compressed gas temperature (T_{ad}') was derived from the equation of state for an ideal, adiabatic, isentropic compression, using the measured pressures at the start and end of compression, p_i and p_c, as described in Section 2.4. The temperature dependence of γ is taken into account using the relationship (Eq. 2.11),

$$\int_{T_i}^{T_{ad}'} \frac{\gamma}{\gamma - 1} \, d \ln T = \ln \left(\frac{p_c}{p_i} \right) \qquad (2.11)$$

The value of γ was varied in order to access a wide range of compressed gas temperatures. Using results obtained for the autoignition of n-pentane and n-heptane, Table 4.1 illustrates the approach to an ideal adiabatic compression (i.e., where $T_{ad} = T_{ad}'$) and the effect of exothermic reaction during the compression stroke (i.e., where $T_c > T_{ad}'$). A more detailed account of the assessment of compressed gas temperature can be found in Section 2.4. The effect of reaction during compression on end of compression temperatures is described in Section 3.2.

Table 4.1 Comparison of T_{ad}, T_{ad}' and T_c for n-pentane, n-heptane and PRF 60 (p_i = 33.3 kPa, CR = 11.00 (± 0.15)).

	T_{ad} / K	T_{ad}' / K	T_c / K
1.0 n-C_5H_{12} + 8.0 O_2 + 17.0 N_2 + 13.2 Ar	807	799	802
1.0 n-C_7H_{16} + 11.0 O_2 + 24.8 N_2 + 16.6 Ar	785	803	861

4.2.1 Ignition delay

The ignition delay (τ) was determined from the pressure record, defined as the time from the end of compression to the maximum rate of pressure increase during ignition. Two-stage autoignition is characterised by a cool flame of very weak light intensity preceding the hot stage of ignition. The first stage duration (τ_1) is defined as the time from the end of compression to the maximum in the light output due to cool flame emission, and the second stage duration (τ_2), is the subsequent interval to the hot stage ($\tau_1 + \tau_2 = \tau$). These features of a two-stage ignition following rapid compression are illustrated by the combustion of n-pentane-air in the RCM (Fig. 4.2), also shown in Figure 2.4.

The light emission and pressure traces give a clear indication of cool flame activity in the first stage, characterised by a relatively small pressure rise and low intensity light output. The total ignition delay time can be divided into two components for the first, τ_1 and second stages ,τ_2, shown in Fig. 4.3 for n-pentane. As T_{ad}' is raised τ_1 decreases and the duration of τ_2 increases. The underlying kinetic reasons for the increase of τ_2 are most likely to be connected with a diminishing ability of the degenerate branching reactions in the first stage to raise the reactant temperature and radical activity sufficiently high at the onset of the second stage.

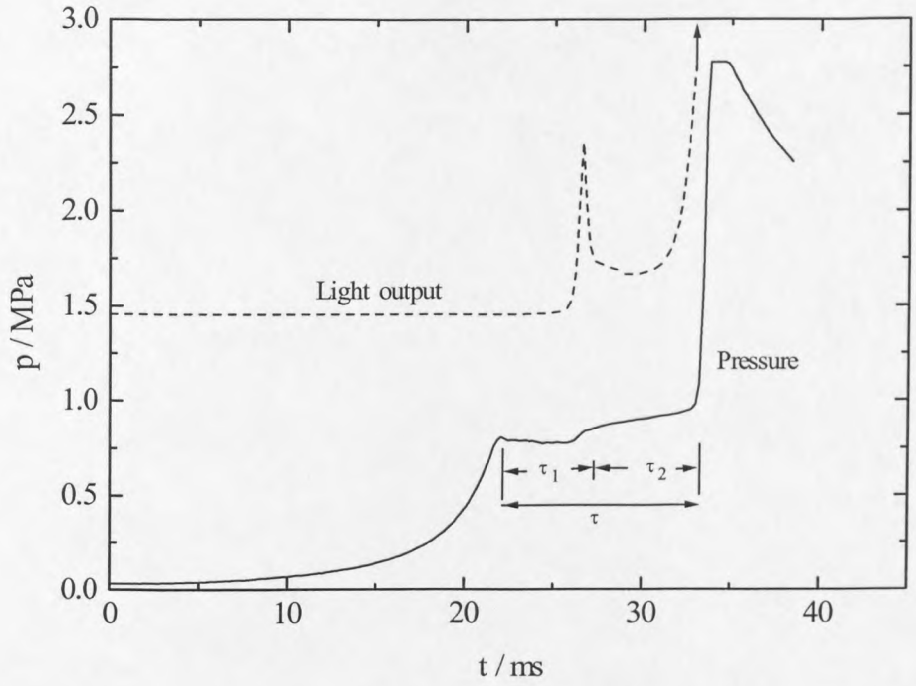

Figure 4.2 Pressure (—) and light output (...) records for the two-stage autoignition of n-pentane in air following compression to 744 K.

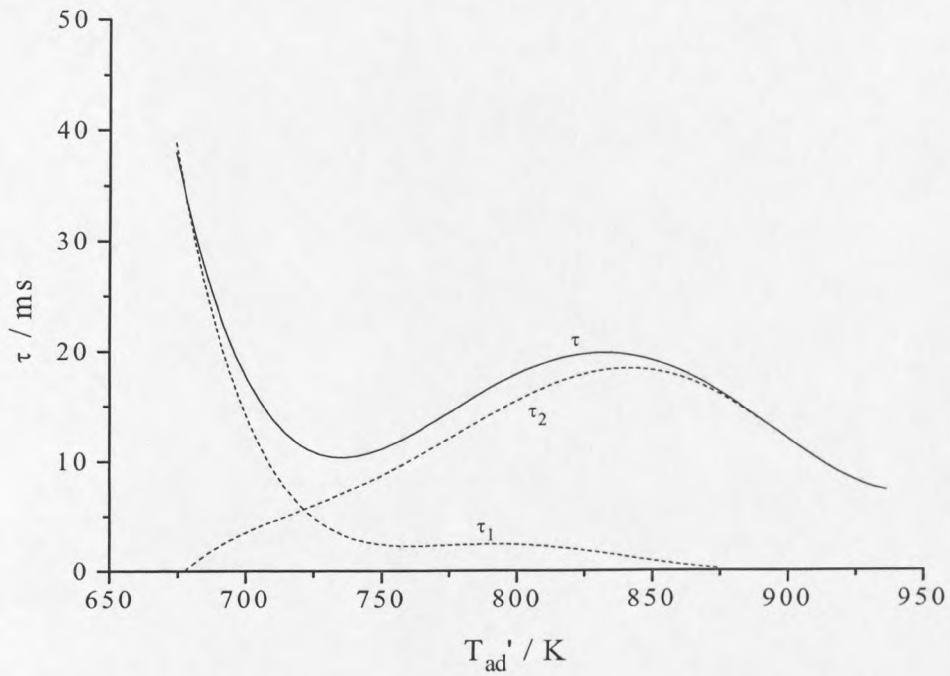

Figure 4.3 The relationship of the duration of the first and second stages in the overall ignition delay for n-pentane autoignition in the RCM.

The existence of a minimum compressed gas temperature for the occurrence of autoignition is an inevitability of the non-adiabaticity of the system and is manifest in the experiments as the ignition delay approaching an infinite duration asymptotically as T_{ad}' decreases.

4.2.2 The effect of changes of compressed gas density

The effect of an increased compressed gas density of the fuel-air mixture on the ignition delay has also been studied to a limited extent, as shown by the variation of the total ignition delay for 2-methylpentane (Table 4.3) and n-pentane (Fig. 4.4). The background is as follows. For an ideal gas,

$p_c V = nRT_c$,

from which the molar density (n/V) is given by,

$$n / V = p_c / RT_c \qquad (4.1)$$

By increasing the initial pressure, p_i, the compressed gas pressure achieved, p_c, is also increased, thereby raising the molar density of the gaseous charge at constant T_c. For example, at an initial pressure of 0.033 MPa and initial temperature of 324 K, compression of a 2-methylpentane-air mixture at a compression ratio of 11:1, gives a compressed gas pressure, p_c of 0.88 MPa, which corresponds ideally to T_{ad}' = 773 K. Thus,

$n / V = (0.88 \times 10^6 \text{ Pa}) / (8.314 \text{ J K}^{-1} \times 773 \text{ K}) = 136.9 \text{ mol m}^{-3}$

By increasing the initial reactant pressure to 0.037 MPa a higher compressed gas pressure (0.97 MPa) but a similar core gas temperature (775 K) is attained. Therefore,

$n / V = (0.97 \times 10^6 \text{ Pa}) / (8.314 \text{ J K}^{-1} \times 775 \text{ K}) = 150.5 \text{ mol m}^{-3}$

Total ignition delay measurements were recorded for 3 mixtures of 2-methylpentane in air ($\phi = 1.0$) at two different compressed gas densities over the range $770 < T_{ad} < 810$ K. As shown in Table 4.2. The compressed gas temperature and the CR remain virtually constant (11(±0.1):1) but the final pressure increases. The associated increase in concentration has the effect of decreasing the total ignition delay throughout the temperature range 650 - 950 K.

Table 4.2 Ignition delay variation with compressed gas density for 2-methylpentane-air mixtures.

Partial Pressure / mmHg									
2-methyl-pentane	O_2	N_2	Ar	p_i / MPa	T_i / K	p_c / MPa	T_{ad}' / K	n / V	τ / ms
12	114	248	184	0.033	324	0.88	773	136.9	28.8
12	114	248	184	0.037	324	0.97	775	150.4	21.4
12	114	230	202	0.033	324	0.89	781	136.4	25.0
12	114	230	202	0.037	324	0.98	782	150.5	20.4
12	114	178	154	0.033	324	0.91	805	135.8	29.4
12	114	178	154	0.037	324	1.00	804	149.4	21.6

However, the change in concentration does not alter the qualitative features of the results, i.e. the ignition delay curve still exhibits 3 branches, as shown for n-pentane ignition (Fig. 4.4). The variations in the range and extent of the ntc region may arise from the effect of heat losses during the longer ignition delays.

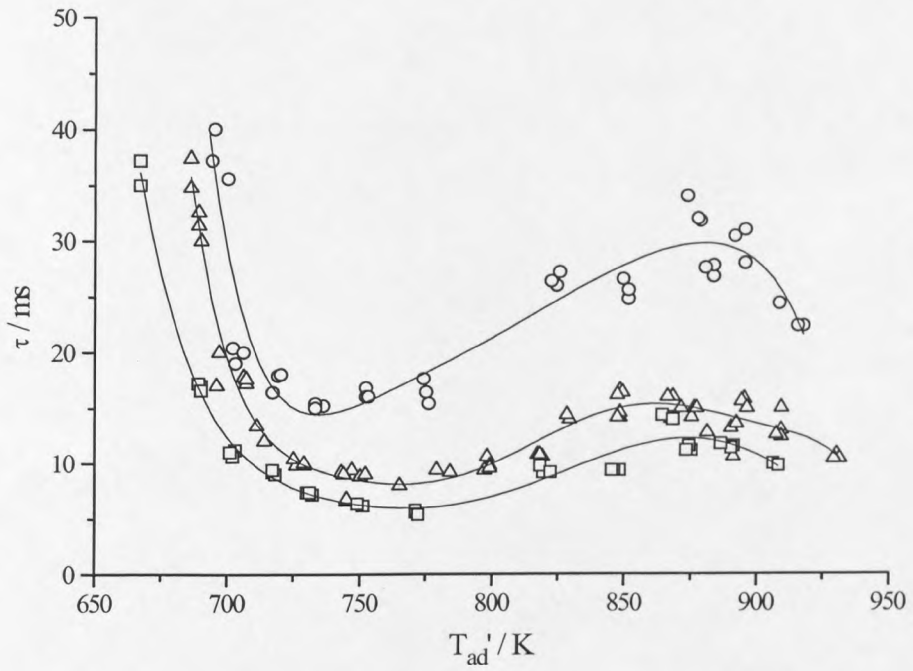

Figure 4.4 Ignition delay variation with compressed gas temperature for n-pentane in air for different compressed gas densities (106.5 (±1.0) mol m^{-3} (O); 131.0 (±1.0) mol m^{-3} (Δ); 157.5 (±1.0) mol m^{-3} (□)).

4.3 Results

Figures 4.5 - 4.8 show pressure-time profiles for the autoignition of selected hydrocarbons at various compressed gas temperatures. Each result provides the necessary information to allow calculation of the adiabatic compressed gas temperature (T_{ad}') and measurement of the ignition delay. Although it is more practical to consider a substantial number of ignition delay data in assessing the relative behaviour of hydrocarbons in the RCM (Section 4.3.1), the pressure-time profiles shown below illustrate some of the characteristics of the ignition delay-compressed gas temperature curves.

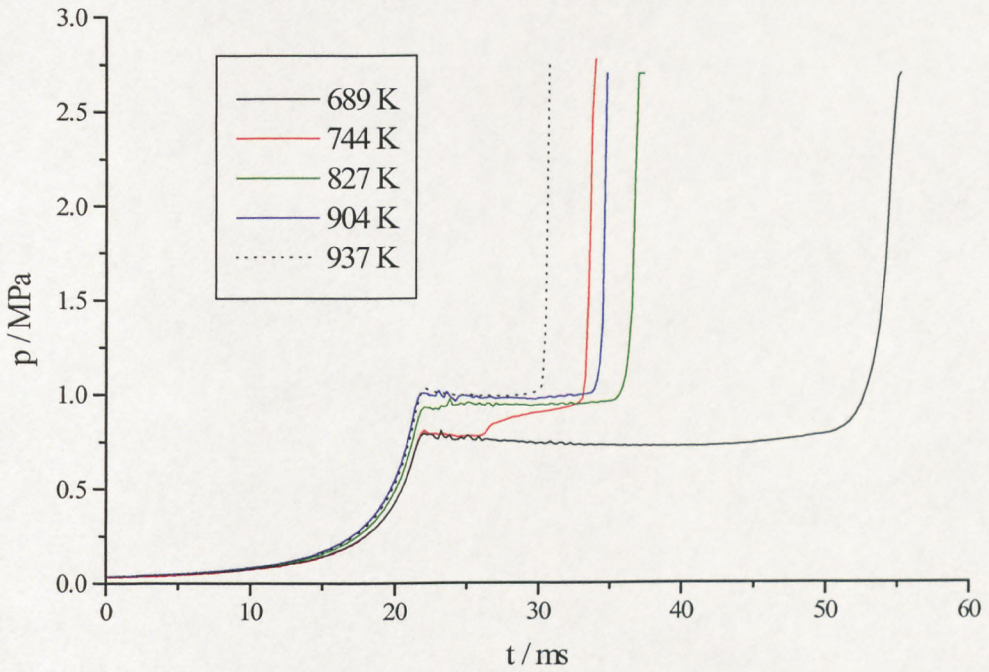

Figure 4.5 Pressure-time profiles for the autoignition of n-pentane at different compressed gas temperatures (T_c).

Figure 4.5 illustrates the role of first and second stages in the overall ignition delay at different compressed gas temperatures as represented by the pressure-time profiles. The graph shows the transition from a long duration single-stage ignition at 689 K to a shorter duration, two-stage ignition following compression to 744 K. As the compressed gas temperature is increased further to 827 K the duration of the first stage

of ignition decreases. However, the second stage duration increases to a greater extent and hence the total ignition delay increases. This is a manifestation of the ntc of the overall reaction rate in this temperature regime. At a higher compressed gas temperature of 904 K the first stage of ignition is no longer evident and a shorter duration, single-stage ignition results. An increase in temperature to T_c = 937 K results in a further decrease in the single-stage ignition delay.

The temperature achieved at the end of the first stage of the autoignition corresponds to the compressed gas temperature above which single stage autoignition occurs. It also represents the temperature at which the maximum in the ntc region of the ignition delay-compressed gas temperature curve occurs (Fig. 4.3).

The contrasting reactivity of the two n-alkanes, n-pentane and n-heptane, during autoignition at different compressed gas temperatures, is illustrated by the pressure-time profiles shown in Figure 4.6. At each of the three temperatures shown, the ignition delay for n-heptane is shorter than for n-pentane. One of the prominent features of this result is the greater extent of pressure increase associated with the first stage of autoignition for n-heptane compared with that for n-pentane. Also, the pressures at the end of compression are not identical for the two n-alkanes, despite choosing the same initial conditions. The n-heptane reaches higher compressed gas pressures than n-pentane. This is a consequence of reaction taking place during the compression stroke (Chapter 3).

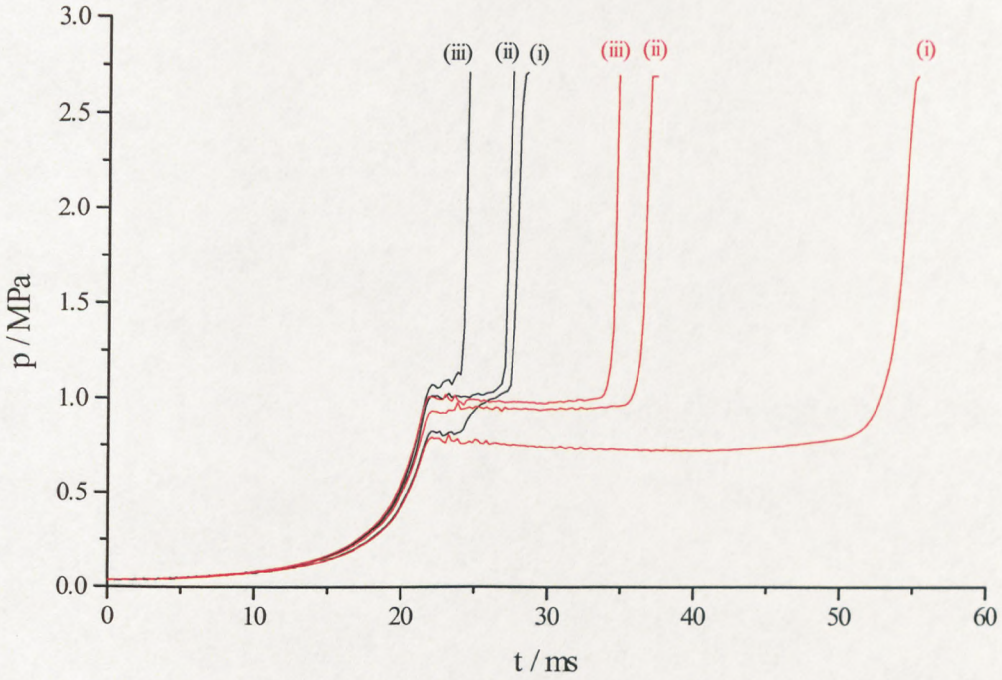

Figure 4.6 Pressure-time profiles comparing the autoignition of n-heptane (black) and n-pentane (red) following compression to different temperatures, (i) 700 K, (ii) 820 K and (iii) 900 K.

In Figure 4.7 the pressure-time profiles for the autoignition of n-pentane and for a PRF 60 mixture following compression to 900 K are compared. The pressure profile for an unreactive mixture is also shown for comparison. The reason for this comparison lies in their similar RON values (n-pentane has a RON of 62.5). The PRF 60 exhibits a shorter ignition delay than n-pentane following compression to 900 K. Closer examination of the pressure profiles and the light output records suggests that the PRF 60 undergoes significant reaction during the compression stroke, whereas n-pentane gives negligible reaction during compression. This may be the key factor in accounting for the different behaviour of the two fuels at this and at other compressed gas temperatures in the range 850-950 K.

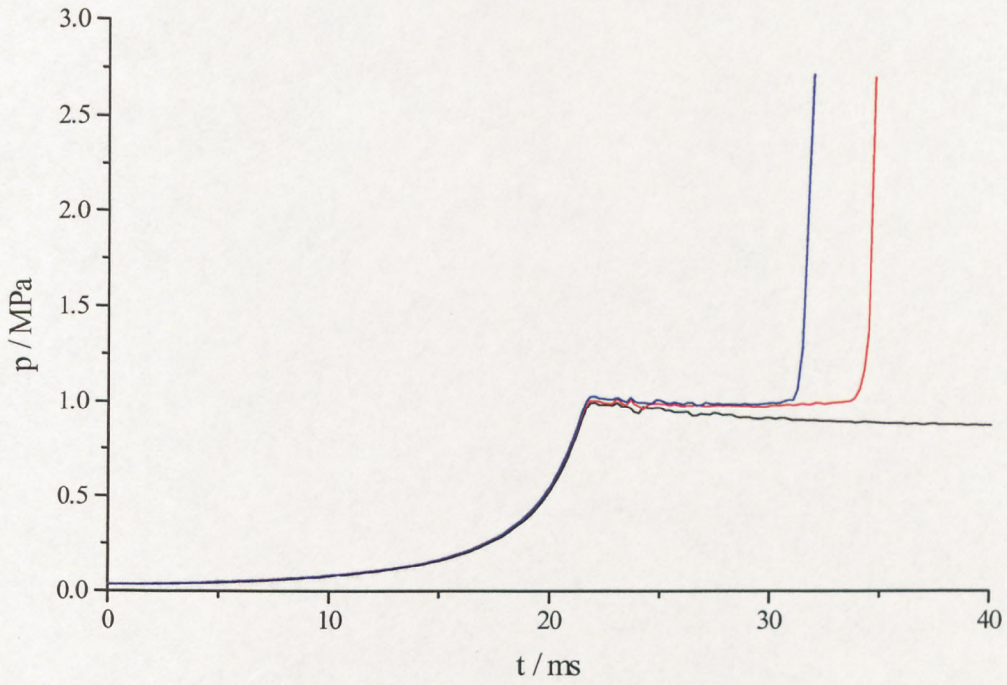

Figure 4.7 Pressure-time profiles for the autoignition of n-pentane (red) and PRF 60 (blue) following compression to 900 K, the pressure profile for an unreactive mixture (black) compressed to 900 K is also shown for comparison.

The pressure profiles for the autoignition of the primary reference fuels for the octane rating scale, n-heptane and i-octane, following compression to 900 K, are compared with that for the autoignition of a PRF 60 mixture under similar compressed gas conditions in Figure 4.8. Normal-heptane has the shortest ignition delay and i-octane the longest ignition delay of the three fuels, with the PRF 60 lying in between the two. To this extent there is a qualitative link between ignition delay and RON.

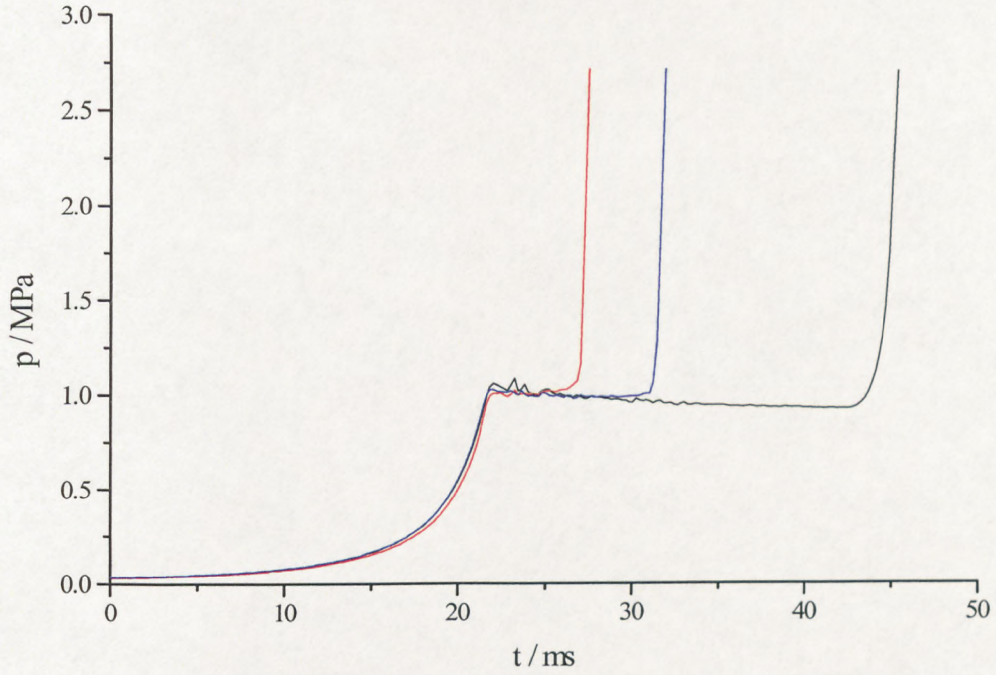

Figure 4.8 Pressure-time profiles for the autoignition of n-heptane (red), i-octane (black) and PRF 60 (blue) following compression to 900 K.

4.3.1 Ignition delay variation with compressed gas temperature

By varying the overall heat capacity of the reactant mixture (as described in Section 2.1) a range of temperatures could be achieved following compression, allowing an investigation of the variation of ignition delay with compressed gas temperature for different hydrocarbons and PRFs, as described below.

The variation of ignition delay, τ, as a function of the adiabatic compressed gas temperature, T_c, is shown in Figure 4.9 for n-heptane, n-pentane and PRF 60 (0.4 n-C_7H_{16} + 0.6 i-C_8H_{18}) over the temperature range 650 - 1000 K and for i-octane over the range 900 - 950 K.

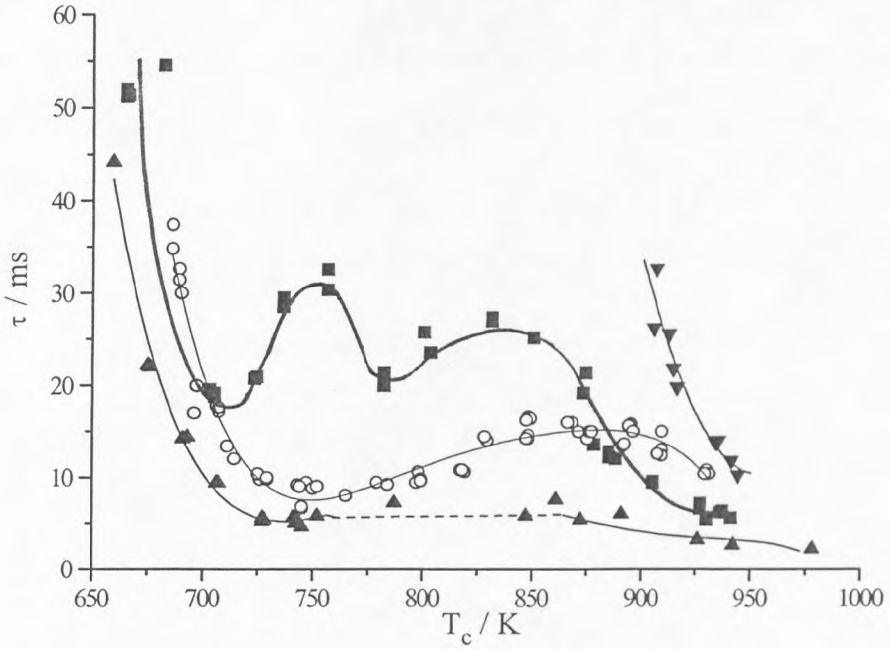

Figure 4.9 Ignition delay variation with compressed gas temperature for n-heptane (▲), i-octane (▼), n-pentane (○) and PRF 60 (■).

The majority of the normal-alkanes exhibit a similar s-shaped curve of ignition delay variation with compressed gas temperature as that shown by n-heptane and n-pentane, where at low ($630 < T_c < 750$ K) and high temperatures ($T_c > 850$ K) the ignition delay decreases monotonically with increasing temperature but in the intermediate temperature regime (750 - 850 K) there is a negative temperature dependence of the overall reaction rate and the ignition delay increases as the temperature increases.

The comparison of PRF 60 and n-pentane is appropriate because the RON for n-C_5H_{12} is 62.5. The ignition delays of these two fuels are most closely matched at the threshold (or minimum) temperature for autoignition and in the high temperature region, $T_c >$ 875 K. The results for i-octane at a compressed gas density of 131 mol m^{-3} extend over the limited range, T_c = 900 - 950 K. This is because, at the lower compressed gas temperatures, the ignition delays are of significantly long duration and heat losses from the chamber in the post-compression period are sufficiently high to cool the reactants and curtail reaction before ignition can fully develop. It is possible to investigate the

lower temperatures by increasing the compressed gas density. This allows the qualitative features of the ignition delay curve to be observed but at an overall reduced ignition delay throughout the temperature range [88].

4.3.2 Alk-1-enes

A comparison of ignition delay variation with compressed gas temperature for n-pentane and hex-1-ene is given in Figure 4.10. It would appear that the comparable RON values (Table 4.3) are vindicated in terms of their similar ignition delays only at the higher compressed gas temperatures (> 850 K).

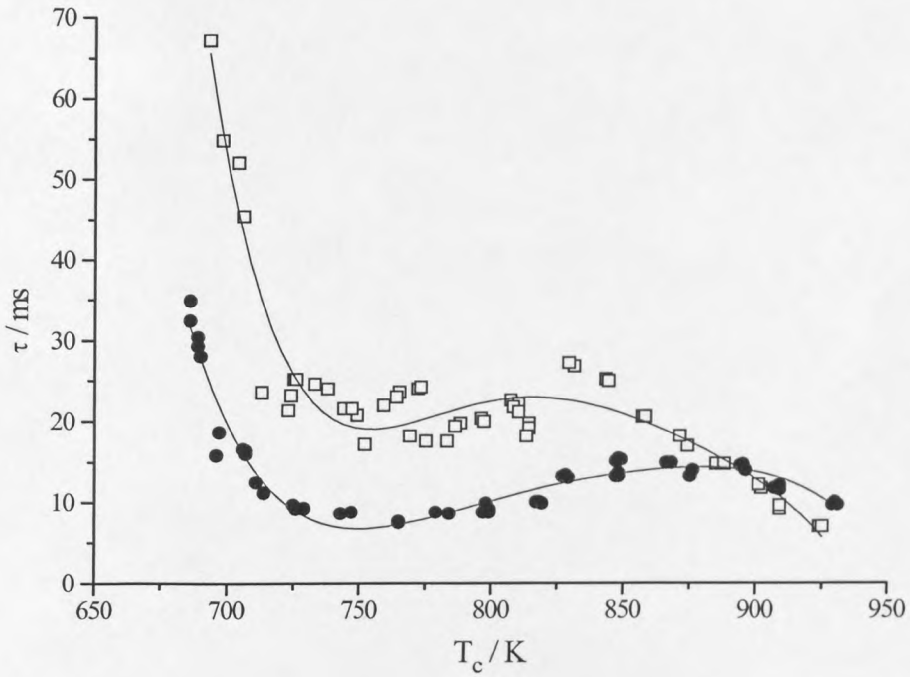

Figure 4.10 Comparison of ignition delay vs. compressed gas temperature for n-pentane (●) and hex-1-ene (□).

Table 4.3 RON values for n-alkanes and corresponding alk-1-enes [11].

Hydrocarbon	RON
n-butane	94
but-1-ene	99
n-pentane	62.5
pent-1-ene	91
n-hexane	25
hex-1-ene	63
n-heptane	0
hept-1-ene	25

4.3.3 Primary Reference Fuel mixtures (PRFs)

Pressure-time profiles illustrating the autoignition of PRFs 60, 70 and 80 following compression to T_c ~ 850 K are shown in Figure 4.11. As the proportion of i-octane in the PRF mixture increases from 60 % to 80 % the total ignition delay increases from 25 ms to 53 ms. The ignition delay for the PRF 70 following compression to 850 K is 36 ms

The ignition delay-compressed gas temperature curves for the PRF mixtures shown in Figure 4.12, illustrate the increasing ignition delay at a given temperature and the increasing threshold temperature as the proportion of i-octane is increased. This is consistent with a decreasing reactivity with increasing proportion of i-octane in a PRF mixture. There is also evidence of a complex variation of ignition delay in the ntc region which falls outside the range of experimental uncertainty. A similar trend has been shown in the numerically predicted ignition delays [152] for a PRF 60 mixture under assumed adiabatic conditions in a closed constant volume following compression (Figure 4.13 and Chapter 6). The existence of this complexity indicates the requirement for a more detailed kinetic appraisal, either by experimental, chemical analysis or by numerical analysis, to interpret the origins of this feature of the ignition delay variation with T_c.

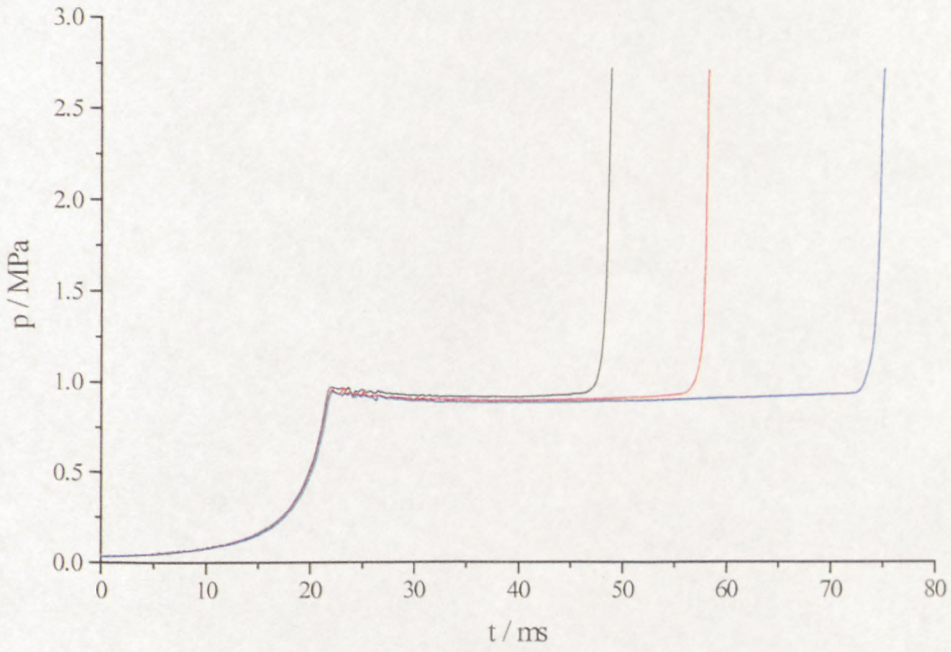

Figure 4.11 Pressure-time profiles illustrating the autoignition of PRFs 60 (black), 70 (red) and 80 (blue) following compression to 850 K.

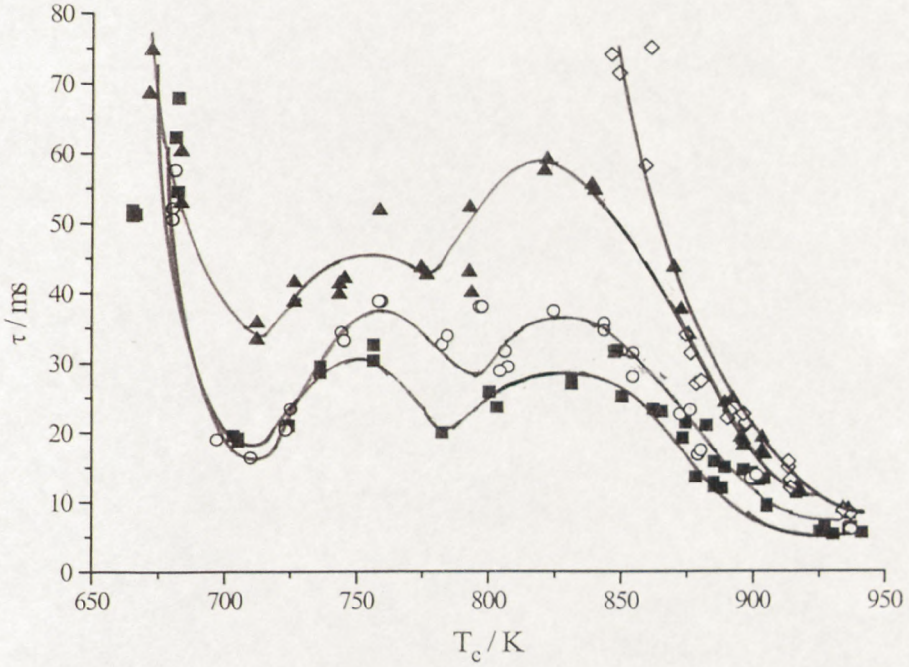

Figure 4.12 Ignition delay variation with compressed gas temperature for the PRFs in the range 60 (■), 70 (○), 80 (▲) and 90 (◊).

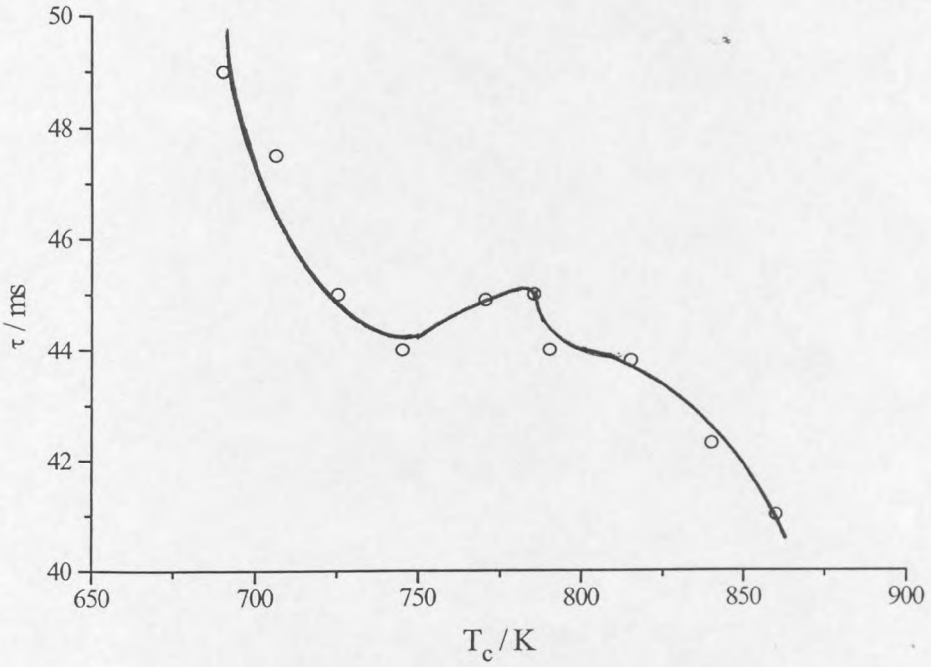

Figure 4.13 Numerical simulation of ignition delay variation with compressed gas temperature for PRF 60 [152].

4.3.4 Ignition delay curves for hydrocarbons of similar RON

The variation of ignition delay as a function of compressed gas temperature for PRF 70 and 2-methylpentane (RON 73) are compared in Fig. 4.14. The ignition delay curves for PRF 80, 3,3-dimethylpentane (RON 81), 2,4-dimethylpentane (RON 83) and 2,2-dimethylpropane (RON 85) are shown in Fig. 4.15. In both sets of results the closest approach to corresponding ignition delays for each fuel occurs at the low and high compressed gas temperatures, with the greatest difference in ignition delay occurring in the intermediate temperature regime (750 - 850 K). Both 2,4- and 3,3-dimethylpentane exhibit an extremely high sensitivity of ignition delay to compressed gas temperature within the ntc region, to the extent that ignition did not occur within a limited temperature range. The virtual absence of an ntc of the ignition delay for 2,2-dimethylpropane is unusual and may be a consequence of a restriction set by the irreversibility of the $RO_2 \rightleftharpoons QOOH$ reaction, as proposed by Hughes et al. [153].

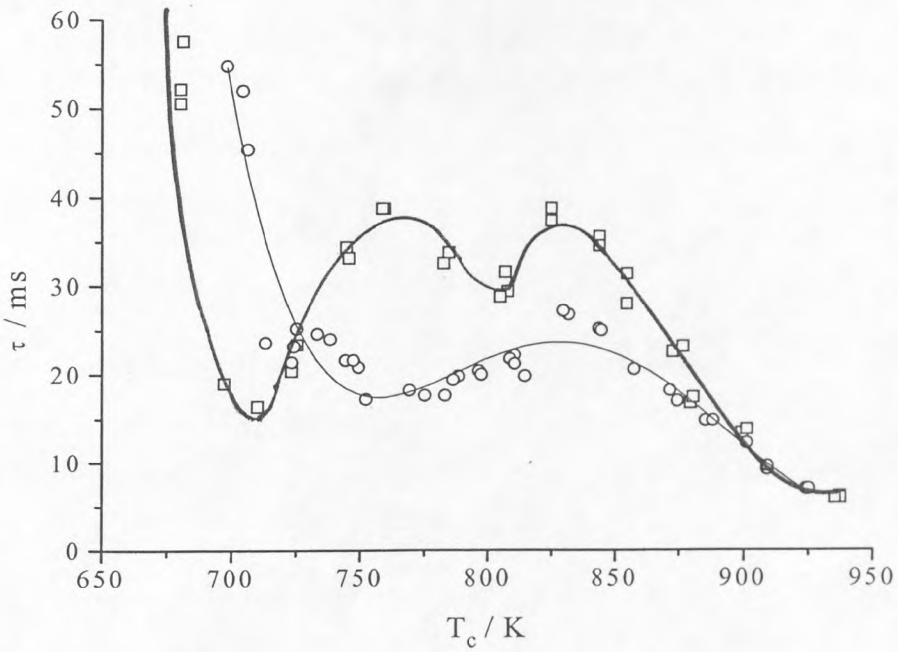

Figure 4.14 Ignition delay variation with compressed gas temperature for PRF 70 (□) and 2-methylpentane (○).

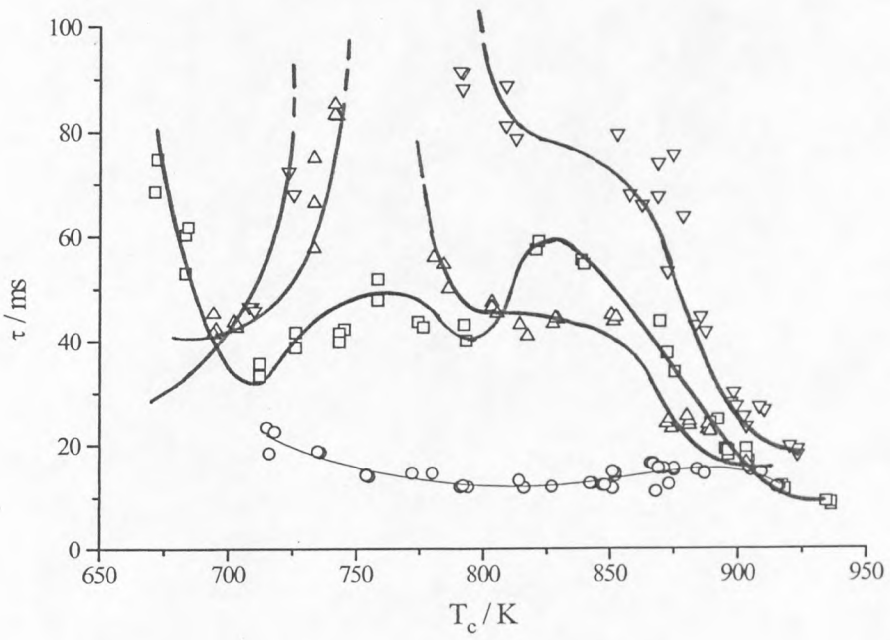

Figure 4.15 Ignition delay variation with compressed gas temperature for PRF 80 (□), 2,4-dimethylpentane (△), 3,3-dimethylpentane (▽) and 2,2-dimethylpropane (neo-pentane) (○).

4.3.5 C_6 hydrocarbons - the effect of molecular structure on reactivity in the RCM

The structure dependent reactivity of hydrocarbons has been described in Sections 1.2 and 4.1.1. The implication is that the short chain, highly branched and cyclic alkanes have a lower reactivity (thus giving longer ignition delays) than the long, linear chain, aliphatic alkanes. This is illustrated by the different ignition delay curves for some of the C_6 hydrocarbons, including several structural isomers of C_6H_{16} (n-hexane (25), 2-methylpentane (73), 2,2-dimethylbutane (92), hex-1-ene (63), cyclohexane (83)) in Figure 4.16 and is also exemplified by their RON values (given in parenthesis).

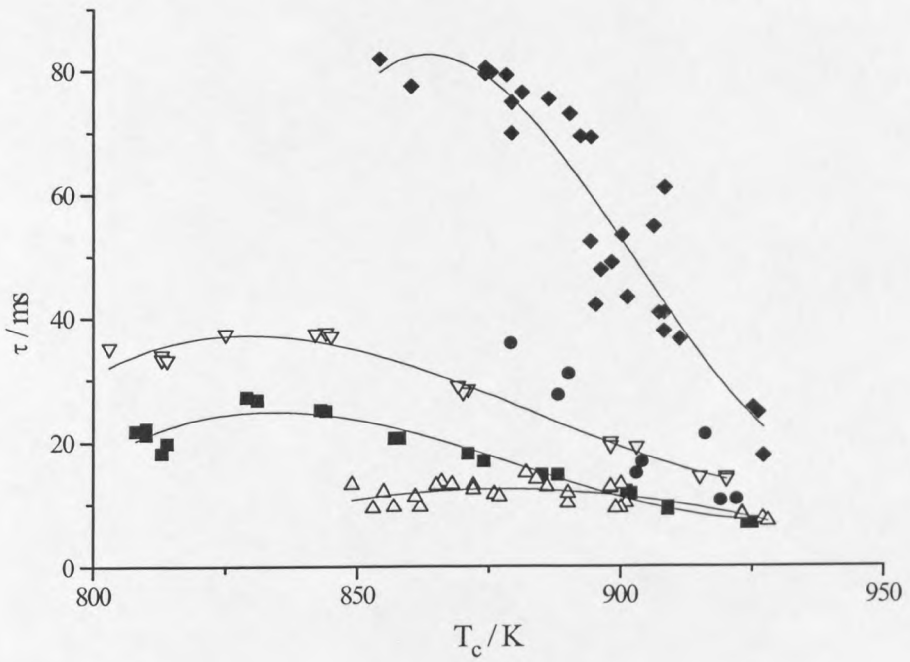

Figure 4.16 Structure dependent reactivity - Ignition delay variation over the temperature range 800-950 K for the C_6 hydrocarbons:- n-hexane (Δ); 2-methylpentane (▽); 2,2-dimethylbutane (♦); hex-1-ene (■); cyclohexane (●).

4.3.6 The relationship between ignition delay and RON

Figure 4.17 illustrates the relationship between ignition delay following compression to 900 K and the RON for selected hydrocarbons and PRF mixtures. To obtain the ignition delay at 900 K it was necessary to measure the ignition delay as a function of

compressed gas temperature at least over the range 860 - 940 K. The value of τ at 900 K was then interpolated from the curve. The error limits include the accuracy of the interpolation and the scatter of experimental results at that temperature. In general, the errors become larger as the value of RON increases, due to an increasing sensitivity of ignition delay to temperature in the high temperature region (see Fig. 4.4).

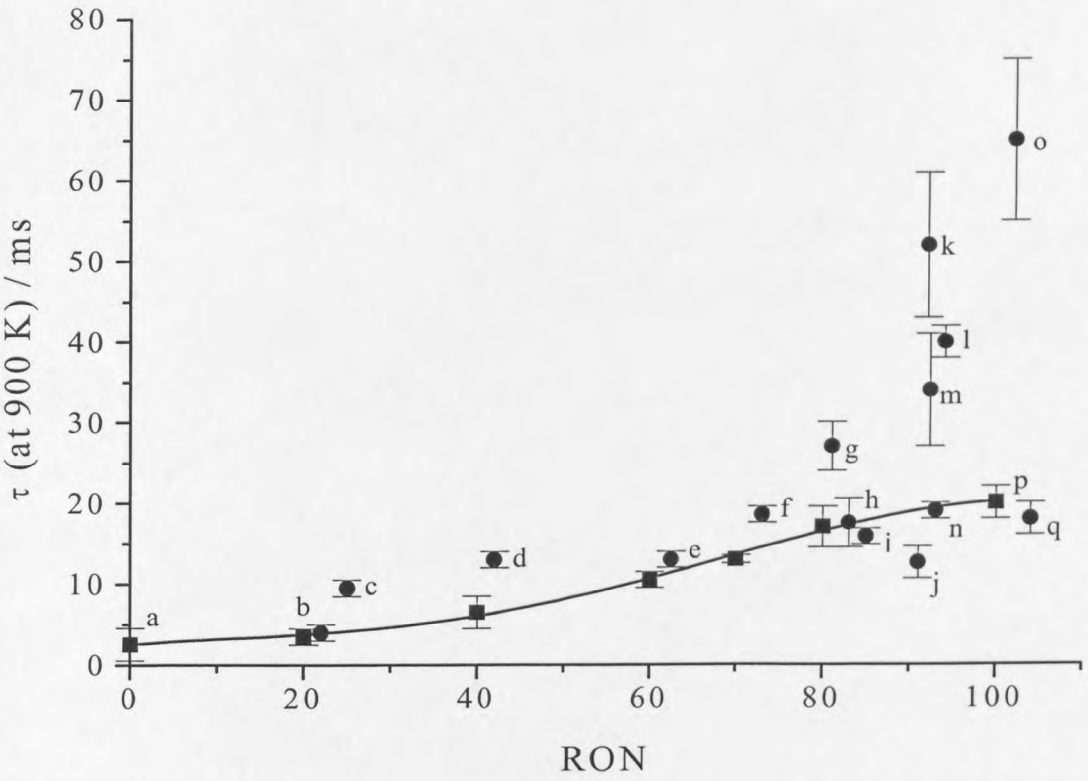

Figure 4.17 Ignition delay at T_c = 900 K as a function of RON for all the compounds studied, PRF mixtures (■) and single component hydrocarbons (●). See Table 4.4 for key to symbols.

The results shown graphically in Fig. 4.17 are also tabulated in Table 4.4, from which the symbols may also be identified. The CCR of each fuel studied, as reported by Lovell [11] and the corresponding RON are also given in Table 4.5.

Table 4.4 Performance of single component alkanes and PRF mixtures.

Fuel			RON [11]	CCR[b] [11]	t_i (± s.d.) / ms at T_c = 900 K (this work)
PRF	Hydrocarbon	Symbol[a]			
0	n-heptane	a	0	3.0	2.6 (2.0)
	2-methylheptane	b	22	3.3	4.0 (1.0)
20			20		3.5 (1.0)
	n-hexane	c	25	3.3	9.5 (1.0)
40			40		6.5 (2.0)
	2-methylhexane	d	42	3.7	13.0 (1.0)
60			60		10.5 (1.0)
	n-pentane	e	62.5	4.0	13.0 (1.0)
70			70		13.0 (0.5)
	2-methylpentane	f	73	4.3	18.5 (1.0)
80			80		17.0 (2.5)
	2,2-dimethylpropane	i	85	4.8	15.8 (1.0)
	2.4-dimethylpentane	h	83	4.9	17.5 (3.0)
	3,3-dimethylpentane	g	81	5.0	27.0 (3.0)
90			90		19.5 (4.0)
	n-butane	l	94	5.5	40.0 (2.0)
	2-methylbutane	m	92.3	5.7	34.0 (7.0)
	2,2-dimethylbutane	k	92	6.0	52.0 (9.0)
	2,2-dimethylpentane	n	93	6.0	19.0 (1.0)
	2,3-dimethylpentane	j	91	6.2	12.6 (2.0)
100	2,2,4-trimethylpentane	p	100	7.3	20.0 (2.0)
	2-methylpropane	o	102	8.0	65.0 (10.0)
	2,3-dimethylbutane	q	104	9.0	18.0 (2.0)

[b] 600 rpm GM engine; Air 310 K; Jacket 373 K; Spark for Max. Power; Mixture Ratio for Max. Knock.

[a] see Figure 4.17

4.4 Discussion

4.4.1 Single and two-stage autoignition and the dependence on compressed gas temperature (T_c)

In general, the autoignition of alkanes develops in two stages at low compressed gas temperatures (< 850 K) and in a single stage at higher compressed gas temperatures (> 850 K). For reactants of low or intermediate reactivity, e.g. n-pentane, the two-stage characteristic persists throughout the ntc region and the maximum ignition delay in the ntc region occurs at the compressed gas temperature equal to the temperature achieved at the end of the first stage. For the highly reactive fuels, such as n-heptane, the first

stage of two-stage ignition can occur in the final stages of the compression stroke [141], resulting in apparent single-stage ignition. For n-pentane, and several other shorter chain hydrocarbons, the low temperature branching reactions are not sufficiently vigorous to cause significant heat release within the time-scale available during the final stages of the compression stroke, as discussed in Chapter 3. The PRFs 60 and 70 behave in a similar way to n-heptane but with less vigorous first stage chemistry occurring during the compression stroke, the rate and extent of reaction being equivalent to that for a lean n-heptane-air mixture. This reactivity during compression and its effect on the overall ignition delay variation with temperature is a characteristic of several of the fuels studied in this work. The occurrence of first-stage reaction during compression and its influence on the overall ignition delay has been described in Chapter 3 and will be discussed in further detail in Chapter 6.

4.4.2 Origin of the negative temperature dependence of ignition delay

The ignition delay of a fuel-air mixture following compression to a given temperature and pressure is a consequence of how the overall reaction rate responds to the temperature and pressure reached at the end of compression and in the post-compression period, where heat losses can also be influential. There is a supplementary effect of reaction which may take place in the compression stroke, as identified in Chapter 3. There is also an additional influence in the post-compression period, where thermal feedback from the exothermic reaction can affect the prevailing temperature and pressure in the combustion chamber of the RCM.

Nevertheless, it is reasonable to use the temperature, reactant density and composition at the end of compression as reference conditions for studying how the ignition delay is affected by a variation in these conditions. In most of the work reported in this chapter, compressed gas density and composition have been fixed and the value of T_c has been varied.

Although there are qualitative differences for all of the fuels or fuel mixtures studied in this work, there is evidence for a negative temperature dependence of the ignition delay

over a certain range of compressed gas temperature. In terms of the detailed structure of the ignition delay, as shown in Fig. 4.3, the ntc is attributable to the net effect of a decrease in τ_1 and a lengthening of τ_2 as T_c is raised. The relationship between the duration of τ_1 and τ_2 must be linked, not only to the reactant temperature which is attained in τ_1, but also to the "chemical conditioning" of the system with respect to intermediate product compositions at the end of τ_1 (including free radical species and molecular intermediates). Some insight into the nature of the species involved can be obtained from chemical analyses, but how the interplay between chemical and thermal effects works is best explored by numerical methods.

A link between a diminishing temperature at the end of τ_1, with an increase in T_c, may be traced to the kinetic origins of the ntc itself. As outlined in Chapter 1, the switch is from low temperature, ketohydroperoxide forming reactions, giving degenerate branching to essentially non-branching reactions (at T ~ 850 K), as a result of the shift of the $R+O_2 \rightleftharpoons RO_2$ equilibrium to the left-hand-side.

If the initial temperature (T_c in this case) is very low then significant yields of the peroxide may be formed. However, when T_c is raised, even though the formation of RO_2 and hence peroxides may still be favoured, the proportion of these compounds must be diminished because the fraction of the alkyl radicals which give rise to RO_2 falls. The further complications that may arise as a result of reaction taking place during the compression stroke have been illustrated in Chapter 3.

4.4.3 Structure related reactivity

The Primary Reference Fuels

The Primary Reference Fuels for the octane rating scale, n-heptane and i-octane, exhibit very different reactivity in terms of their tendency to cause engine knock in a CFR engine under standard operating conditions. The difference in reactivity of the two fuels in terms of their ease of autoignition in the RCM is also evident from the results presented in this chapter. The high reactivity of n-heptane is manifest in very short first

and second stage of autoignition development times. However, i-octane exhibits no ignition at low compressed gas temperatures, despite there being some first stage chemistry under the conditions achieved in the Leeds RCM (Fig. 3.7). The failure of ignition is a result of heat losses which occur during the very long duration of τ_2 for i-octane, to the extent that the high temperature branching reactions leading to the second stage of ignition cannot be established. This comparison may represent an extreme case of the point of principle described in 4.4.2.

The different behaviours are a consequence of the different molecular structures of the two compounds (Sections 1.5 and 4.2). The long, uninterrupted chain of n-heptane renders the internal isomerisation reactions which lead to vigorous chain-branching in the low to intermediate temperature regime much more facile than for the small, highly branched structure of i-octane (reactions 16 and 17).

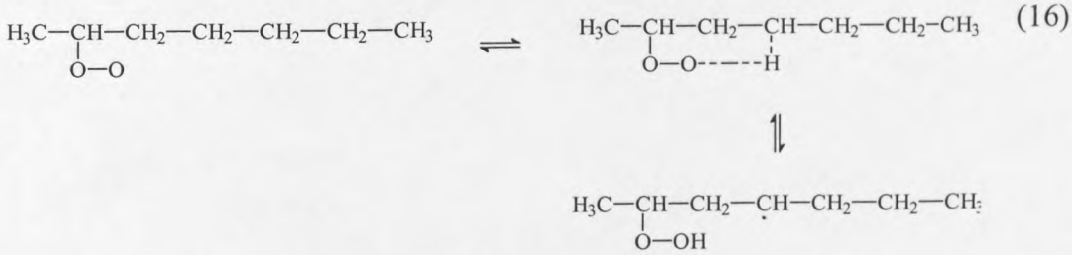

(16)

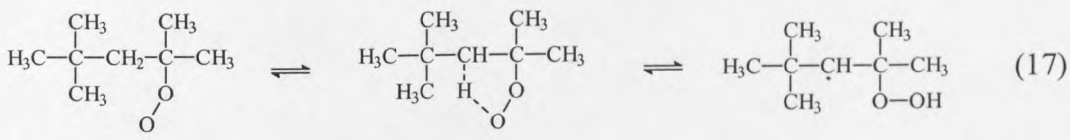

(17)

Lignola et al. [33] proposed that the differences in reactivity between n-heptane and i-octane were due to the amount of acetaldehyde that was formed during alkylperoxy radical isomerisation and decomposition. However, it is now more commonly accepted that differences in reactivity of higher carbon number alkanes may lie in constraints of the alkyldiperoxy radical (O_2QOOH) rearrangement and decomposition. For the alkanes of low carbon number ($n < 4$) the inability to undergo spontaneous ignition at very low temperatures may be attributed to the existence of very high energy barriers associated with alkylperoxy radical isomerisation and the failure of diperoxy species to be formed.

There is ample experimental evidence for the formation of alkyldihydroperoxides, especially from the longer chain n-alkanes [154,155] but the rate of chain branching which arises from the homolysis of molecular hydroperoxides, regardless of whether they are alkylhydroperoxides or alkyldihydroperoxides, is too slow to account for the short duration of ignition delays in high pressure gases at low temperature. There is also experimental evidence for the formation of alkylketohydroperoxy radicals, illustrated here for the pentylketohydroperoxy radical,

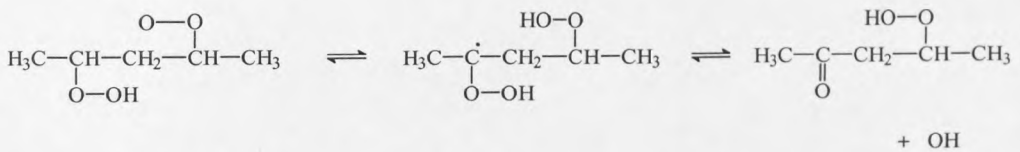

(18)

Similar rearrangements may also occur involving an H atom other than that at the hydroperoxy site, but in these circumstances the product is not a molecular species, but a free radical which decomposes via a branching reaction, e.g.,

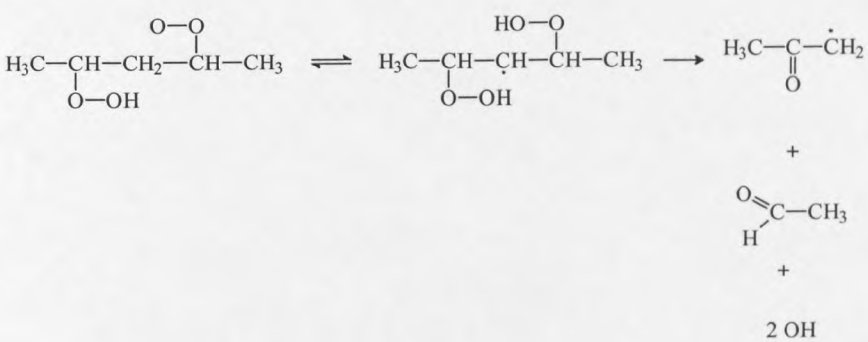

(19)

This is likely to occur with an activation energy which is appreciably lower than that for molecular hydroperoxide decomposition, and typically that of the energies involved with the decomposition of QOOH. These particular mechanisms can satisfactorily account for the high reactivity of long chain n-alkanes [156]. It is now commonly accepted that the ketohydroperoxide is the chain-branching agent, the formation and decomposition of which results in a net production of 2 hydroxyl radicals and vigorous exothermic chain branching. This step continues to be an important inclusion in reduced models of hydrocarbon oxidation [96,97,137].

Other Alkanes

It has been well established that the molecular structure of a fuel contributes to its overall reactivity via the rate of RO_2 and O_2QOOH isomerisation. Let us compare the reactivity of two C_6 isomers (Fig. 4.11), n-hexane and 2,2-dimethylbutane. The ignition delay curve for the straight chain alkane is characteristic of a "reactive fuel", exhibiting short ignition delays, low threshold temperature for autoignition and negligible ntc. In contrast to this, the branched chain alkane exhibits relatively long ignition delays, and does not give low temperature autoignition, both characteristics of a low reactivity fuel. The distinctive behaviour of the two isomers can be rationalised in terms of their different molecular structures.

The more facile isomerisation of RO_2 for n-hexane via 5, 6, 7 or 8-membered ring transition states renders it a more significant contributor to the subsequent chain-branching, exothermic reaction and OH radical production. The linear alkylperoxy radical undergoes internal H-atom abstraction involving predominantly 2° C-H transitions. Typical activation energies for this internal H-atom abstraction reaction are given in Table 4.5. The result of a 1,5 transition (where position 1 refers to the O atom and the H-atom is abstracted from position 5) from a secondary carbon position (commonly referred to as a 1,5s transition) is shown in reaction (20).

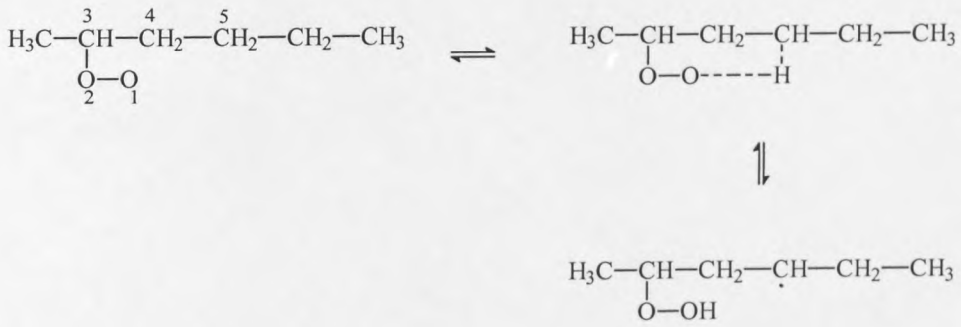

(20)

The dimethyl-substituted isomer, however, results in a more compact and highly strained cyclic transition state during the internal H-atom abstraction which involves exclusively 1° C-H bond fission in either a 1,5p or a 1,6p (21) transition.

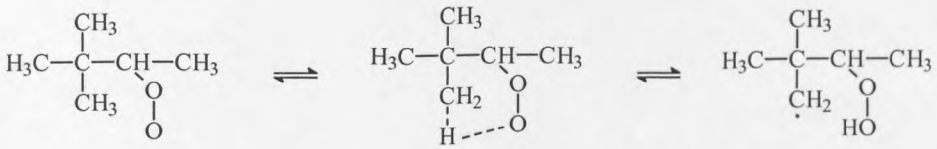

(21)

Table 4.5 Activation energies for the internal H-atom abstraction reaction via a cyclic transition state, for an RO_2 species with the peroxy group attached to a secondary carbon.

Number of atoms in ring	Type of internal H-atom abstraction reaction	Activation Energy / kJ mol^{-1}	
		[140]	[137]
5	1,4p	124.4	155.1
	1,4s	116.8	137.5
	1,4t	106.3	
6	1,5p	100.1	122.7
	1,5s	92.7	108.7
	1,5t	82.5	
7	1,6p	88.3	104.0
	1,6s	81.0	108.7
	1,6t	68.7	
8	1,7p	100.1	92.5
	1,7s	92.7	
	1,7t	82.5	

The higher reactivity of straight chain alkanes compared with branched-chain alkanes can also be explained by the formation and decomposition of the ketohydroperoxide. The straight chain alkane tends to result in the net production of 2 OH radicals (22), whereas the branched alkanes result in OH and HO_2 (23). As illustrated below for n-hexane (22) and 2,3-dimethylbutane (23).

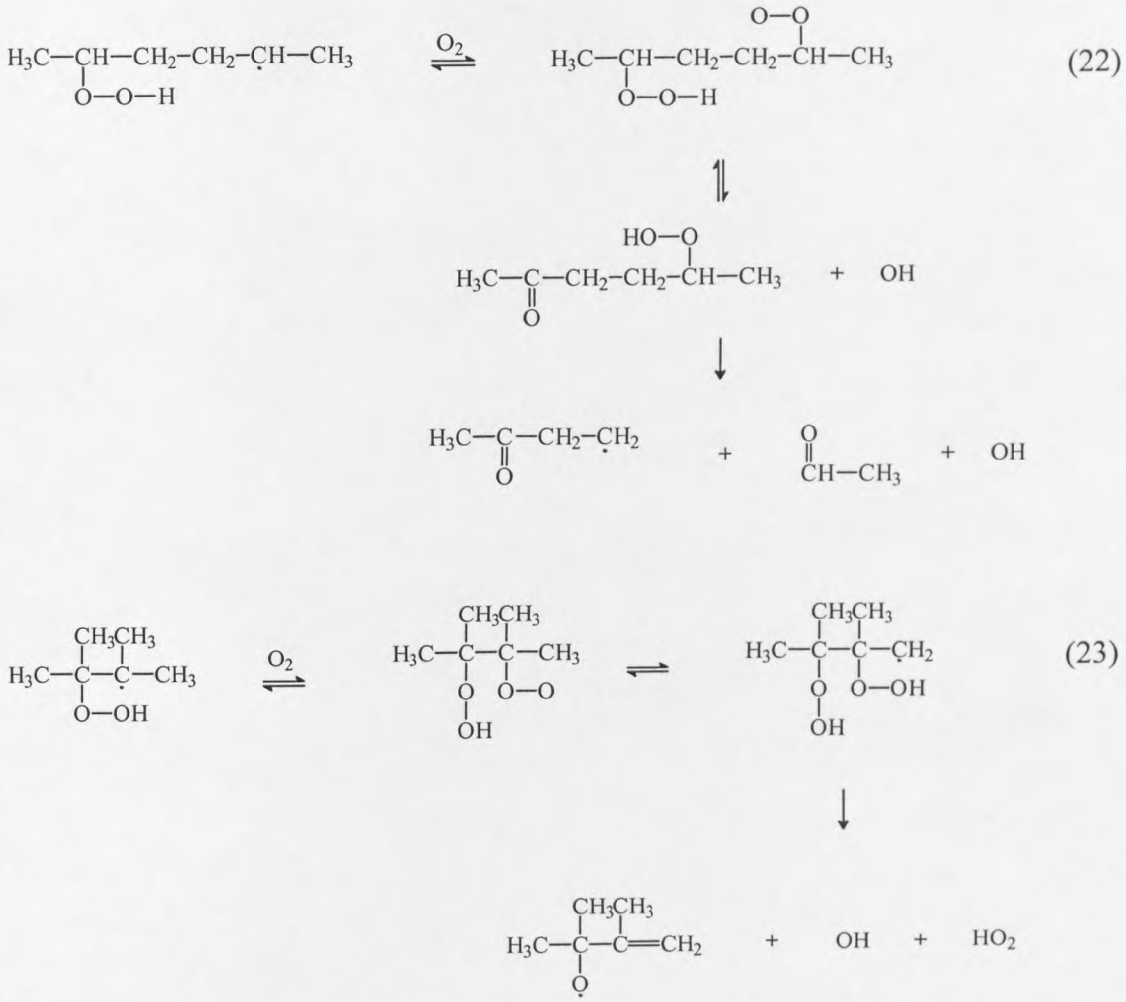

(22)

(23)

The much more restricted activity of 2,2- and 2,3-dimethylbutane means that they would have to be raised to a higher temperature than n-hexane to achieve the same overall rate of low temperature oxidation. There is then a counter effect of the displacement of the R/RO_2 equilibrium towards the dissociation. Correspondingly, in an engine, 2,2- and 2,3-dimethylbutane would lack the rapid low temperature paths to OH production and chain-branching exhibited by n-hexane under similar conditions. This different low temperature reactivity supports the different RON values of the three fuels; n-hexane with RON 25, 2,2-dimethylbutane with RON 92 and 2,3-dimethylbutane with RON 104.

Neo-pentane

Neo-pentane oxidation is anomalous amongst the normal alkanes (C_4-C_8), in that the $RO_2 \rightleftharpoons QOOH$ reaction has been regarded to be irreversible [153]. However, recent numerical simulations have maintained the reversibility of the equilibrium [157], but with a more significant rate of forward reaction. Even with increased compressed gas density the ntc region could not be distinguished for neo-pentane autoignition in the RCM. This might be explained by the assumption that the reverse reaction to form the alkylperoxy radical, and hence the subsequent non-branching pathway via the dissociation of RO_2 is not favourable. Only one type of alkyl radical is formed by the H-abstraction from neo-pentane and because all the C-H bonds are equivalent, only one type of $RO_2 \rightleftharpoons QOOH$ reaction is possible. Neo-pentylperoxy radicals undergo a 1,5p H-abstraction and isomerisation, as follows,

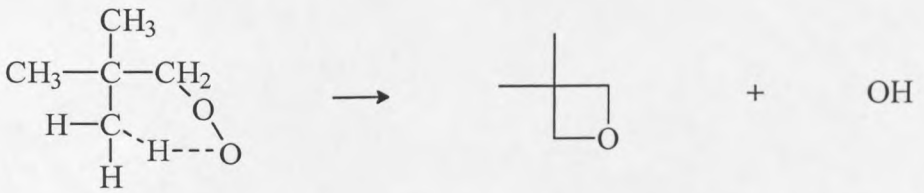

(24)

,

so forming 2,2-dimethyloxetan and an OH radical by ring closure. Also possible is the formation of formaldehyde, 2-methylpropene (or iso-butene) and an OH radical (25).

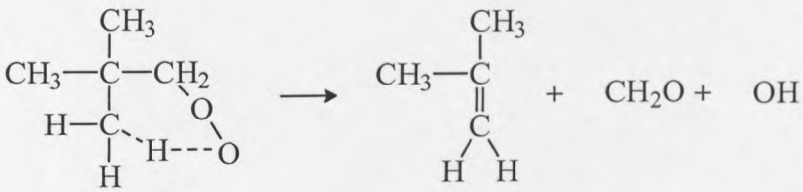

(25)

The neo-pentyl radical cannot react with O_2 to form a conjugate alkene and HO_2 because the adjacent C atom is a quaternary carbon. It can be postulated that the origin of the lack of ntc for the oxidation of neo-pentane in the low to intermediate temperature regime lies in the competing propagation and branching pathways of the QOOH radical.

Sensitivity analyses of the n-heptane oxidation system [140] have illustrated the significant sensitivity of ntc behaviour to the reaction

$QOOH \rightleftharpoons AB + HO_2$.

Since this reaction is not possible in the low to intermediate temperature oxidation of neo-pentane, this could provide a suitable explanation for the lack of ntc behaviour.

Alkenes

The autoignition chemistry of alkenes has been studied extensively in a motored engine [151] and the contrasting behaviour of alkanes under similar operating conditions examined. One obvious distinction lies in the initiation step of the oxidation mechanism. Alkanes tend to undergo H-atom abstraction by a radical or molecular oxygen, whereas alkene autoignition is controlled by radical addition across the double bond. The results showed that alkenes require a higher compression ratio in order to initiate chemical activity and to induce autoignition. There was also evidence in support of the previously encountered lack of ntc behaviour for alkenes [94]. A previous investigation of the autoignition of a binary mixture of n-heptane and hept-1-ene (RON 0 and 50 respectively) has been performed using an RCM [158]. Results indicate that the allylic radical + O_2 reaction is less exothermic than the alkyl + O_2 reaction and the resulting peroxy radical can isomerise less easily due to restriction to rotation by the π-bond. The present study has illustrated the reactivity of hex-l-ene in relation to n-pentane (Fig. 4.10). The results suggest that the alk-1-ene with n carbon atoms exhibits a similar reactivity to the n-alkane with (n-1) carbon atoms in the higher compressed gas temperature region.

The alkenes follow a unique oxidation pathway in the low to intermediate temperature regime (dictated by their unique structure) which differs distinctly to that of the corresponding alkane. The first possibility is the non-branching route to a carbonyl species and an alkyl radical (26). Alternatively, at high pressure, the addition of molecular oxygen and subsequent carbon-carbon bond fission to form two carbonyls and an OH radical (27) is favoured.

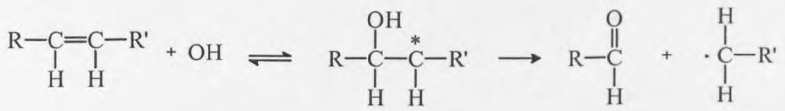

(26)

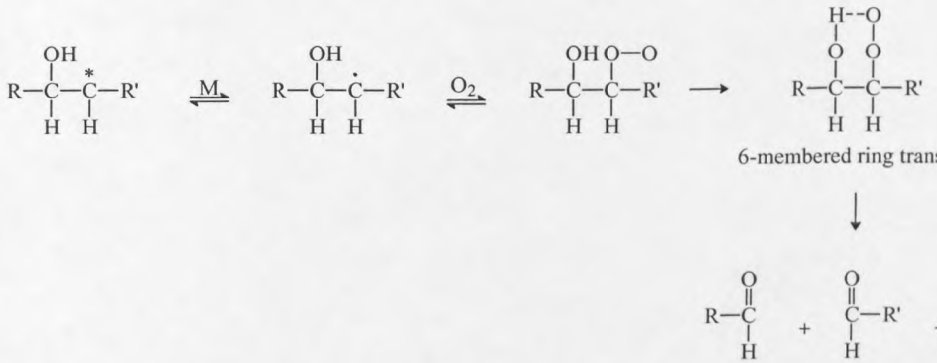

(27)

4.4.4 Ignition delay and octane rating - what is the relationship?

The most satisfactory temperature regions in which precise values of ignition delay would be obtained for comparisons to be made between different fuels are where the temperature sensitivity is at a minimum, i.e. at the maxima or minima either side of the ntc region. Nevertheless, a reference temperature of 900 K was chosen for the following reasons:-

i. the end-gas temperature under knocking conditions for fuels of high RON in a CFR engine has been calculated and is approximately 900 K [144]

ii. as illustrated in Figs. 4.5, 4.9 and 4.10, the closest correlation between fuels of similar RON appears to be in the range $850 < T_c < 950$ K

iii. in the RCM it was not possible to cause fuels of high RON to autoignite at $T_c < 850$ K at the reactant density employed in these experiments.

In general, the autoignition delays at 900 K exhibit an increase as the RON increases and for isolated cases there is reasonable quantitative agreement with the equivalent PRF mixture. However, the discrepancies are greatest in the range of RON most pertinent to combustion in s.i. engines (RON > 90). An explanation for the discrepancies may lie in the extent of reaction during the compression stroke, as described in Chapter 3. Both n-C_7H_{16} and i-C_8H_{18} are capable of a significant extent of

fuel consumption before the end of compression, whereas negligible reaction of n-C_5H_{12} occurs under similar conditions.

The performance of the PRF mixtures may be governed, ultimately, by the comparatively high reactivity of both n-heptane and i-octane giving some reaction during the compression stroke. From these results there appears to be little foundation for the use of autoignition delay as a quantitative basis for the comparison of the octane number of fuels at any compressed gas temperature in the range 700-900 K. There is, however, some indirect relevance of ignition delays to engine knock prediction, as a basis for the validation of kinetic models which may be used in the prediction of end-gas autoignition in an engine.

In addition to this, a link between the ignition delay in an RCM and the tendency of a fuel to knock in a s.i. engine may be anticipated from the principle that the occurrence of knock in engines depends not only on the temperature achieved just before autoignition, but on the entire temperature history of the end-gas during the compression and firing cycle [159]. In RCMs and in s.i. engines the reactions of RO_2 and QOOH species influence the overall reaction rate for compressed gas temperatures above 850 K, because part of the compression history allows lower temperature chemistry to occur. The variety of primary, secondary and tertiary alkyl radicals which can be formed from a given parent alkane complicates the interpretation of the overall kinetic response to the alkyl/alkylperoxy radical equilibrium and the subsequent reactions. This is most satisfactorily established from numerical simulations based on comprehensive chemical kinetic models, or from reduced kinetic models which account for molecular structure on an *ab initio* basis [160].

There is some indication that a more satisfactory basis for an experimentally measured or numerically predicted correlation to the octane rating scale may be the minimum autoignition temperature (AIT) in a given system, determined in statutory ASTM and CEC (BS 4056) tests. The variation of minimum autoignition temperature (T_{ign}) with number of carbon atoms is shown in Fig. 4.18 for some of the C_3-C_9 hydrocarbons. The

qualitative features appear to be in good agreement with those shown in Fig. 1.2 for the dependence of CCR on number of carbon atoms.

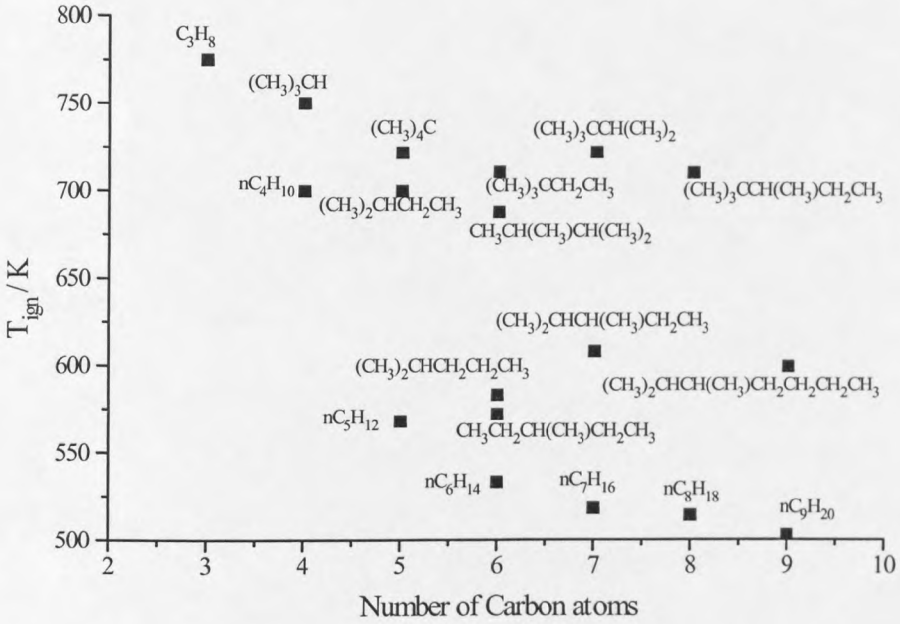

Figure 4.18 Minimum AIT variation with number of carbon atoms.

4.5 The effect of fuel:air ratio on ignition delay

Experiments have been performed to investigate the effect of fuel:air equivalence ratio (ϕ) ((actual fuel:oxidant):(fuel:oxidant for complete combustion)) on the total ignition delay for premixed gaseous n-pentane-air mixtures. The equivalence ratio was varied between 0.5 and 2.0 by varying the proportion of n-pentane in the reactant mixture. The results indicate that as ϕ was increased from 0.5 to 1.0, the ignition delay decreased but there was relatively little influence on ignition delay as ϕ was increased above stoichiometric ($\phi = 1.0$).

4.5.1 Background

Studies of the effect of fuel:air equivalence ratio on the ignition delay characteristics of hydrocarbons are useful in terms of enhancing the fundamental understanding of the phenomenon, they also hold some relevance to the autoignition of lean mixtures in engines under swirl conditions [161] and to the identification of hazardous operating conditions in industrial applications [162]. In addition to the practical applications, the results can also be used in the validation of numerical models [134,163] and so broaden the range of validated conditions.

Previous investigations of the effect of fuel:air ratio on the ignition delay in an RCM have revealed the complexities encountered when comparing results from different experimental systems. The importance of the effect of increasing fuel concentration on the overall heat capacity of the mixture, and hence on the results obtained has been emphasised [116]. The study by Taylor et al. [164] implies that ignition delay decreases as the fuel-air mixture becomes leaner. However, if one considers that the accompanying increase in T_c for a change in ϕ from 0.47 to 1.32 is from 725 K to 813 K, then the comparison is seen to be more complicated. In the present study the effect of increasing fuel concentration on the overall heat capacity of the mixture was compensated for by the preparation of a fuel-oxygen-inert mixture which allowed a range of compressed gas temperatures to be accessed by varying the relative proportion of the inerts, and so a valid comparison could be made.

The rate of pressure rise during the first stage of two-stage autoignition is proportional to the fuel concentration. Figure 4.19 shows the results of an investigation by Levedahl [165] into the effect of ϕ ratio on the rate of pressure rise during the cool flame stage of n-heptane autoignition in an RCM. The measurements at three different compressed gas densities and fuel:air ratios in the range ϕ = 0.25 - 1.5 show that this relationship holds true for lean to stoichiometric mixtures, but for $\phi > 1.0$ no additional increase in the rate of pressure rise was evident.

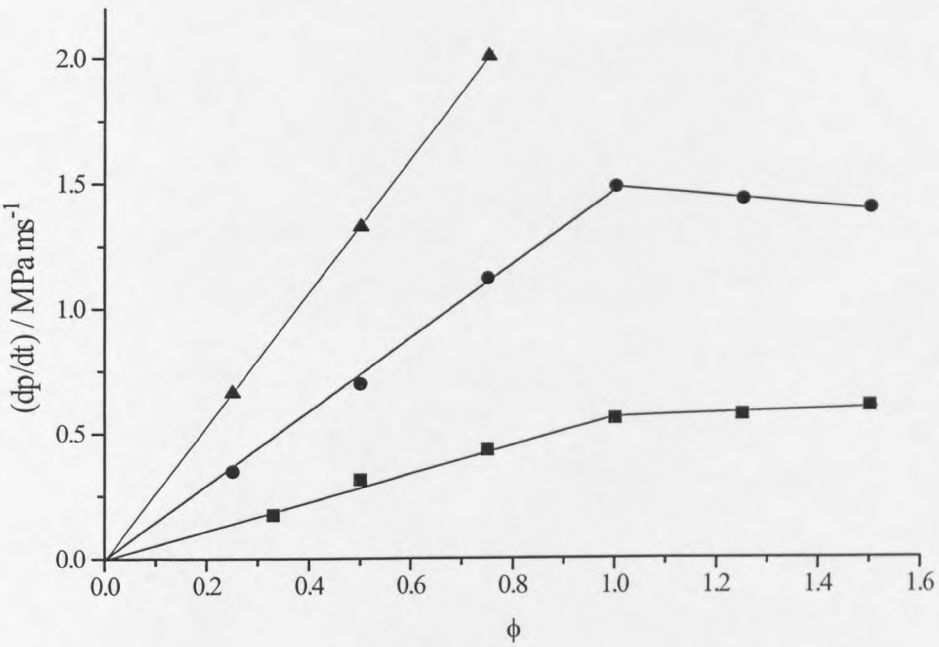

Figure 4.19 Maximum rate of pressure rise during the cool flame stage of the autoignition of n-heptane as a function of fuel:air ratio, at three compressed gas densities (0.288 lb mol ft^{-3}(■), 0.216 lb mol ft^{-3}(●), 0.014 lb mol ft^{-3}(▲)) [165].

In an experimental and numerical investigation of the autoignition of n-butane-air ($0.8 < \phi < 1.2$) in an RCM it was concluded that the autoignition of n-butane-air is inversely proportional to the fuel:air equivalence ratio [134]. It is well established that the autoignition delay is dependent on the experimental conditions of temperature, pressure and the fuel:air equivalence ratio. The results described in this chapter illustrate the effect of equivalence ratio ($0.5 < \phi < 2.0$) on the autoignition delay of n-pentane in an RCM throughout the range of compressed gas temperatures 650 - 950 K.

4.5.2 Results

The results presented in Figure 4.20 illustrate the effect of fuel:air equivalence ratio on the ignition delay of n-pentane following compression to 765 K. As ϕ is decreased from 1.0 to 0.5 the total ignition delay increases from 6.2 ms to 40.8 ms (Fig 4.20 (a)). The effect on the duration of the first stage of autoignition (τ_1) is negligible. However the rate and extent of pressure rise associated with the first stage of autoignition is very strongly affected and consequently the duration of the second stage (τ_2) increases dramatically as the mixtures become more fuel-lean. In addition to the effect on ignition delay, the maximum pressure during ignition and the rate at which it is achieved decreases as the equivalence ratio decreases. This effect of fuel:air ratio on the extent and rate of pressure rise during the hot stage of ignition in the RCM has been reported previously [166].

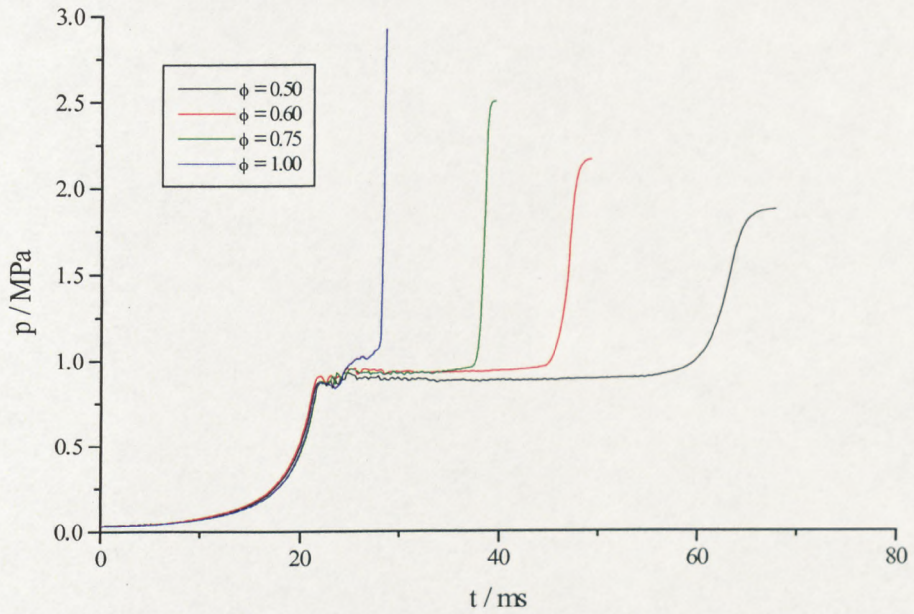

Figure 4.20 (a) Pressure-time profiles for the autoignition of n-pentane in air following compression to 765 (±5) K, for different fuel:air equivalence ratios (ϕ = 0.5 - 1.0).

The pressure-time profiles shown in Figure 4.20 (b) illustrate the effect of increasing fuel:air equivalence ratio in the range $1.0 \leq \phi \leq 2.0$ on the ignition delay of n-pentane

following compression to about 725 K. The pressure profiles indicate a more vigorous first stage of autoignition as the fuel:air equivalence ratio is increased and a shorter duration first stage. This rapid rate of pressure rise associated with the first stage results in the attainment of a high enough temperature and a sufficient radical pool for the development of the second stage of autoignition to proceed after a relatively short delay for the more fuel-rich mixtures compared with the more fuel-lean mixtures.

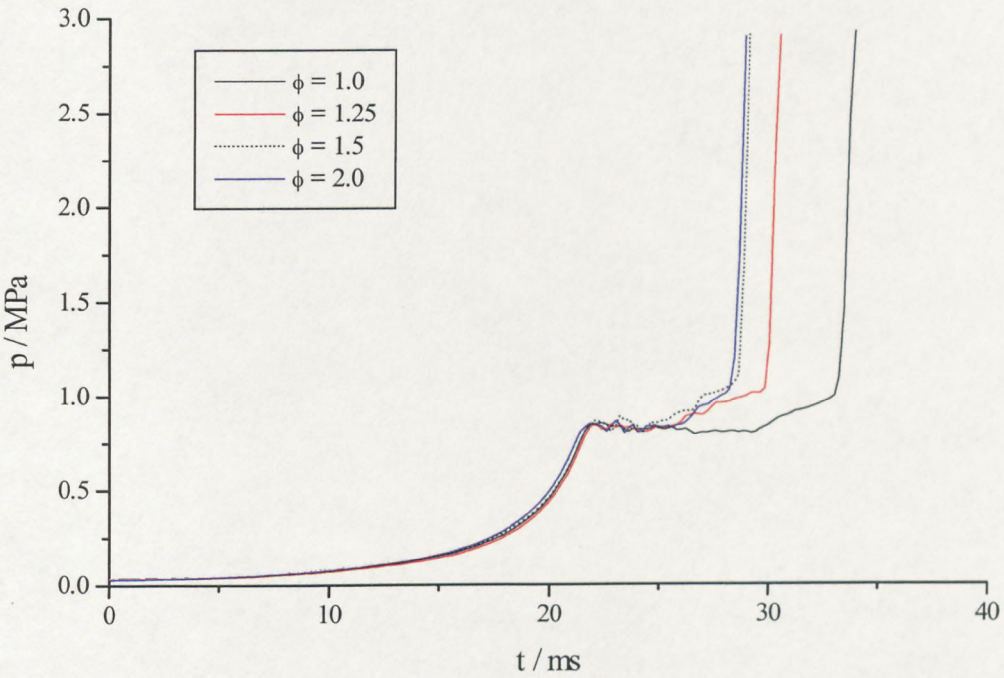

Figure 4.20 (b) Pressure-time profiles for the autoignition of n-pentane in air following compression to 724 (±6) K, for different fuel:air equivalence ratios (ϕ = 1.0 - 2.0).

The effect of equivalence ratio on ignition delay has been investigated in the range 650 < T_c < 950 K for n-pentane, the results are given in Figure 4.21 (a) and (b). Figure 4.21 (a) shows results for fuel-lean (ϕ = 0.5) to stoichiometric (ϕ = 1.0) mixtures and in Fig. 4.21 (b) the results obtained for stoichiometric to fuel-rich (ϕ = 2.0) mixtures are presented. The results suggest that the ignition delay is most sensitive to changes of equivalence ratio in the range 0.5 - 1.0, and further increases in ϕ have negligible effect

temperature range and at any given compressed gas temperature the ignition delay decreases as ϕ increases from 0.5 to 1.0.

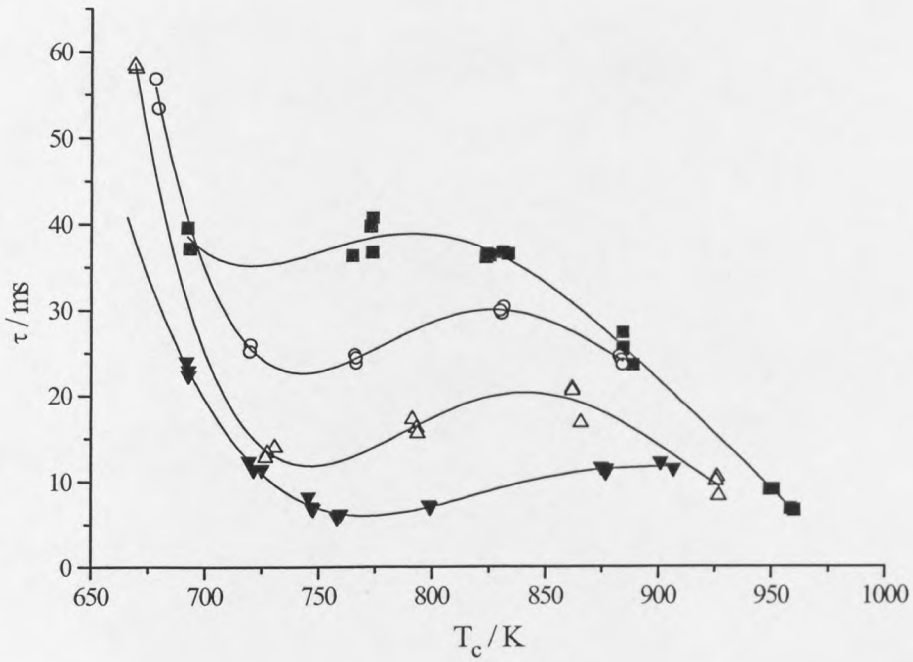

Figure 4.21 (a) Ignition delay variation with compressed gas temperature for n-pentane for $\phi \leq 1.0$ ($\phi = 0.5$ (■); $\phi = 0.6$ (○); $\phi = 0.75$ (Δ); $\phi = 1.0$ (▼)).

As the fuel:air equivalence ratio was increased from 1.0 to 1.25 the threshold temperature for autoignition decreased and there was an overall decrease in ignition delay at temperatures below about 750 K. As the equivalence ratio was increased beyond 1.25 there is no further effect on the ignition delay variation with temperature and at temperatures above 750 K the effect of increasing fuel:air equivalence ratio (from 1.0 to 2.0) on ignition delay was seen to be negligible.

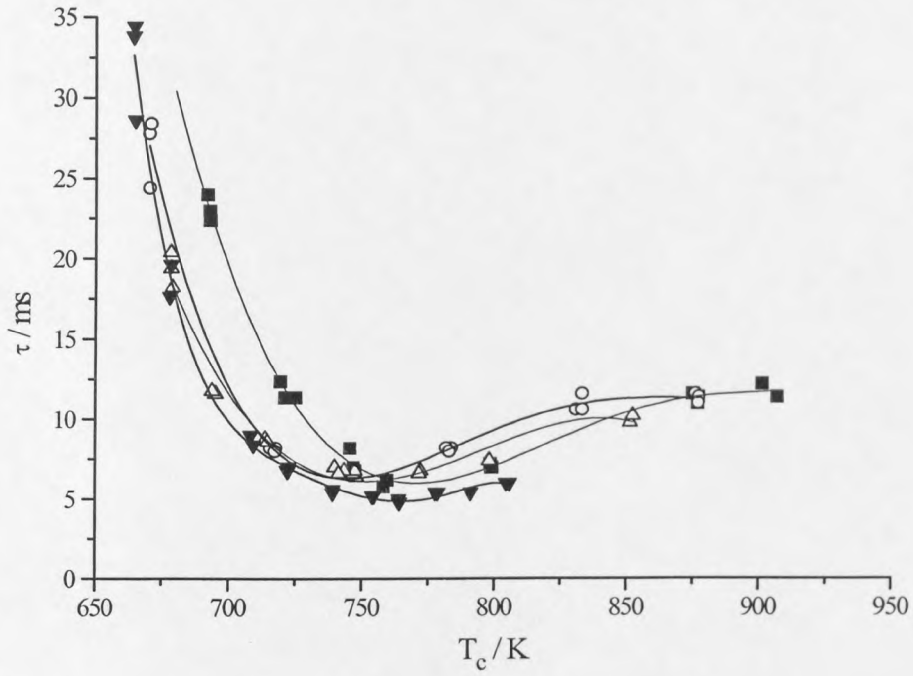

Figure 4.21 (b) Ignition delay variation with compressed gas temperature for n-pentane $\phi \geq 1.0$ ($\phi = 1.0$ (■), $\phi = 1.25$ (○), $\phi = 1.5$ (△), $\phi = 2.0$ (▼)).

4.5.3 Summary and Conclusions

In accordance with the mechanism for high temperature autoignition, τ_2 may be expected to decrease as the mixture becomes leaner, but the simultaneous decrease in cool flame intensity should in turn cause the second stage to become longer.

The variation of ignition delay is due to the complex dependence on both ϕ and temperature. There is also an apparatus-related dependence. The difference in the chain-branching mechanisms at low and high temperatures leads to varying reactivity depending on the fuel:air equivalence ratio. Because the chain branching mechanism at high temperatures is due to the $H + O_2 \rightleftharpoons O + OH$ reaction, fuel-lean mixtures are more reactive in this regime. However, at low temperatures, because chain branching is dependent on radical species formed directly from the parent fuel, fuel-rich mixtures are oxidised more quickly. At low temperatures the controlling reaction is

$R + O_2 \rightleftharpoons RO_2$.

Increases in the concentration of R due to increases in concentration of the parent fuel, result in a shift of the equilibrium toward the formation of the alkylperoxy radical and subsequent chain-branching first-stage of autoignition is favoured. The results presented in this chapter support this explanation of the effect of fuel:air ratio on the ignition delay.

4.6 Combustion of a liquid fuel spray

The application of a diesel injection system to the RCM has enabled a study of hydrocarbon autoignition following direct injection of a liquid fuel spray into the combustion chamber, the results are presented and discussed in this section. The aim of the study was to compare the ignition delay of a single component hydrocarbon fuel, n-heptane, following direct liquid spray injection, with that obtained for the premixed gaseous fuel-air mixture. The ignition delay following injection of the fuel into the combustion chamber following rapid compression of air was measured over a range of compressed gas temperatures for n-heptane.

4.6.1 Background

The occurrence of autoignition following direct injection of a liquid fuel spray into the combustion chamber (as in a direct injection diesel engine) incurs a delay which is dependent on the physical processes of evaporation and mixing and the chemical reaction rate determined by the local composition and temperature. Evaporation tends to result in a lowering of the gas temperature in the region of the spray thus there is a markedly non-uniform temperature field and a non-uniform composition resulting from incomplete mixing of the fuel and air in the time available. The combination of complex physical and chemical processes involved in the combustion of sprays provides scope for an independent area of combustion research which has been reviewed elsewhere [167,168].

Spray combustion was first utilised in the 1880s as a powerful method of burning relatively involatile liquid fuels and continues to have several practical applications [169]. The process of spray formation involves atomisation of the liquid to form a spray of small droplets so increasing the total surface area and thereby increasing the rates of heat and mass transport between the liquid and gas phase. A burning spray, unlike premixed combustible gases, does not have a uniform composition. Droplets may range in size and the fuel:air ratio can be anything between zero and infinity in different regions of the combustion chamber. The autoignition of droplets of fuel under diesel engine-like conditions and the influence of droplet diameter, fuel:air ratio, etc. has been investigated previously [170,171]. The mixing of fuel and oxidant takes place inside the combustion chamber and is controlled by the geometry of the chamber, the spatial distribution and momentum of injected spray and the direction and momentum of the air flow.

In practical combustion systems atomisers produce a spray with a spectrum of droplet sizes. A fine spray of liquid is formed by injecting a narrow diameter jet or by increasing the surface area of a sheet of the liquid until it becomes unstable and breaks down. The process of jet break up follows the mechanism suggested by Rayleigh in 1879 [172], that a column of liquid is unstable and breaks into droplets if its length is greater than its circumference. The most common method of atomisation is the forcing of a liquid through an orifice at high pressure (e.g., 100 atm).

The majority of compression ignition (c.i.) engines rely on the injection of a fuel spray either into the inlet manifold or directly into the combustion chamber. The four-stroke diesel cycle differs from the s.i engine cycle, where the fuel and air are premixed in the appropriate proportions in the carburettor then drawn into the engine cylinder via an inlet valve. In diesel engines air is drawn into the cylinder on the downward stroke and then compressed to approximately 35-50 atm and up to 900 K. The liquid fuel is injected by a pressure jet atomiser in the form of a fine spray just before tdc. After a delay, ignition occurs and combustion of the reactive fuel-air mixture occurs at a time near the end of the compression stroke. During combustion pressures in excess of 70 atm and temperatures of approximately 2800 K are achieved. The energy released and

subsequent work done on the piston during the downward stroke provides the power for mechanical motion. The amount of fuel injected is metered according to the power required, i.e. setting the throttle. The duration of injection constitutes a sufficient fraction of the engine cycle such that ignition may be initiated before the fuel injection is complete. Finally, in the expansion stroke, the exhaust valve opens and the burned gases are expelled to the exhaust system.

The c.i. engine relies on the autoignition of fuels; there is no spark-ignition of the fuel-air charge. If the ignition delay of the fuel used in a compression ignition engine is too long then too much fuel is injected prior to ignition and so pre-ignition can occur. The quality of diesel fuel is measured on a scale of cetane number (CN) where CN 0 corresponds to α-methylnapthalene, which is very difficult to autoignite and cetane (n-hexadecane, CN 100) which autoignites very easily under diesel engine conditions.

4.6.2 Experimental

A schematic diagram of the coupling of the RCM to the fuel injection system is shown in Figure 4.22. The injection pump used was an in-line injection pump with a mechanical (flyweight) governor. The principle of operation was as follows. Fuel was fed into a reservoir at the top of the pumping element through a tube, in the present study it was gravity fed. A central camshaft rotates and the lobes displace a plunger in a plunger-barrel assembly. The displacement of the plunger causes the fuel to be forced through the injection pipe. The diesel pump generates the pressure to force the liquid fuel through a small orifice in the injection nozzle. Thus, a fine spray of fuel was injected into the chamber. A detailed mechanical description of the operation of in-line diesel fuel-injection pumps can be found elsewhere [173], a summary of the experimental features is given below.

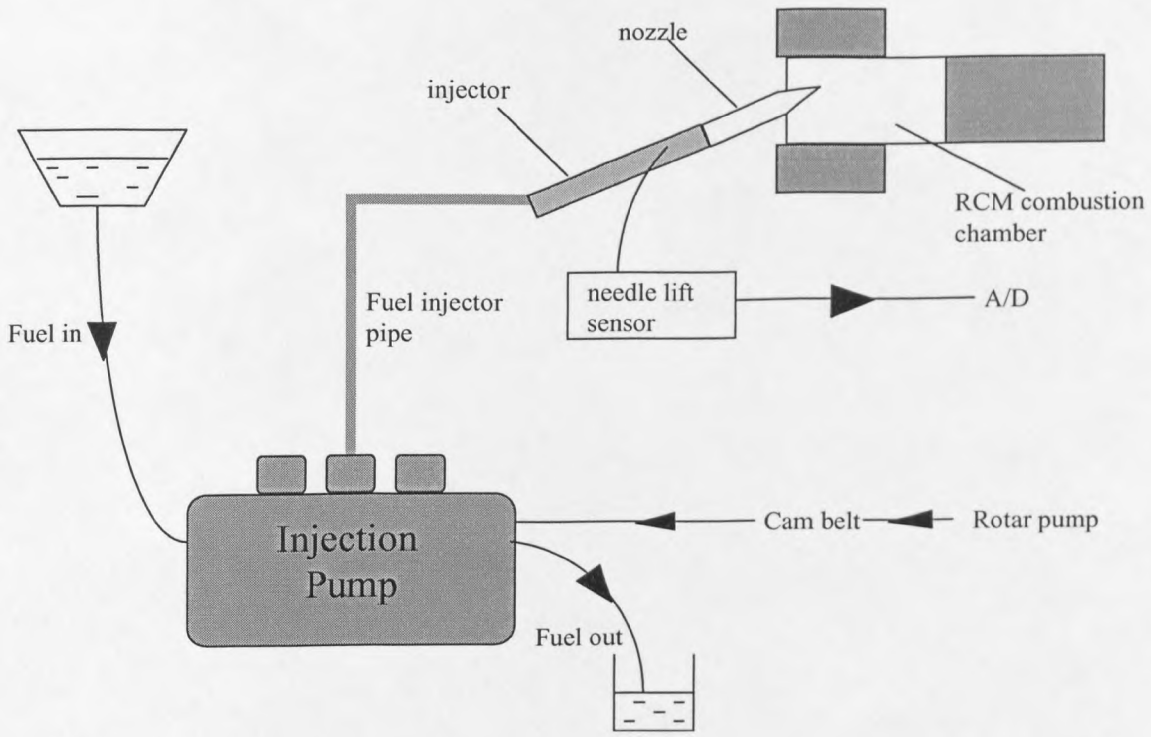

Figure 4.22 Schematic diagram of fuel injection experiment.

The purpose of the fuel injection pump was to pressurise the liquid and deliver it to the injector nozzle for injection into the combustion chamber. The injector used is typical of most direct injection diesel injectors. The nozzle contains 4 holes, 3 of which were blocked with an epoxy resin so leaving just one single hole for the injection of fuel. It was important to flush out the system with the fuel in use at the start of operation and bleed out any air from the system to maximise the injection pressure. It was also necessary to prime the injector before each experiment to obtain sufficient pressure build-up in the pump-injector system. The injector could be operated manually (during priming) or electronically, via the computer data capture software and the A/D converter. The timing of the injection was an important consideration. We were aiming for injection times at or around the end of compression where possible. To achieve this the RCM data capture software had to be modified to allow for the discrepancy between the electromechanical delay in the opening of the solenoid valve on the RCM and the electronic operation of the fuel injection pump. This has presented some difficulties which are currently being resolved. The time of injection was recorded in each

experiment by use of a needle lift sensor (operating on the principle of the Hall Effect) [174] which outputs a signal to the A/D converter at the time of injection.

The main experimental difficulty encountered was that of the viscosity of the fuel used. The pump and injector were designed to operate with diesel fuel which is significantly more viscous than the pure hydrocarbons (Table 4.6). The solution to this difficulty was to alter the number of spacers in the injector body below the spring, this had the effect of increasing the spring-loaded pressure needed to inject the liquid. The initial pressure of air in the combustion chamber was 33.3 kPa. On the basis of the average volume per shot being 0.006 cm^3 and assuming complete evaporation of the fuel, the fuel equivalence ratio (ϕ) was approximately 0.6.

Table 4.6 Viscosity measurements, defined as the time taken for the test liquid to flow through a specified length of capillary tube, measured at 20 °C.

Fuel	time / s
n-pentane	116 (±1)
n-heptane	184 (±1)
PRF 60	208 (±1)
Diesel	~ 1320

4.6.3 Results

Figure 4.23 illustrates the variation of ignition delay with compressed gas temperature for the direct injection of a liquid n-heptane spray into the combustion chamber at tdc. It was not possible to achieve autoignition at temperatures below approximately 750 K and at temperatures above this the ignition delay exhibited a monotonic decrease with increasing compressed gas temperature. The ignition delays at around 900 K are comparable (± 2 ms) with those which were measured for the premixed gaseous n-heptane-air mixtures (Fig. 4.9).

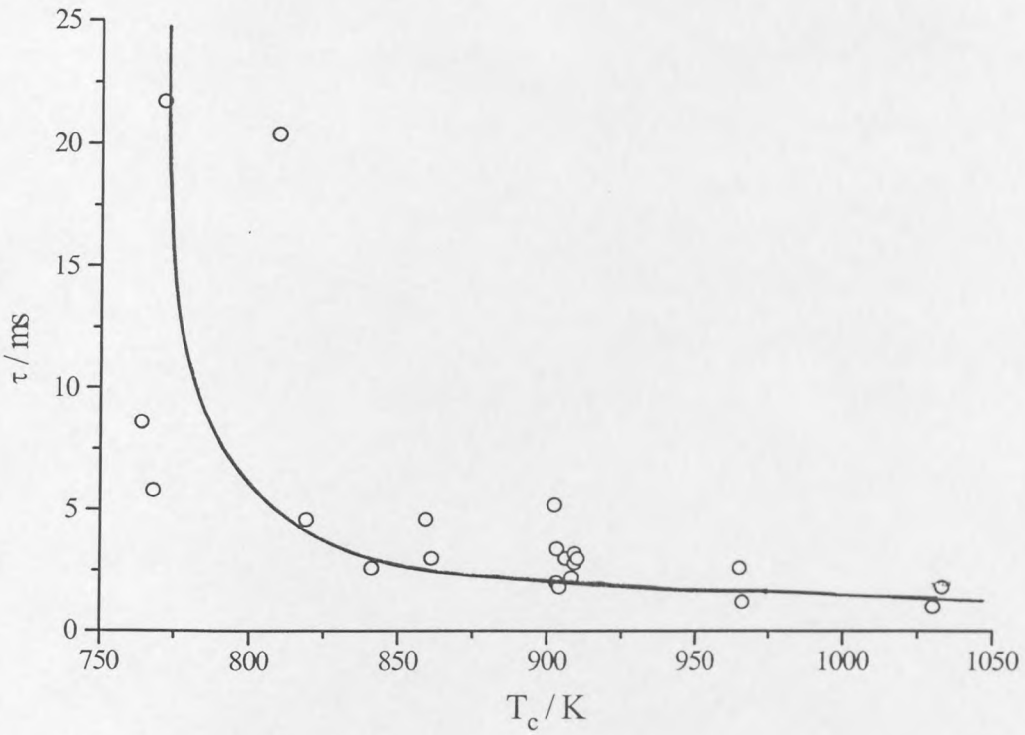

Figure 4.23 Ignition delay variation with compressed gas temperature for n-heptane following liquid spray injection into a compressed oxygen:inert (21:79) mixture.

The results shown in Figures 4.24 and 4.25 for the injection of PRF 60 into an oxygen-inert mixture compressed to 895 K, illustrate the effects of fuel injection on the surrounding gas and the effect of the gas phase on the development of autoignition. The evaporation of the liquid spray following injection incurs a latent heat of vaporisation and so tends to absorb heat from the surroundings and an overall decrease in the average temperature within the combustion chamber, as followed by the pressure measurement, is evident (Fig. 4.24). Also, the injection of the fuel occurred after a considerable delay from the end of compression (11 ms), a time when the gas is almost stagnant. Therefore, it is unlikely that the spray experienced significant turbulent gas motion within its vicinity and the droplets may have remained a significant size. Evaporation and mixing with the surrounding gas would, therefore, be slow and chemical reaction may not readily develop in the cooling mixture. In Figure 4.25, similar end of

compression conditions were achieved but injection occurred just after tdc where the advantageous effects of turbulent gas motion could be encountered by the spray. Under these circumstances autoignition occurred after a relatively short delay of 6.0 ms. In addition to the pressure-time profile a 2-dimensional image of the light output from the chamber at a time corresponding to 2 ms after injection was captured using the CCD camera (Figure 4.26). The injection point was at the top of the image and there was intense light output from the opposite side of the chamber. A few small spots of light are also visible near the centre of the image. Although it is difficult to draw any definitive conclusion, this could possibly be characteristic of a burning droplet. Unfortunately the extent of this study was also limited due to difficulties with coincident timing, but the initial evidence suggests that there is scope for further studies of spray combustion in the RCM. (The imaging procedures are described in detail in Chapter 5).

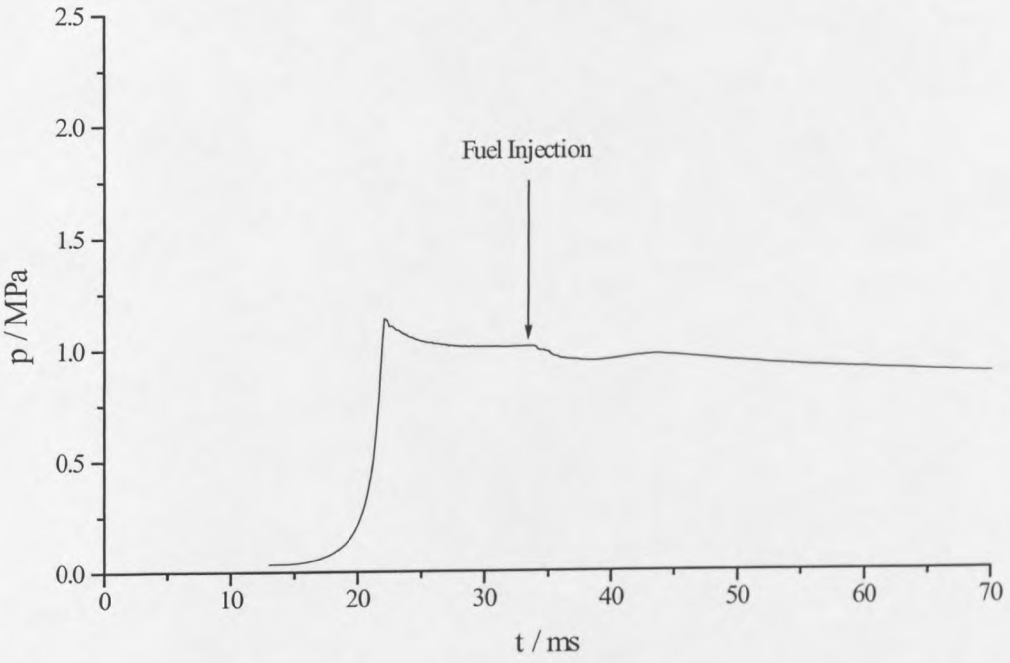

Figure 4.24 Pressure-time profile for the injection of PRF 60 into a compressed oxygen:inert (21:79) mixture, T_c = 895 K, injection at 11 ms atdc, non-ignition.

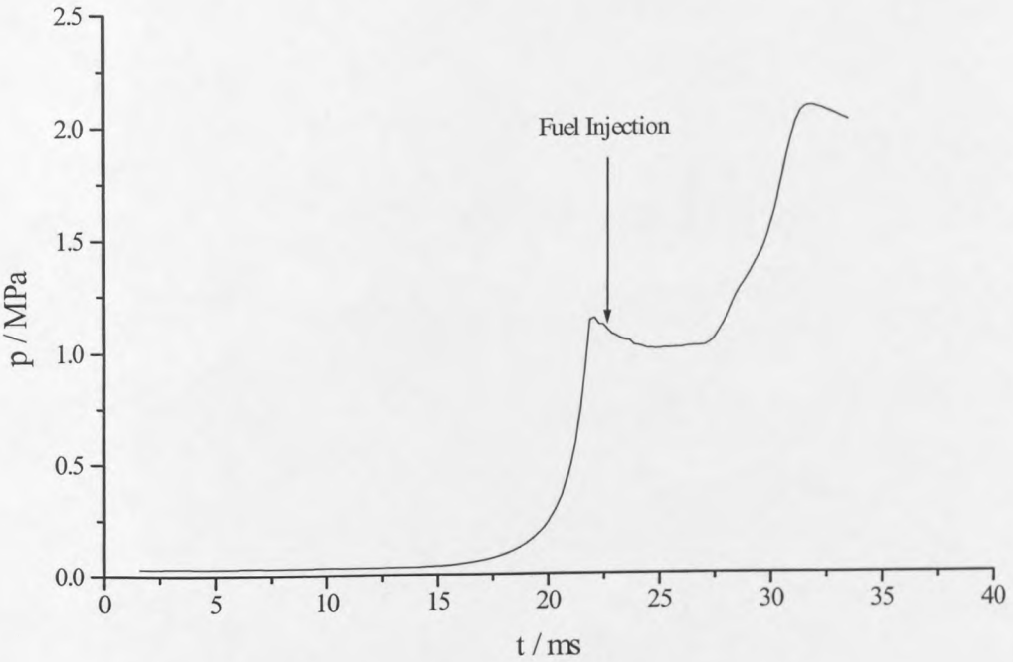

Figure 4.25 Pressure-time profile for the injection of PRF 60 into a compressed oxygen:inert (21:79) mixture, T_c = 895 K, injection at 0.6 ms atdc and autoignition at 6 ms after injection.

Figure 4.26 CCD image of the light output from the combustion chamber of the RCM 2 ms after the injection of PRF 60 into a compressed oxygen-inert mixture (T_c = 895 K). Exposure time was 1 ms. (White areas represent regions of light emission).

4.6.4 Discussion and Conclusions

The autoignition of a liquid fuel spray incurs additional complexities which do not occur during homogeneous combustion in the gas phase. The dispersion of the spray within the oxidant and the size distribution of the droplets are affected by the method of spray formation and by the condition of the gas into which it is injected. A highly turbulent gas will tend to break up the larger droplets into smaller droplets forming a finer dispersion within the gas phase. An additional effect of turbulence within the chamber is to enhance contact between the fuel and the oxidant and therefore promote the initiation of reaction. The extent of mixing of the fuel and oxidant varies within the chamber, and spatial variations in fuel:air ratio result, therefore the assumption of a fuel:air equivalence ratio made on the basis of complete evaporation of the spray is inaccurate. However, this assumption can be made in the qualitative analysis of the global features of spray injection and ignition.

Despite the complexities involved in this experiment the results shown in Figure 4.23 demonstrate the potential value of the RCM in determining the effect of low volatility additives on the ignition delay of hydrocarbons following direct injection of a liquid spray into the combustion chamber. In general the results obtained for n-heptane show a comparable behaviour as the premixed gaseous autoignition in the RCM. The ignition delay exhibits an approximately monotonic decrease with increasing compressed gas temperature and there is negligible ntc effect in the intermediate temperature regime. However, for the spray injection, the threshold temperature for autoignition is greater than that for the premixed gaseous autoignition of n-heptane.

A potential advantage of this method over the study of homogeneous gas phase autoignition lies in the ability to use low vapour pressure liquid additives, such as NMA, which do not give a sufficient vapour pressure at room temperature for the accurate preparation of gaseous reactant mixtures.

Chapter 5

Autoignition centres and knock features in the RCM

5 AUTOIGNITION CENTRES AND KNOCK FEATURES IN THE RCM

In this chapter the spatial development of autoignition in the combustion chamber of the RCM is addressed. The first section (Section 5.1) describes the experimental investigation of the spatial evolution of single and two-stage ignition in the RCM, using visual imaging techniques. The occurrence of hydrocarbon autoignition in the end-gas following spark-ignition has also been studied using 2-dimensional imaging methods and the intensity of the resulting "knock" for different fuels under different conditions has been characterised (Section 5.2).

5.1 The spatial development of hydrocarbon autoignition in an RCM

The light emission from different regions of the combustion chamber of the RCM has been monitored using photomultiplier tubes positioned at a partially blackened end window. In addition to this, the optical imaging techniques of schlieren imaging and intensified CCD digital image capture have been used to investigate the spatial development of hydrocarbon autoignition in the combustion chamber of the RCM. The autoignition of premixed gaseous fuel-air mixtures has been studied following compression to different temperatures for two n-alkanes (n-pentane and n-heptane) and also for a PRF 60 mixture, although only results pertaining to the autoignition of normal alkanes will be presented here.

These spatial imaging techniques have been usefully applied to the investigation of the effect of spatial temperature inhomogeneities within the combustion chamber of the RCM on the location of autoignition centres during the post-compression period. Experiments have shown that, within the negative temperature coefficient (ntc) regime, autoignition centres may originate in the cooler regions of the combustion chamber, whereas at the higher compressed gas temperatures autoignition tends to originate in the

hot, adiabatically compressed core gas. The qualitative features of the images obtained will be discussed.

5.1.1 Background

Visualisation and spatial resolution of light output

The visualisation of light output during hydrocarbon autoignition has traditionally been conducted using photomultiplier tubes and, more recently, with fibre optical devices [175]. However, as early as 1929, the technique of shadowgraphy had been applied to the study of autoignition and detonation waves ahead of a moist $CO + O_2$ combustion wave [176,177]. Prior to the advent of advanced laser based imaging techniques, substantial progress had already been made in the field of 2-dimensional imaging of combustion systems. Direct natural light photography [4,125,178-185], proved remarkably informative considering its simplicity. Interferometry [186-188] and schlieren imaging were also widely applied to the study of flames and their radiation and to fluid motion [189-203]. A detailed review of laser techniques used in combustion research can be found elsewhere [204].

Throughout the 1940s and 1950s much of the emphasis lay on the observation of candles [186,197], laminar premixed flames [180] and turbulent premixed flames on a burner [183,192-193,205] and propagating flame fronts [195]. The majority of the photographs obtained were instantaneous and long exposure. However, as photographic technology advanced there was a move toward high speed filming methods, particularly coupled to shadowgraphy [124,206] and schlieren imaging [185,190,194,199,203,207]. One of the first experiments of this type involved the observation of the early stages of flame development in flowing methane-air mixtures [190]. At a later date the autoignition in a rapid compression machine for different fuels was studied using schlieren methods and a framing rate of 2000 frames per second (fps) [207] (Figure 5.1). In 1985 Hyashi et al. developed this theme with particular relevance to the study of knocking combustion in a rapid compression machine [124]. The technique employed was shadowgraphy, with ciné filming at much faster framing rates of up to 100,000 fps.

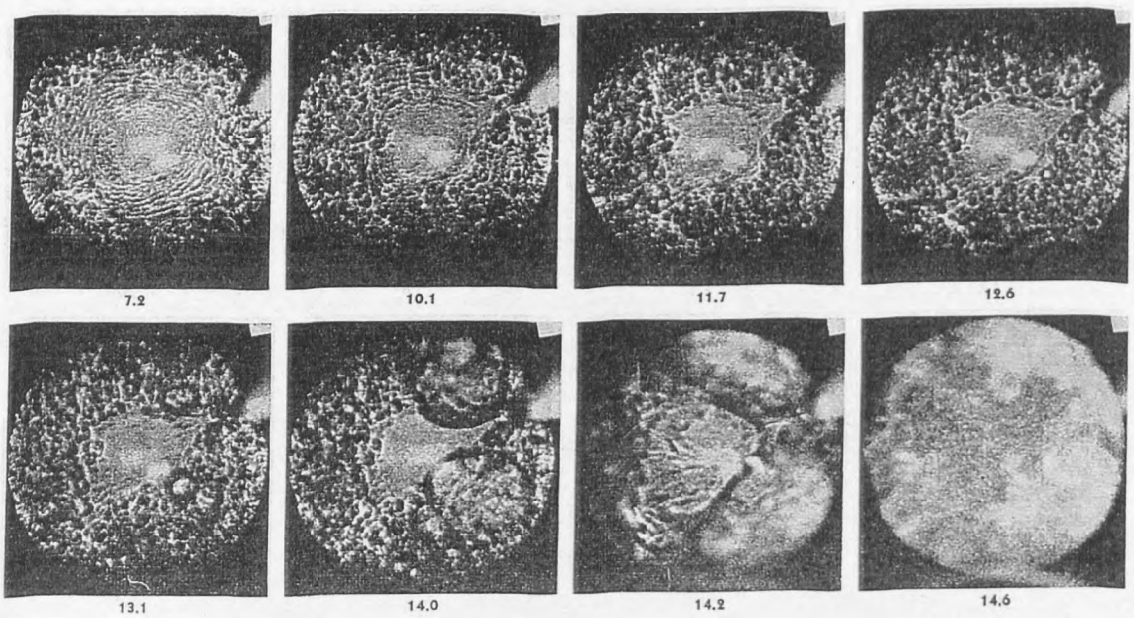

Figure 5.1 Schlieren imaging of the autoignition of i-octane in an RCM. (p_i = 1.1 atm; T_i = 65 °C; CR = 12.6; ϕ = 0.095). The frame number corresponds to the time in milliseconds after the end of compression [207].

Aside from the shadowgraphy and schlieren methods, several non-invasive laser based imaging techniques have since been developed, providing a valuable means of examining flame structure and measuring temperature, species concentration and flow fields in combustion systems, particularly in relation to spark-ignition and diesel engines. Technological advances in laser diagnostics and digital image capture using Charge Coupled Devices (CCDs) have led to a more direct and sophisticated approach to the study of hydrocarbon combustion phenomena and the associated light output. Image intensifiers have been employed as a means of detecting very low light intensities over short time intervals when coupled to a CCD camera [208], as in the present study. Laser diagnostic methods have also been applied to the study of autoignition in engines [144,206,208-212] and RCMs [213,214]. Methods including laser induced fluorescence (LIF) spectroscopy [206], Coherent Anti-Stokes Raman Spectroscopy (CARS) [144], Rayleigh Scattering [209] and Mie Scattering [206] have all led to a broadening of the

understanding of combustion phenomena. A detailed description of these laser diagnostic methods and their application to combustion systems has previously been published [215]. In addition to the principle laser diagnostic techniques, novel planar (2-dimensional) imaging techniques [216] have provided the means for a useful progression from single-point laser diagnostics.

Status of numerical modelling in relation to spatial structure

Thermokinetic modelling of hydrocarbon autoignition in an RCM is commonly represented in terms of a spatial uniformity of temperature and species concentrations within the combustion system and therefore fails to capture the real features which relate to the spatial variations within the majority of combustion applications. Numerical studies of the spatial structure in hydrocarbon autoignition in the RCM have been performed using a computational fluid dynamics code (KIVA II) [217], modified to include the simulation of hydrocarbon autoignition based on reasonably detailed kinetics and heat release [139]. The temperature and vectorial flow fields created by the simulation of piston motion within the axisymmetric plane of the combustion chamber were calculated and the spatial temperature and concentration inhomogeneities which exist throughout the post-compression period as combustion proceeded were predicted.

At the end of the compression stroke the maximum gas velocity was shown to be in the direction of piston travel and corresponds to the piston velocity (~ 10 m s^{-1}) [121]. A roll-up vortex is formed by the shearing at the cylinder wall. This causes re-circulation at the periphery of the cylinder and creates a stagnation zone close to the corner between the piston and the chamber surface, consistent with the observations by Tabaczynsky et al. [113]. This stagnation zone survives throughout the ignition delay. Following the transient pressure gradients created at tdc, the flow patterns are predicted to cycle from the axis to the edge in a clockwise direction with the centre of the vortex lying axisymmetrically towards the piston crown and the wall. Within a short interval the

effects of gas viscosity and momentum transfer cause a reduction in predicted velocities and the gas motion begins to decay.

Numerical simulations of the spatial temperature and concentration distributions and autoignition chemistry of alkane-air mixtures in the end-gas ahead of a spark-ignited flame in a rapid compression machine have illustrated that, within the region of the ntc, autoignition centres may originate close to the piston crown and the chamber walls [139].

Purpose of study

The relevance of the foregoing remarks is that these predictions were made prior to the performance of the experimental studies.

The aim of the work described in this chapter was to investigate the spatial evolution of cool flames and autoignition in the RCM and to seek experimental evidence in support of the numerical prediction that within the temperature range of the ntc, autoignition tends to occur in the cooler regions of the combustion chamber adjacent to the walls. Spatial imaging techniques have been used to illustrate the existence of temperature inhomogeneities in the combustion chamber of the RCM during the post-compression period. The two fuels studied, n-pentane and n-heptane, were chosen on account of their similar molecular structure but different reactivity, as discussed in Chapter 3. Normal-heptane undergoes significant reaction during the compression stroke when compressed to high temperatures in excess of about 770 K, whereas, in the Leeds RCM, n-pentane does not undergo significant reaction during compression throughout the accessible temperature range.

5.1.2 Experimental

A full description of the RCM and its operation can be found in Chapter 2. Liquid fuel vapour was premixed with "air" in stoichiometric proportion ($\phi = 1.0$). Reactants were

admitted to the combustion chamber at an initial pressure of 33.3 kPa, then compressed by a solid stainless steel piston driven by compressed air. Pressure-time data during the compression stroke (duration = 22 (± 1) ms) and throughout the post-compression period were measured by a pressure transducer (Kistler 601A, natural frequency 100 kHz) and recorded digitally via an A/D converter onto a pc for a total duration of 200 ms at 0.2 ms intervals.

Light Output

In the majority of experiments a temporal, qualitative record of the total light output from the chamber was obtained using a photomultiplier. This viewed events either through the transparent (Perspex or quartz) cylinder head of the combustion chamber or at a small quartz window set into the side wall of the combustion chamber, depending on the accessibility of the end-window, which was dictated by the type of experiment being performed and the associated experimental set-up.

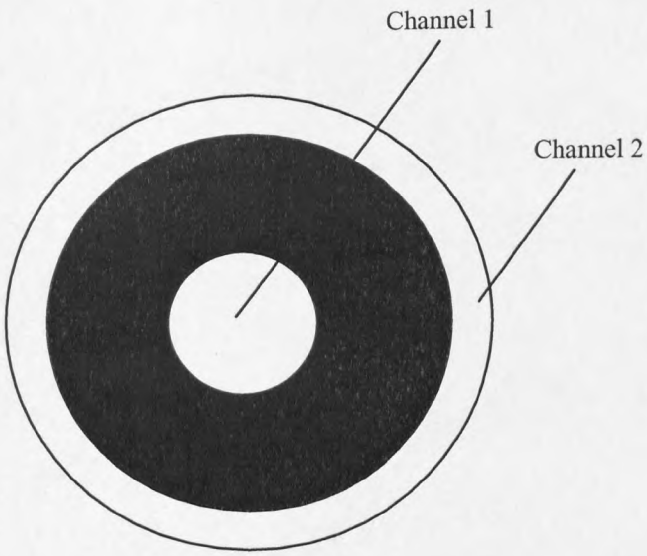

Figure 5.2 Schematic diagram of end-on view of partially blackened Perspex window.

Two light output records were obtained in some experiments, each one representing light from spatially distinct regions of the chamber. This was done using a partially blackened Perspex window (Figure 5.2) and two photomultiplier tubes. This allowed direct comparison of the light output record from the outer region of the chamber

adjacent to the wall (Channel 2) with that from the central core gas region (Channel 1). Each signal was averaged over the chamber depth and therefore some allowance had to be made for the possibility of detection of internally reflected light from the other regions of the chamber.

Schlieren Imaging

The technique of schlieren imaging relies upon the refraction of a light beam as a result of density gradients in the test gas. The optical arrangement used in the present work was for reflected mode schlieren imaging (Figure 5.3) in which an optically flat mirror was attached to the piston crown. A low power (25 mW) He/Ne laser beam was directed onto the mirrored piston. The optical axes of the incident and reflected beams were slightly mis-aligned, and the undisturbed reflected beam directed onto a screen to allow filming of the image using a Hitachi ciné camera (5000 fps).

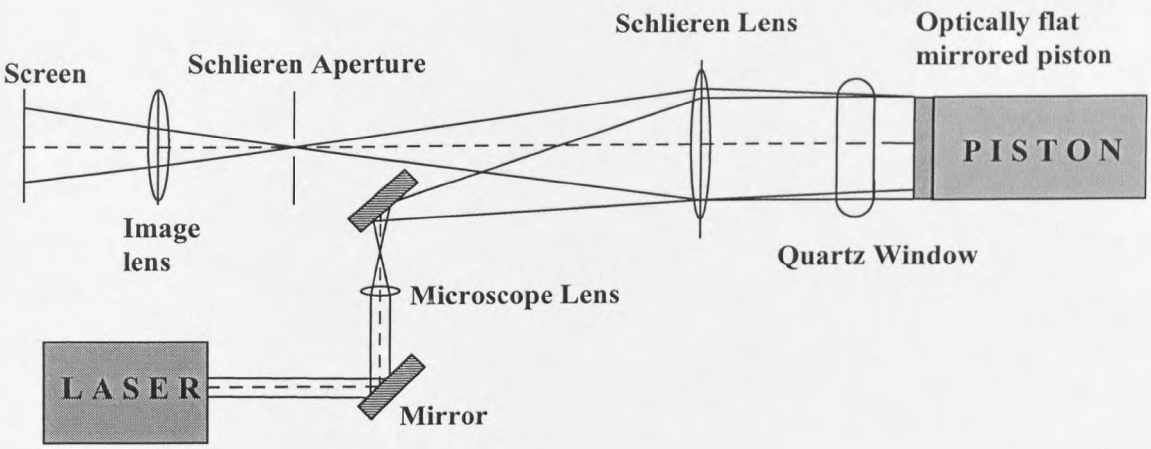

Figure 5.3 Schematic representation of the schlieren optical arrangement.

The schlieren aperture, placed at the focal point of the schlieren lens, excludes the unwanted deflected light, due to refractive index gradients (or density gradients) in the region of interest. Optical studies were by end-on viewing of the full cross-section of

the cylindrical combustion chamber (45 mm diameter × 18 mm depth) through a quartz window, providing a full field of view of the cross-section. Observations were averaged over the clearance distance between the piston crown and the internal surface of the quartz window.

Image Intensified CCD camera

In order to obtain a 2-dimensional image of the light output from the chamber a cooled scientific grade CCD (charge coupled device) camera, lens-coupled to a phosphor screen image intensifier device, was employed. The CCD camera parameters, such as gain factor and exposure time, were controlled using a computer software package. A programmable gating unit for delay and pulse generation (Photek PSU 100G) was used to control the image intensifier and gate the duration and timing of the image capture. Permanent damage to the intensifier can be incurred if the phosphor screen is exposed to light intensity exceeding 3 Cd m^{-2} for more than a few seconds. Therefore, in the majority of experiments the phosphor screen was exposed to the chamber for no more than 5 ms. As an additional precaution, when investigating the hot stage of autoignition, a filter (100 % transmission in the range 283-410 nm) was placed over the front of the chamber to absorb the high intensity yellow and white light emitted during ignition.

In selected experiments a Perspex window positioned at the spark plug port allowed the simultaneous measurement of the total light output from the chamber and the CCD image capture, therefore allowing the two to be related with respect to time.

Image Processing (AVS)

Digital images were saved as 12-byte binary data files of 2 bytes per pixel on a grid 600 × 400 pixels, with a grey scale. It was then necessary to convert the files to a readable file type, i.e. remove the 6 byte header and convert to integers, to enable image

processing using AVS (application visualisation system) software [218]. The aim of image processing was to remove unwanted features from the image and also to enhance the required information such as the intensity of the image. The complete image processing procedure is encapsulated within a network of individual operations (thresholding and contrasting), or modules, chosen from a module library. These processes are performed in succession on the original image (file descriptor module), resulting in the final processed image (image to postscript module). Figure 5.4 shows the AVS software display with a network used to process images of spark-ignited flames, this enabled the identification of the flame edge (4 conn and sketch roi modules).

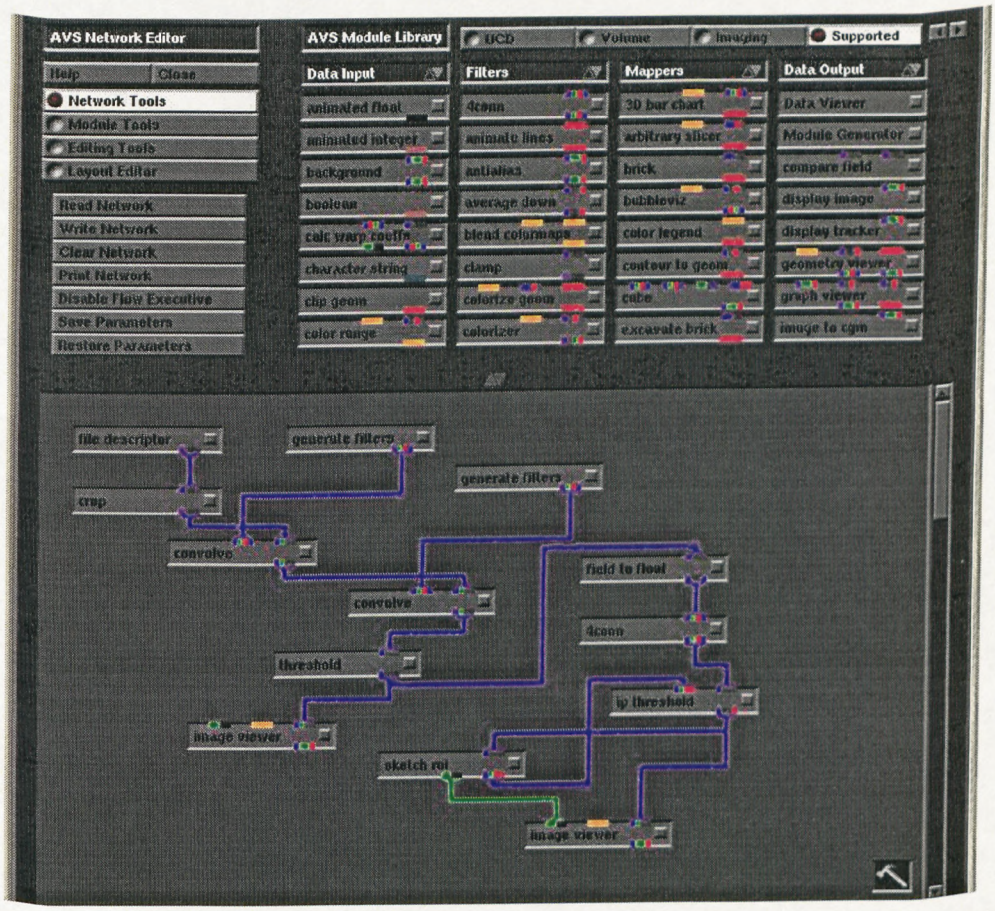

Figure 5.4 AVS Network for the processing of CCD images of spark-ignition in the RCM.

The AVS image processing network shown in Figure 5.5 was employed to enhance images from autoignition experiments. At each step in the process an image viewer module can be connected to view the image at intermediate stages in the image

processing. It is important to note that, for the CCD images shown in this chapter, regions of light emission are represented as dark regions and regions of no significant light output appear as light regions on the processed image.

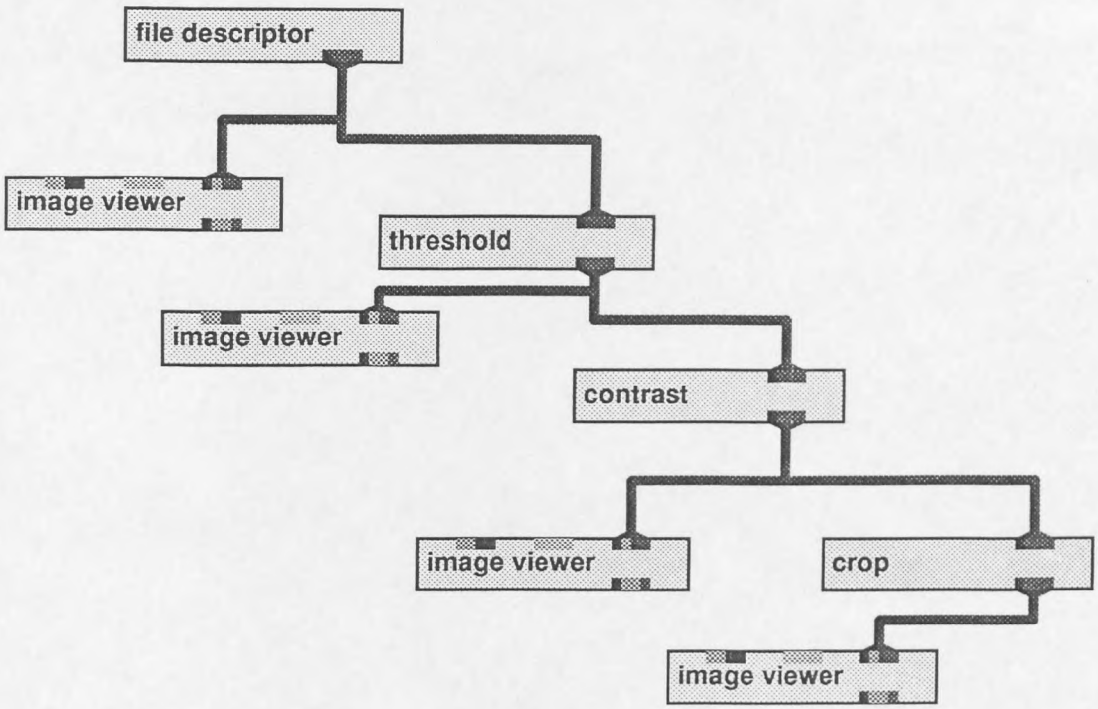

Figure 5.5 AVS Network for the processing of CCD images of autoignition in the RCM.

5.1.3 Results

General Features of Schlieren Images

In general the image on the film was satisfactory in terms of size and clarity, although there was some loss of definition at the edges. All films gave comparable evidence for gas motion during and up to 5 ms post-compression, which appears to be almost symmetrical over the cross-section of the combustion chamber and gradually decays throughout the post-compression period. Several of the films exhibit an alternating loss and regain of the image over an approximately 1.6 ms interval, at a time coinciding with or near the end of the compression stroke (see Fig. 2.6). This is believed to be a consequence of the slight recoil of the machine when the piston reaches the end of its travel.

It is important in all of these experiments, where two-dimensional imaging of a three-dimensional region is carried out, to consider the chamber depth over which the photographic image is averaged. The effect of the depth of the chamber may obscure the fully burned region and therefore ambiguities could arise in the analysis of the photographic images due to three-dimensional effects.

n-Pentane autoignition, T_c = 750 K

The first evidence obtained for the existence of spatial temperature variations within the combustion chamber of the RCM during the autoignition of n-pentane-air (ϕ = 1.0) was obtained using the partially blackened window and two photomultiplier tubes. A typical result for the two-stage autoignition of n-pentane following compression to 760 K is given in Figure 5.6. The two light output records represent the light output from different regions of the chamber at a given time. Light from one region could also be detected by the other photomultiplier, hence the weak light output seen in record 1

(detecting light from the centre of the chamber) at the corresponding time to the maximum in record 2 (detecting light at the edge of the chamber).

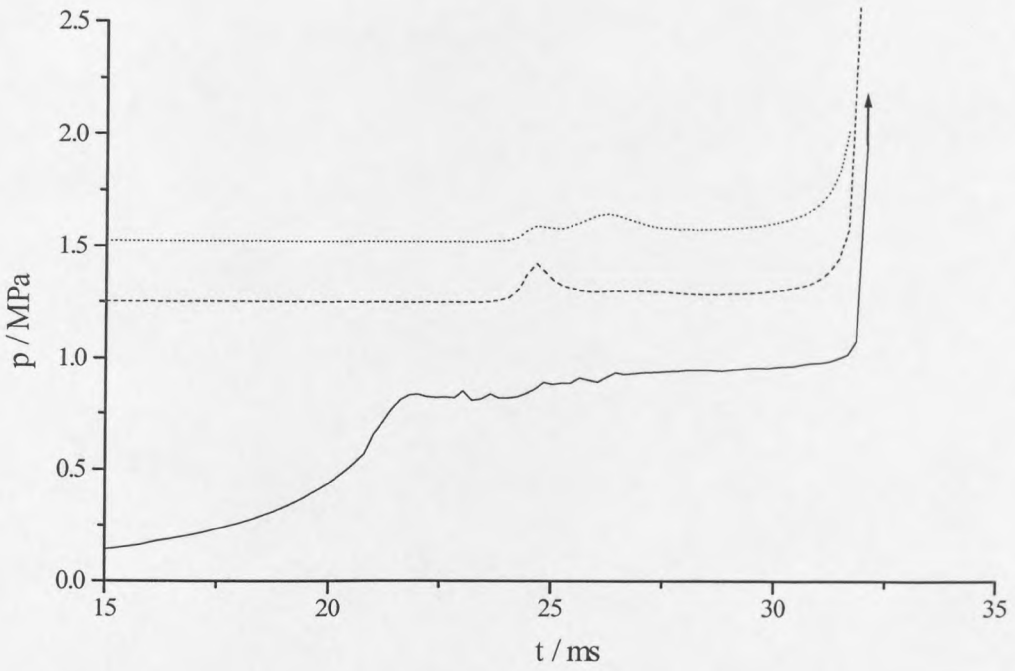

Figure 5.6 Pressure and light output records for the two-stage autoignition of n-pentane following compression to 760 K. Light output records corresponding to Channels 1 (...) and 2 (---) in Figure 5.2 are shown.

The implications of this result were that the occurrence of the cool flame was not spatially homogeneous but was initiated in the cooler boundary layer of the chamber then gradually propagated into the central core gas region of the chamber. This method alone was not deemed sufficiently explicit for studies of the spatial development of autoignition centres because the total light output from a given region is too intense to be completely spatially resolved by a partially blackened window. Thus, further experimental evidence in support of the spatial temperature inhomogeneity was sought.

The technique of schlieren imaging has proved to be a valuable method of visualising the occurrence of autoignition centres in the unburned end-gas of spark-ignition engines

in several previous investigations [4,185,203]. This method was also employed in the study of the autoignition of hydrocarbons in the RCM. A photographic record of the schlieren imaging of the two-stage autoignition of n-pentane-air following compression to 744 K has been obtained (Figure 5.7a), the corresponding pressure-time profile for this experiment is given in Figure 5.7b.

The filming speed was 5000 fps, therefore each photographic frame represents a time interval of 0.2 ms. Frames are read left to right, downwards. The image is essentially uniform at the end of compression. After 3.0 ms some structure begins to develop and becomes increasingly more prominent with time, until after 5.4 ms there is a distinct central dark region on the film as illustrated by Frame 27. An autoignition centre, characterised by a large density gradient, originates at the wall (Frame 33) and as it grows in size and intensity, the density gradients in the remaining unburned gas become more significant. By Frame 41 (8.2 ms after tdc) a second autoignition centre is initiated, also at the wall but in a different region of the chamber. In the subsequent frames the combustion accelerates until complete reactant consumption occurs during ignition.

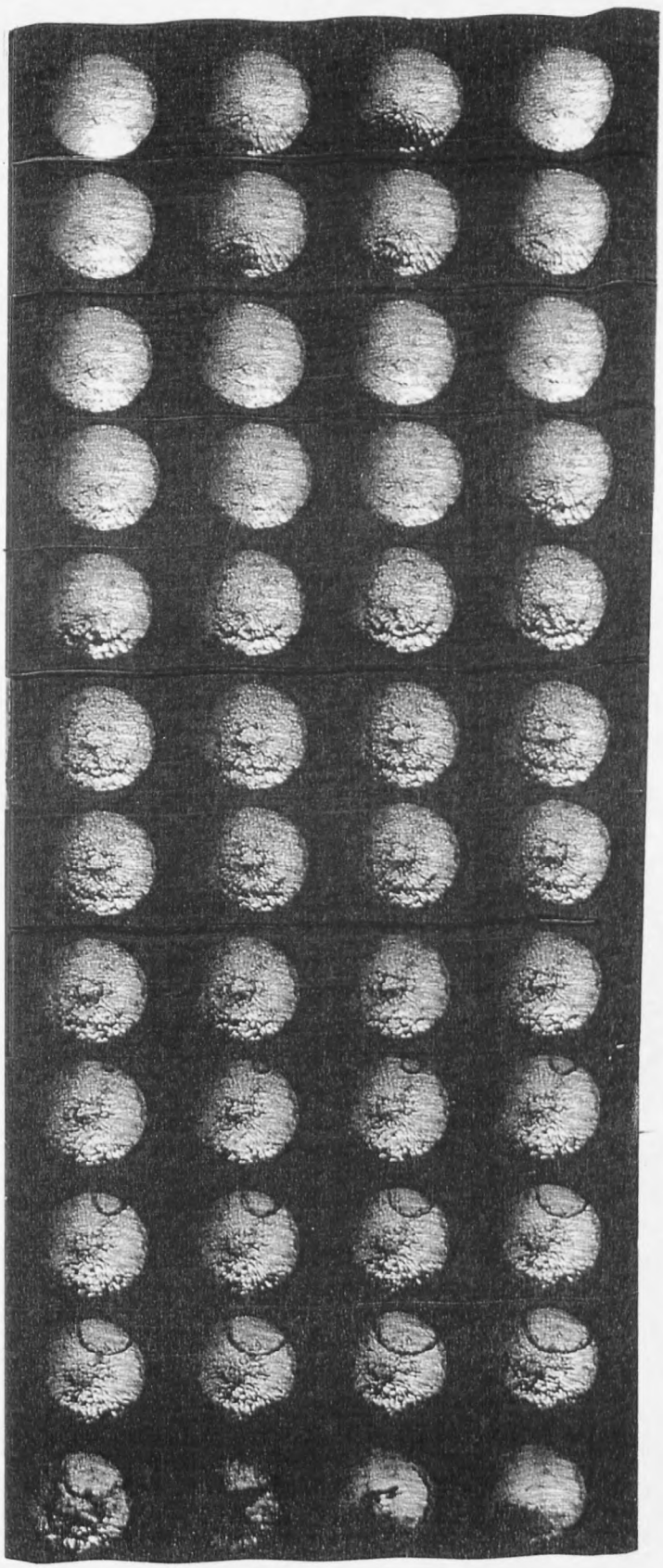

Figure 5.7 (a) Schlieren image sequence for the two-stage autoignition of n-pentane following compression to 744 K. Filming speed was 5000 fps, Frame 1 corresponds to the end of compression.

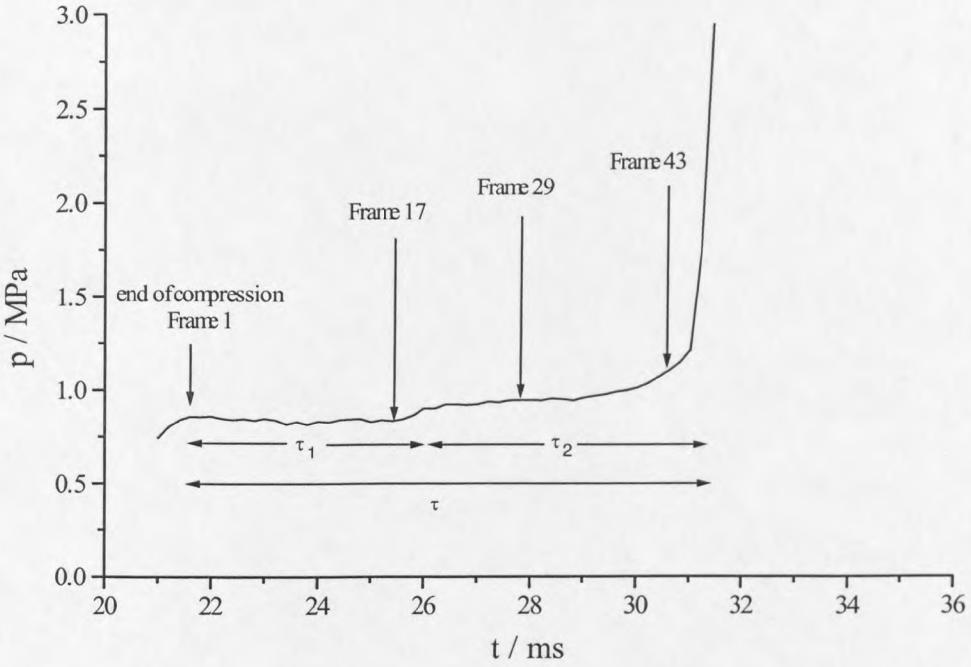

Figure 5.7 (b) Pressure-time profile for the two-stage ignition of n-pentane following compression to 744 K corresponding to the schlieren sequence shown in Fig. 5.7 (a). The times of selected frames are also indicated on the pressure profile.

The digital images captured using the CCD camera exhibit similar features during the autoignition of n-pentane following compression to ~750 K (Fig. 5.8). Each image is obtained in a separate experiment, i.e. a single shot at a predetermined time during the event. The intensity of the images obtained does not represent the quantitative light intensity because the image intensifier gain was varied from experiment to experiment. The images shown in Figure 5.8 illustrate the cool flame light output during the two stage ignition of n-pentane following compression to ~750 K, the pressure history is also given, illustrating the time of image capture. The CCD images given in Figure 5.9(a) and (b) illustrate the light output due to autoignition centres at the wall of the combustion chamber in agreement with the previously described Schlieren films (Fig. 5.7). The pressure profiles are also shown and illustrate the relatively slow pressure rise

associated with the initial growth of the autoignition centre following compression to 690 K and 730 K respectively.

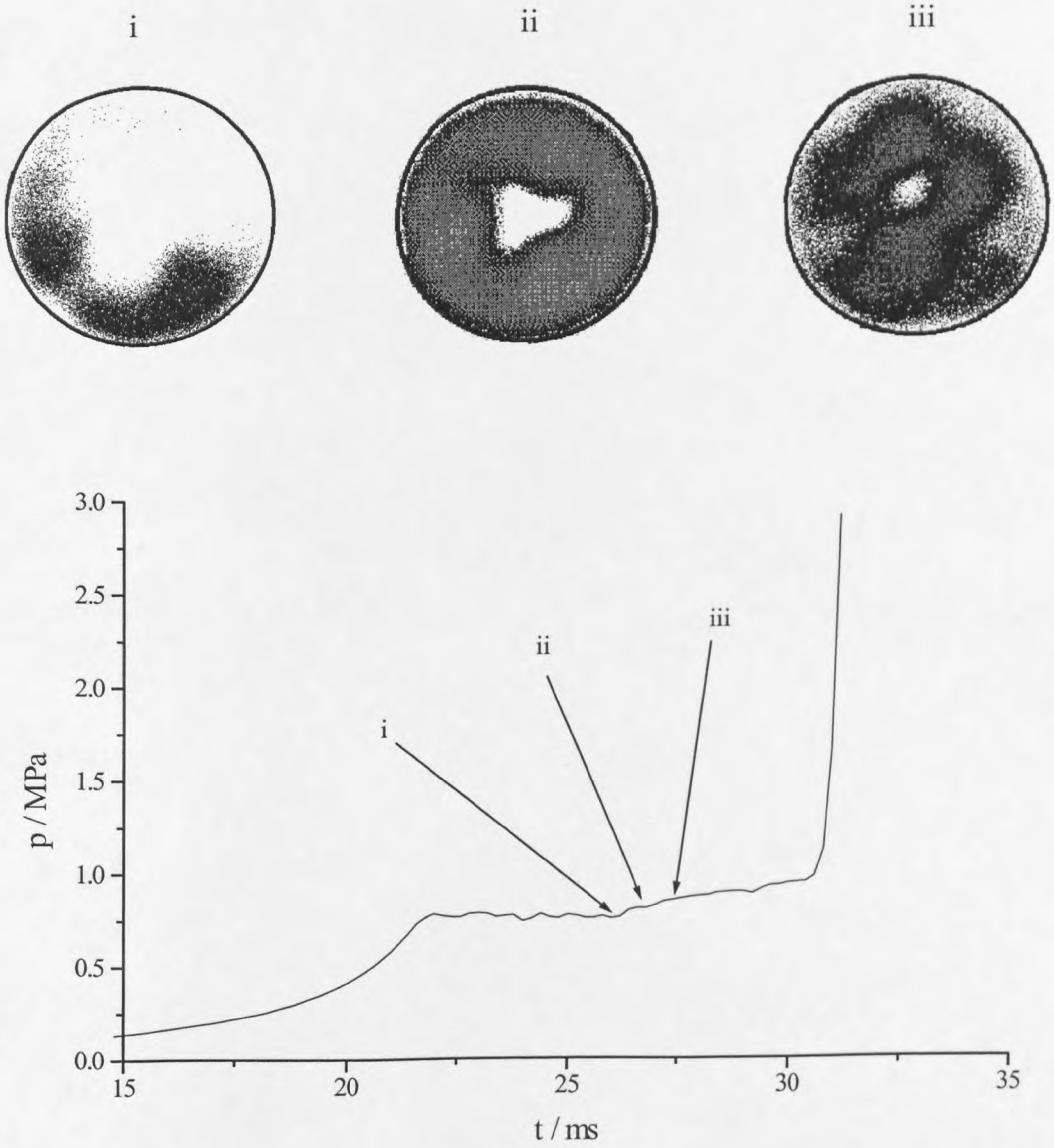

Figure 5.8 CCD images obtained during the cool flame period of the first stage of two-stage ignition of n-pentane following compression to 750 K. The three images correspond to different times on the pressure rise associated with the first stage of autoignition as illustrated on the pressure profile.

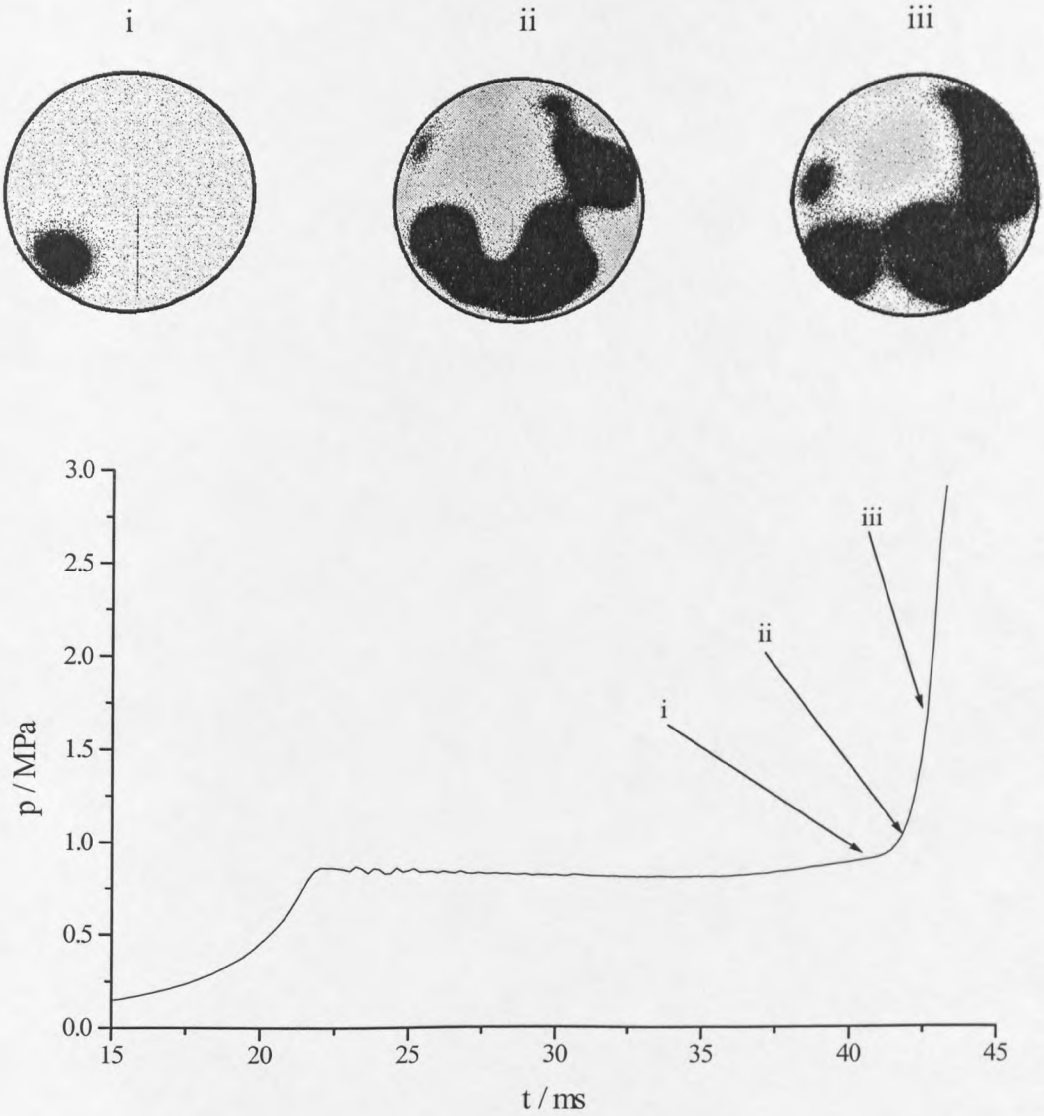

Figure 5.9(a) CCD images taken during the initial stages of the hot stage of ignition for n-pentane following compression to 690 K. The three images were acquired at different times during ignition as shown on the pressure profile.

The rate of pressure rise in the initial part of the hot stage of ignition (~ 1.0 - 2.0 MPa for images (i) to (iii) is seen to be a consequence of the developing hot flame. There are especially marked inhomogeneities at this stage of the autoignition. Allowance for this should be made in the quantitative validation of numerical simulations of ignition delays when the assumption of spatial homogeneity is made in the model.

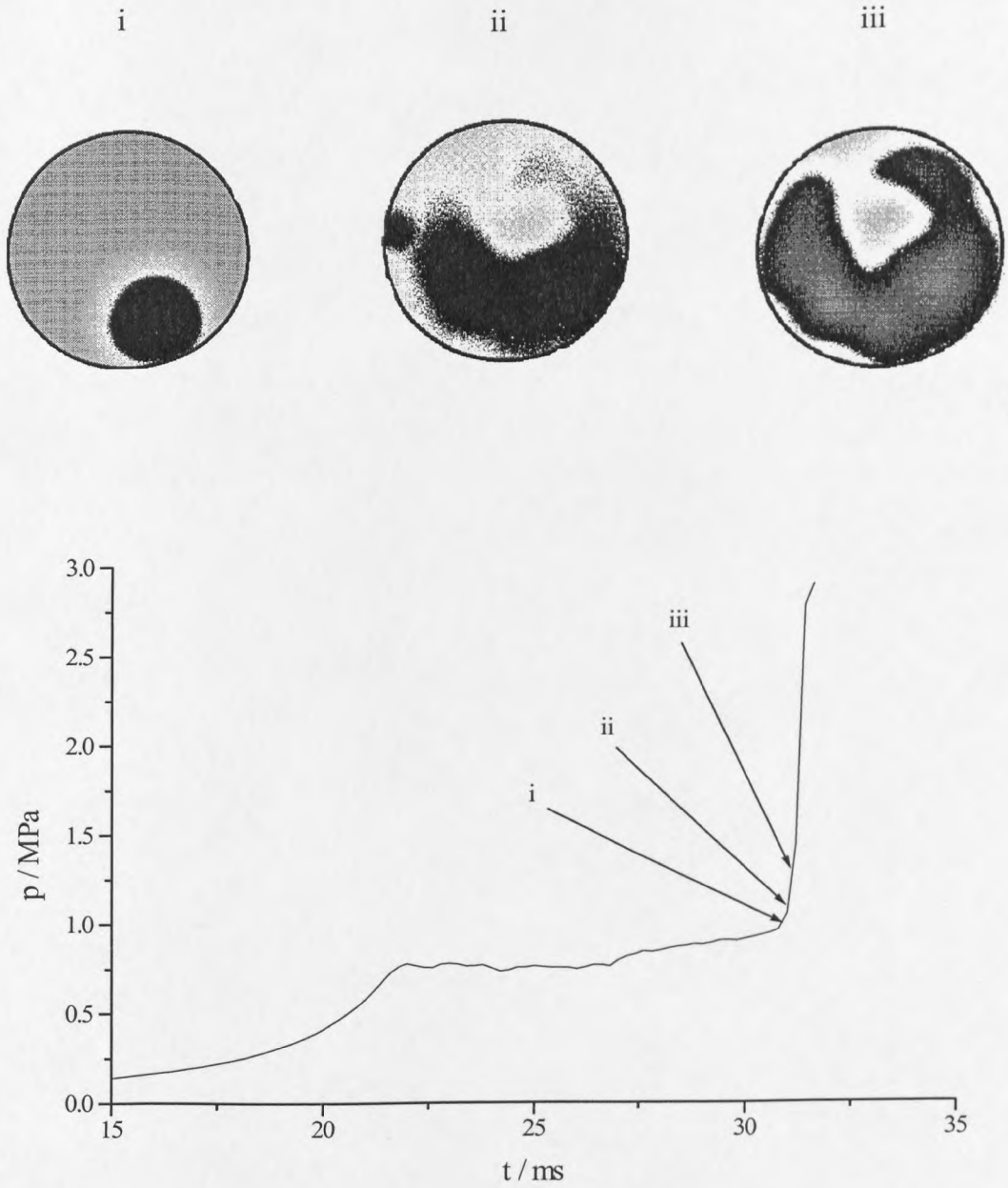

Figure 5.9(b) CCD images taken during the initial stages of the hot stage of the two-stage ignition of n-pentane following compression to 730 K. The three images were acquired at different times during ignition as shown on the pressure profile.

n-Pentane autoignition, T_c = 875 K

The schlieren and CCD images obtained for the single-stage autoignition of n-pentane following compression to 877 K are shown in Figures 5.10 and 5.11 respectively.

Frame 1 of the sequence of schlieren Film in Figure 5.10 (a) corresponds to a time during the ignition delay approximately 2 ms before the maximum pressure rise due to ignition (the pressure profile is given in Figure 5.10 (b)). Frame 4 illustrates multiple autoignition centres in the core gas region of the combustion chamber. By Frame 11 virtually all of the reactant has been consumed by autoignition and the opacity of the image was possibly due to aqueous and carbonaceous deposits on the internal surface of the window. Similarly, the CCD images in Figure 5.11 represent the development of one or more autoignition centres within the central core gas region of the combustion chamber for n-pentane autoignition following compression to temperatures greater than about 850 K.

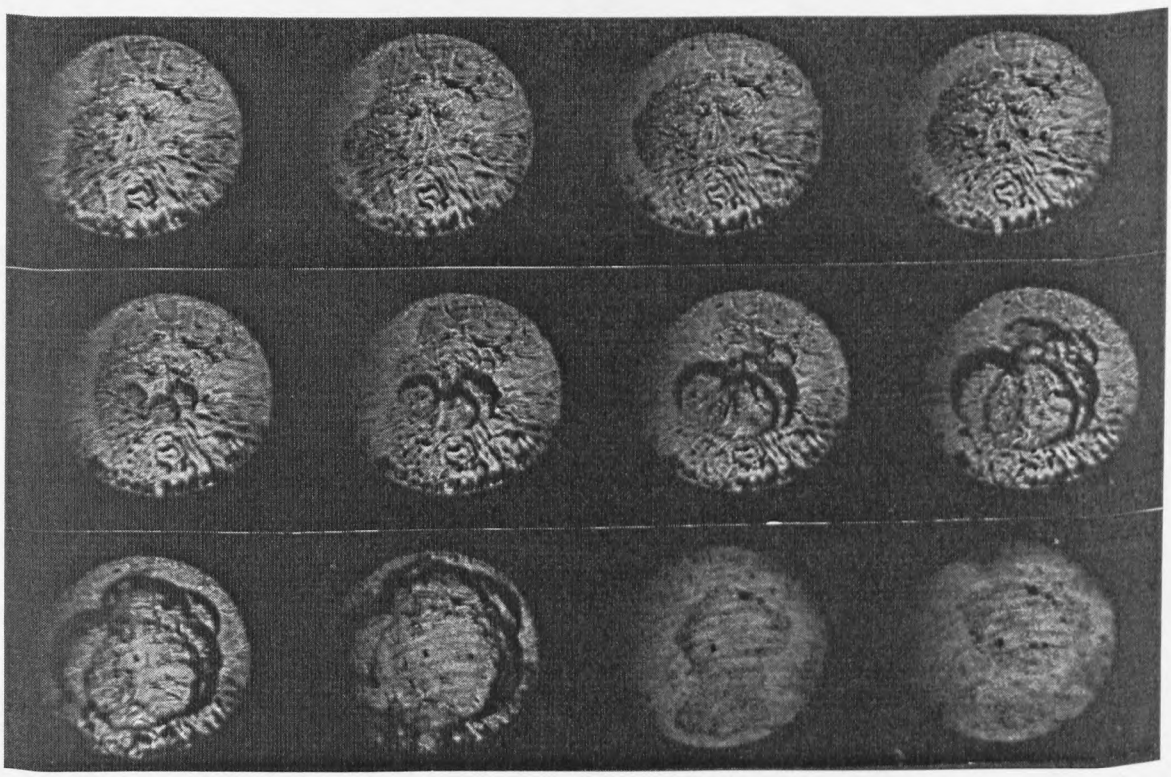

Figure 5.10 (a) Schlieren image sequence for the autoignition of n-pentane following compression to 877 in the RCM. The corresponding pressure profile is given in (b).

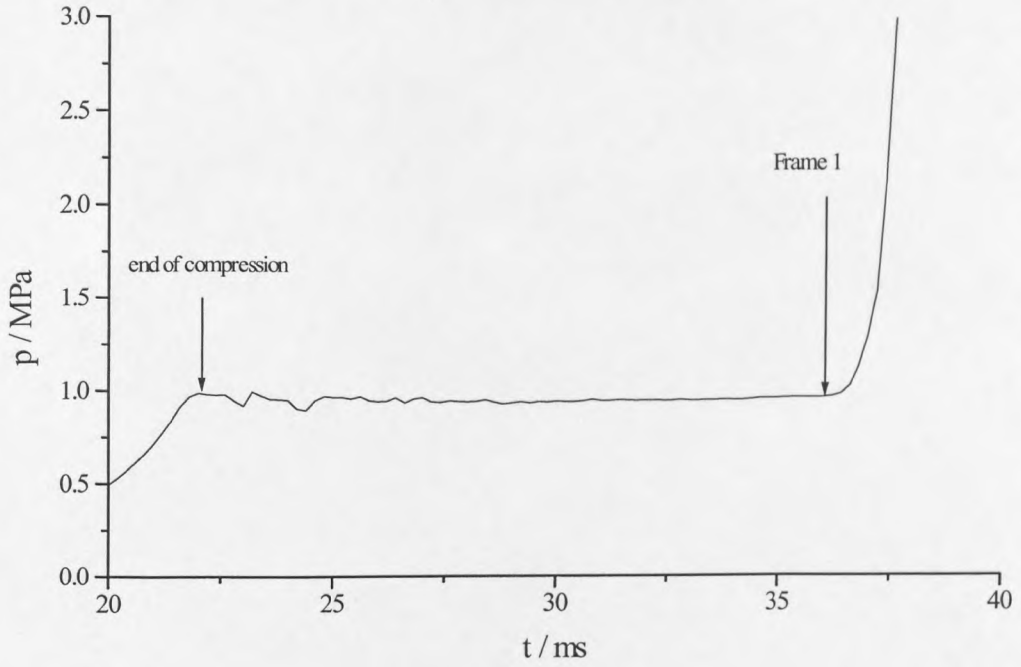

Figure 5.10 (b) Pressure-time profile for the autoignition of n-pentane following compression to 877 K in the RCM. The timing of frame 1 is indicated on the pressure profile.

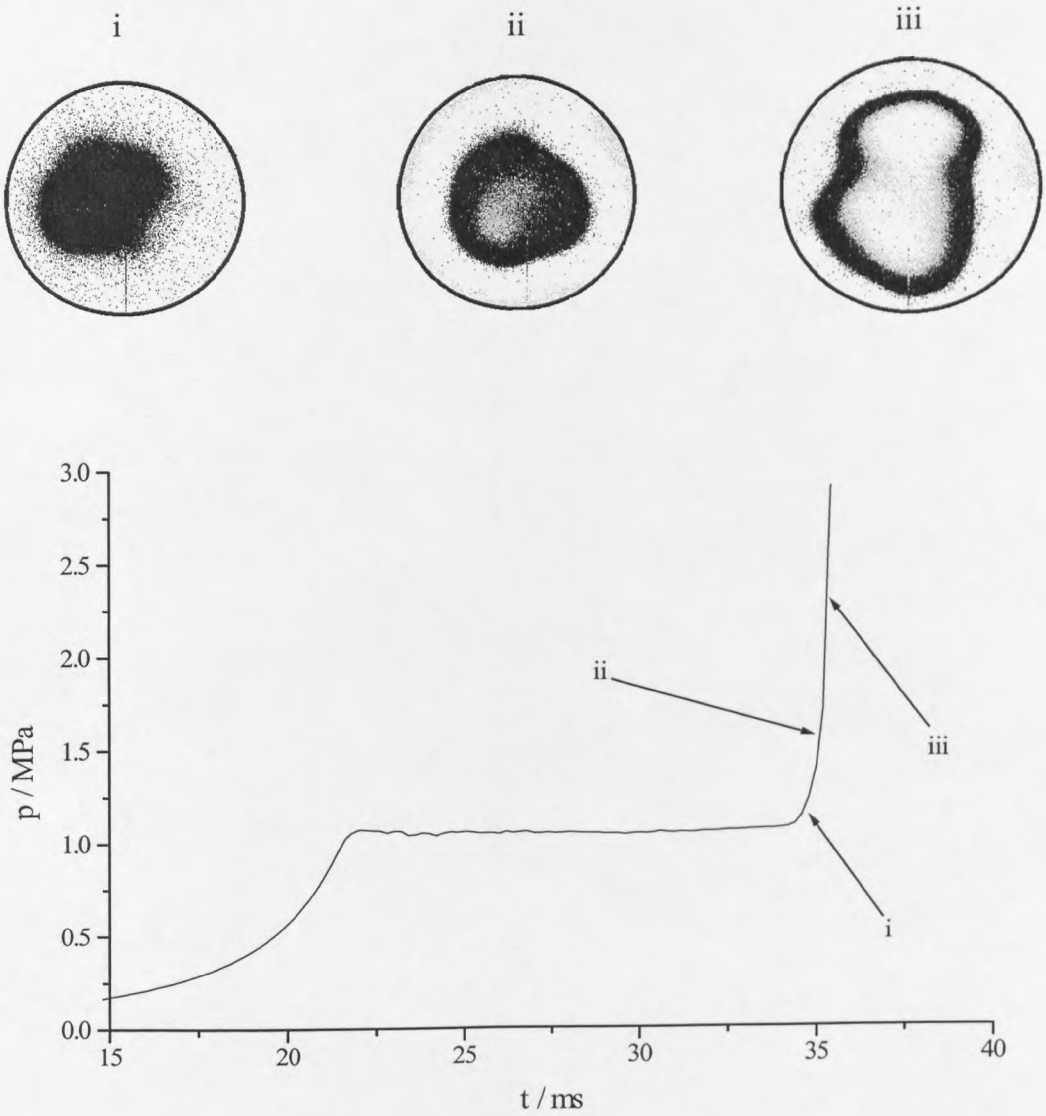

Figure 5.11 CCD images taken during the autoignition of n-pentane following compression to 890 K. The three images were acquired at different times during ignition as shown on the pressure profile.

n-Heptane autoignition

The fractional extent of consumption of n-heptane occurring in the late stages of compression has been measured experimentally (Chapter 3) and confirmed in numerical simulations [141]. All or part of this reaction occurs during the course of compression when the compressed gas temperature is above approximately 770 K. Figure 5.12 is a

representative experimental result for the autoignition of n-heptane in air following compression to 870 K in which the cool flame activity associated with the first stage of autoignition occurs before the end of compression. Evidence for the occurrence of the first (cool flame) stage before the end of compression is given by the light output record. In this case only one photomultiplier was used and the fully transparent window to allow a record of the total light output from the chamber to be obtained. Where significant reaction has occurred before the end of the compression stroke, it is necessary to calculate the end of compression temperature (T_c) using the ideal gas law. Therefore, one can obtain an appropriate value for T_c which accounts for the augmentation of the gas temperature due to exothermic low temperature oxidation reactions during the compression.

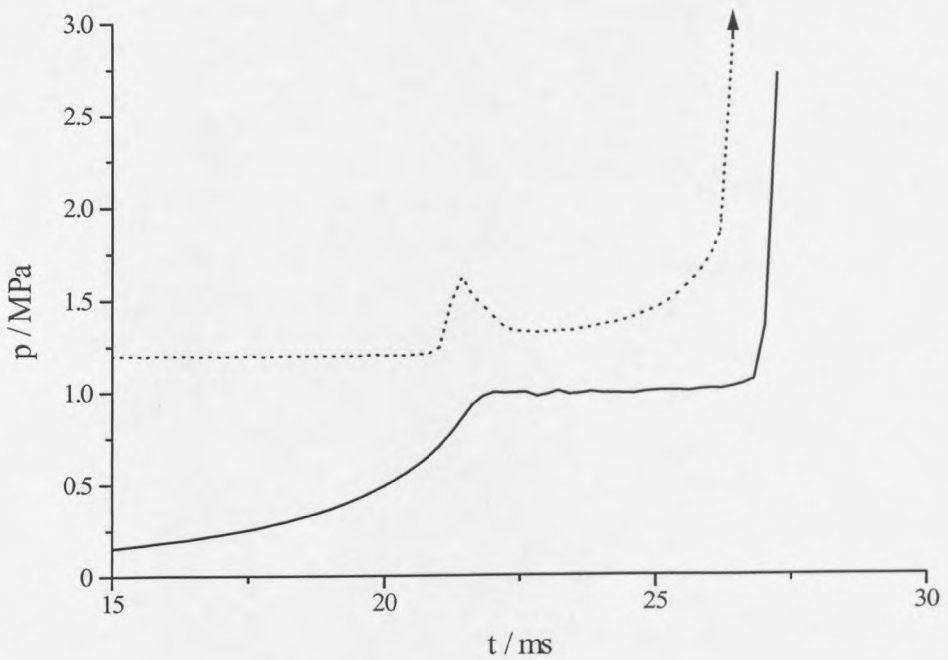

Figure 5.12 Pressure (—) and light output (---) profiles for the autoignition of n-heptane following compression to 870 K, illustrating first stage reactivity during the compression stroke.

The existence of spatial temperature inhomogeneities within the combustion chamber during the post-compression period has also been confirmed for n-heptane autoignition using the two photomultiplier tubes set-up (Figure 5.13(a) and 5.13(b)). At the lower compressed gas temperature (758 K) negligible reaction occurs during the compression stroke and two-stage ignition occurs, with the cool flame appearance during the post-compression period. Therefore, where the cool flame occurs in the post-compression period, heat losses have occurred and a boundary layer developed and a spatial structure of the cool flame exists (Figure 5.13(a)). In contrast to this, where the cool flame occurs during the late stages of compression to a higher temperature (T_c = 970 K), there has been insufficient time available during the rapid compression for heat losses to occur and hence a spatially homogeneous region of cool flame activity results (Figure 5.13(b)).

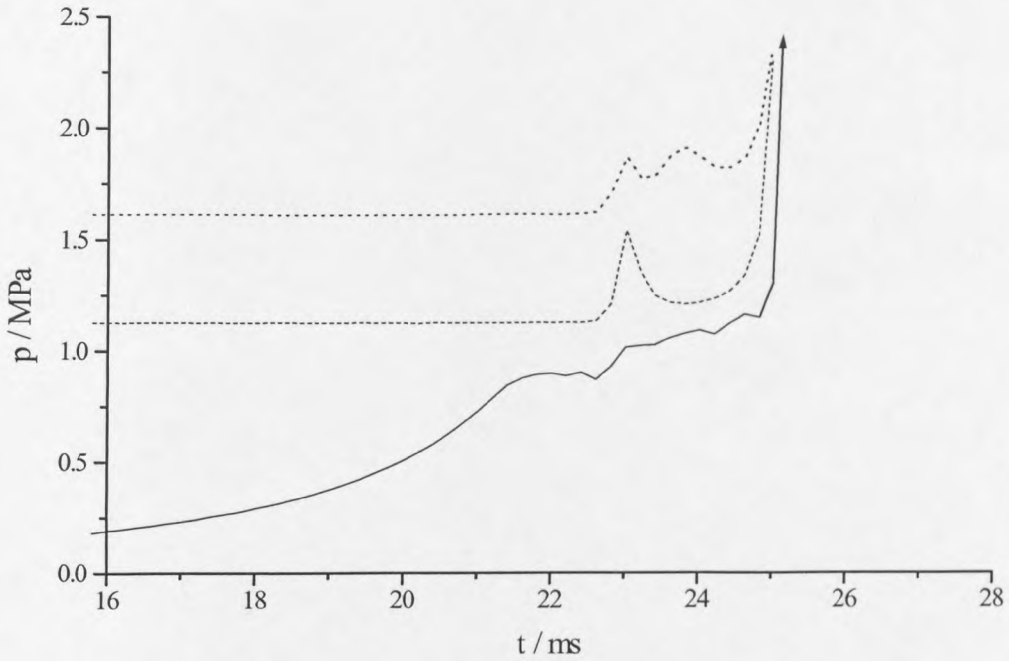

Figure 5.13(a) Pressure and light output records for the two-stage autoignition of n-heptane following compression to 758 K. Light output records corresponding to Channels 1 (...) and 2 (---) (Figure 5.2) are shown.

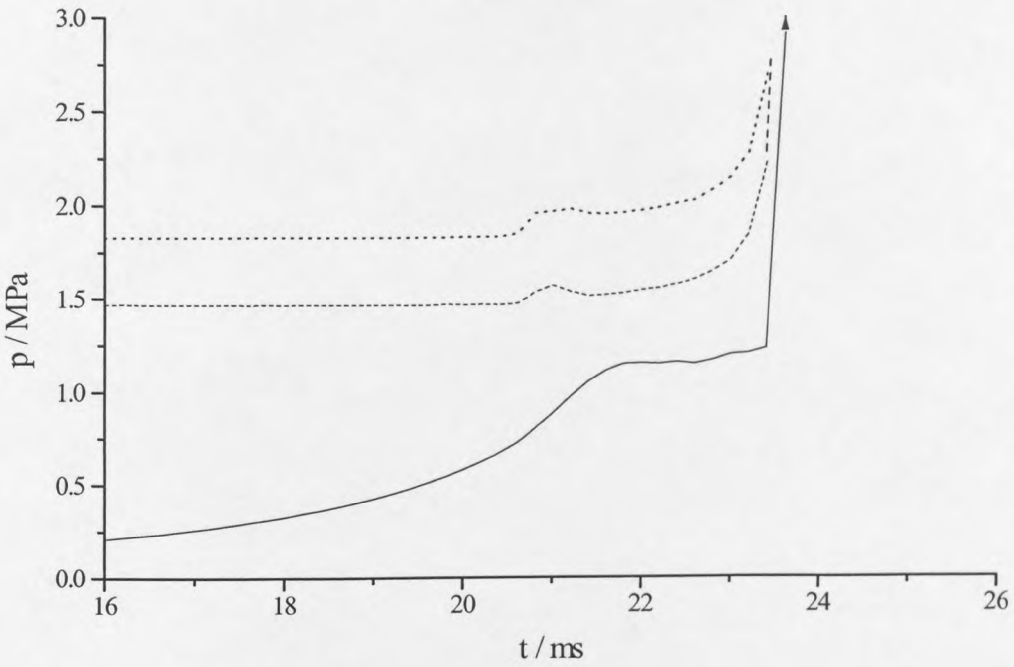

Figure 5.13(b) Pressure and light output records for the autoignition of n-heptane following compression to 970 K. Light output records corresponding to Channels 1 (...) and 2 (---) (Figure 5.2) are shown.

Imaging techniques have proved very valuable in provision of evidence for the occurrence of the "cool flame" stage of two-stage ignition before the completion of the compression stroke. Selected CCD images obtained at different conditions of temperature and time of image capture are shown in Figure 5.14 (a-c). A total light output record was obtained simultaneously using a small Perspex window in replacement of the spark plug for Fig. 5.14 (b) and (c). The experimental results provide further supporting evidence for the occurrence of first stage reaction before the end of compression. However, the intensity and spatial structure of the cool flame images differ markedly to those for the n-pentane two-stage autoignition. The light output due to the cool flame occurring in the final stages of compression is much less intense and implies negligible spatial inhomogeneity, occurring almost uniformly across the chamber diameter.

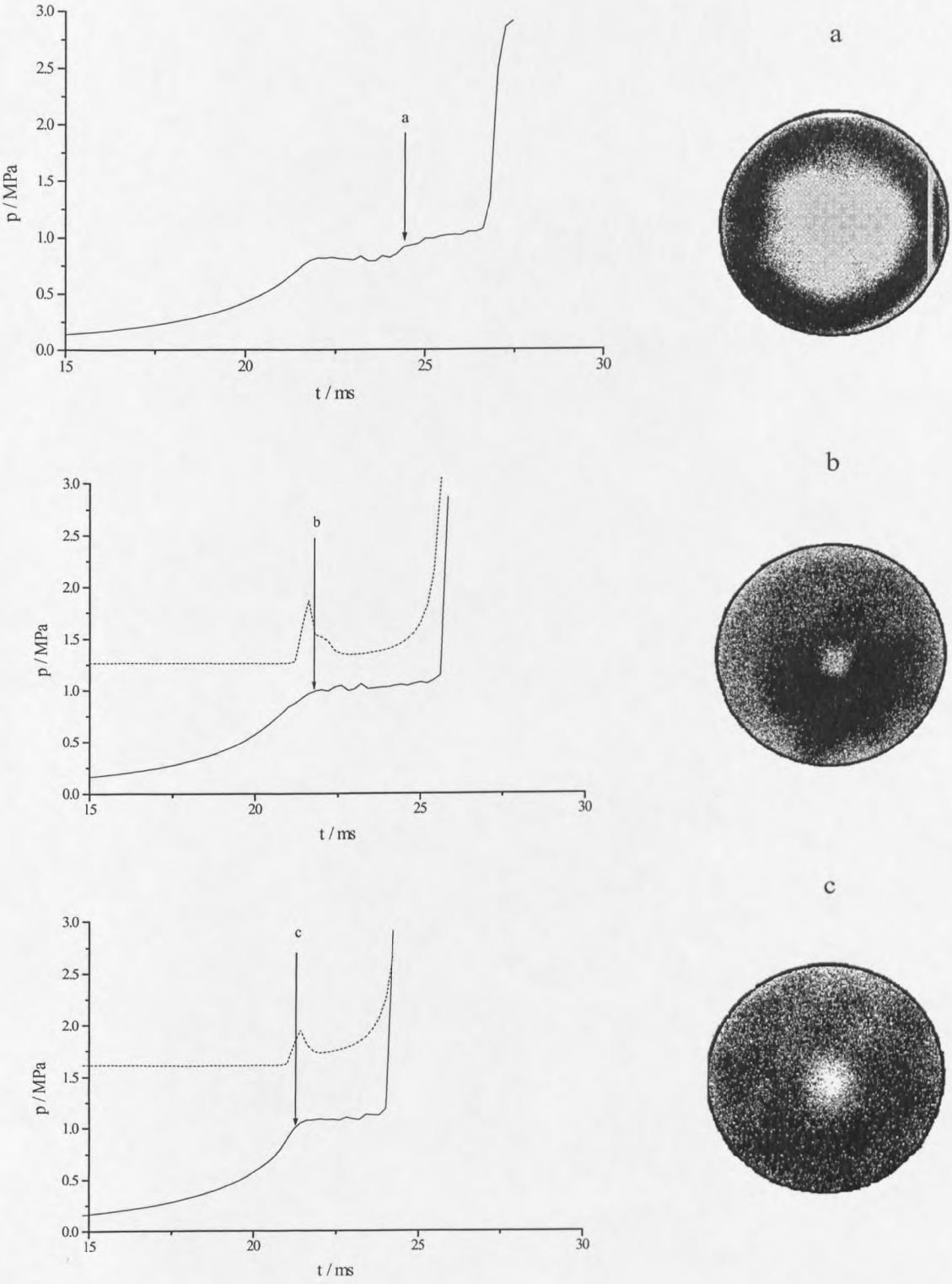

Figure 5.14 CCD images illustrating cool flame light emission during the autoignition of n-heptane at different compressed gas temperatures ((a) 708 K, (b) 832 K, (c) 911 K). The time of image capture is indicated on the accompanying pressure and light (for b and c) profiles.

5.1.4 Summary and Conclusions

In an ideal RCM experiment, autoignition would represent non-steady state, homogeneous reaction and the gas temperature would increase uniformly in that region. One would, then, expect an autoignition centre to appear as a complete black region on the film rather than the relatively light region enclosed by a dark line (or "schliere"). The schliere is representative of a discontinuity of temperature and pressure, as in a flame front, separating burned and unburned gases. In reality however, the autoignition centre appears to propagate as a combustion wave into the surrounding unburned gas. Spatial temperature variations exist within the combustion chamber in the post-compression period and the dependence of reaction rate on temperature is non-linear, exhibiting a region of non-Arrhenius (or negative) temperature dependence in the region of 750 - 850 K. These factors influence the occurrence and spatial distribution of autoignition centres.

The compression stroke of the RCM is sufficiently fast to provide adiabatic compression of the reactant gases and this has been confirmed for the majority of experiments by the comparison of T_{ad}' and T_c (Table 4.2). The vigorous gas motion and gas flow vortices formed as a result of the rapid compression, sweep hot gases across the internal surfaces of the chamber walls, which are at a lower temperature than the compressed gases. Thus, a temperature gradient is likely to exist at the internal surfaces of the combustion chamber and heat losses result due to heat transfer down the thermal gradient. The post-compression period is non-adiabatic and spatial inhomogeneities of temperature exist within the combustion chamber. This physical environment, coupled to the existence of a negative temperature dependence of the overall reaction rate at intermediate temperatures, results in an acceleration of the overall rate of oxidation in the lower temperature regions of the chamber and a tendency for autoignition centres to originate in the cooler boundary layer adjacent to the chamber walls.

The appearance of autoignition centres is a consequence of a localised acceleration of the reaction rate due to the pressure, temperature, composition and reactivity of the gaseous charge at a given point. For example, n-pentane compressed to 750 K exhibits a spatial structure during the subsequent development of the cool flame stage of two-stage autoignition, which occurs within a localised region of the combustion chamber, adjacent to the wall. This implies that the temperature is low enough for cool flame activity only in this part of the chamber. This suggests that free radical and molecular intermediate concentrations are highest in this region. The overall reaction rate is lower in any other part of the chamber where the gas is hotter, and especially in the adiabatic core. The "cool flame conditioned" boundary region is the most reactive zone, from which the second stage chemistry can be initiated. Consequently, the ignition centres are first seen in the regions close to the wall and not at the centre.

When the reactants are compressed to a sufficiently high temperature that there is no opportunity for cool flame activity or an influence of the negative temperature dependence, the most active region is the hottest gas region. Thus, autoignition is most likely to be initiated in the adiabatic core gas region of the chamber. This would appear to be supported by the results for n-pentane shown in Figures 5.7 and 5.10.

The autoignition centre begins to develop and appears to propagate outward as a flame front consuming the surrounding unburned gas. Therefore, in addition to the mechanical compression of the gaseous charge by the piston, there is a further compression by the expanding autoignition centre and the flame front that subsequently develops from it. These further raise the pressure and temperature of the unburned gas in the combustion chamber and can result in the initiation of one or more additional autoignition centres in other regions of the chamber (Figure 5.7(a), Frame 42).

The first experimental evidence for the existence of spatial inhomogeneities in the Leeds RCM combustion chamber was found using the experimental method described earlier

with two photomultipliers each monitoring the light output from spatially distinct regions of the chamber. Following this data acquisition, further verification for the occurrence of autoignition centres in the cooler regions of the chamber was sought using the two-dimensional imaging methods. The combination of these methods for visualising the light output from the chamber has led to the acquisition of incontrovertible evidence in support of the existence of spatial inhomogeneities within the combustion chamber of the RCM. In addition to this, evidence for the occurrence of autoignition centres in the cooler regions of the chamber adjacent to the chamber walls, following compression to temperatures within the ntc region, has been obtained.

These experimental results confirm the existence of spatial temperature inhomogeneities within the combustion chamber of the Leeds RCM during the post-compression period. The results also support the numerical prediction that, within the region of the ntc, autoignition centres may originate in the cooler boundary layer adjacent to the chamber walls.

5.2 Spark-ignition and "knock" in the RCM

5.2.1 Introduction

Engine knock is the physical manifestation of the abnormal oscillations in the cylinder pressure during combustion. The localised overpressures generated at an exothermic centre are dissipated by the propagation of pressure waves away from the hot centre with an acoustic frequency. The severity of the knock induced in the end-gas determines the extent of the damage that may be caused in an engine [185].

In the past, the common practice was to define knock intensity as the ratio of knocking cycles to the total number of firing cycles sampled. More quantitative methods now exist and knock intensity may be characterised in a variety of ways which are commonly based on the amplitude and frequency of the measured pressure fluctuations in the

combustion chamber. The calculation of the integral knock parameter, KIrms, is one such method [203]. KIrms is defined as the root mean square amplitude of the cylinder pressure oscillations measured over an interval of 2 ms from the onset of knock, after the mean cylinder pressure has been filtered by a high pass filter with a cut-off frequency of 2 kHz (Appendix D).

Khalghatgi et al. [144] adopted a knock intensity defined as the difference between the maximum and minimum of the filtered pressure record, but other parameters, such as a "knock onset time" and a "knock onset pressure", were deemed also to be of importance. In a quite different approach, Kono et al. [123] determined knock intensity from the energy of the gas vibrations resulting when the end-gas ignites spontaneously. This method assumes that the gas vibration energy originates from the difference between the displacement of the 2 types of burned gases produced by the flame propagation and the spontaneous ignition processes.

Purpose of study

The use of imaging techniques coupled with high frequency sampling of pressure data has enabled the association of autoignition in the end-gas region ahead of an expanding spark-ignited flame in the RCM with a knock-like oscillating pressure profile for n-pentane and for a PRF 60 mixture. A quantitative comparison of knock intensities has been made by determining the value of the knock intensity, KIrms, for different fuels, compressed gas temperatures and spark timings. The imaging techniques have been used to verify the relationship between the occurrence of autoignition centres in the unburned end-gas and the high frequency pressure oscillations associated with knocking combustion in spark-ignition engines. A common link between the knock intensity and the ignition delay variation with T_c can be made for the spark-ignition of n-pentane-air and n-heptane-air mixtures.

5.2.2 Experimental

The incorporation of a motorcycle engine spark plug (NGK CR7HS) into the side wall of the chamber has enabled a comparison of spark-ignition and autoignition of hydrocarbons in the RCM. The spark plug discharge was generated by a LUCAS variable duration arc ignition supply via a 12V ignition coil. The timing of the spark was controlled by use of a spark delay unit (Appendix E), which electronically generates a variable delay on the output signal to the spark generator. The data capture software was also adapted to include a transient data recorder (DATALAB DL905) which sampled the amplified pressure transducer signal over a 10 or 20 ms interval at a high frequency (100 or 50 kHz). This pressure profile could then be used to give a quantitative measure (by calculation of the parameter KIrms) of the knock intensity of a spark-ignited fuel-air mixture in the RCM.

5.2.3 Results

Using schlieren imaging and fast photography applied to the study of spark-ignition in the RCM, the knock-like oscillatory pressure profile obtained can be associated with the occurrence of autoignition centres ahead of the spark-ignited flame (Figure 5.15). In other instances where a knock-like pressure profile was obtained, the rapid pressure oscillations appear to be associated with either a rapid burn-up of the end-gas (Figure 5.16) or an acceleration of the flame front propagation as it coincides with the hot reacting gases in the central core region of the combustion chamber (Figure 5.17).

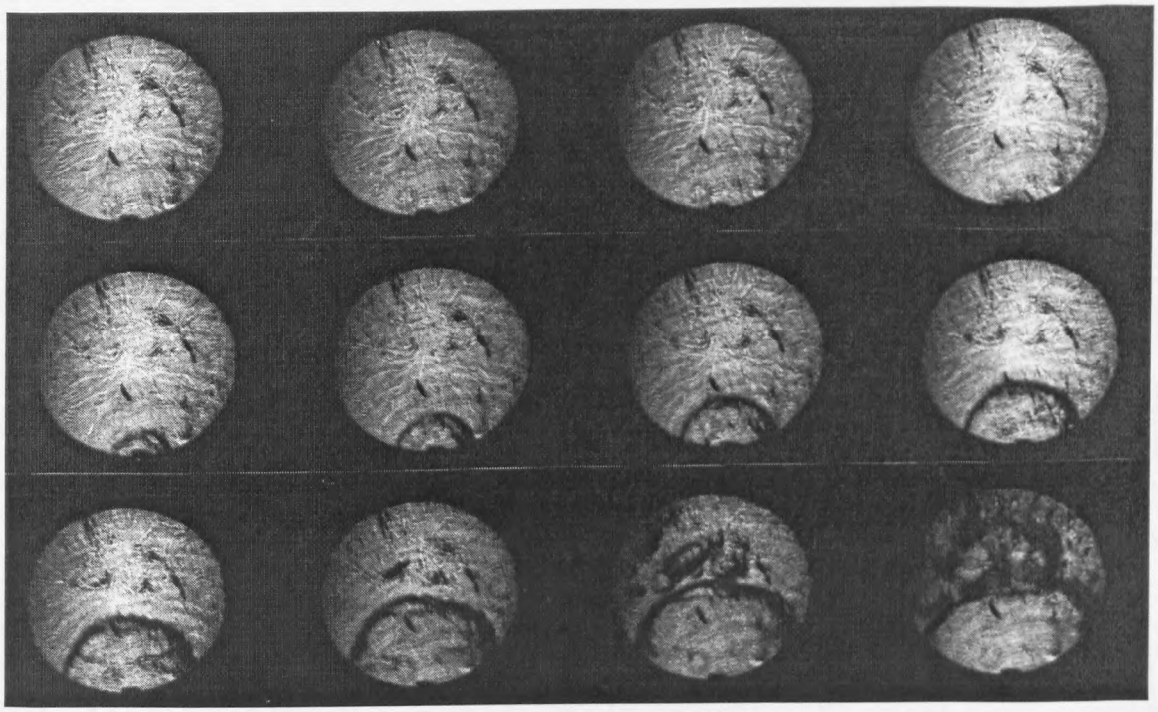

Figure 5.15 (a) Schlieren image sequence illustrating the spark-ignition of n-pentane and the occurrence of autoignition ahead of the spark-ignited flame. Spark-ignition occurred at 10 ms after compression to 872 K.

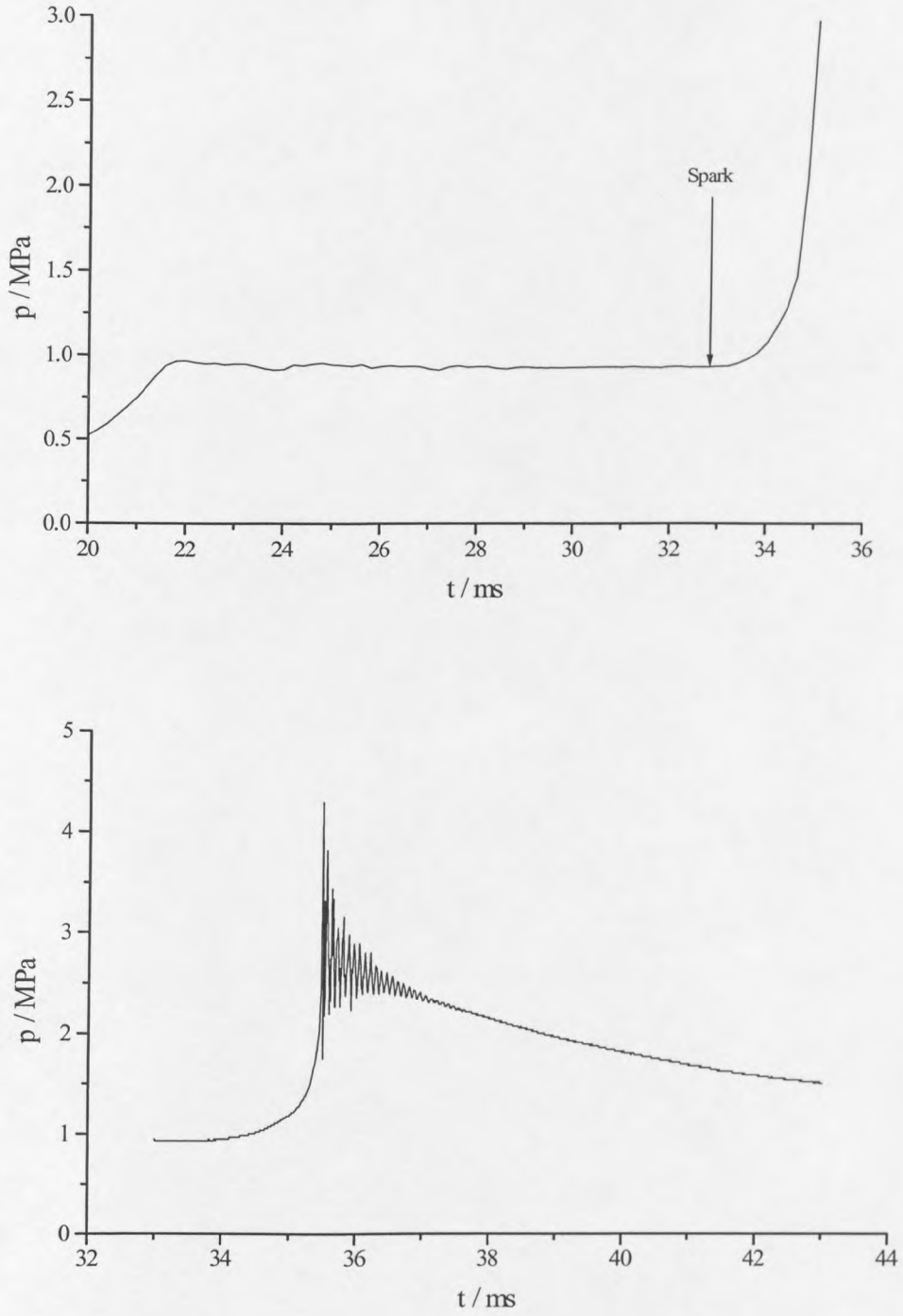

Figure 5.15 (b) (i) Pressure-time profile and transient data recorder knock profile for the spark-ignition of n-pentane, corresponding to the schlieren image sequence shown in Fig. 5.15 (a).

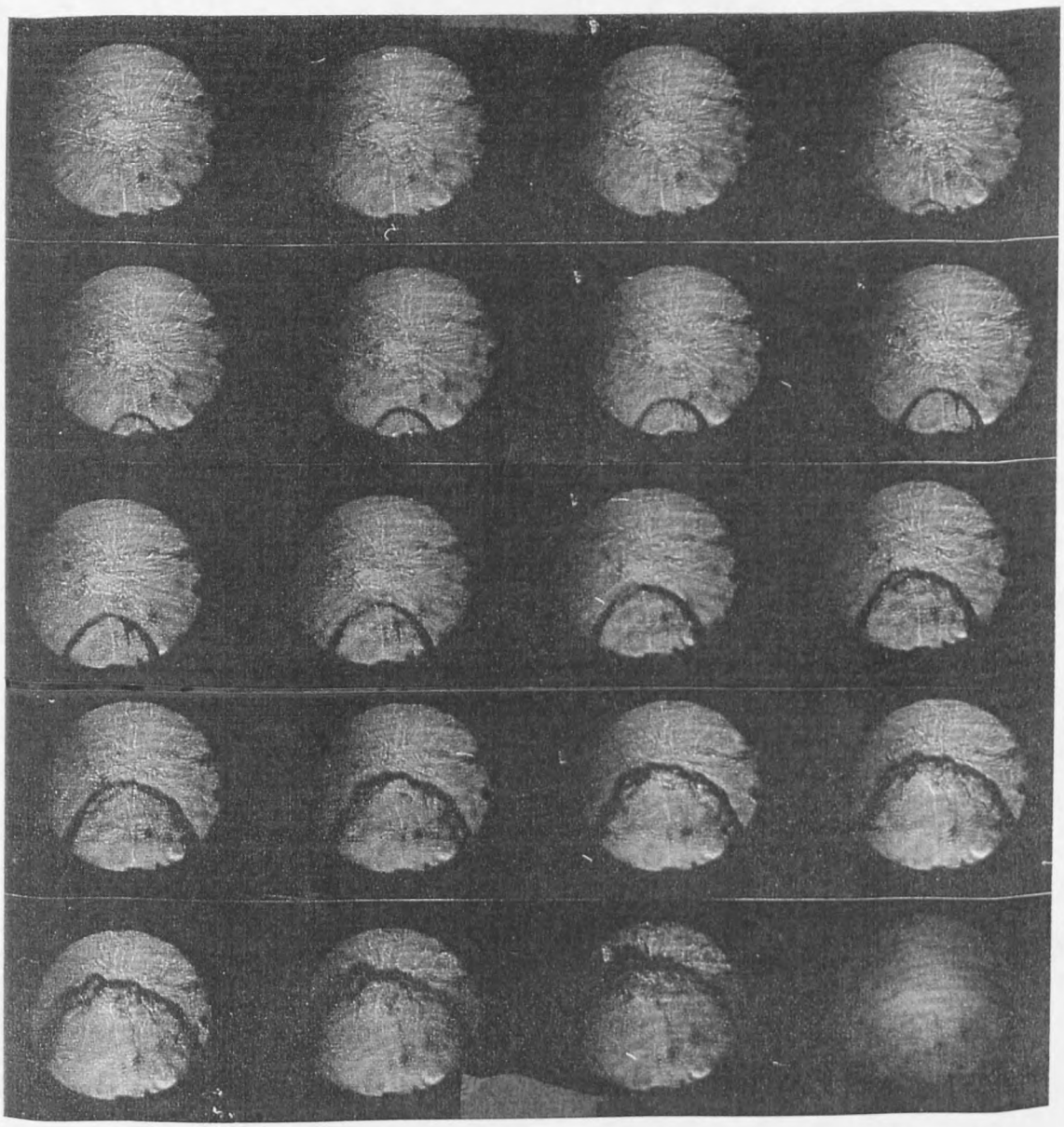

Figure 5.16 (a) Schlieren image sequence illustrating the spark-ignition of a PRF 60 mixture spark-ignited at 6 ms after compression to 877 K.

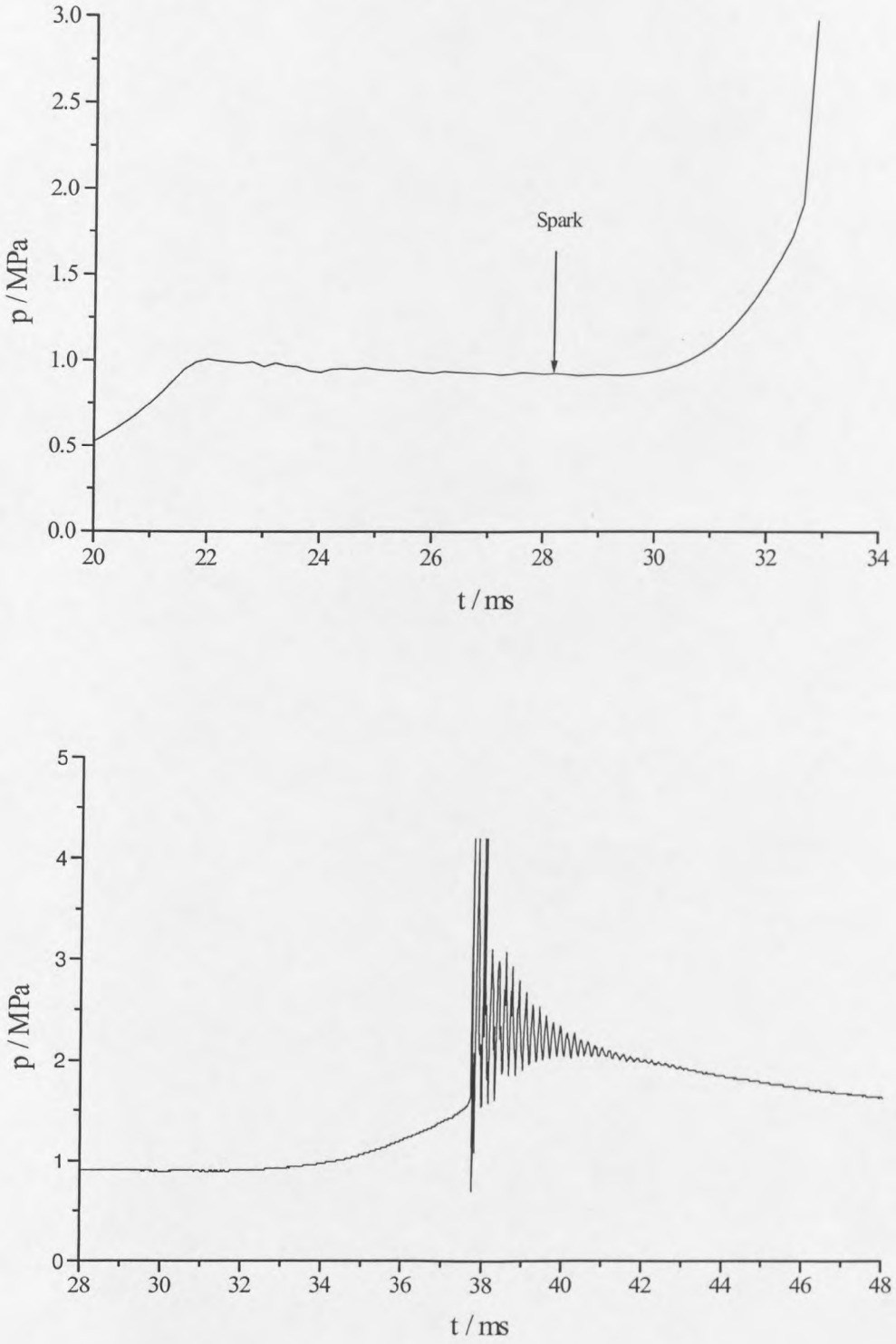

Figure 5.16 (b) Pressure-time profile and transient data recorder knock profile for the spark-ignition of a PRF 60 mixture, corresponding to the schlieren image sequence shown in Fig. 5.16 (a).

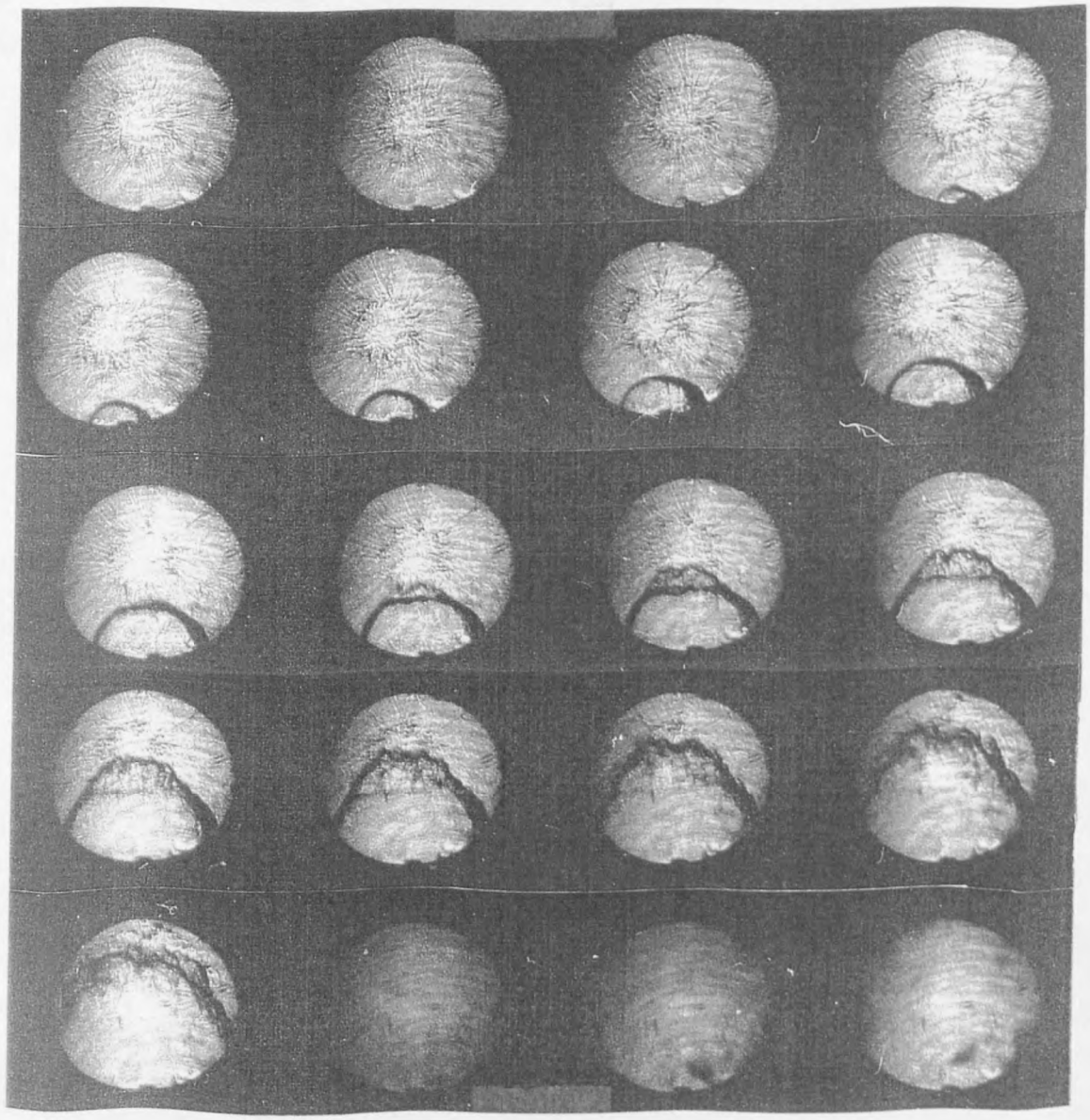

Figure 5.17 (a) Schlieren image sequence for the spark-ignition of a PRF 60 mixture spark-ignited at the end of compression to 876 K.

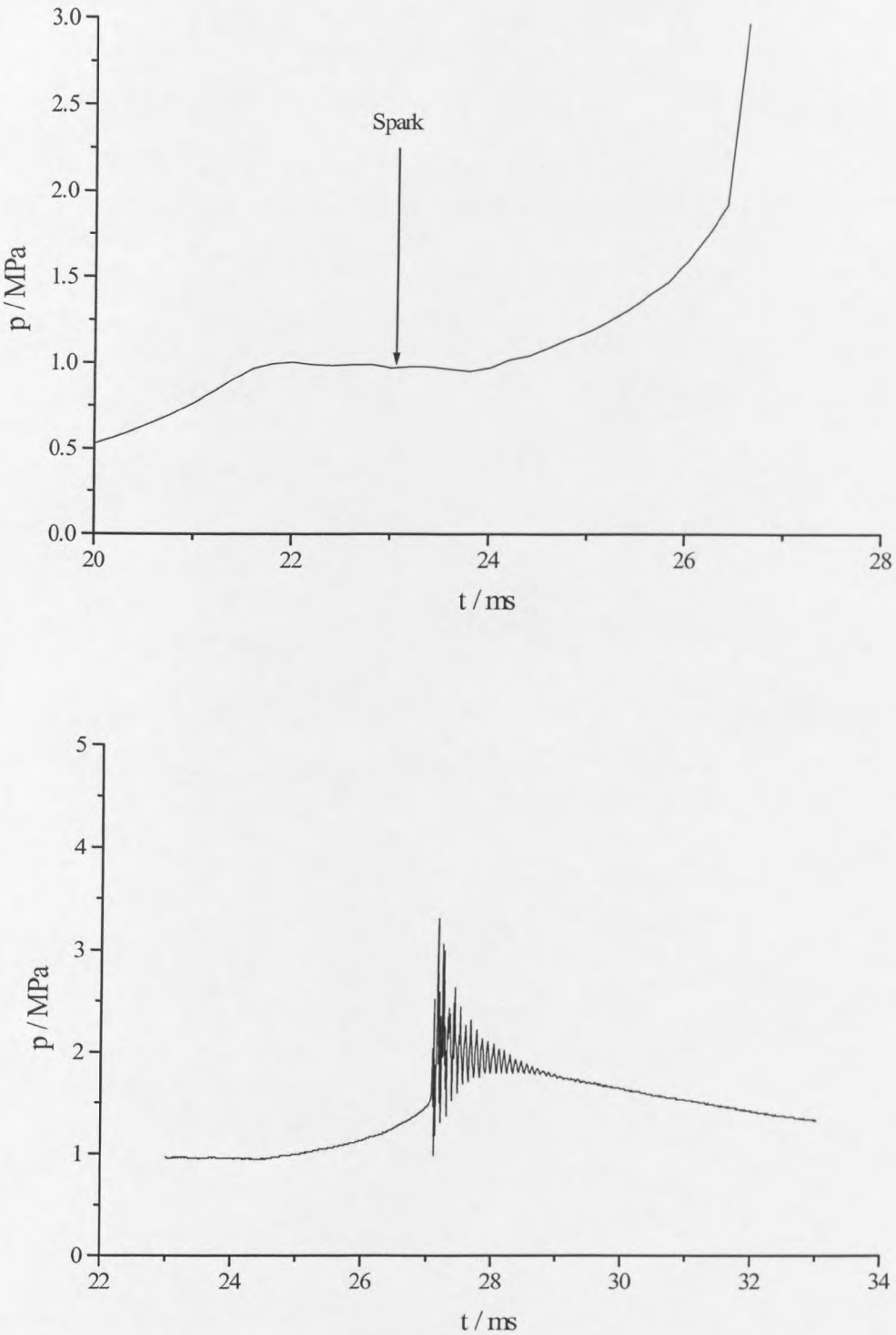

Figure 5.17 (b) Pressure-time profile and knock profile for the spark-ignition of a PRF 60 mixture, corresponding to the schlieren image sequence shown in Fig. 5.17 (a).

The image intensified CCD camera can not be used to illustrate the occurrence of both autoignition centres and the spark-ignited flame on the same frame due to the different operating gain of the image intensifier required for the study of each of these events.

The spark-ignited flame kernel development has been followed and documented using the CCD camera for the spark-ignition of n-pentane at the end of compression following compression to 750 K (Fig. 5.18 (a)) and to 875 K (Fig. 5.18 (b)). The image processing software (AVS) has been used to identify the flame edge as described in Section 5.1.2. The time of image capture relative to the spark (at the end of compression) is shown. The images suggest a more rapid flame propagation of the spark-ignited flame following compression to the higher temperature, 875 K.

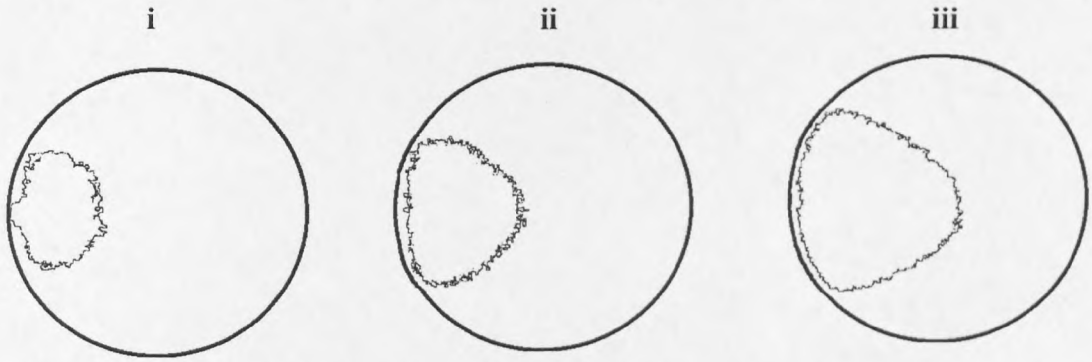

Figure 5.18 (a) CCD images showing flame edge propagation during the spark-ignition of n-pentane at tdc following compression to 750 K. Frames at (i) 1.6 ms, (ii) 2.0 ms, and (iii) 2.6 ms after the spark initiation.

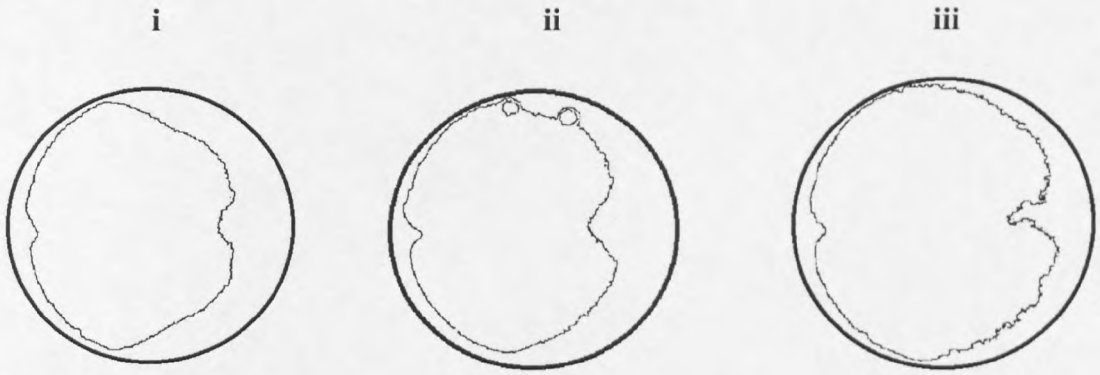

Figure 5.18 (b) Spark-ignition of n-pentane at tdc following compression to 875 K. Frames at (i) 2.2 ms, (ii) 2.4 ms and (iii) 2.6 ms after the spark initiation.

In general, the rate of development of the spark-ignited flame is indicative of the temperature of the reactant gases within the chamber. The flame propagates at an increased rate through hot gas. The mass fraction of fuel consumed during the autoignition of the end-gas influences the knock intensity. The greater the amount of fuel burned due to autoignition the more rapid the rate of energy release and thus more violent knocking combustion results. However, engine experiments have illustrated that knock intensity is more sensitive to the mean end-gas temperature than to the mass of unburned gas available for autoignition [203]. This would appear to be vindicated by the results presented in Figure 5.18 (a) and (b), where the volume of unburned gas available for autoignition (based on an approximation of the flame area) is similar in both cases but the calculated knock intensities differ significantly (KIrms values of 1.2 (±0.5) bar and 4.0 (± 0.5) bar respectively). The additional compression and heating of the end-gas by the expanding spark-ignited flame results in the autoignition chemistry proceeding at a much faster rate in the higher temperature gas and knocking combustion results.

Normal-pentane-air and n-heptane-air mixtures were spark-ignited at the end of the compression stroke, at T_c in the range 650 - 910 K. Pressure records for n-pentane combustion, obtained using the transient data recorder, are shown in Figure 5.19. Pressure oscillations were detected during both n-pentane and n-heptane combustion at all compressed gas temperatures in excess of 700 K. The pressure oscillations showed and increasing severity with T_c at first. However, in both cases KIrms decreased at intermediate compressed gas temperatures before a further increase was detected at higher compressed gas temperatures (Figures 5.20(a) and 5.20(b)). An additional parameter used to characterise the severity of the ensuing events following spark-ignition was the elapsed time from the initiation of the spark to the maximum rate of pressure rise during ignition (t_s) as illustrated in Figure 5.19. In figures 5.21 (a) and 5.21 (b) the dependence of t_s on T_c for n-pentane (Fig. 5.21 (a)) and n-heptane (Fig. 5.21 (b)) is illustrated.

For n-pentane there was a marked decrease in t_s at compressed gas temperatures at which knock was observed, but this interval became virtually insensitive to T_c

throughout most of the knock region (725 < T_c < 900 K). Results for the PRF 60 mixture show similar sensitivity (Fig. 5.21 (a) (x)). There was a high sensitivity of t_s to T_c during n-heptane combustion at the lowest compressed gas temperature but this was followed by a significant negative temperature dependence of t_s as T_c was raised. The longest duration of t_s, at T_c = 875 K, was associated with the lowest knock intensities (Figure 5.21). Severe knock was associated with very short intervals (t_s) at compressed gas temperatures above 875 K. The absence of experimental data from the n-heptane results in the range T_c = 775 - 850 K arises from the occurrence of extensive exothermic reaction in the final stage of the compression stroke, which raises the compressed gas temperature considerably as discussed in Chapter 4.

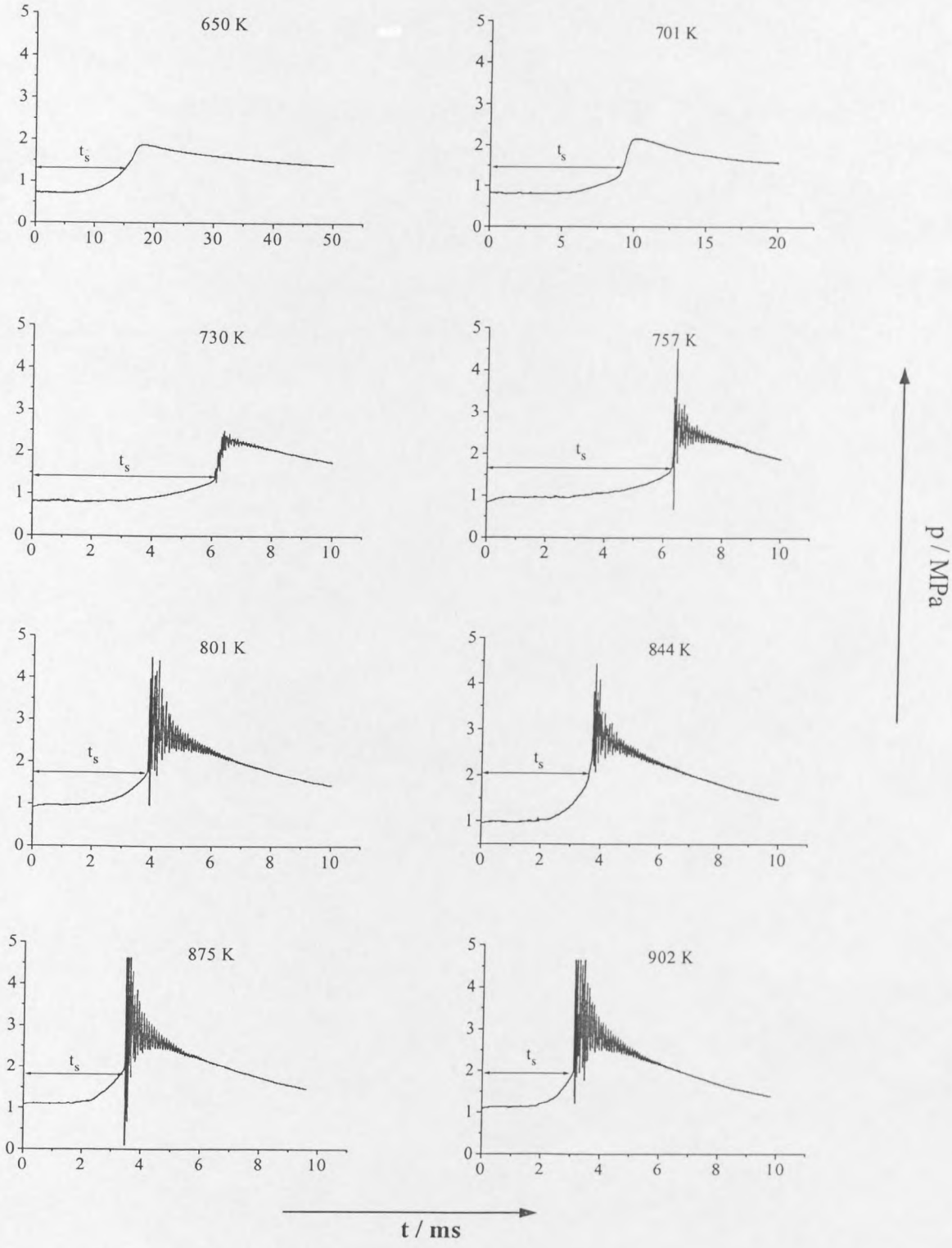

Figure 5.19 Transient data recorder pressure profiles for spark-ignition of n-pentane at tdc in the range of compressed gas temperatures 650 - 910 K.

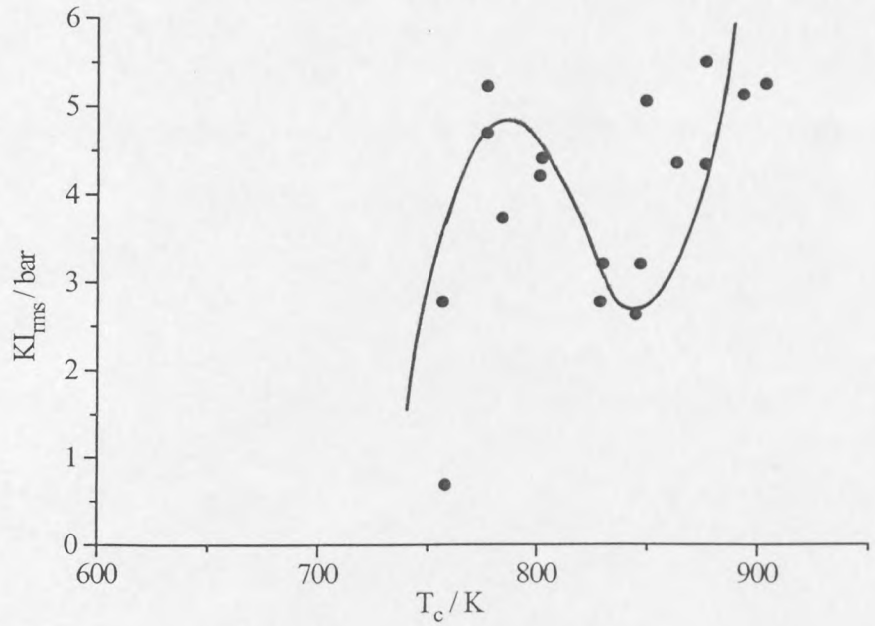

Figure 5.20 (a) Knock intensity (KIrms) vs. compressed gas temperature for the spark-ignition of n-pentane at the end of compression in the range T_c = 650 -910 K. Negligible knock occurred at T_c < 700 K.

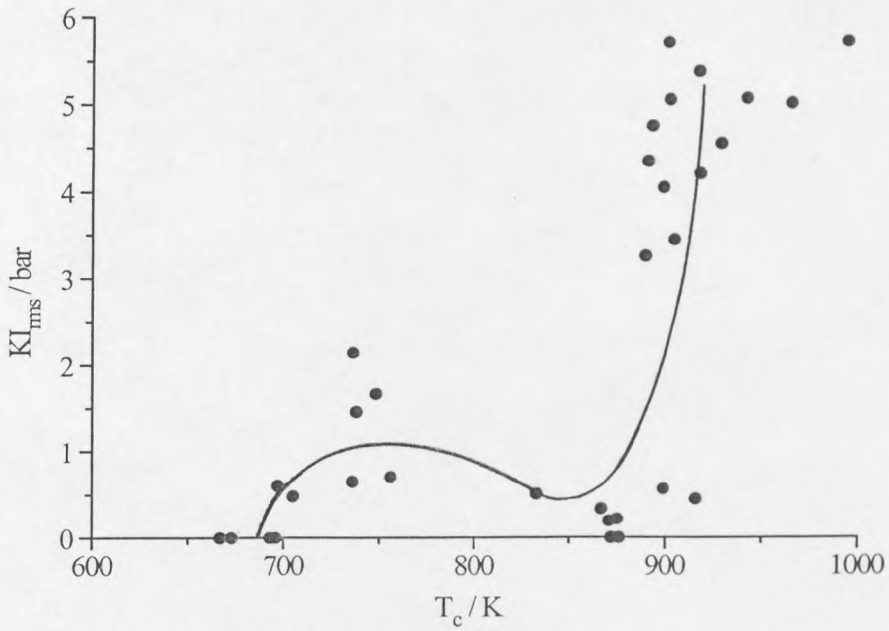

Figure 5.20 (b) Knock intensity (KIrms) vs. compressed gas temperature for the spark-ignition of n-heptane at tdc in the range T_c = 650 - 1000 K.

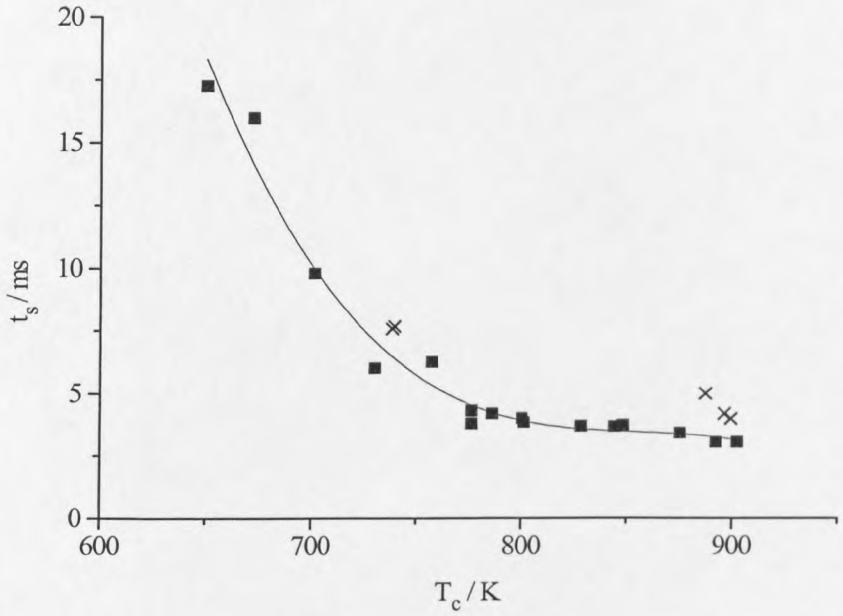

Figure 5.21 (a) Time from initiation of spark to maximum rate of pressure rise in ignition (t_s) vs. compressed gas temperature for the spark-ignition of n-pentane at the end of compression. Limited results for the spark-ignition of a PRF 60 mixture are also shown (x).

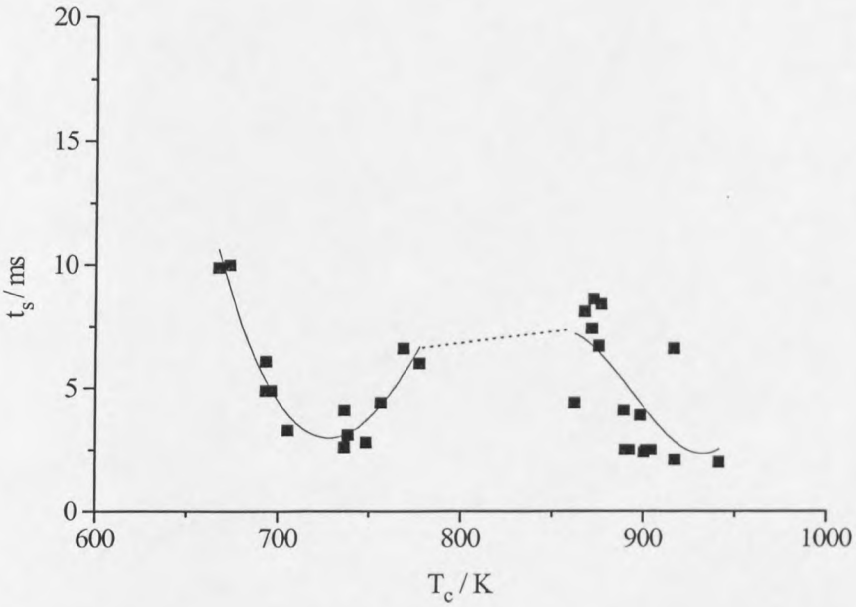

Figure 5.21 (b) Time from initiation of spark to maximum rate of pressure rise in ignition (t_s) vs. compressed gas temperature for the spark-ignition of n-heptane at the end of compression in the range T_c = 650 - 1000 K. The dotted line signifies the inaccessible temperature range as discussed in Chapter 3.

5.2.4 Summary and Conclusions

In the present study, the most severe knock, in terms of KIrms, during n-pentane and n-heptane combustion occurred both at relatively low as well as at the highest compressed gas temperatures (Figure 5.20). These were interspersed by a region of low knock intensity. The compressed gas temperatures at which KIrms decreased corresponded to those at which there was an ntc of the ignition delay. These experimental features appear to be consistent with previous experimental results and numerical predictions of knock intensity variation with compressed gas temperature, using a CFD code [139].

The timing of the spark initiation is significant in terms of the condition of the gas being ignited, this is exemplified in this and in previous work [219]. As described previously (Section 2.3.3 and 5.1.1), immediately after compression the gas motion within the combustion chamber is vigorous and the temperature is at a maximum before heat losses occur to the walls. Therefore, the high temperature and turbulence provide the optimum conditions for favourable propagation of a flame from the spark. In the absence of turbulence, after long delays to the spark initiation, the flame is unwrinkled and almost symmetrical. However, the near spherical propagating flame is constrained by the more violent autoignition centre ahead of it (Figs. 5.15 and 5.22).

The conditions at the end of the compression, when spark-ignition occurred, are well defined. The gaseous reactants are compressed and further heated as the spark-ignited flame develops. This affects, not only the rate of spontaneous oxidation in the end-gas, which eventually leads to autoignition and possibly knock, but also the burning velocity of the propagating flame itself. Consequently, the time to the onset of autoignition in the end-gas shown as a function of T_c, given in Figure 5.21, does not represent identical behaviour to the dependence of t_i on T_c. Nevertheless, there are qualitative similarities, particularly in the weak dependence of t_s on T_c during n-pentane combustion and the negative temperature dependence of t_s during n-heptane combustion, which correspond to the regime in which a negative temperature dependence of τ was detected (Section 4.2).

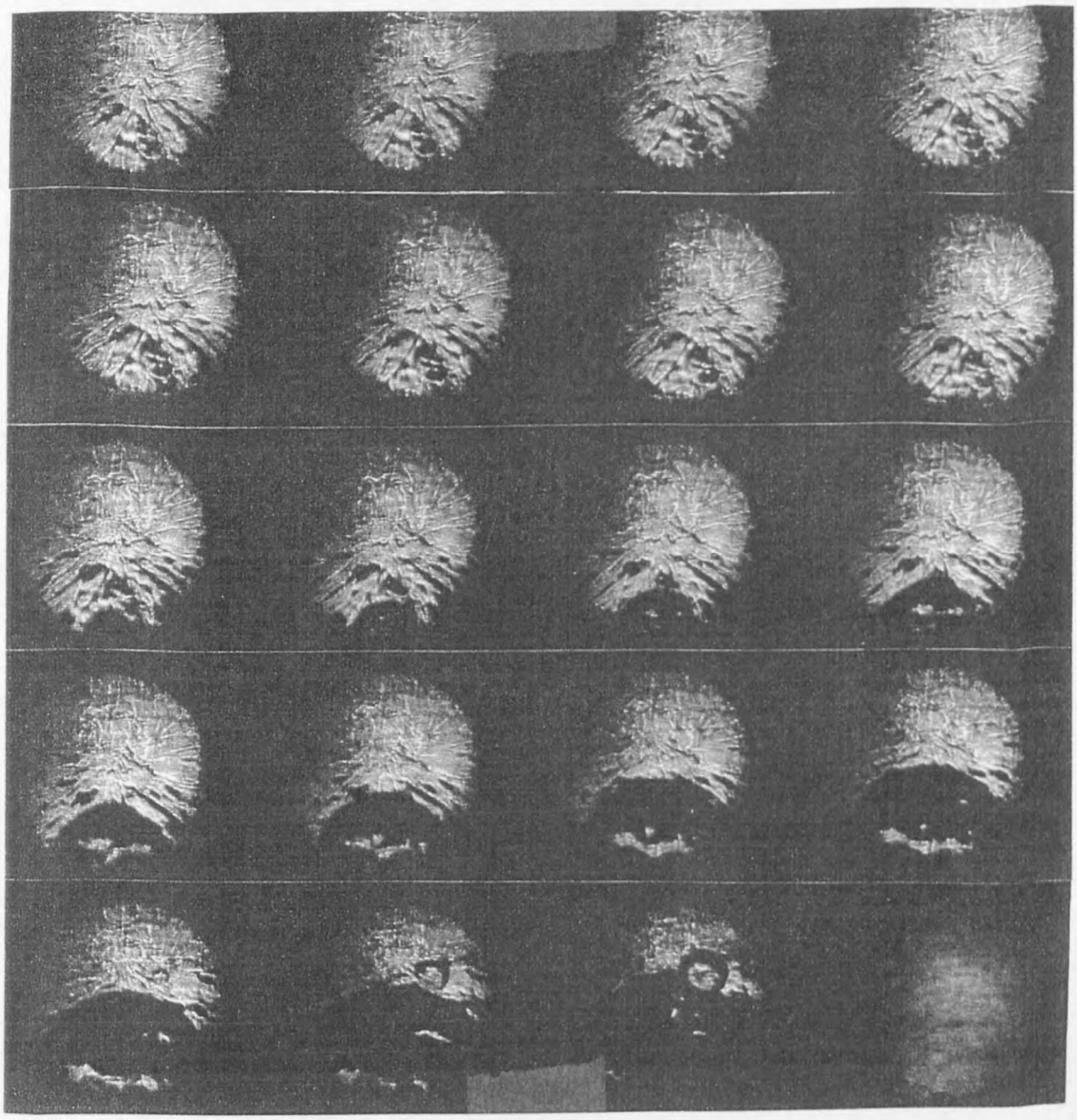

Figure 5.22 Schlieren image sequence for the spark-ignition of a PRF 60 mixture, spark occurred at 15 ms after the end of a compression to 885 K.

The end-gas temperature during spark-ignition experiments can be estimated using the measured pressure record and the schlieren photographs of the flame propagation to estimate the volume of burned and unburned gas, assuming ideal gas behaviour. However, such methodology does not account for the additional compression and

heating of the end-gas due to the expanding spark-ignited flame or the effects of heat transfer from the hot flame to the surrounding gases. A modified version of the LUSIEDA (Leeds University Spark Ignition Engine Data Analysis) thermodynamic model [220] has been developed for application to the RCM, which allows the end-gas temperature and the burned mass fraction to be estimated, without any chemical contribution. A brief description of this method and an example of the results obtained will be given in Chapter 6.

There is insufficient experimental information to explain the distinction between n-pentane and n-heptane with respect to the ntc of t_s, which is a reversal of the characteristics measured for the dependence of τ on T_c. It is known that the failure of n-heptane to show an ntc of τ in the RCM is determined by the extent of reaction that occurs in the compression stroke [221] (Chapter 3). The response of t_s may also be related to this. One qualitative perception is that if the overall rate of oxidation were to exhibit a strong positive dependence throughout the entire range of compressed gas temperatures, the duration of t_s would be expected also to diminish monotonically. Neither an independence nor a negative temperature dependence of t_s on T_c would be a possibility.

At its minimum, the duration of t_s is related to the reactivity of the fuel, that for n-heptane being shorter than that of n-pentane (Figure 5.21). These similarities between the results in Figure 5.21 (a) and 5.21 (b) appear to offer an experimental vindication that the spontaneous ignition delay is a practical criterion for the propensity of a fuel to cause engine knock.

The occurrence of knocking combustion following the spark-ignition of n-pentane and n-heptane-air mixtures in the RCM, measured in terms of KIrms, also exhibits some features associated with the negative temperature dependence of the overall reaction rate. These experimental results provide some support for the relevance of ignition delay as a diagnostic of the propensity of a fuel to cause engine knock.

Since the pressure and temperature conditions of the end-gas in a spark-ignition engine are continually changing with time due to the continuous cycle and the compression by the spark-ignited flame, it is possible that the knock intensity might be better correlated with the calculated mean end-gas temperature at the onset of autoignition. For low end-gas temperatures the overall reaction rate is relatively slow and does not exceed the critical value required for knocking combustion.

Chapter 6

Numerical modelling as a tool to understanding engine knock and examples of its application

6 NUMERICAL MODELLING AS A TOOL TO UNDERSTANDING ENGINE KNOCK AND EXAMPLES OF ITS APPLICATION

An introduction to the development of kinetic modelling techniques for the study of hydrocarbon autoignition has been provided in Section 1.5. Methods ranging from the early skeleton schemes of Yang and Gray [90], through reduced models [160] to the detailed chemical kinetic models [100-102] have been described briefly. The purpose of this section is to analyse and discuss the present status of numerical modelling techniques, with particular emphasis on their application to the study of engine knock.

6.1 Background to numerical approaches

The use of numerical modelling techniques in combustion science and technology has intensified over the last 30 years [107], particularly in relation to combustion in engines [141,222], and combustion hazards [223]. In this section the use of modelling techniques in the study of hydrocarbon combustion in relation to engine knock will be addressed. A detailed understanding of the chemistry of combustion can be realised from the chemical kinetic modelling of hydrocarbon oxidation, an extremely valuable technique for the fundamental scientific understanding of hydrocarbon combustion in practical systems. It holds enormous potential also as a powerful tool for the prediction and analysis of engine knock occurrence through this kinetic insight. However, the development of a successful chemical kinetic model is not facile and involves a variety of scientific disciplines. The provision of reliable kinetic parameters from experimental and numerical methods employed by elementary reaction kineticists is essential. Mathematical methods are needed to solve the complex non-linear differential equations in the model. Also, powerful and robust mathematical techniques for model reduction (such as sensitivity analysis and principle component analysis) are required. There have been extensive developments in the methods of model reduction techniques in recent years [108]. In addition to this, advanced, state-of-the-art, computer technology is required to enable efficient computation. Finally, and arguably most importantly, there is a need for experimental chemical validation of the kinetic models.

A chemical kinetic model for hydrocarbon combustion cannot be assumed to be an accurate representation of the practical combustion system without sufficient chemical validation, it must be capable of successfully predicting well-established combustion phenomena under the specified conditions. A synergy between experimental study and numerical modelling evolves. The modeller relies on the experimentalist for the validation of the chemical kinetic mechanism over a wide range of conditions and in a variety of experimental systems. The experimentalist can then use an accurate model to interpret combustion phenomena in practical systems and gain an insight into the chemical kinetic interactions, which would otherwise not be possible by experiment.

The present status of numerical modelling suggests that, although enormous progress has been made in the development and validation of comprehensive chemical mechanisms for the oxidation of hydrocarbons over a wide range of conditions, the use of chemical kinetic modelling as a reliable tool for the direct simulation of complex combustion phenomena such as engine knock remains an anticipation of the future. The overall goal is to develop a detailed chemical kinetic model which will reliably predict the response of practical combustion systems to changes in operating conditions.

As a consequence of the broad range of physical and chemical conditions which are pertinent to combustion science the requirement is for an oxidation mechanism which can simultaneously be applied to a wide variety of conditions. This may preclude the need for extensive development and testing of the model over a wide range of conditions and in a variety of experimental devices.

Chemical validation from experimental analyses is probably the most important validation technique. However, ignition delays measured in different experimental devices, including RCMs, shock tubes, flow reactors and closed vessels, are also used for the validation of detailed chemical kinetic models which might later be applied to the simulation of autoignition in practical systems, such as s.i. engines. Direct comparisons of numerically predicted and experimentally measured results for the occurrence of knock in a reciprocating engine may also be used.

6.2 Modelling engine knock - how much detail?

Reduced and detailed chemical models have previously been used to predict the onset of knock in a s.i. engine via the comparison of ignition delay with the duration of flame propagation [224]. The two models were both able to predict results which were in good agreement with the experimentally observed results (Fig. 6.1). However, the choice of reduced or detailed kinetic modelling involves a trade off between their inherent advantages and disadvantages. A reduced kinetic model of hydrocarbon oxidation comprises a series of global reactions most of which represent a class of individual elementary reactions of a similar type. Therefore the total number of reactions in the model is comparatively small (~20 reaction steps) and so can be readily applied in a multi-dimensional analysis. However, the parameters themselves cannot be derived from elementary kinetics but may have to be interpreted empirically by matching predictions to experimental results.

The move to a detailed chemical kinetic model can involve an increase in the number of species by a factor of up to 100 and in the number of reactions by a factor of about 500. This additional complexity of the detailed model results in much longer computer run times (30 minutes on the most powerful computers, compared with a few seconds for a reduced model on a workstation, to the same precision).

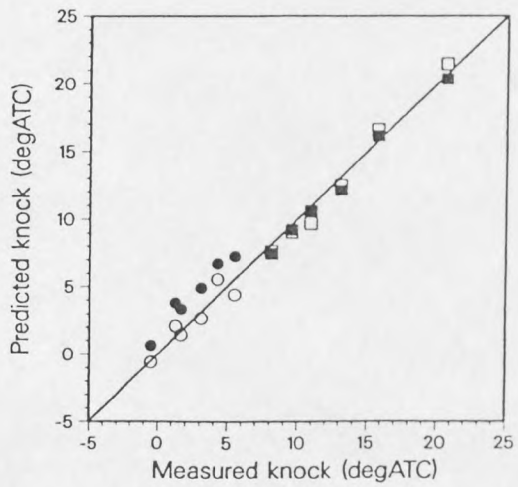

Figure 6.1 Correlation of predicted and experimentally measured times of knock occurrence (degrees crank angle) for i-octane (circles) and n-pentane (squares). Open symbols are results from the reduced kinetic model and solid symbols from the detailed kinetic model [224].

The nature of combustion systems, ideally requires a detailed treatment of the chemical kinetic mechanism which includes all the possible elementary reaction steps and accounts for the influence of fuel molecular size and structure on the rates of low temperature oxidation reactions leading to autoignition (Section 1.3). The occurrence of ignition might often be misconstrued as a purely high temperature phenomenon resulting from the vigorous chain branching reactions of small species. However, it is now well established that the inclusion of low to intermediate temperature reaction steps is essential to an accurate description of the events which occur in the end-gas of a s.i. engine [100]. In the use of numerical modelling techniques to predict engine knock it is assumed that knock occurs as a result of homogeneous autoignition in the end-gas. The low to intermediate temperature chemistry of autoignition influences the time taken for the end-gas to achieve a high enough temperature for the hot stage of ignition to occur and therefore is critical to the definition of engine knock in kinetic modelling.

In addition to the chemical complexity associated with hydrocarbon oxidation in practical combustion systems, the physical environment in which the reactions develop exerts an influence on the overall behaviour of the system. Apart from when ideal adiabaticity is assumed, heat loss must always be taken into account. In addition to this, in a s.i. engine the end-gas experiences turbulent gas motion, non-uniformities due to incomplete mixing, boundary layer effects and heat transfer, all of which can significantly affect the prevailing chemical kinetics. The assumptions of spatial homogeneity and negligible heat and mass transfer are far removed from the reality of the end-gas environment and these simplifications in the model can lead to an inaccurate interpretation of the kinetic interactions. Thus, the inclusion of variables for the treatment of fluid motion and heat transfer effects becomes a requirement as the modelling moves from an idealisation to the practical application.

The inference is that to obtain a reliable understanding of practical combustion devices a numerical model should include a detailed chemical kinetic model in addition to heat and mass transport terms. The mathematical solution methods required for such a model are extremely difficult to develop and the computation resource required would be costly and time-consuming compared with a purely kinetic model. There are two

possible solutions to the problem. The first is to use a purely kinetic analysis with a detailed chemical mechanism and treat the combustion system on a zero-dimensional basis, as a spatially homogeneous system so that heat and mass transfer effects are neglected. The second solution is to use a less detailed chemical mechanism and broaden the spatial domain over which the computation is made.

Numerical modelling on a zero-dimensional basis, cannot give a fully quantitative analysis of the combustion system, where spatial variations in temperature and concentration usually exist. There is clearly a balance to be reached between the need for multi-dimensional modelling and the amount of detail in the chemical mechanism used. A 2-dimensional code which can simulate the heat and mass transport characteristics of a combustion system in a computational fluid dynamics (CFD) code might only rely on very simple kinetics in a reduced model to simulate the chemistry of hydrocarbon autoignition [139]. The zero-dimensional modelling of engine knock employs detailed chemical kinetics and is based on the temporal relationship between the ignition delay in the end-gas (τ) and the time for the complete combustion of the fuel-air mixture by the propagating spark-ignited flame (τ_c). It is assumed that when τ_c is greater than τ, then knocking combustion results. The ignition delay of the end-gas is computed from a detailed chemical kinetic model and the treatment of fluid motion is neglected.

6.3 Numerical modelling of hydrocarbon autoignition in the RCM

6.3.1 Zero-dimensional modelling and chemical validation

Over the last decade Westbrook et al. [102] have developed a comprehensive chemical kinetic model which now includes hydrocarbon oxidation chemistry for C_1-C_8 hydrocarbons in the temperature range 500 - 2000 K. The model has been developed from the earlier mechanisms used to describe the high temperature oxidation of smaller species such as hydrogen, carbon monoxide, methane and C_2 hydrocarbons which had previously been used to describe laminar flame chemistry [225]. The development of

the model to include higher hydrocarbons has led to a hierarchical structure of the model, where the oxidation mechanism of a more complex fuel such as n-heptane includes sub-mechanisms for the oxidation of C_1-C_7 hydrocarbon species validated over a wide range of conditions [140]. This kinetic model of hydrocarbon autoignition has been used to simulate the autoignition of hydrocarbons in the Leeds RCM, some of the results and their interpretation will be presented in this section.

The reaction mechanism includes more than 2000 elementary reaction steps with their reverse reactions and 365 species. The kinetic structure for the low temperature oxidation of hydrocarbons follows that outlined in Section 1.3 with a fully detailed kinetic treatment of all the possible R, RO_2, QOOH and O_2QOOH species, distinctions being made between their different rate parameters.

The numerical modelling calculations were carried out using the HCT code [226] which solves the coupled non-linear differential equations for the conservation of mass, momentum, energy and each chemical species. The compression was simulated on an *ab initio* basis from the initial conditions of pressure, temperature and composition assuming adiabaticity throughout the compression. The output from the compression stage of the simulation was then used as the input for the beginning of the post-compression period, in which the RCM combustion chamber was treated as a spatially homogeneous reactor. This is the adiabatic core assumption, also used by Keck et al. in their modelling of engine knock [224]. The post-compression period could either be assumed to be adiabatic or a Newtonian heat loss term could be included, derived from the pressure fall in the post-compression period for an inert gas. In the present work both possibilities were investigated and their influence on the results obtained will be discussed in the next section. A comparison of experimental and computational pressure profiles for an inert gas mixture is shown in Figure 6.2, illustrating the compression stroke simulation.

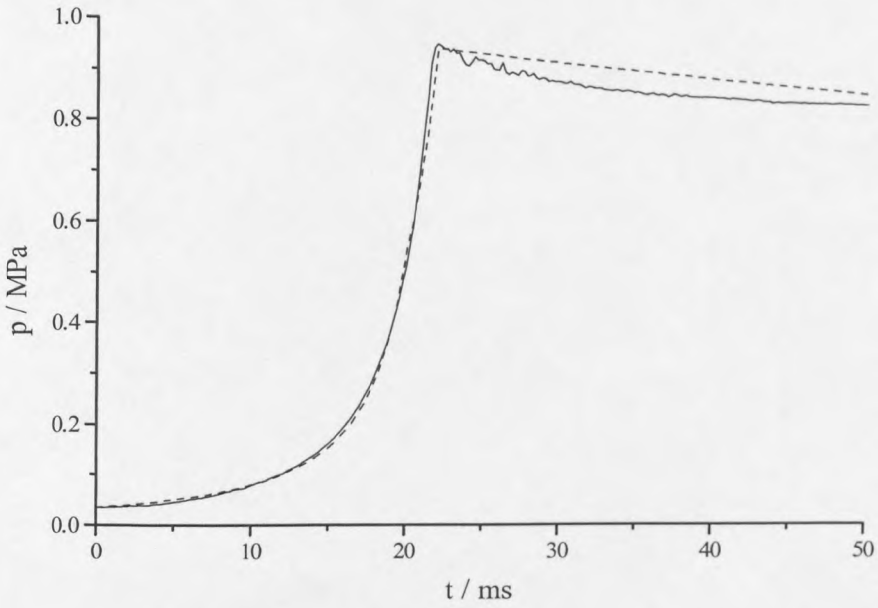

Figure 6.2 Comparison of experimental (—) and numerically simulated (---) pressure-time profiles for the compression stroke of RCM.

The computation provides pressure, time and fuel concentration profiles as well as intermediate product concentrations. The interpretations of ignition delays and % fuel consumption have been compared with the experimental observations discussed in Chapters 3 and 4 [141]. The comparison of experimentally measured and predicted extents of fuel consumption is a rigorous test of the kinetic detail in the model and provides important validation of the chemical kinetic model under engine-like conditions.

The results for n-pentane autoignition shown in Figures 6.3 and 6.4 were particularly satisfactory and demonstrate that the predicted reactivity from the detailed kinetic model is in good agreement with the experimentally observed features of n-pentane autoignition in the RCM. The model satisfactorily predicts the evolution of single and two-stage ignition in the RCM under similar conditions as those observed experimentally. Although the model predicts a greater extent of fuel consumption during the first stage of two-stage ignition, the times of onset of first and second stages are in very good agreement with the experimental results. The prediction of a more

vigorous first stage is believed to be a consequence of the idealisation of the model, as described in the next section (Section 6.4).

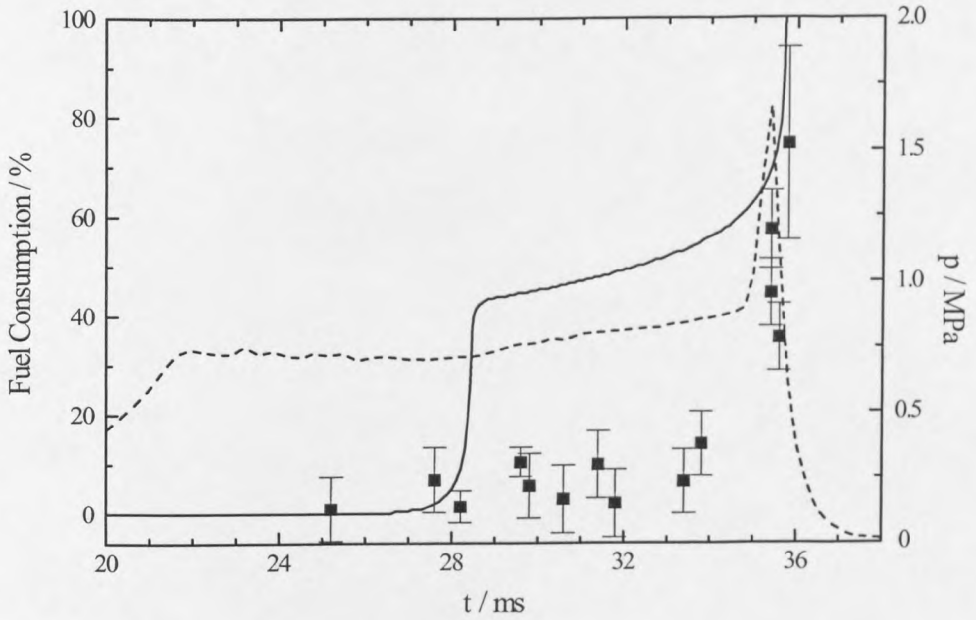

Figure 6.3 Comparison of experimentally measured (■) and numerically predicted (—) fractional extents of consumption (%) of n-pentane during two-stage ignition following compression to 750 (±5) K. The experimental pressure record (---) is also shown.

The results shown in Figures 6.3 and 6.4 exhibit negligible fuel consumption at the end of compression. For the single-stage event shown in Fig. 6.4, the computed extent of fuel consumption increases gradually throughout the ignition delay with less than 10 % being consumed at approximately 10 ms after the end of compression, this is in excellent agreement with the experimental results. The comparison of measured and predicted extents of fuel consumption during n-heptane autoignition emphasises the importance of the inclusion of low temperature oxidation reactions during the simulation of the compression stroke (Figure 6.5). This is discussed further in Section 6.3.2.

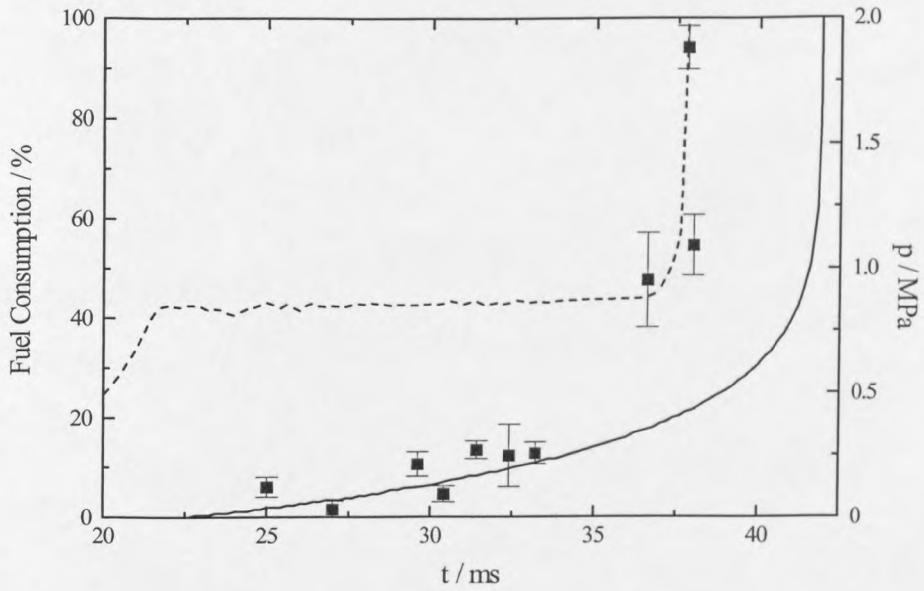

Figure 6.4 Comparison of experimentally measured (■) and numerically predicted (—) fractional extents of consumption (%) of n-pentane during single-stage ignition following compression to 853 (±4) K. The experimental pressure record (---) is also shown.

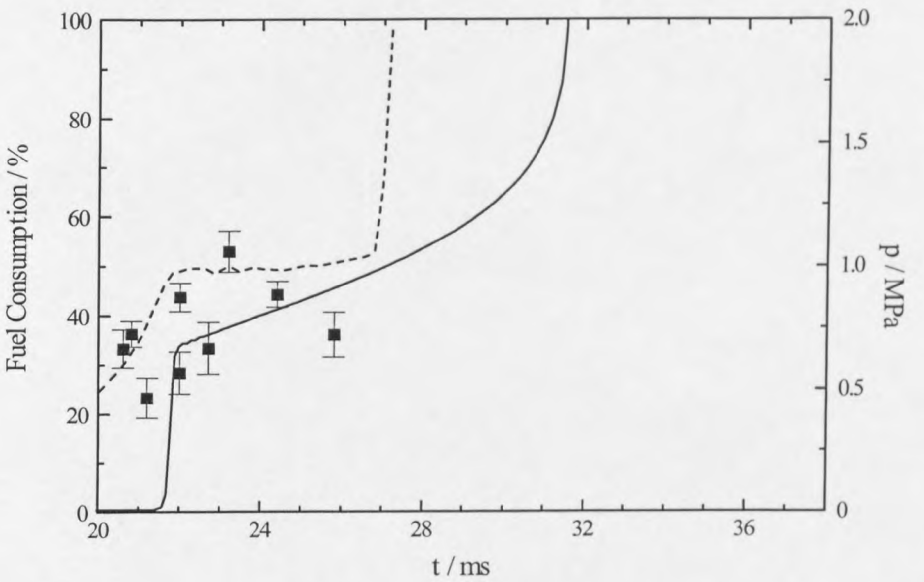

Figure 6.5 Comparison of experimentally measured (■) and numerically predicted (—) fractional extents of consumption (%) of n-heptane during ignition following compression to 870 (±5) K. The experimental pressure record (---) is also shown.

6.3.2 Prediction of ignition delay in the RCM

Figure 6.6 illustrates the comparison of computed and experimental pressure-time profiles for the autoignition of n-pentane following compression to (a) 730 K and (b) 860 K. There are two prominent features of the results shown in Fig. 6.6. The first relates to the development of the first stage of two-stage ignition following compression to 730 K. The model predicts a more prominent first stage than that observed experimentally, this however may be a correct representation of the idealisation of the model, where no heat losses occur during the post-compression period. In reality the effect of the first stage chemistry may be dampened due to spatial inhomogeneities within the combustion chamber as a result of heat transfer.

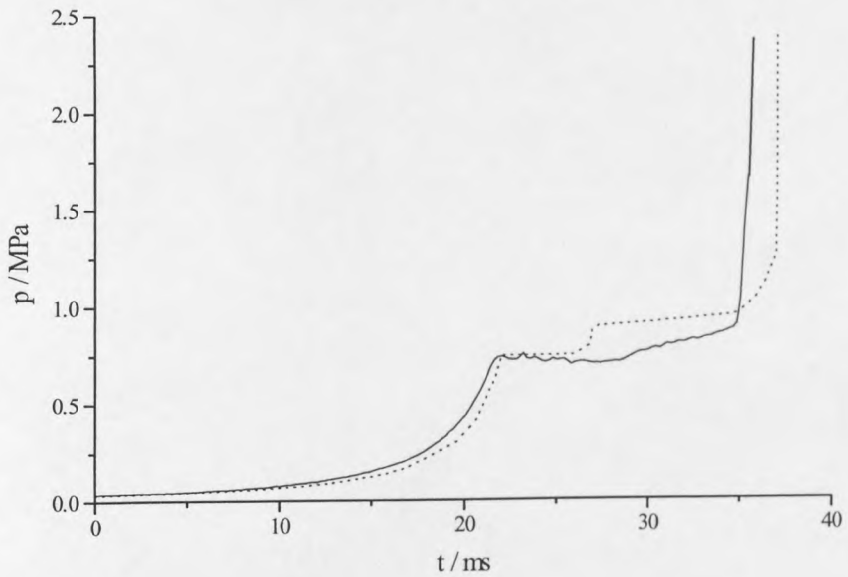

Figure 6.6(a) Computed (...) and experimental (—) pressure-time profiles for the autoignition of n-pentane following compression to 730 K.

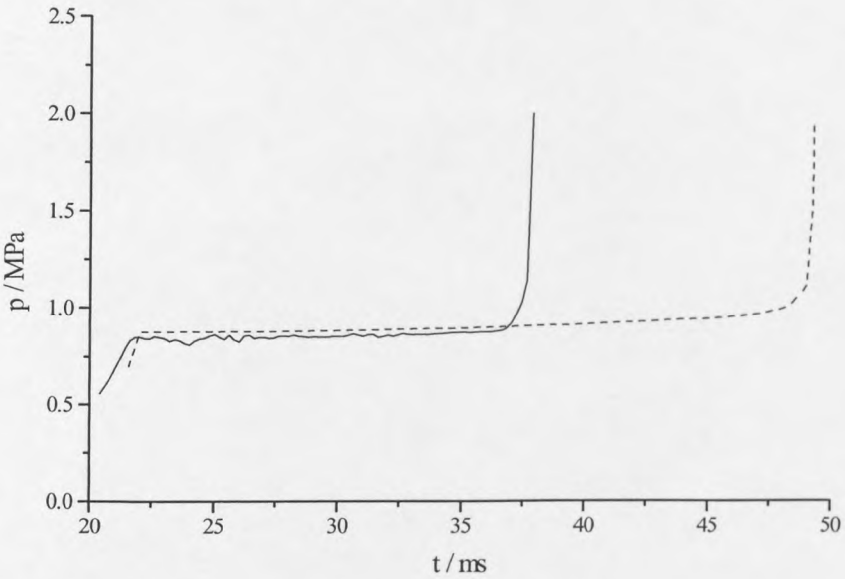

Figure 6.6(b) Computed (...) and experimental (—) pressure-time profiles for the autoignition of n-pentane following compression to 860 K.

The second feature of the comparison of the experimental and modelling pressure profiles is the difference in overall ignition delays. In both examples shown above the model predicts longer ignition delays and a slower rate of pressure rise associated with hot stage of ignition than was observed experimentally. It is unlikely that the source of this inconsistency lies in the chemical mechanism as it occurs in the high temperature region where the reactions are well characterised. The reason for the discrepancy probably lies in the assumption of spatial uniformity of temperature and species concentration in the model. It is inevitable that the pressure during the hot stage of ignition increases at the rate it does in the numerical simulation because it is assumed that the behaviour of the fuel-air mixture is identical in all regions of the combustion chamber. However, as discussed in Chapter 5, schlieren imaging of the autoignition of n-pentane in the rapid compression machine has shown that the hot stage often begins at a single centre and then propagates into and consumes the unburned gases, often initiating additional autoignition centres. In these highly non-uniform circumstances the rate at which the pressure rises in the late stages of ignition is governed by the rate of propagation of the combustion wave, this cannot be accounted for in a zero-dimensional model.

An approximate approach to the inclusion of a heat transfer at the wall term in the numerical simulation is by deriving a Newtonian heat transfer coefficient from the pressure-time profile of an inert gas mixture compressed in the RCM. Whilst this global heat transfer coefficient is a useful first step, it cannot account quantitatively for the effect on the reaction kinetics of heat loss via temperature gradients in the gas. The problem is that the non-linear response of reaction rates to temperature change means that an averaging of the temperature reduces the reaction rate far more than is appropriate to the hotter gas regions that exist in the combustion chamber.

In addition to the consideration of heat losses, in order to perform a meaningful simulation of hydrocarbon autoignition in the RCM it is imperative that the low temperature oxidation reactions must be included in the simulation of the compression stroke. The effect of including low temperature hydrocarbon oxidation reactions during the compression stroke in the simulation of the overall ignition delay for the autoignition of n-heptane in the RCM is illustrated in Figure 6.7. The experimental results revealed an inaccessible range of compressed gas temperatures (750-850 K). This is because, when n-heptane is compressed to these high temperatures, the low temperature oxidation reactions are sufficiently vigorous to occur during the final stages of the compression and hence raise the temperature achieved at the end of compression to 850-900 K, that is, to the "cut-off" temperature induced by the onset of the ntc.

The simulation of n-heptane autoignition in the RCM without the allowance for reactivity during compression provides a means of quantifying this effect of reaction during compression on the ignition delay. When the numerical simulation is started at the beginning of the compression stroke the low temperature oxidation reactions which can occur during the last 2 ms of the compression stroke, as observed experimentally, are allowed to evolve and so the overall predicted ignition delay is in very close agreement with the experimental results. These results confirm the pre-conditioning effect of reactivity during compression and its influence on ignition delay throughout the temperature range 650 -1000 K.

Experimental and numerically simulated results are in reasonable agreement in the low temperature region because there is no potential for reaction during compression to these temperatures. However, at higher compressed gas temperatures (> 800 K) there is a marked discrepancy. The numerical model simulation, without "conditioning" in the compression stroke, shows the existence of a negative temperature dependent region and a considerable lengthening of the ignition delay at T_c > 850 K, which was not observed experimentally.

Modelling of hydrocarbon autoignition in the RCM in this way has served two main purposes. The first is to show that when simulating the autoignition of hydrocarbons in RCMs and in engines it is essential to include reactions taking place during compression in order to perform a successful prediction of ignition delay. It also demonstrates very clearly that, for the most reactive fuels, the knock initiating processes are capable of beginning from "bottom dead centre" as the fuel-air mixture is heated due to the compression stroke.

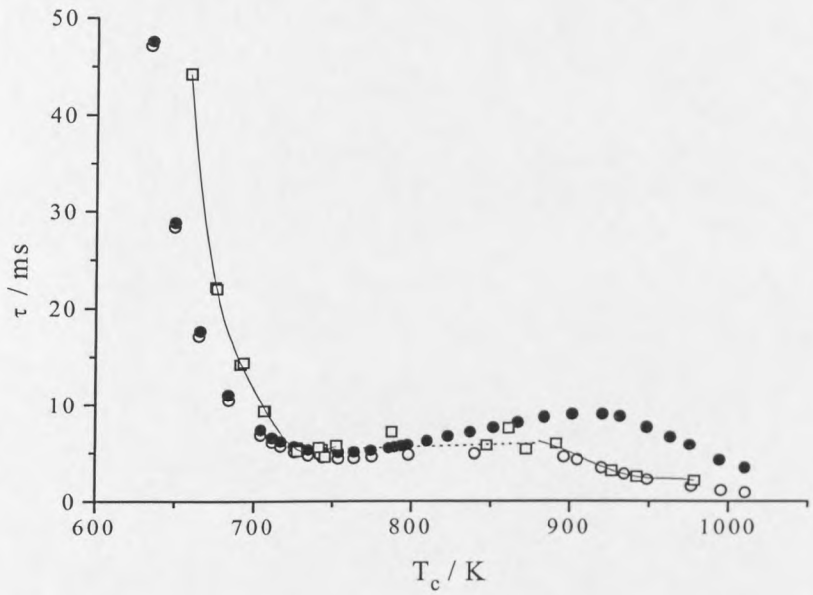

Figure 6.7 A comparison of experimental results (□) and numerical predictions of ignition delay variation with compressed gas temperature for n-heptane in air, illustrating the effects of numerical simulation without reaction during compression (●) and with reaction during compression (○) on the predicted ignition delays.

The second purpose is as a means of performing the "impossible experiment", or the "what if...?" approach. In order to establish experimentally how pre-conditioning during compression has affected the ignition delay it would have been necessary to somehow contrive a shock tube experiment or closed vessel experiment to give an identical pressure, temperature and composition at the reference conditions as those achieved in the RCM. The numerical simulation of effectively "switching off" or "switching on" the chemistry, provides an insight into the experimental system, which would otherwise not be possible, in the quantification of the effect of reaction during compression on the ignition delay. The calculations for n-C_7H_{16} combustion at $T_c >$ 850 K show that when about 33 % of the fuel has already been consumed in the compression stroke, and has conditioned the system accordingly, the ignition delay is about half of that predicted from a 'non-reacted' compressed gas state [221].

The effect of inclusion of a Newtonian heat loss term in the calculation is illustrated in Figure 6.8. The inclusion of the heat loss term appears to give better agreement between predicted and experimentally measured ignition delays for n-heptane in the low temperature regime. However, the model tends to over-predict the ignition delay within the region of the ntc, possibly due to an overcompensation for heat losses within this temperature regime. The assumption of adiabaticity may be a better approximation than the Newtonian heat loss term because the non-linear kinetic response of low temperature oxidation reactions does not respond well to this simplified approach.

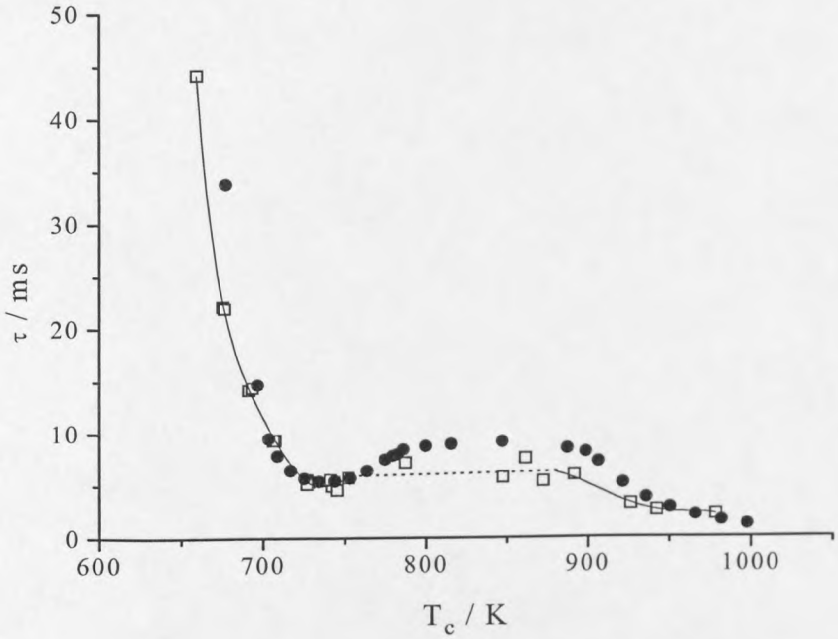

Figure 6.8 A comparison of experimental results (□) and numerical predictions of ignition delay variation with compressed gas temperature for n-heptane in air, illustrating the effect of the inclusion of a heat loss term and reaction during compression in the numerical simulation (●) on the predicted ignition delays.

6.3.3 One- and two-dimensional modelling of hydrocarbon autoignition in the RCM

The complications that can arise from the assumption of a zero-dimensional system are apparent. The move to multi-dimensional modelling techniques applied to the simulation of hydrocarbon autoignition in the RCM is possible, the trade off being the use of a reduced kinetic model instead of a detailed chemical model. A two-dimensional model has previously been used in the simulation of hydrocarbon autoignition ahead of a spark-ignited flame in the RCM [139]. Using a reduced chemical kinetic model for hydrocarbon autoignition derived from the "Shell model" [96] coupled to KIVA II [217], a CFD code which simulated the heat and mass flow characteristics, the model was able to predict the temperature variation within the unburned region of the chamber and simulate the hydrocarbon oxidation within these regions. The numerical prediction was that spatial temperature variations exist during the post-compression period and autoignition centres can originate in different regions

of the chamber determined by the end-gas temperature. The experimental results of the visualisation of hydrocarbon autoignition in the RCM by schlieren imaging (Chapter 5) confirm this numerical prediction.

A one-dimensional thermodynamic analysis of the experimental results from the RCM has also been carried out, this involved a purely thermodynamic treatment of the system and did not include chemical reaction kinetics. The method employed the Leeds University Spark Ignition Engine Data Analysis (LUSIEDA) program which was designed for use by engineers to provide estimates of the unburned gas temperature and unburned mass fraction in the combustion chamber of a reciprocating engine cycle. The aim of this study was to modify and use the program to estimate the mass fraction burned and the unburned gas temperature ahead of a propagating spark-ignited flame in the RCM. LUSIEDA requires a 2-dimensional image of the propagating flame and the corresponding pressure history. The combustion chamber is treated as a two zone constant volume chamber comprising burned and unburned regions. Convection heat transfer coefficients were derived for each zone and the flame speed was calculated, assuming spherical flame growth. At any given time during the event, assuming ideal gas behaviour, the mass fraction burned and the burned and unburned temperatures could be estimated.

Results have been obtained for the spark-ignition at tdc of PRF 60 in the RCM (Fig. 5.17). The estimated unburned gas temperature at a time just before the rapid pressure rise which is associated with complete consumption of the reactants, is 850 K. At a similar time the mass fraction of unburned gas is estimated to be 60 %. These end-gas conditions of temperature and fuel available for reaction are consistent with conditions which might preclude the occurrence of end-gas autoignition and vigorous knocking combustion, in agreement with the observed pressure profile. This study demonstrates the valuable information which can be obtained by thermodynamic analysis, which could otherwise not be obtained by the experimental technique.

6.4 Why model hydrocarbon autoignition?

The benefits to be gained from the successful modelling of hydrocarbon oxidation are apparent, but so too are the problems which can arise. A detailed chemical kinetic model which can reliably simulate combustion phenomena in practical devices provides a valuable tool for the prediction and interpretation of combustion systems. Numerical modelling provides the power to gain quantitative insight into the kinetic interactions at the elementary reaction level, which govern the global behaviour. As a consequence an enhanced understanding of experimental and practical combustion systems can be gained.

The development of comprehensive mechanisms for the oxidation of hydrocarbons which have been validated over a wide range of conditions enables their application over a broad range of conditions. Such detailed mechanisms are necessary for the accurate simulation of hydrocarbon oxidation. In addition to this, comprehensive kinetic models provide a formal starting point for the generation of reduced models, using mathematical techniques. The function of sensitivity analyses and other mathematical procedures is to show which reactions are important to the overall behaviour of the model. However, the practical application is to be able to identify the processes which are of such little importance that they may be disregarded. If this is performed satisfactorily then the reduced scheme should be as robust as the comprehensive scheme for the prediction of behaviour over a wide range of conditions and will ultimately enable the affordable and reliable simulation of hydrocarbon autoignition in a multi-dimensional analysis.

The use of sensitivity analyses in numerical modelling also allows detailed interpretation of the kinetic interactions. The effect of fuel molecular size and structure on octane rating has been made possible in this way. Coupled numerical modelling and experimental studies have confirmed that the kinetic chain branching agents responsible for the vigorous low temperature chain-branching in hydrocarbon oxidation are the ketohydroperoxide species.

Numerical modelling of hydrocarbon oxidation and engine knock has developed tremendously over the last decade, from the high temperature flame chemistry of small hydrocarbons [225] to the detailed chemical kinetic models for the oxidation of n-heptane and i-octane [102]. In the present status detailed chemical models exist for the oxidation of C_7 and C_8 hydrocarbons which have been sufficiently validated over a broad range of conditions. However, the application of these models in 2- and 3-dimensions is presently limited by the availability of the necessary computing resource. The assumption of spatial homogeneity in a zero-dimensional analysis is a wholly inaccurate description of highly non-uniform combustion systems such as the end-gas in a s.i. engine. Thus, there is a pre-requisite, either for the development of more reliable reduced models of hydrocarbon oxidation, or the evolution of the necessary computing power.

As mentioned at the beginning of this section, in addition to detailed mechanisms which give a valid description of hydrocarbon oxidation, the development of successful models requires accurate elementary reaction kinetic data and advanced mathematical and computing techniques. Through developments in the future of sufficiently powerful computing resources which will enable the detailed chemical kinetic modelling of hydrocarbon oxidation in a 3-dimensional space, accurate prediction and interpretation of engine knock may be possible.

The ultimate goal for the future is the development of reliable and robust models which can accurately predict the occurrence of combustion phenomena. In particular, the direct simulation of engine knock and its kinetic interpretation for a multi-component gasoline will enable an improved understanding of the physical and chemical processes which lead to engine knock. This in turn will enable accurate predictions of the influence of antiknock additives and octane boosters on the knock characteristics of gasoline.

Chapter 7

Conclusions and future work

7 CONCLUSIONS AND FUTURE WORK

In the main part of this thesis the autoignition of hydrocarbons in relation to engine knock has been explored. The experimental results described in Chapters 3-5 broaden the current status of physical and chemical understanding of hydrocarbon autoignition at high pressures and temperatures (p_c = 0.8-1.1; T_c = 600-1000 K) in a rapid compression machine. The main reasons for using an RCM for these types of investigation are as follows:-

i. In common with s.i. engines, the RCM provides a means for the compression of a reactive fuel-air mixture by a piston in a cylinder. The combination of speed and duration of compression in the RCM are comparable with the typical performance in a reciprocating s.i. engine operated at 2000 rpm.
ii. Conditions approaching those which occur in the end-gas of a spark-ignition engine can be accessed experimentally, i.e. p_c = 8-11 atm; T_c = 650 - 1000 K.
iii. A variety of measurements and investigations of hydrocarbon autoignition can be made.
iv. The RCM provides a cleaner and more ideal system for the investigation of hydrocarbon autoignition than a reciprocating s.i. engine, i.e. gas mixing, opening and closing of valves and expansion strokes do not occur in the RCM.

The simplifications offered by the RCM also present some important distinctions from combustion in s.i. engines. The lack of reciprocation in the RCM does not enable a build-up of residuals from the previous cycle or cycles, as occurs in a motored engine. Experimental and numerical modelling investigations [145] have illustrated the effect that residuals in the combustion chamber can exert on the time taken for autoignition to develop.

7.1 Conclusions

The pressure records, ignition delays and the light output from the combustion chamber throughout the post-compression period are global features which help to resolve features of the overall development of reaction leading to autoignition. However, a detailed kinetic interpretation is not possible from these measurements alone. Nevertheless, global ignition delay measurements remain an important experimental observation, in their application to the validation of numerical models and also with regard to understanding and verifying the structure-related reactivity of hydrocarbons at conditions of temperature and pressure comparable to those which occur in the end-gas of a s.i. engine. For example, the results shown in Chapter 4 illustrate the ignition delay variation with compressed gas temperature, which encompasses several of the common features of low to intermediate temperature hydrocarbon oxidation chemistry.

An objective of Chapter 4 was to determine the relationship between the ignition delay of a fuel, as measured in the RCM, and the RON as measured in a CFR engine under standard operating conditions. Following a detailed investigation of the ignition delay characteristics of several single component hydrocarbons (C_4-C_8) and mixtures of the PRFs in the range 0-100 mol% i-octane, the lack of quantitative agreement between ignition delay at 900 K and RON became apparent. This would suggest that ignition delay alone is unsatisfactory for the purpose of defining knock ratings.

The poor correlation between the ignition delay at 900 K for the single component hydrocarbons and the PRFs of corresponding RON can be reasoned in light of the results presented in Chapter 3. The potential for consumption of n-heptane and i-octane during the compression to 900 K in the RCM has been emphasised. Evidently, throughout the range of PRFs studied, some extent of reaction is likely to have occurred before the end of the compression stroke to 900 K. The same may not be true of all the single component hydrocarbons investigated in that range. A quantitative interpretation of the effect of reaction during compression on the ignition delay in the RCM can be obtained by numerical modelling analysis, as described in Chapter 6.

In the experimental results shown in Chapter 3 and in the supplementary modelling analysis described in Chapter 6, it has been shown that considerable fuel consumption can take place prior to completion of the compression stroke when sufficiently high compressed gas temperatures are accessed. By implication, this will occur in other machines with comparable or slower compression rates. In addition, when knock occurs in a spark- ignition engine (at < 2000 rpm, at an average piston speed of 4-6 m s^{-1} with a compression stroke of 6 - 10 cm) there is a similar time interval during which spontaneous oxidation of the fuel-air mixture can develop appreciably, especially at high gas densities.

In addition to an improved understanding of the temporal evolution of hydrocarbon autoignition in the RCM, an understanding of the spatial evolution of hydrocarbon autoignition in the combustion chamber has also been obtained, via the application of non-intrusive, 2-dimensional imaging techniques to the RCM. The visualisation of autoignition in the RCM provides evidence for the existence of spatial temperature inhomogeneities within the combustion chamber of the RCM throughout the post-compression period and the resulting effect on the initiation of autoignition centres. The results clearly demonstrate the inhomogeneous development of the hot stage of ignition and provide experimental evidence to support the numerical prediction [139] that within the region of the ntc, autoignition may originate in the cooler regions of the combustion chamber adjacent to the wall.

7.2 Future studies of hydrocarbon autoignition in the RCM

The schlieren imaging study of the development of hydrocarbon autoignition in the RCM was extremely informative. However, although the results give a clear indication that spatial temperature inhomogeneities exist in the combustion chamber throughout the post-compression period, they do not provide a quantitative measure of the prevailing temperature variations. As a progression from the schlieren imaging studies, a research programme is currently in progress with the aim of obtaining a spatial temperature profile across a 2-dimensional plane of the combustion chamber of the

RCM throughout compression and post-compression periods, using Laser Rayleigh Scattering and Coherent Anti-Stokes Raman spectroscopy.

The limitations set by the maximum safe operating driver pressure of the Leeds RCM have been outlined in Section 2.4. The design and manufacture of a mechanically more robust, driver gas chamber has recently been commissioned and will enable operating initial pressures of up to and in excess of 0.1 MPa. This will permit the study of the autoignition of low reactivity fuels such as i-octane and toluene at lower compressed gas temperatures. At the present operating conditions, autoignition of these fuels is not possible due to the long ignition delays during which heat losses become significant and can curtail reaction. This modification will also provide initial conditions of pressure and molar gas density at the end of compression, more comparable with those which occur in the end-gas of s.i. engines.

The effect of diethylamine on ignition delay has been demonstrated and the experimental study would clearly benefit from a numerical modelling analysis using a mechanism for oxidation, which includes reactions for alkylamines, to assess and interpret the kinetic interactions which result in the observed behaviours of inhibition and sensitisation during the autoignition of n-pentane in the RCM.

The extent and scope of the study of hydrocarbon autoignition following direct injection of a liquid fuel spray into the combustion chamber of the RCM was limited by difficulties encountered with the coincident timing of the electromechanical devices on both the RCM and the injection pump. Initial results illustrate the potential for a new and exciting area of combustion research in the field of heterogeneous combustion of fuel droplets. This opens up the possibilities of imaging the spray formation in a high temperature and pressure vessel under diesel engine-like conditions and the application of laser diagnostics to provide information of the spatial development of autoignition chemistry.

Numerical modelling could be usefully applied to the study of the effect of fuel:air ratio on the ignition delay of n-pentane in the RCM an may well be extended to the

simulation of fuel injection or other studies. A successful prediction of the experimentally observed behaviour coupled to a sensitivity analysis could provide valuable information relating to the chemical kinetic interactions which govern the behaviour.

7.3 Overall summary

The main conclusions which can be made from the results presented in Chapters 3-5 are:-

- the ignition delay variation with compressed gas temperature is indicative of the overall reactivity of the hydrocarbon and is related to the molecular structure
- in general, as RON increases, the ignition delay at T_c = 900 K, measured in the RCM, also increases. However, a quantitative correlation of the two parameters was not observed
- when a reactive fuel is compressed to a high enough temperature, then a significant extent of fuel consumption can occur during the compression stroke in the Leeds RCM
- the potential for reactivity during compression in the Leeds RCM, in other RCMs and in engines, imposes an influence on the subsequent development of autoignition within the combustion chamber
- the addition of a small proportion of diethylamine to n-heptane, significantly suppresses the extent of reaction during the compression to high temperatures and consequently lengthens the measured ignition delay
- spatial temperature variations exist within the combustion chamber of the RCM during the post-compression period and when fuel-air mixtures are compressed to temperatures within the region of the ntc then autoignition centres may originate in the cooler gas region adjacent to the wall
- the occurrence of autoignition in the RCM combustion chamber originates from a small hot centre of reactivity which propagates into and consumes the surrounding unburned gas, it is not a rapid homogeneous ignition.

- the occurrence of autoignition centres ahead of a spark-ignited flame can be associated with the characteristic knock pressure profile observed under engine knock conditions
- the variation of knock intensity with T_c illustrates some of the features characteristic of the autoignition delay variation with temperature, i.e. ntc, threshold temperature.

Chapter 8

The ignition of methane in the RCM

8 THE IGNITION OF METHANE IN THE RCM

The results described in Chapters 3-5 relate to the autoignition of (C_4-C_8) hydrocarbons in air using the RCM, at compressed gas temperatures in the range 600-1000 K and compressed gas pressures in the range 0.8-1.1 MPa. This chapter describes the experimental investigation of the autoignition of methane in the RCM and how ignition may be induced by carbon particles.

8.1 Summary

The aim of the experiments described in this chapter was to investigate the conditions of temperature and pressure at which methane-oxygen-inert mixtures are able to autoignite in the RCM. In addition, the effect of small proportions (5-15 mol%) of higher alkanes (ethane, propane and n-butane) on the autoignition of CH_4-O_2-inert mixtures in the RCM was investigated over a range of compressed gas temperatures (700-800 K).

The results suggest that the autoignition of methane-oxygen in the RCM is extremely difficult under the normally accessible conditions of pressure, the lowest practical temperature being approximately 900 K. However, in the presence of higher alkanes the initiation of autoignition is significantly enhanced. The experimental study has also shown that carbonaceous particles are able to induce ignition at relatively mild compressed gas temperatures and pressures (T_c < 750 K; p_c < 0.8 MPa). A detailed investigation into the effect of soot particles on the initiation of ignition of methane-oxygen-inert mixtures and the self-heating properties of carbon particles in the presence of oxygen over a range of compressed gas temperatures and pressures has been carried out.

Supplementary studies were also made of the ignition of soot particles in oxygen, in the absence of any other gaseous fuel. This served two purposes. The first was to establish unequivocally that the particles could be heated to combustion temperatures and that

heterogeneous ignition could occur. In this instance ignition was diagnosed from the light output from the combustion chamber alone because there was no significant pressure change associated with the ignition of the particles. The second purpose was to expose the particles to more extreme compressed gas pressures, whilst remaining within the safe operating conditions of the RCM. This would not have been possible in the presence of methane because its ensuing ignition would have generated unsafe pressures in the system.

8.2 Background

8.2.1 Natural gas blends and the effect of higher alkanes on the ignition of methane

The search for alternative, cleaner burning transportation fuels has escalated over the last decade and this is emphasised by the recent introduction of natural gas-fuelled vehicles onto the market. Gaseous fuels result in cleaner burning combustion than conventional liquid fuels because the fuel-air mixing is improved in the homogeneous gaseous phase and also the higher H:C ratio is more likely to result in complete oxidation to CO_2 and H_2O. In general, natural gas comprises a mixture of 80-95 % CH_4 and a 5-20 % composite of CO_2, C_2H_6 and C_3H_8, the relative proportions of which vary depending on the source.

Commercial grade CH_4 fuel (or natural gas) presents several advantages as a transportation fuel, it is readily available, low cost, clean burning and has a high heat of combustion. Methane gas has a high octane rating (RON 130), so higher compression ratios are accessible (15:1), making it an attractive alternative fuel to gasoline. The higher operating CR allows increased power output and thermal efficiency. Also, cold start fuel enrichment is not required, therefore the pollutant emissions of unburned hydrocarbons and carbon monoxide are reduced. However, although natural gas vehicles present a very low ground level ozone forming potential, CH_4 is a more powerful (albeit shorter lived) greenhouse gas than CO_2. Arguably, the most ideal alternative fuel to gasoline would be hydrogen gas, this would not produce any CO_2, CO, unburned hydrocarbons or particulates. Therefore, in terms of reduced pollutant

emissions, this would be an extremely attractive alternative to gasoline. However, the additional complications posed by the storage of large volumes of hydrogen gas in a transportation vehicle present some obvious disadvantages.

8.2.2 Methane oxidation, ignition delay and sensitisation

At pressures in the range 1-10 atm and temperatures below about 700 K the oxidation of methane is extremely slow. The reason for the relative stability of methane at low pressures lies in the strength of the 4 primary C-H bonds, rendering H-abstraction during propagation relatively difficult. Also, further reaction of the relatively stable methylperoxy radical is not facile. However, at very high pressures (> 30 atm), the rate of low temperature oxidation becomes more significant.

The low temperature (550-700 K) oxidation of methane in oxygen at high pressures (25-35 atm) has received considerable attention in relation to the optimisation of conditions for the production of methanol on an industrial scale [227-228]. Experimental studies of the partial oxidation of methane in a high pressure plug flow reactor have illustrated the influences of partial oxygen pressure and the reactant temperature on the onset and duration of oscillatory combustion [228]. The results suggest that at low oxygen concentration the number of oscillations is limited by the concentration of oxygen but at higher oxygen concentrations the onset of temperature oscillations is limited by the reactant temperature.

The ignition delay time for methane in oxygen, usually obtained in shock tube studies, can be correlated in the following way [76],

$$\tau = A \exp^{(-E/RT)} [CH_4]^a [O_2]^b .$$

Several studies [76,229,230] have shown that the value of b is of the order -1.0, i.e. the ignition delay is inversely proportional to the oxygen concentration. For example, Lifshitz et al. [230] studied the autoignition of $CH_4/O_2/Ar$ mixtures in a shock tube at temperatures between 1500 and 2500 K and pressures of 2.1 atm, the results led to the following relationship between ignition delay and reactant concentration,

$$\tau = 3.62 \times 10^{-14} \exp^{(46.5\times10^3/RT)}[Ar]^0[CH_4]^{0.37}[O_2]^{-1.03}.$$

One of the earliest studies which reported the sensitising effect of higher alkanes on methane autoignition was the shock tube investigation by Higgin and Williams in 1969 [231]. This study showed that the addition of a trace amount of n-butane to a lean methane-oxygen mixture results in a significant reduction in the ignition delay. It has previously been suggested that the addition of a small amount of easily ignited fuel to CH_4/O_2 had no effect on the combustion chemistry of methane and the influence could be explained on a purely thermal basis, i.e. the heat release due to reaction of the higher hydrocarbon raises the reactant mixture to a higher temperature [230]. Recent studies by Tan et al. [232,233] have also illustrated the importance of trace amounts of hydrocarbons in the oxidation of methane in a jet-stirred reactor in the range 800 K<T<1240 K and pressures between 1-10 atm. Their explanation for the behaviour was one of kinetic interaction. The higher hydrocarbons react with O_2 before CH_4 producing OH, H and O radicals which subsequently initiate the oxidation of methane. Experimental measurements showed that approximately 50 % of the initial consumption of CH_4 is due to its reaction with OH radicals when ethane or propane are present in the mixture. This contrasts with the initiation by O_2 during the oxidation of CH_4 and O_2 alone. As the length of the higher hydrocarbon chain increases the radical pool is increased more rapidly and to a greater extent, so the influence on the initiation of autoignition is stronger. The competition between methane and higher hydrocarbons was demonstrated in other studies of the sensitisation of methane-air autoignition in a closed vessel at atmospheric pressure [162].

The observed reduction in ignition delay is due to the presence of the higher alkanes and the chemical coupling of the oxidation mechanisms, rather than thermal effects arising from the preflame exothermic oxidation of the higher alkane. The enhanced early generation of CH_3 radical by the more reactive minor species, leads to more rapid overall reaction. Experimental and numerical investigations have verified that this sensitisation originates predominantly in the kinetic interactions [225,234-236].

8.2.3 Heterogeneous initiation of ignition in relation to engine combustion

High boiling point additives in gasoline tend to cause the formation of combustion chamber deposits (ccds) which can act in a number of ways and ultimately result in the occurrence of knock in the engine. Therefore, the tendency of a car to knock and its octane requirement tend to increase with use as carbonaceous deposits collect in the combustion chamber [237]. Combustion chamber deposits can act in one or more of the following ways:

- solid particle initiator for autoignition of the unburned end-gas
- heat sink
- the particles have a finite volume so can increase the CR and result in higher temperatures at tdc
- absorb and release, in a subsequent cycle or cycles, unburned fuel or pro-knock species
- promote chemical reaction through catalytic surface effects

Generally, ccds will act as a hot spot, which is generally a deposit on the combustion chamber wall, piston or valve surface which raises the local gas temperature and accelerates reaction in the surrounding gases. The characteristics of ccds as initiators to ignition ultimately have detrimental effects in s.i. engines but on the other hand could be usefully applied to the initiation of ignition in diesel engines.

8.2.4 Surface combustion and the heterogeneous initiation of ignition

In solid-gas systems, combustion can be initiated either at the surface where the oxidant is adsorbed or at the solid-gas interface. The size dispersion of the solid particles determines the extent to which the solid fuel can mix with the gaseous oxidant and under turbulent conditions the contact between fuel and oxidant is enhanced. Combustion of a solid fuel involving adsorption of the oxidant onto the surface can be considered in following simplified way:

a) the gaseous reactant/oxidant (O_2) is transferred from the bulk gas to the solid surface

b) the reactant is adsorbed onto the surface

c) reaction occurs at the surface

d) gaseous products are desorbed from the surface and diffuse away from the surface into the bulk gas.

In general, the rate of heterogeneous combustion experiences diffusion or kinetic control, depending on the surface temperature. At low temperatures the surface reaction is slow compared with diffusion therefore kinetic control predominates at low temperature. At higher surface temperatures the surface reaction is sufficiently rapid and diffusion control predominates.

For a carbon particle exposed to an oxidising atmosphere, the occurrence of ignition is determined by the balance between the rate of heat generation at (R) and the rate of heat loss from (L) the particle surface. A condition of criticality exists where L = R and dL/dT = dR/dT, above which thermal runaway occurs (Figure 8.1). This is reminiscent of the criteria which determine criticality in thermal explosion theory, although the interpretation of the chemical reaction rate and the physical processes may take a different form.

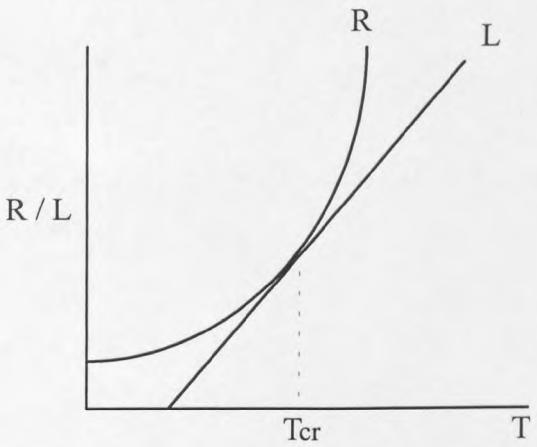

Figure 8.1 Heat release and heat loss rates vs. temperature, representing critical condition for the autoignition of a carbon particle in a high temperature oxidising atmosphere.

Heat release at an autoigniting centre (or particle) is lost initially by conduction to the surrounding gas. Since the heat release rate increases exponentially with increasing temperature, eventually a steady state is sustained in the vicinity of the particle, where reaction "runs away" and a flame kernel is initiated at and propagates from the hot centre. There is a critical radius of an autoigniting centre [238] which is the smallest radius at which the heat release within the autoigniting centre can be sustained in a

steady state just prior to thermal explosion. When the radius of the autoigniting centre exceeds the critical radius, then it can act as a hot spot. The probability of an autoignition centre becoming critical depends on the size distribution of the centres (or particles). Since ignition can originate from a hot centre and propagate through the surrounding gas, the core gas temperature may be of greater significance than the average bulk gas temperature. The dependence of the rate of soot oxidation on the partial oxygen pressure has been studied in a shock tube at high temperatures (1500-2000 K) [239]. The results illustrate that as the temperature is increased from 1600 K to 2000 K, the order of reaction with respect to oxygen concentration, increases from 0.36 to 0.57.

A previous investigation of the effect of particles on the ignition of fuels in an RCM has shown that the initiation of a flame by a dust particle can occur more readily than spontaneous ignition in the gas phase [240]. After compression the particle is heated by conduction from the hot gas and the gaseous fuel also begins to oxidise so the temperature of the particle increases further, either until a flame is ignited from the hot centre or until gas-phase ignition occurs.

The aim of this study was to determine the minimum pressure and temperature at which the ignition of carbonaceous particles is possible under engine-like conditions.

8.3 Experimental

The experimental system (the RCM) has been described in detail in Chapter 2. The apparatus and experimental method was essentially the same as that used previously. However, slight modifications to the system were made in order to allow higher initial pressures (hence compressed gas pressures) and lower compressed gas temperatures to be achieved.

The premixed gaseous reactants were admitted into the combustion chamber at an initial pressure in the range 0.033 MPa - 0.152 MPa, then compressed to pressures in the range

1.0 - 2.8 MPa. The requirement for higher initial pressures in selected experiments will be discussed in Section 8.3.2.

8.3.1 Carbonaceous particles (soot)

The soot particles used in this study were products of methane pyrolysis at 1100 K and 70 atm. X-ray diffraction and transmission electron microscopy showed that the structure was a fine carbon filament structure.

A small amount (~ 7.0 mg) of soot was distributed on internal surface of the Perspex window and the inside wall of the combustion chamber before each experiment. It was assumed that the surface tension retains a sufficient proportion of the particles during evacuation of the chamber. It was also assumed that the total quantity of particulate matter in the chamber was not crucial as only one particle in the right place is required to initiate ignition of the surrounding gas.

There was a significant statistical error incurred in the amount of carbon particles of the optimum size for reaction placed in the chamber due to the inaccuracy in loading the sample into the chamber and also due to the particle size distribution within a given sample. The existence of statistical variations in these experiments is an important consideration when assimilating the results obtained.

8.3.2 Operating conditions

A range of compressed gas temperatures (T_c) could be achieved following compression to a final volume which could be varied to a limited extent by varying the thickness of the end-window, thus varying the CR (CR = 18.0 (± 0.2):1, 11.0 (± 0.5):1, 6.8 (± 0.1):1 or 6.1(± 0.2):1). In the early experiments the compressed gas temperature was limited to the high temperature region as a consequence of the relatively low C_p/C_v (γ) of the methane fuel proportion (compared with longer chain hydrocarbons in previous experimental investigations) and the reduced dilution by inert gases.

In the initial studies of the autoignition of methane-oxygen mixtures in the RCM the higher pressures were achieved by using a "stepped-out" window (Fig. 8.2(a)) to give a lower final volume and hence higher compression ratio. However, as shown below (Fig. 8.3), the increase in CR also results in increased compressed gas temperatures so there was a limit to the minimum accessible compressed gas temperature for a given mixture and CR. Subsequent investigation at high pressure and low temperature required the use of a "stepped-in" window (Fig. 8.2(b)) to achieve low temperatures and higher initial pressures were required to compensate for the lower CR.

(a) Normal operation, CR = 11:1

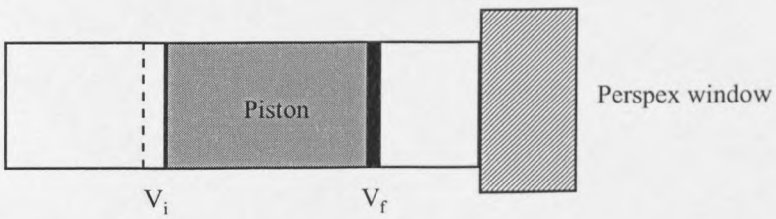

(b) Stepped-out window, CR = 18:1

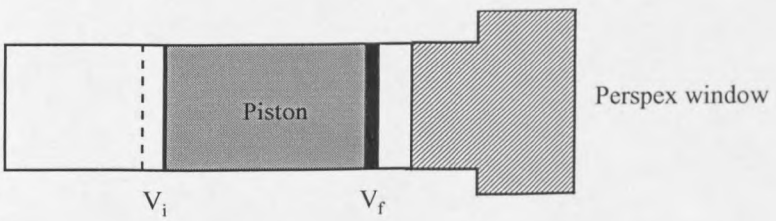

(c) Stepped-in window, CR = 6.8 or 6.1:1

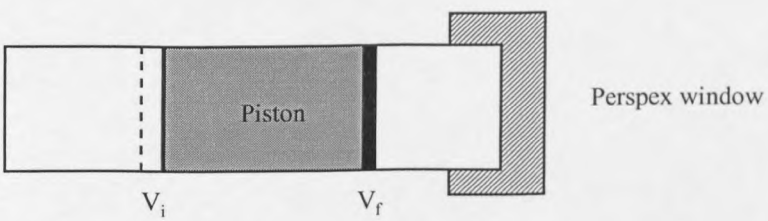

Figure 8.2 Different Perspex end-windows used to access different end of compression conditions of temperature and pressure. The initial volume, V_i remains constant but the final volume is changed, so CR is changed.

Figure 8.3 illustrates the variation of compressed gas conditions with changing CR, T_o and p_o. This figure represents the limited range of operating conditions that could be obtained in the series of experiments performed.

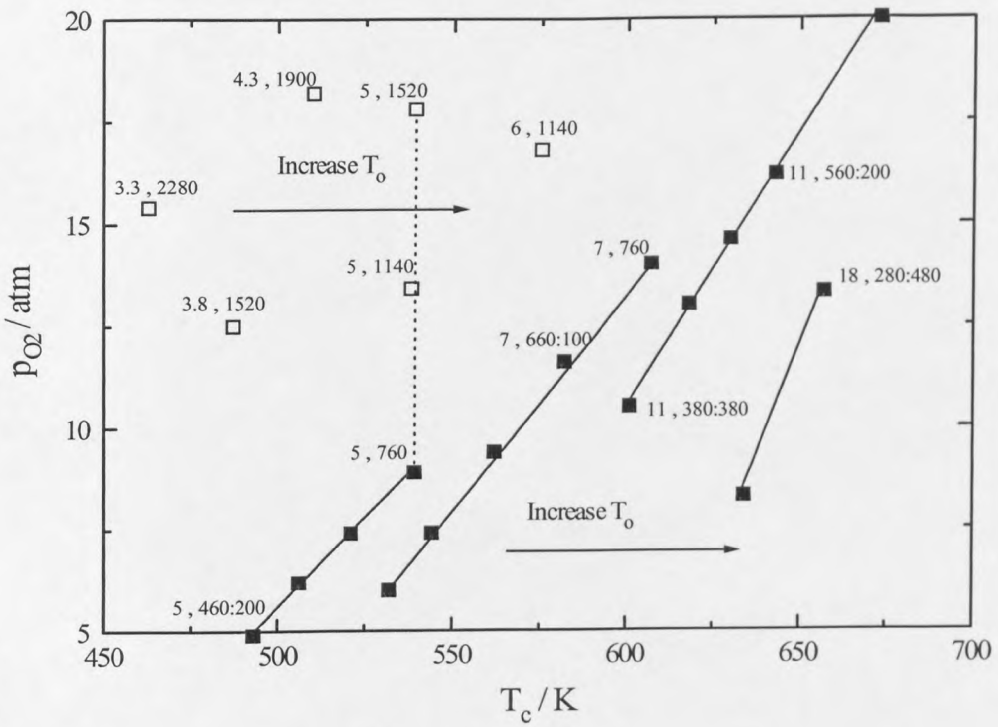

Figure 8.3 Conditions at the end of compression in the RCM and the effect of CR, mixture composition (O_2:CO_2), initial pressure (mmHg) and temperature. Data markers represent (CR, O_2:CO_2). Initial pressures greater than 1 atm (□) and up to and including 1 atm (■) are shown on this figure. Solid lines connects mixtures of oxygen and carbon dioxide with the same CR. The dashed line connects the same mixture composition and same CR for increasing initial pressure.

For an ideal adiabatic compression in the RCM the compressed gas temperature is given by,

$$T_c = T_o (CR)^{\gamma-1}$$

and the expected compressed gas pressure can be calculated by the following relationship,

$p_c = p_o (CR)^{\gamma}$.

The need for higher p_o is important because, as Fig. 8.3 illustrates, the low pressures achieved by low compression ratios (3.3:1) must be compensated for by an increase in p_o so that a high p_c (and hence p_{o2}) can still be achieved whilst achieving low T_c.

The initial temperature of the system, (the wall temperature of the combustion chamber), can be maintained at room temperature, ~20°C, which also assists in the approach to lower T_c.

A simple calculation to determine the CR and p_o required to achieve T_c = 500 K and p_c = 15 atm, taking γ = 1.34 (pure O_2 at the high temperature limit):

$(T_c/T_o)^{1/\gamma-1} = CR$

$(500/293)^{2.94} = 4.8$

for a CR = 4.8, to achieve a pressure of 15 atm following compression,

$p_o = p_c/(CR)^{\gamma} = 15/(4.8)^{1.34} = 1.8$ atm

The value of T_c can be varied by adjusting:-

- the relative proportions of oxygen and carbon dioxide to vary the value of γ
- the initial temperature T_o
- the compression ratio (using different thickness end-windows)

And p_o can be varied accordingly to keep p_{o2} within the required range.

With a "stepped-in" window, giving CR = 6.8 or 5.5

The required conditions can be achieved by using a range of initial pressures, 1-2 atm, and using mixtures of CO_2 and O_2 (Table 8.1). The mixtures were prepared and stored in a high pressure mixing vessel and transferred directly to the combustion chamber at the required pressure.

1 atm = 14.5 psi = 760 mmHg

pV^{γ} = constant

$p_1V_1^{\gamma} = p_2V_2^{\gamma}$

$(V_1 / V_2 = CR)$

$p_c = p_o (CR)^{\gamma}$

$T_c = T_o (CR)^{\gamma-1}$

Table 8.1 Effect of variation in mixture composition, initial pressure and CR on the end of compression temperature and partial oxygen pressure.

CR = 6.8 ; T_o = 298 K

O_2 / psi	+ CO_2/ psi	= p_o / psi	p_c / atm	po_2 / atm	γ	T_c / K
14.5	-	14.5	13.3	13.3	1.35	601
12.0	2.5	14.5	12.3	10.2	1.31	568
10.0	4.5	14.5	11.9	8.2	1.29	547
21.7	-	21.7	19.9	19.9	1.35	601
18.0	3.7	21.7	18.5	15.3	1.31	568
14.0	7.7	21.7	17.4	11.3	1.28	541
28.9	-	28.9	26.6	26.6	1.35	601
24.0	4.9	28.9	24.6	20.5	1.31	568
20.0	8.9	28.9	23.7	16.4	1.29	547
16.0	12.9	28.9	22.8	12.6	1.27	530
CR = 5.5 ; T_o = 298 K						
14.5	-	14.5	10.0	10.0	1.35	557
12.0	2.5	14.5	9.5	7.9	1.32	531
21.7	-	21.7	15.0	15.0	1.35	557
18.0	3.7	21.7	14.2	11.8	1.32	531
17.0	4.7	21.7	14.0	11.0	1.31	525
28.9	-	28.9	20.0	20.0	1.35	557
26.0	2.9	28.9	19.3	17.4	1.33	541
24.0	4.9	28.9	19.0	15.8	1.32	531
22.0	6.9	28.9	18.7	14.2	1.31	522
20.0	8.9	28.7	18.3	12.7	1.30	514
18.0	10.9	28.9	18.0	11.2	1.29	507

Much lower CRs could not be achieved by modification to the end window because there is a limit to how thin the end wall can be in order to withstand the pressures achieved during the post-compression period.

8.4 Results

8.4.1 Sensitisation of methane autoignition by higher alkanes

Mixtures were either 1:2 or 1:1 (CH_4:O_2), i.e. ϕ = 0.5 or 1.0, with appropriate dilution with inert gases to obtain the required value of γ. Selected experiments using a 2:1 (ϕ = 2.0) mixture have also been carried out. The first studies of methane-oxygen combustion at T_c in the range 700 - 900 K and p_c = 0.8 - 1.5 MPa, showed that autoignition does not occur under these conditions in the RCM. Note that, where reference to methane-oxygen mixtures is made, this signifies methane in equimolar, stoichiometric or half stoichiometric proportion with oxygen but with suitably selected proportions of N_2/Ar/CO_2 added to maintain a constant initial pressure and to obtain the appropriate γ value.

Since autoignition did occur within these ranges when higher alkanes were added in small quantities, the effect may be interpreted as one of sensitisation. The results are summarised in Table 8.2 and Figure 8.4. Figure 8.4 illustrates the effect of the percentage of n-butane, O_2 proportion and T_c on the ignition delay (τ) of methane-oxygen-inert mixtures in the RCM for compressed gas pressures in the range 8-15 atm and T_c in the range 800 - 825 K. The influence of propane and ethane on the autoignition of methane-oxygen mixtures is summarised in Table 8.2. In general, the results show that the sensitisation effect of the higher alkanes on the autoignition of methane-oxygen decreases as the carbon chain length decreases. Figures 8.5(a) and 8.5(b) are pressure-time profiles illustrating the effect of various proportions of n-butane on the autoignition of methane-oxygen mixtures (1:1 and 1:2 respectively).

Each of the pressure profiles shown in Figure 8.5 exhibits a pressure fall after the end of compression, followed by a further increase in pressure after approximately 10 ms. This is a consequence of the high pressures achieved towards the end of the compression. The driver pressure is not sufficiently high to force the piston to the completion of its stroke against the high pressures in the combustion chamber. However, following some heat losses in the early part of the post-compression period, the piston is then able to

proceed to the completion of the compression stroke, encountering a reduced resistance to forward motion due to the pressure in the chamber, thus causing a mechanical enhancement of the pressure in the chamber. In addition to this, several of the pressure profiles for the experiments where ignition did not occur, exhibit a small, gradual pressure rise during the post-compression period for up to 80 ms after the end of compression. This is also believed to be an artefact of the piston motion and can be attributed to a gradual "creep" forward of the piston.

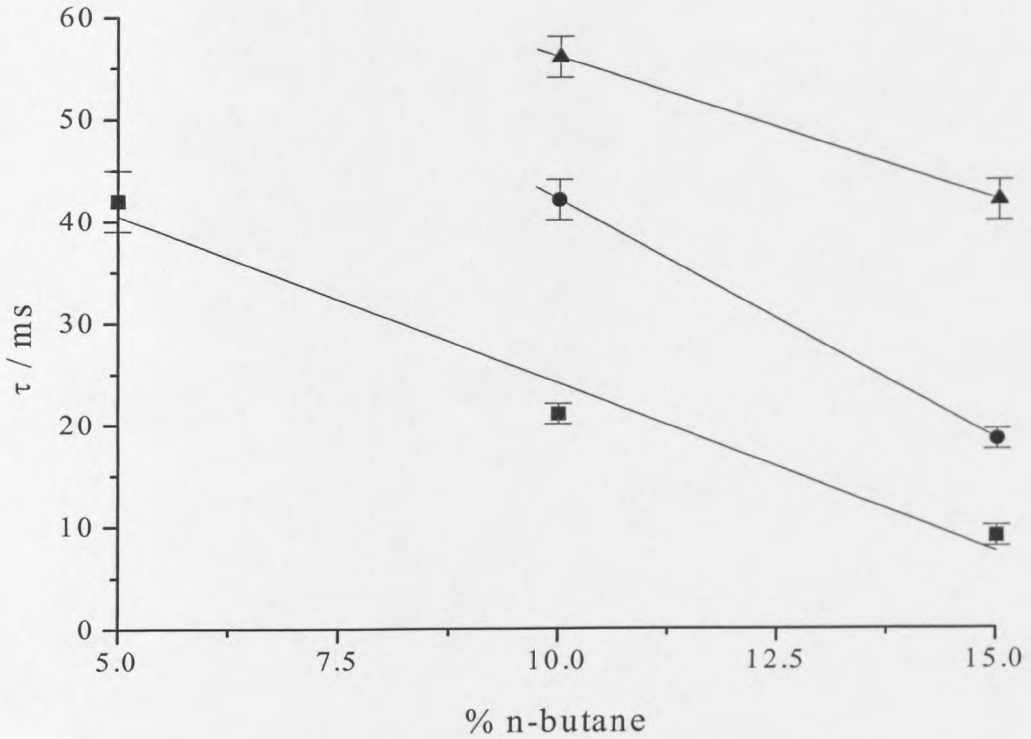

Figure 8.4 Effect of % n-butane, compressed gas temperature and fuel:oxygen ratio on autoignition delay of CH_4:O_2:inert mixtures (1:2:2, 820-825 K (■); 1:1:2, 810-820 K (●); and 1:1:2, 800-810 K (▲)).

Table 8.2 Effect of higher alkane additives on the autoignition of methane-oxygen mixtures in the RCM (n/i = no ignition).

Reactant Mixture / mmHg				T_c / K	τ / ms
CH_4	O_2	N_2/Ar/CO_2	RH (%)		
100	200	200	-	750-950	n/i
100	100	200	-	750-950	n/i
100	100	100	-	750-950	n/i
200	100	200	-	750-950	n/i
			C_4H_{10}		
100	200	200	2	820-825	n/i
			5	820-825	42 (±3)
			10	820-825	21 (±1)
				730-900	*(Fig. 8.7)*
			15	820-825	9 (±1)
100	100	200	5	800-810	n/i
			10	800-810	56 (±2)
				810-820	42 (±2)
			15	800-810	42 (±2)
				810-820	18.5 (±1)
200	200	200	0-15	< 740	n/i
200	100	100	15	715-725	60
			C_3H_8		
100	200	200	0	820-830	n/i
			2	820-830	55, n/i
			5	820-830	44, n/i
			10	820-830	55, 34, n/i
			C_2H_6		
100	200	200	0	835-840	n/i
			2	835-840	37, n/i, n/i
			5	835-840	37, n/i
			10	835-840	n/i
			15	835-840	n/i

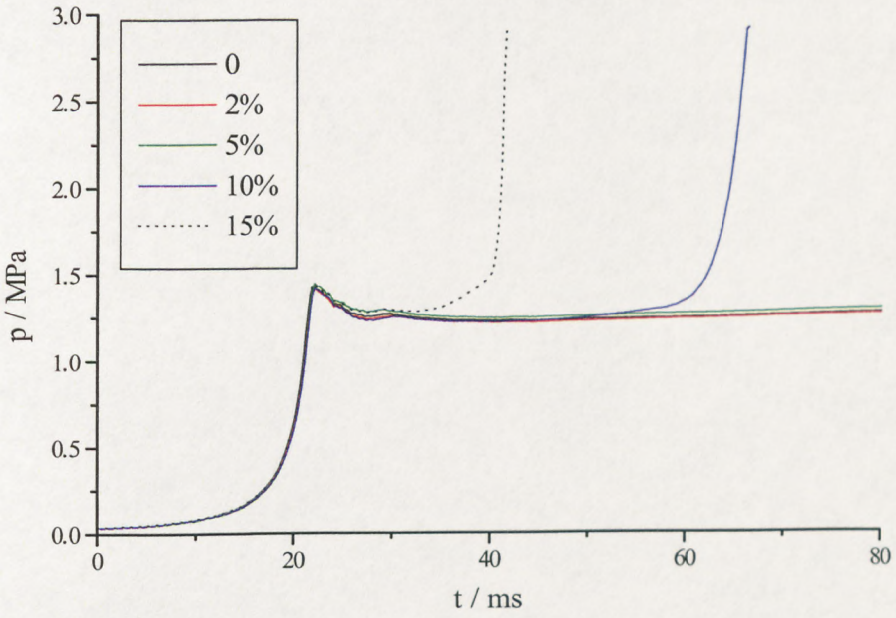

Figure 8.5 (a) Pressure-time profiles illustrating the autoignition of CH_4:O_2:(N_2/Ar):C_4H_{10} = 1:1:2:(0-0.15) mixtures for varied proportions of n-butane, following compression to 815 (±4) K and ~1.45 MPa.

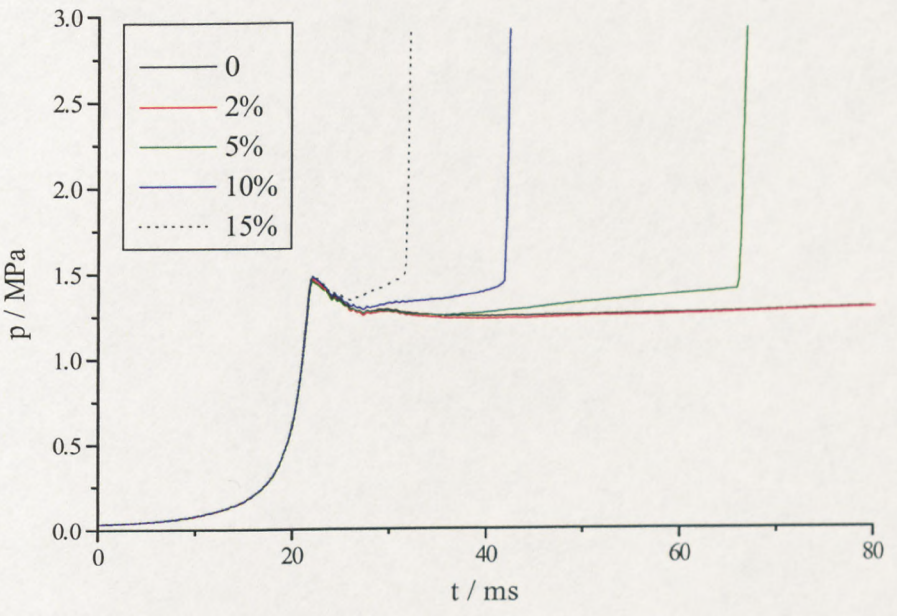

Figure 8.5 (b) Pressure-time profiles illustrating the autoignition of CH_4:O_2:(N_2/Ar):C_4H_{10} = 1:2:2:(0-0.15) mixtures for varied proportions of n-butane, following compression to 820 (±2) K and ~1.45 MPa.

8.4.2 The initiation of ignition by soot particles of methane-oxygen mixtures and of methane-oxygen mixtures sensitised with n-butane

The effect of soot particles on the ignition of CH_4:O_2:(N_2/Ar/CO_2) (1:2:2) mixtures and on CH_4:O_2:(N_2/Ar/CO_2):C_4H_{10} (1:2:2:0.1) mixtures has been studied at compressed gas temperatures in the range 650-900 K and pressures in the range 0.8 - 1.5 MPa. The second reactant mixture is of some interest because it is representative of natural gas, which may contain up to 10 % higher alkanes. The results are shown in Figures 8.6 and 8.7 respectively. Ignition of the CH_4-O_2-inert mixtures did not occur at compressed gas temperatures in the range 650 - 900 K in the absence of soot, or at temperatures below 700 K in the presence of soot.

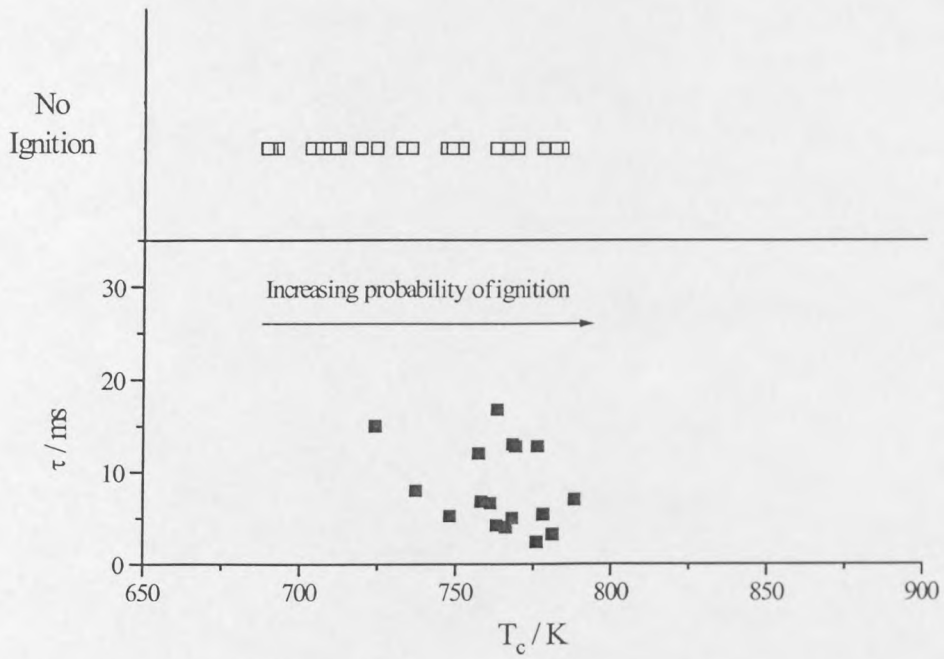

Figure 8.6 Effect of soot particles on the ignition of CH_4:O_2:(N_2/Ar) = 1:2:2 (ignition with soot (■); no ignition with soot (□)).

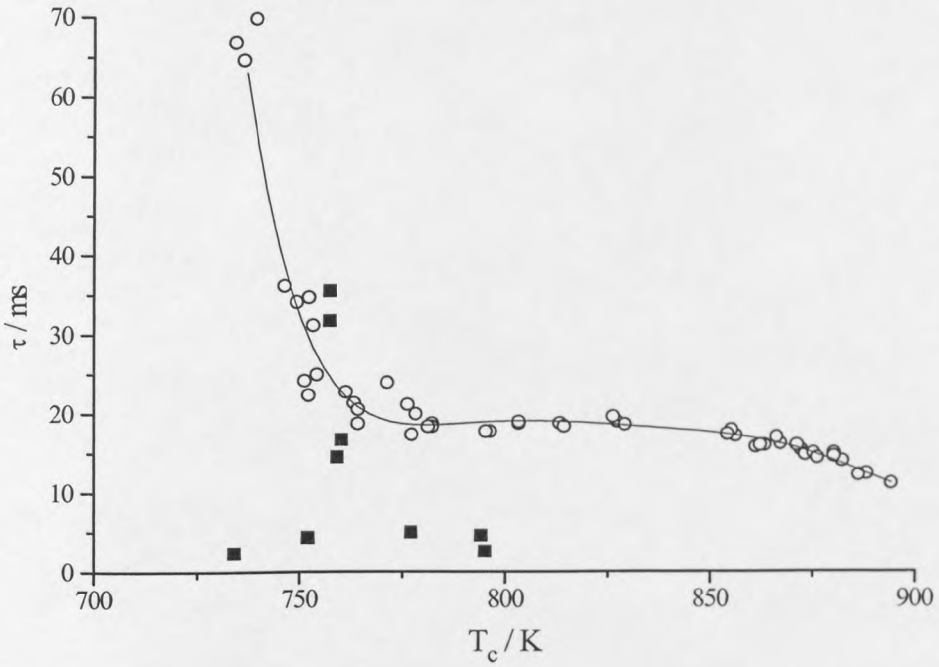

Figure 8.7 Effect of soot particles on the ignition of CH_4:O_2:(N_2/Ar):C_4H_{10} = 1:2:2:0.1, (ignition with soot (■); autoignition without soot (O)). Three more experiments were performed at T_c ~730 K in the presence of soot, in which ignition was unsuccessful.

Soot particles were found to strongly affect the onset of ignition of methane-oxygen mixtures in the RCM at $T_c > 750$ K, but with negligible temperature dependence of the ignition delay ($\tau = 8$ (±5) ms). In methane-oxygen mixtures sensitised with n-butane the minimum temperature at which particle initiated ignition occurred did not differ significantly from that for the autoignition of the gaseous sensitised mixture. However, the time delay was shorter than and somewhat similar to that for the ignition of methane-oxygen mixtures by soot particles.

These results suggest that there is a threshold temperature (~700-750 K) below which the soot particles are unable to ignite methane or "natural gas" mixtures, at least at pressures up to 1.5 MPa. Table 8.3 illustrates the effect of increasing temperature on the probability of soot particles initiating ignition in a CH_4:O_2:inert (1:2:2) mixture following compression to pressures in the range 0.7-1.1 MPa in the RCM. These results

emphasise the highly statistical nature of the experiments and the need for many experiments repeated at the same conditions to obtain a reliable indication of the probability of soot particles acting as ignition initiators. As the temperature range is increased from 650-700 K to 700-750 K, the probability of ignition in the presence of soot particles increases from 0 in 9 to 3 in 23. An additional increase in temperature to 750-800 K results in a further increase in probability of ignition given soot particles, to 14 in 22. The evidence suggests that a lower limiting temperature exists between 650 and 700 K. However, this should not be regarded as a definitive ignition boundary in the same sense as that applied to the autoignition of gaseous hydrocarbons in air.

The effect of increasing oxygen partial pressure on the autoignition of methane:oxygen mixtures in the presence of soot has also been studied (Table 8.4). For each mixture two compressed gas temperature regions were investigated, thus providing further verification of the effect of increasing temperature on the autoignition of methane-oxygen in the presence of soot. The results show that as the partial oxygen pressure and the temperature are increased, the probability that ignition may be initiated by soot particles increases and the ignition delay decreases.

Table 8.3 Proportion of total number of experiments carried out which result in successful and unsuccessful ignition of methane:oxygen:inert (1:2:2) mixtures in the presence of soot in the range of compressed gas temperatures 650 - 800 K.

T_c / K	650 - 700	700 - 750	750 - 800
Total number of experiments	9	23	22
No. of unsuccessful ignitions	9	20	8
No. of successful ignitions	0	3	14
Ignition delay / ms	-	8.0, 4.0, 5.2	Average = 8.0 s.d. = 4.4

Table 8.4 The effect of soot as an initiator to methane ignition and the influence of partial oxygen pressure and compressed gas temperature on ignition. A comparison between soot and non-soot containing experiments is made. (n/i = no ignition).

Reactant mixture / mm Hg			Ignition Delay / ms	
CH_4	O_2	T_c / K	with soot	without soot
100	100	734 (±2)	n/i	n/i
			n/i	n/i
			n/i	n/i
100	150	730 (±2)	n/i	n/i
			n/i	n/i
			-	n/i
100	200	733 (±2)	n/i	72.8
			n/i	n/i
			-	n/i
100	250	736 (±3)	17.6	n/i
			2.6	n/i
			17.8	11.2
			2.8	n/i
100	300	733 (±4)	4.2	16.6
			n/i	n/i
			2.0	n/i
			5.0	-
100	100	814 (±3)	n/i	-
			n/i	-
			n/i	-
100	150	814 (±1)	n/i	-
			14.0	-
			n/i	-
100	200	~820	0.0	-
			0.6	-
100	250	~820	0.0	-
			0.0	-
100	300	~820	0.0	-

8.4.3 The self-heating properties of soot in oxygen-inert mixtures at high pressure

It has been established that as the compressed gas temperature and the partial pressure of oxygen are increased, there is an enhanced reactivity of the soot particles leading to self-heating and ignition. The combustion of soot particles in a compressed oxygen-inert

mixture has also been used to illustrate this to be the ignition source. For this purpose the light output, i.e. the intensity and duration of light emission, from incandescent particles was detected (Figs. 8.8 and 8.9).

Figure 8.8 Effect of partial pressure of oxygen (O_2:N_2/CO_2/Ar) on the light emission (—) from soot particles at T_c = 830 (±3) K.

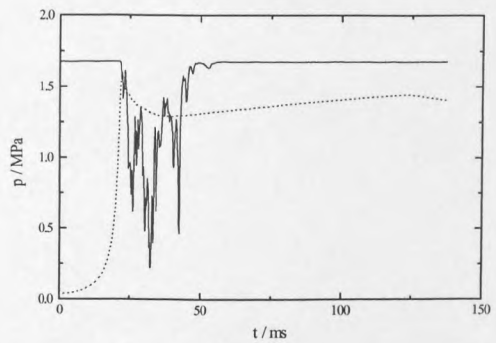

(1:5)

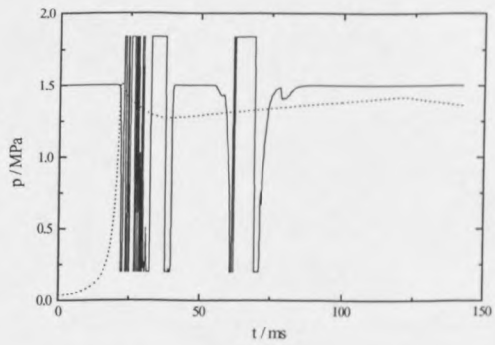

(1:2)

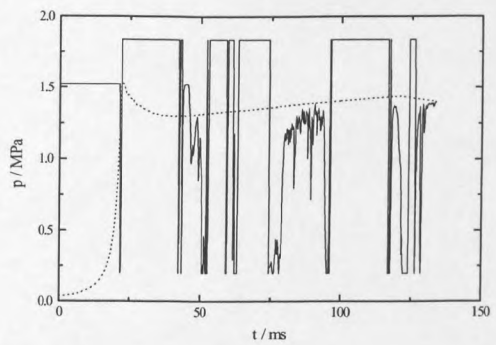

(1:1)

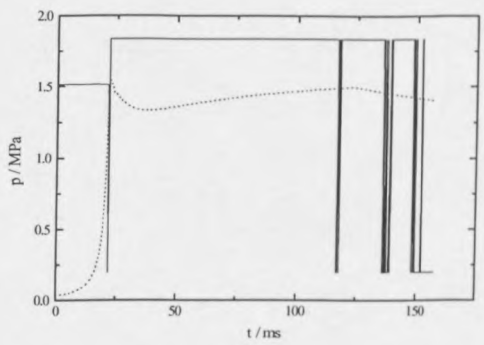

(2:1)

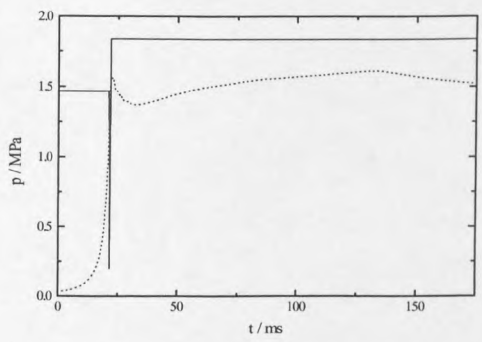

(5:1)

Figure 8.9 Effect of compressed gas temperature (T_c) on light emission (—)due to hot soot particles at constant partial oxygen pressure (O_2:N_2/CO_2/Ar = 1:1)

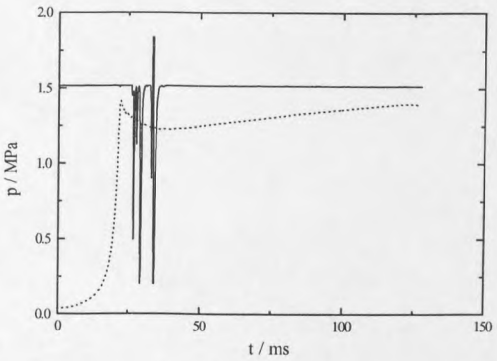

T_c = 720 K

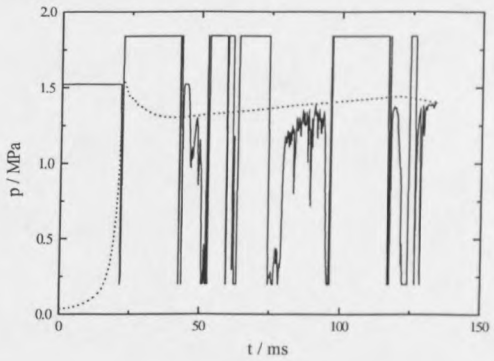

T_c = 830 K

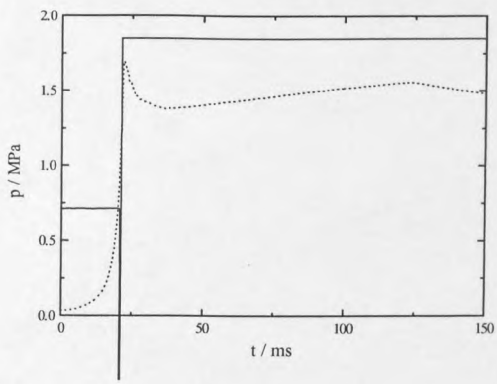

T_c = 928 K

In the light output records, a negative deviation from the baseline signifies the detection of light, except where the PMT has been saturated with light. In these circumstances the light output record gives a rapid positive deviation from the baseline, as illustrated by the figure above at T_c = 928 K.

Given that heat transfer must occur to the soot particles and that gas cooling occurs fairly rapidly in the RCM, it might be inferred that there is a limiting particle size that is capable of ignition or there is a minimum particle temperature for it to ignite . In a given experiment, where a wide range of particle sizes exist, there are likely to be

varying intensities of light emission occurring at different times throughout the post-compression period (Fig. 8.8 and 8.9).

The less intense, short duration of light output due to the soot particles which was observed at the lower temperatures (T_c <720 K) might reasonably account for the ineffectiveness of soot as a promoter to autoignition of methane-oxygen-(butane) mixtures below 700 K. Presumably, insufficient small particles are present or those that do ignite cannot generate a large enough hot spot to initiate a flame kernel.

The light given off from a glowing soot particles is essentially black body radiation, with some shortfall in the infrared region of the spectrum. A 2-dimensional image of the light output due to glowing soot particles within the combustion chamber has been obtained using the CCD camera (Figure 8.10). The image was obtained at a time during the post-compression period, for a 1:1 (O_2:inert) mixture following compression to 810 K. This result provides evidence for the dispersion of particles of varying size and light emission intensity throughout the combustion chamber during the post-compression period.

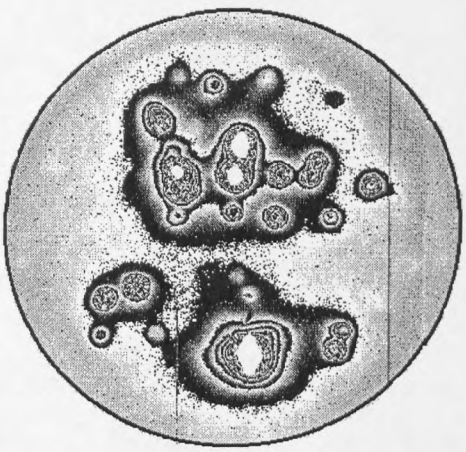

Figure 8.10 CCD image illustrating the light output due to self-heating soot particles in the combustion chamber of the RCM. (Dark regions indicate light output, except where saturation occurs, signified by white regions)

Following compression, a single carbon particle near the centre of the combustion chamber is likely to ignite the surrounding fuel-air mixture. The number of particles in the combustion chamber is not crucial providing there are a sufficient number for there

to be a realistic probability of one particle being subject to the core gas temperature. It is only necessary to have one particle, which is capable of self-heating, in the right place in order for it to initiate ignition. The probability of a particle of a given size being the first to ignite depends on the number fraction of the particles of that size present.

It is thought that the size of the particle has a predominant effect on its ability to self-heat and release heat and light into the surroundings, thus acting as a hot centre for the initiation of autoignition. Small particles will tend to lose heat rapidly, at a more rapid rate than they release heat due to exothermic reactions. Large agglomerates with voids filled with oxygen can self-heat at a more rapid rate and give off heat and light. Therefore an optimum particle size for ignition exists. The heat transfer from the hot particle to the surrounding fuel-air mixture increases the gas temperature and therefore the rate of reaction in the vicinity of the particle and a combustion wave propagates outward from the hot centre.

The particle temperature lags behind the gas temperature during and directly after the compression and thereafter heat transfer from the gas heats the particle. Eventually, the particle temperature exceeds the gas temperature and the particle ignites. Temperature, partial pressure of O_2 and particle size all influence the ability of a particle to self-heat. Therefore variations in light output from experiment to experiment occur.

The results presented in this chapter appear to suggest the existence of an ignition boundary of the conditions of partial oxygen pressure and temperature below which soot particles are unlikely themselves to ignite or to be a sufficiently large energy source to initiate ignition in flammable mixtures.

The study has so far been limited to relatively low partial oxygen pressures. The aim of the remainder of the study was to widen the scope of the investigation to include higher partial oxygen pressures. The results shown in Table 8.5 and Figure 8.11 illustrate the probability of soot particles igniting in the RCM across a wider range of compressed gas conditions of temperature and partial oxygen pressure.

The evidence suggests that at partial oxygen pressures in excess of 15 atm the ignition of soot particles is relatively insensitive to pressure and the probability of ignition occurring above 15 atm increases as the temperature exceeds 550 K. In addition to the effect of temperature and pressure, the problem is also subject to a degree of statistical control, a general characteristic of heterogeneous combustion systems. In some experiments light output was observed in the absence of soot, in these cases it was assumed that a sufficient amount of residual soot from the previous experiment was present in the combustion chamber.

Table 8.5 Effect of temperature and partial oxygen pressure on the probability of ignition of soot particles in the RCM.

pO_2 / atm	T_c / K	No. of Experiments	No. of successful ignitions
8.4 (±1)	544 (±1)	3	0
10.5 (±1)	564 (±1)	3	0
11.9 (±1)	577 (±1)	3	0
13.4 (±2)	545 (±2)	3	0
13.6 (±3)	597 (±3)	9	6
15.4 (±2)	564 (±2)	4	0
17.8 (±3)	576 (±2)	4	1
20.5 (±2)	598 (±1)	5	4

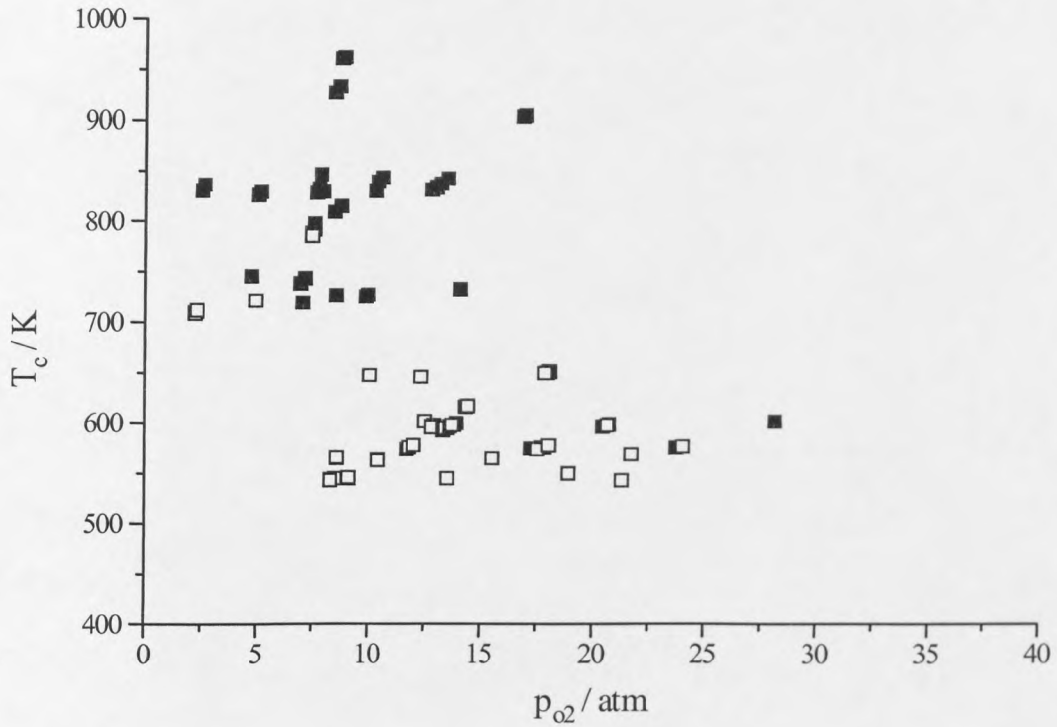

Figure 8.11 Effect of compressed gas temperature and partial oxygen pressure on the ignition of soot particles in the RCM (ignition (■); non-ignition (□)).

8.5 Summary and Conclusions

- Higher alkanes have a sensitising effect on methane:oxygen mixtures. The longer chain alkane, n-butane, had the most significant effect on the reactivity of the mixture and increasing the proportion of butane in the range 0-15 % resulted in a reduction in ignition delay at a given compressed gas temperature and pressure.
- The presence of soot particles in the chamber has the effect of promoting the ignition of methane:oxygen mixtures which would otherwise not autoignite in the RCM under the conditions studied.
- There appears to be a threshold temperature at approximately 700 K below which soot particles fail to initiate ignition in methane-oxygen mixtures and the reduction in delay for the methane-oxygen-butane mixture is no longer evident at p_c in the range 0.8-1.5 MPa.

- Soot particles have the effect of reducing the ignition delay of the methane-oxygen-butane mixtures when compared with that of the autoignition of the gaseous mixture.
- At partial oxygen pressures above 15 atm there appears to be a minimum temperature for the ignition of soot particles in oxygen at approximately 580 K. However, the statistical variations inherent in heterogeneous ignition suggest that this "ignition boundary" is more likely to be representative of a region of varying probability of soot particles igniting.

Finally, it should be noted that two different types of combustion phenomena have been described in this chapter. First, there is the spontaneous ignition process which is defined by the temperature and pressure to which a gaseous mixture must be raised in order for ignition to be possible in the absence of an external stimulus. Secondly, there is the possibility of initiating the ignition of a gaseous fuel-oxidant mixture within a certain range of composition, defined by the rich and lean limits of flammability. The flammable range has not specifically been studied in this work but such limits must exist even at high temperature and pressure, especially in a small combustion chamber. The important distinction is that spontaneous ignition can occur in reactant compositions that fall outside the flammable limits for flame initiation by a spark or other external stimulus.

APPENDICES

APPENDIX A

(i) Predict 3 - Calculation of compressed gas temperature (1)

In order to simplify the process of choosing the appropriate reactant mixtures for use in the RCM, a FORTRAN program (Predict 3) has been compiled which allows the prediction of end of compression temperatures and a final value of γ, for a given mixture at a known initial temperature and pressure given a fixed value for the compression ratio, i.e.,

$$\frac{T_{ad}}{T_i} = \left(\frac{V_i}{V_c}\right)^{\gamma - 1}$$

Taking into account temperature dependence of specific heat capacities throughout the compression stroke the computer performs an iterative calculation, represented as follows,

$$\int_{T_i}^{T_{ad}} \frac{1}{(\gamma - 1)} \, d\ln T = \ln\left(\frac{V_i}{V_c}\right)$$

The program uses the CR, C_p data for the mixture components and the initial temperature, T_i, to predict the adiabatic compressed gas temperature of the reactant mixture, T_{ad}.

The program is not shown here but the main steps are as follows:-

1 the input data file (predict.dat) is opened and read
2 the CR is adjusted for the number of cycles in the calculation, i.e., for a 200 cycle iteration, $CR2 = CR^{(1/200)}$ (the reason for this is described in further detail below).
3 heat capacities are calculated from the C_p polynomial data using a temperature TGUESS and the value of γ is derived for that temperature
    a) the total vapour pressure of the blend, X_T is calculated

b) the total heat capacity of the blend is calculated, C_{pT}

c) the mole fraction averaged heat capacity, C_p, of the blend is calculated

$C_p = C_{pT} / X_T$

$C_v = C_p - R$

d) $\gamma = C_p / C_v$

4 The compressed gas temperature, T_{ad}, is calculated from the equation,

$T_{ad} = T_o (CR2)^{\gamma-1}$

5 the calculated value of T_{ad} from one iteration is used as the value TGUESS in the subsequent iteration

6 steps 1-5 are repeated 200 times (for a 200 iteration calculation) until the values of TGUESS and T_{ad} converge to within 0.5 K, hence, $T_o = T_{ad}$.

Assuming the number of cycles in the calculation is 3, the justification for step 3 is as follows:-

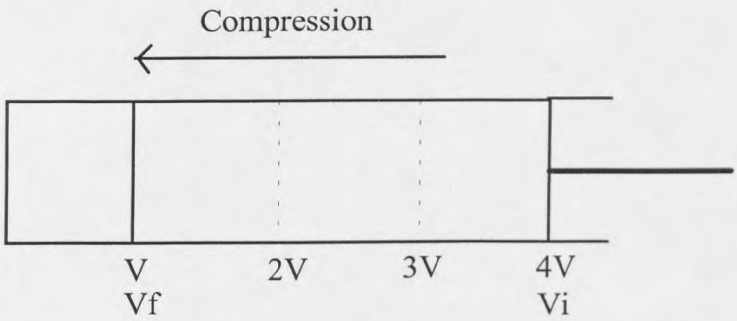

For the step $4V \rightarrow 3V$: $T_3/T_4 = (4/3)^{\gamma4-1}$

The value T_3 is then used to calculate γ_3, used in the next step of the calculation,

$3V \rightarrow 2V$: $T_2/T_3 = (3/2)^{\gamma3-1}$

The value T_2 is then used to calculate γ_2, used in the next step of the calculation,

$2V \rightarrow V$: $T_1/T_2 = (2/1)^{\gamma2-1}$

Overall,

$T_f/T_i = T_1/T_4 = (4/3)^{\gamma4-1} (3/2)^{\gamma3-1} (2/1)^{\gamma2-1}$

$T_f/T_i = (CR2)^{\gamma-1}$

where, $CR2 = CR^{(1/3)}$ for this three cycle iteration

$CR = V_f/V_i = 1/4$

$CR2 = (1/4)^{1/3} = 0.63$

and so,

$V_3/V_4 = V_3/4 = 0.63$

$V_3 = 2.54$

Repeating this for each step in the compression stroke calculation,

$V_2 = 1.59$

$V_1 = 1.0$

Therefore, using CR2 accounts for the true variation in initial and final volume at stages throughout the compression stroke.

(ii) Predict 4- Calculation of compressed gas temperature (2)

Predict 4 is a similar programme to Predict 3, based on the same principle for treatment of the compression stroke. The program uses best fit C_p data to calculate the end of compression temperatures from the measured initial and compressed gas pressures and calculates γ by an iterative procedure with respect to the compression stroke, i.e. takes into account the change in pressure and temperature at intervals throughout the stroke of the piston (200 iterations). The equation of state,

$$\frac{T_{ad}'}{T_i} = \left(\frac{p_c}{p_i}\right)^{\frac{\gamma-1}{\gamma}}$$

is adapted for the iterative procedure, taking into account the variation of specific heat capacities with temperature and becomes,

$$\int_{T_i}^{T_{ad}'} \frac{\gamma}{\gamma - 1} \, d \ln T = \ln \left(\frac{p_c}{p_i} \right)$$

The compression ratio is adjusted for the number of cycles in the calculation, i.e. 200 cycles. The heat capacity of the mixture is calculated from the polynomials of the specific heat capacity data using a guessed value for temperature and the vapour pressures of the mixture components as described earlier for Predict 3. At each iteration the temperature used in the calculation is adjusted so that the value, T_{ad}', calculated at the end of the previous iteration is used as T_i in the next iteration.

In this programme, the pressure ratio (p_c/p_i) is adjusted for the number of cycles in the calculation (200), in a similar way as performed for the volume ratio in Predict 3.

In Predict 4 the actual compression ratio is calculated at the end of the iterative procedure, from the ideal gas law using the measured pressures at the start and end of compression, the initial temperature and the calculated final temperature, i.e.

$CR = V_i/V_f = p_c T_i / p_i T_c$

APPENDIX B

Piston Speed measurement

The compressing piston speed has been measured using three different methods of differing degrees of precision. The first and most simplistic method is to measure the total distance travelled by the piston during the compression stroke using a ruler to measure the position of the piston at the start and end of the compression stroke and, assuming the compression time to be 22 ms, derive the average piston speed throughout the compression stroke.

The distance travelled by the piston during compression = 24 cm
Therefore, average piston velocity = 0.24 m / 0.022 s = 11.4 m s^{-1}

The average speed of travel of the RCM compression piston has also been measured using perfluoropropane (C_3F_8) as the gaseous charge. Perfluoropropane has a specific heat capacity ratio, γ (= C_p/C_v) of 1.06. When a gas of polytropic ratio approaching or equal to 1 is compressed there is negligible adiabatic heating so the pressure-time history follows the isothermal pressure change due to mechanical compression alone. Therefore the rate of pressure change gives some indication as to the rate of change of piston speed throughout the compression stroke (Figures 1 and 2).

Figure 1 below illustrates the rate of pressure change during the compression of perfluoropropane from an initial pressure of 0.033 MPa, the final pressure achieved at top dead centre was 0.43 MPa. Applying the ideal gas law and the known combustion chamber dimensions, one can calculate the distance travelled by the piston during the compression stroke using the measured pressures and use this to calculate the average piston velocity during the compression stroke. Averaged over 4 experiments, the value obtained was 9.6 (±2) m s^{-1}.

The compression of perfluoropropane alone will result in no adiabatic heating due to the inherent heat capacity of the polyatomic molecule and no additional rise in pressure due

to exothermic reaction of the fuel. Therefore any pressure increase or decrease during the post-compression period is due to movement of the piston. The slow pressure rise during the 70 ms of the post-compression period is due to a gradual creep forward of the piston to give further compression. The hydraulic oil surrounding the piston provides a means for dampening the effect of the impact of the rapidly moving solid piston with the end-plate at the end of compression. A small volume of hydraulic fluid is gradually squeezed out of a small depth annulus in the end plate as the piston gradually "creeps" forward.

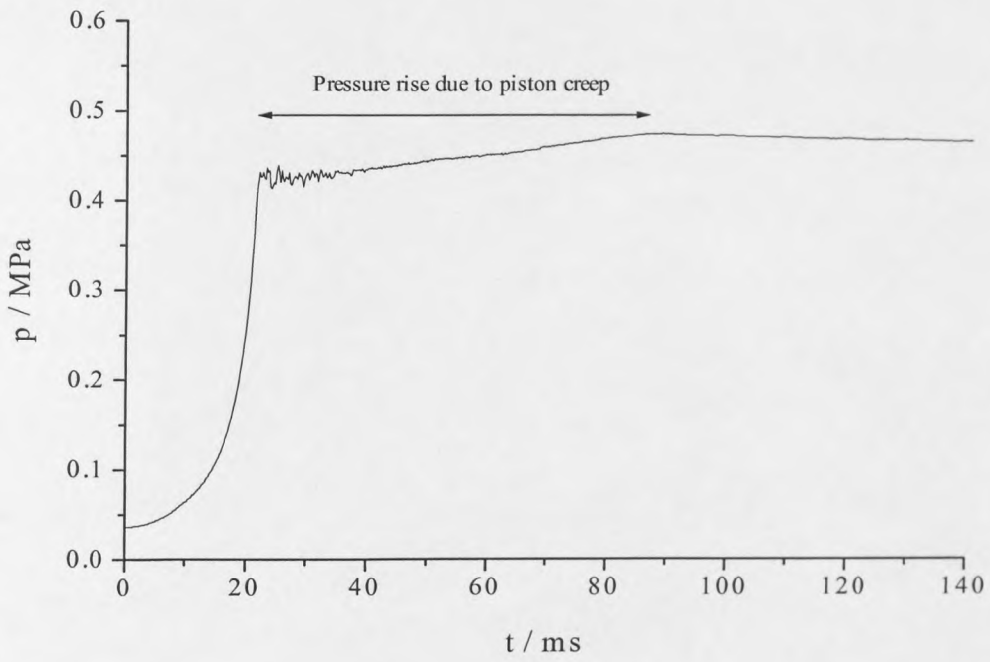

Figure 1 p-t history for compression of C_3F_8 (P_i = 0.033 MPa).

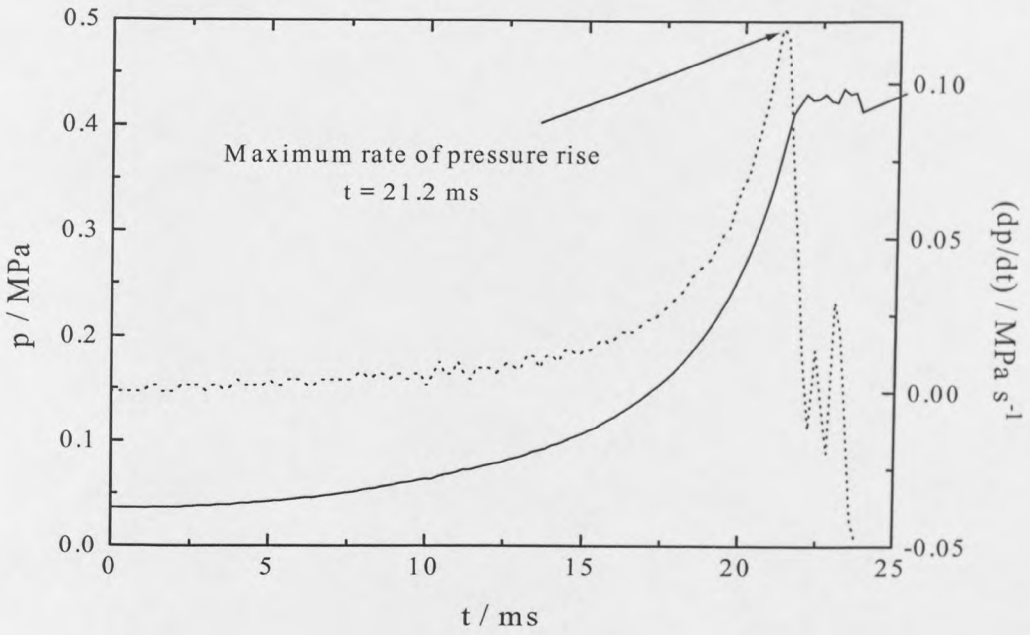

Figure 2 p-t history (—) for compression stroke and derivative curve (...) illustrating rate of pressure change during compression.

An alternative method for calculating piston velocity is to deduce an equation for the piston velocity directly from the ideal gas law, given that the temperature (T) and the cross-sectional area of the combustion chamber (πr^2) are constant.

For an ideal gas,

$pV = nRT$

and

$$p = \frac{nRT}{V} = \frac{nRT}{\pi r^2 (l_o - l)}$$

where l_o is the full distance travelled by the piston during compression and l is the distance moved by the piston after a given time during compression. This rearranges to,

$$(l_o - l) = \left(\frac{nRT}{\pi r^2}\right)\left(\frac{1}{p}\right)$$

Since πr^2 and T (at γ = 1.0) are constant, then the piston velocity is given by the relationship,

$$-\frac{dl}{dt} = \left(\frac{nRT}{\pi r^2}\right)\left(\frac{d(1/p)}{dt}\right)$$

where $(nRT/\pi r^2)$ is a constant equal to 8283 J m^{-2}. Therefore a plot of 1/p vs. t gives a graph, the gradient of which yields the piston velocity at any time (Figure 3).

The compression stroke includes the acceleration of the piston at the start of compression and the deceleration of the piston at the end of compression. The calculated gradient of the best fit line throughout the entire compression stroke is -0.00128 J^{-1} m^3 s^{-1}, which gives the average velocity of 10.6 m s^{-1}.

The piston velocity throughout any given time interval during compression can be calculated by calculating the gradient of the line of best fit for that time range. The greatest change in gradient occurs at the start and at the end of the compression stroke due to the acceleration and deceleration of the piston respectively. During the time interval from 5 to 20 ms after the start of compression the piston velocity is fairly constant and corresponds to 11.8 m s^{-1}. Between 2 and 3 ms after the start of compression the average piston velocity was calculated to be 10.3 m s^{-1}, in good agreement with the value obtained at a similar time during compression, using the Michelson Interferometer method described below.

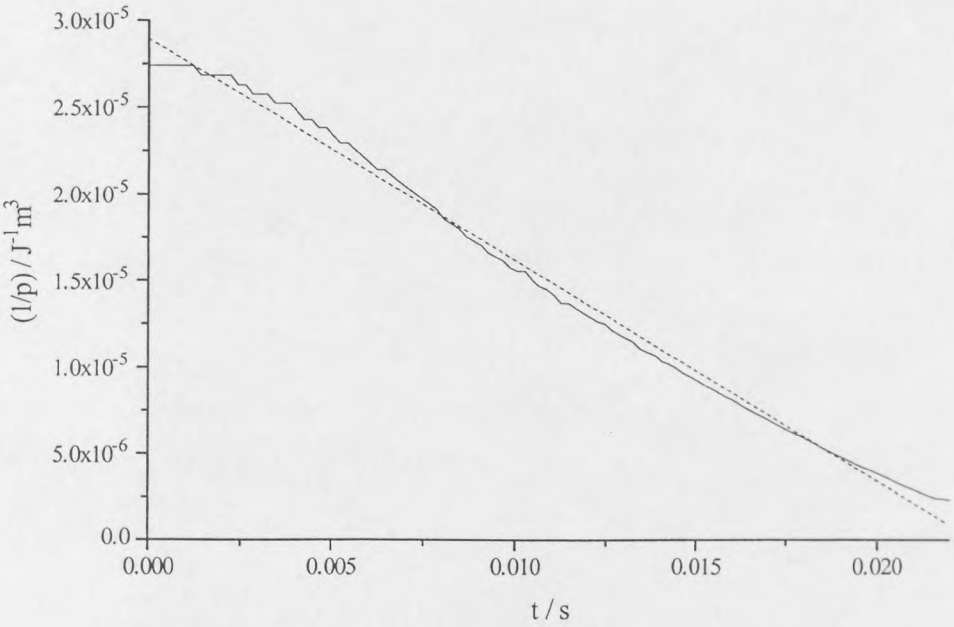

Figure 3 Graph of reciprocal pressure vs. time throughout the compression stroke duration. A line of best fit is also shown, the gradient of which gives the average piston velocity throughout the compression stroke.

The Michelson Interferometer method for measuring piston velocity

The Michelson interferometer provides a method for accurately measuring the velocity of a moving object [241]

Figure 4 below is a diagrammatic representation of the experimental set up. M1 is a stationary mirror for the reflection of the reference beam, M2 is the mirror fixed onto the piston crown, BS is a beam splitter and PD is a photodiode, the output from which was displayed on an oscilloscope. A low power (25 mW), single wavelength (632.8 nm) He-Ne laser was used. As M2 moves forward, the reflected laser light mixes with and interferes with the undisturbed laser beam reflected off M1, the photodiode detects the constructive and destructive interference patterns of the two laser beams.

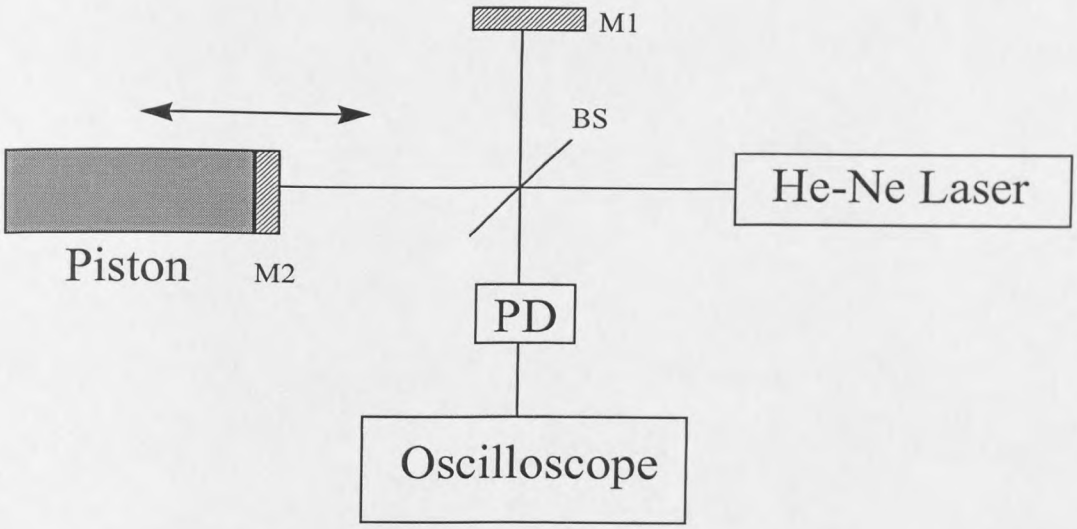

Figure 4 Schematic diagram of the Michelson Interferometer method applied to the RCM experiment

Figure 5 illustrates the underlying theory which enables a velocity, v, to be measured. At t = 0 the point source and the image of the point source are an equal distance, x_o, away from the mirror. As the mirror moves towards the source at a constant velocity, v, the distance from the mirror to the source at a given time is $(x_o\text{-}vt)$, which is also the distance from the mirror to the image. The light wave travels to the mirror and is then reflected back along its path so the total distance is $2(x_o\text{-}vt)$. Since this is equal to the total distance between the image and the source, x_T, one can assume that the image approaches the source at velocity, v_{rel}. The relative velocity between the source and the image is given as follows:-

$x_T = 2(x_o\text{-}vt)$

and

$v_{rel} = dx_T/d_t = 2v$

and the mirror approaches the source at velocity, v.

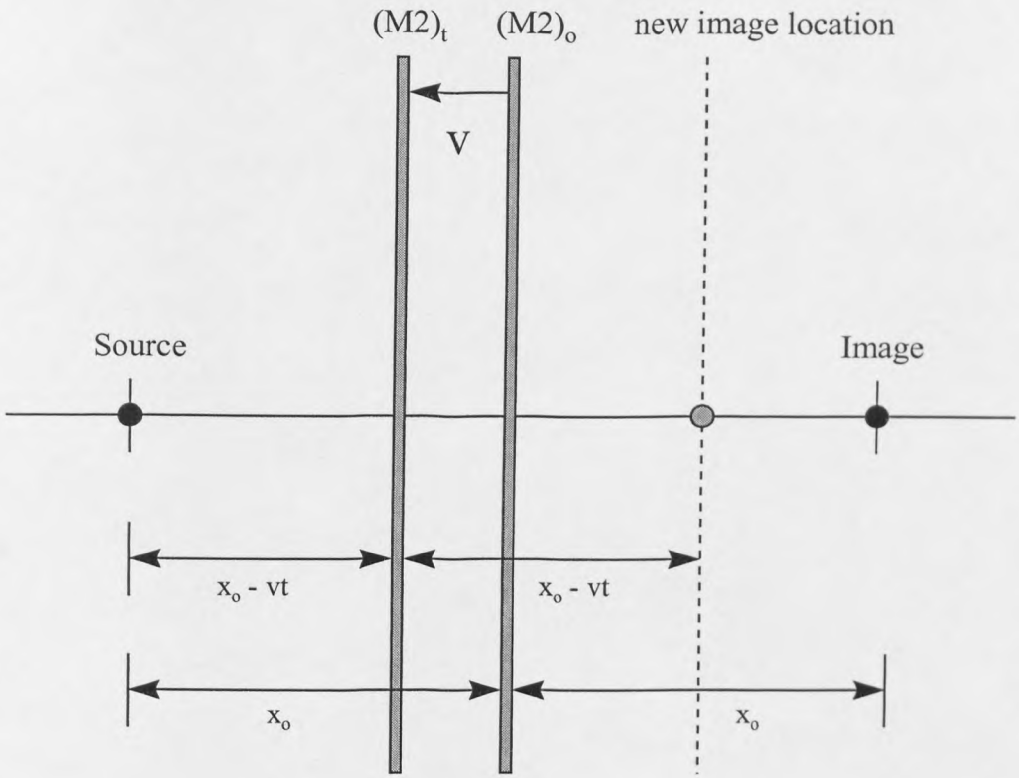

Figure 5 Diagram illustrating the effect of mirror movement on the distance between image and source

It was important to acquire a rapid data sampling frequency in order to satisfactorily capture the interference pattern because the events which are being recorded evolve over a relatively short time interval, a consequence of the rapid piston motion. The result obtained, operating at a sampling rate of 1×10^{12} samples/second (1 GHz) over a 200 ns range, is shown in Figure 6. This represents the interference pattern for a 200 ns time period taken near the start of piston motion. The high frequency vibrations characteristic of each of the fringes is relatively periodic and can be assumed to be a result of background "noise". The interpretation of the result to give a velocity measurement is as follows:-

The number of interference fringes corresponds to the number of whole wavelengths ($n\lambda$) travelled by the laser beam. Given that the time for the capture of data was 200 ns, a piston velocity can be calculated. An important consideration is that the light beam is

also reflected along its path so the distance must be halved to give the true distance travelled by the piston in the 200 ns interval.

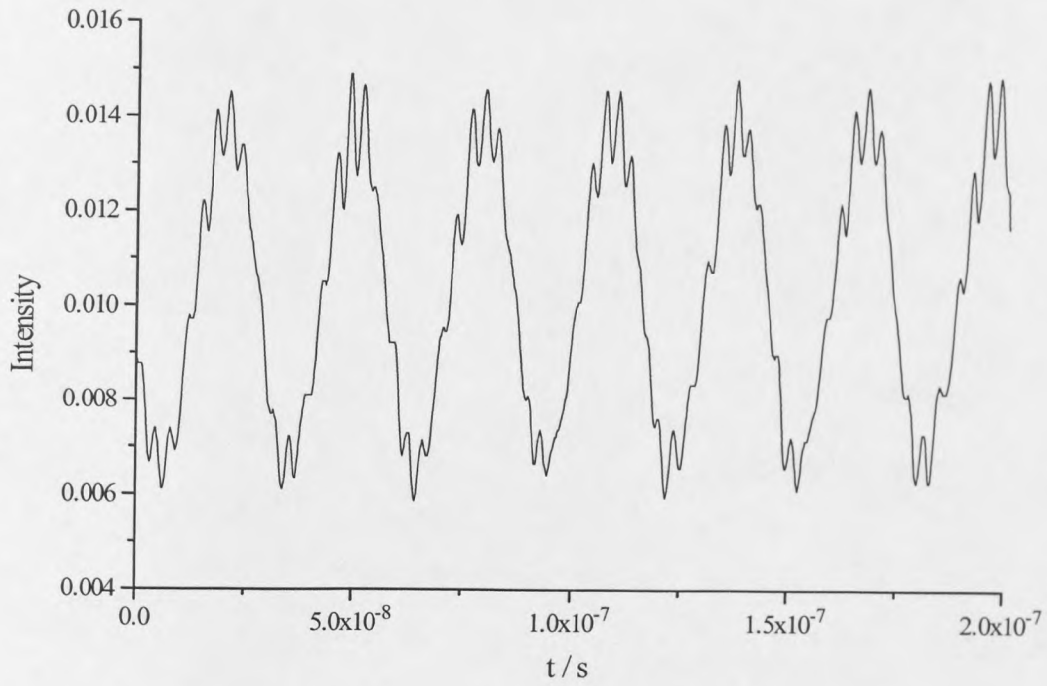

Figure 6 Interference pattern obtained using a Michelson interferometer to measure the piston velocity at the start of compression.

Total number of fringes in 200 ns = 6.75

Wavelength of He/Ne laser (λ) = 632.8 nm

$\therefore$ Distance travelled in 200 ns, $x = 6.75 \times (632.8 \times 10^{-9})$

$= 4.27 \times 10^{-6}$ m

Velocity,

$v = x / t$

$= (4.27 \times 10^{-6} / 2) / 200 \times 10^{-9}$

$= 10.68$ m s^{-1} at a time 2-3 ms after the start of the compression stroke.

APPENDIX C

Monitoring the start of piston motion

The method employed to monitor the start of piston motion utilises the rapid release of air from a small hole in the cylinder which encloses the driver piston as an indication of the start of motion of the driver piston. The start of piston travel was monitored by using the deflection of a thin strip of paper into the cavity between two arms of a photoelectric diode (Figure 7). When the passage of light between the two arms of the photoelectric diode is obstructed, there is a discontinuity in the signal output relayed to the pc via the A/D converter. This signal can be related to the temporal pressure profile.

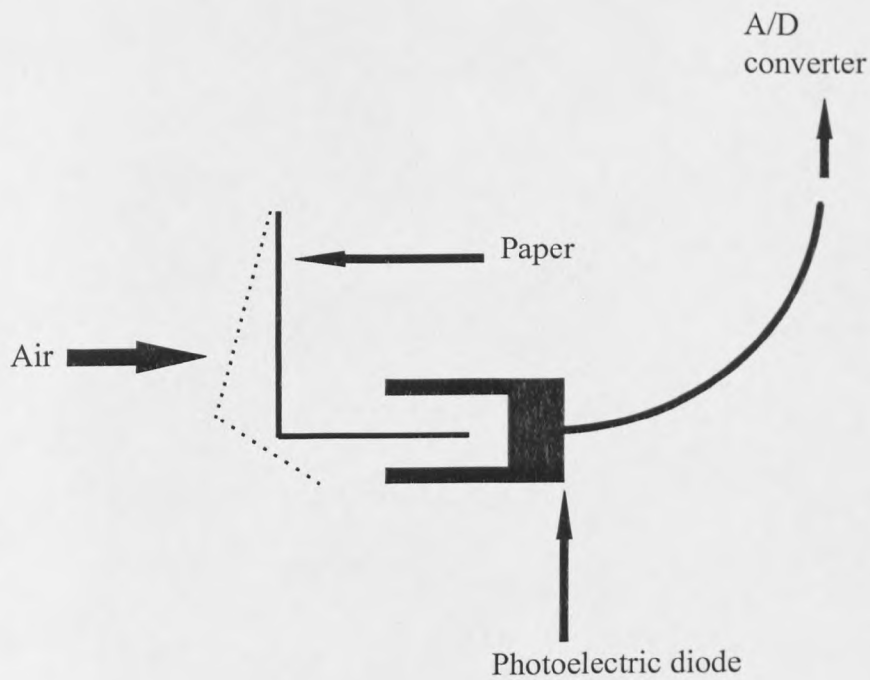

Figure 7 Schematic representation of method of monitoring the start of piston motion

Over several experiments, with the combustion chamber charged with an initial pressure of 0.033 MPa of air, the total duration of the compression stroke was measured as 22 (±1) ms.

APPENDIX D

Calculation of Knock Intensity

The method employed for the calculation of knock intensity was similar to that previously used by Pan et al. [203] in their quantification of individual engine knock cycles.

Figure 8 is a representative knock pressure profile from the RCM, obtained using the transient data recorder for a higher sampling frequency, thus enabling the characteristic pressure oscillations to be distinguished.

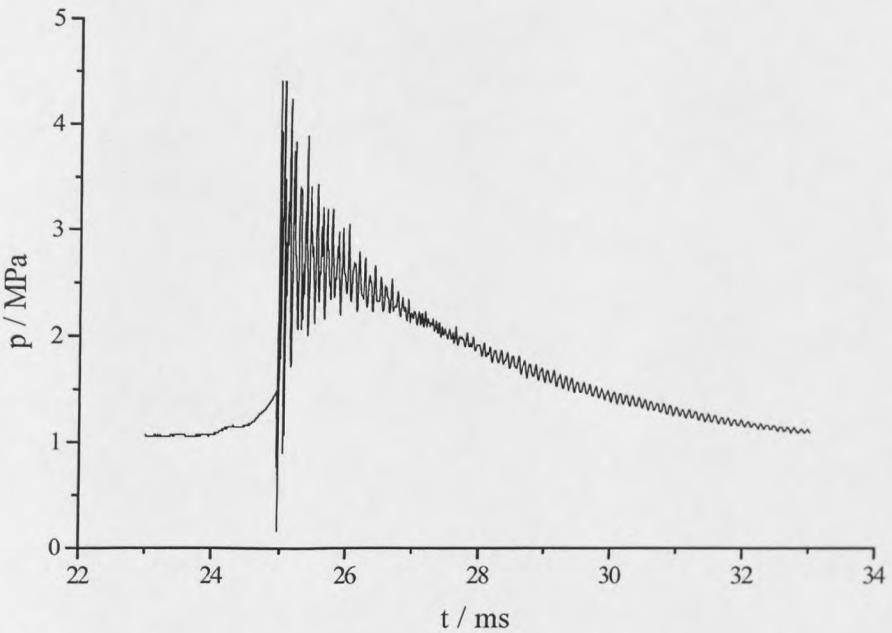

Figure 8 Knock pressure profile obtained using the transient data recorder for the spark-ignition of n-heptane following compression to 940 K, spark initiation occurred at 1.0 ms after the end of compression.

The primary knock signal data file was used as the input file and the knock intensity calculation program performed the following routine:

1. read the knock signal data file and its sampling rate
2. design a digital filter according to the specifications given
3. filter the knock signal and output a filtered data file (e.g. Figure 9, filtered pressure profiled for the knock profile shown in Figure 8)
4. calculate various knock intensity parameters using either original data or the filtered data
5. output the results

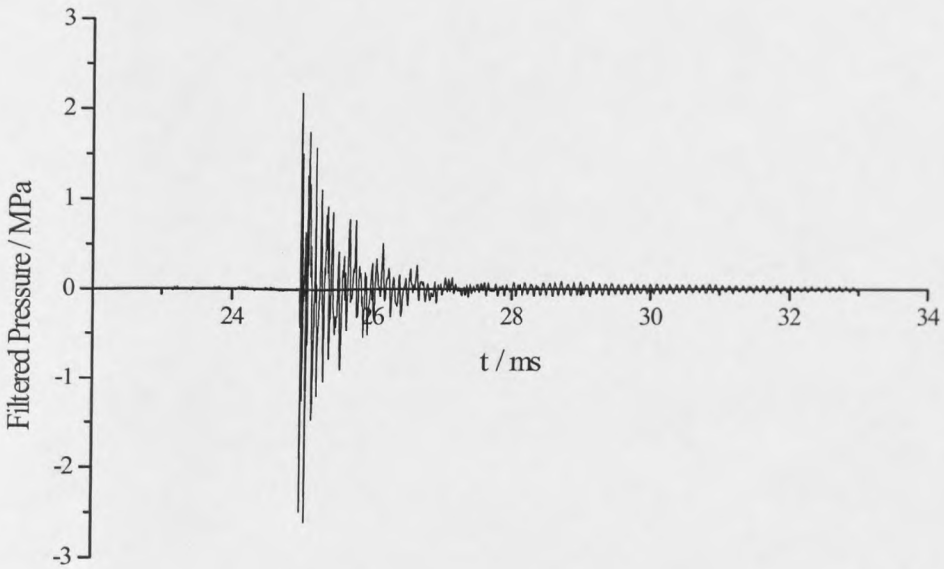

Figure 9 Filtered knock profile for the data shown in Figure 8.

The results were given as follows:-

Knock onset - time from start of data point
Pressure at onset - Pressure at knock onset

P max - maximum pressure
RPR max - maximum rate of pressure rise
DEV max - maximum of deviation of filtered signal

from its mean

KI20 - knock intensity calculated over an equivalence of 20 degrees crank angle at 1500 rpm

KIrms - knock intensity calculated over 2 ms (as defined elsewhere [203])

A20 - area covered by filtered knock signal over 20 degrees crank angle

Since there were some over flows in the data sampling, i.e. where the pressure transducer is saturated, and the sampling rate was relatively low (51.2 kHz in most cases), the parameters RPR max and DEV max, which require the maximum pressure measurement, were not as reliable as the time integrated parameters, KIrms, KI20 and A20.

The sampling frequency for the data was either 50 kHz or 100 kHz depending on the duration of transient data capture, i.e. 1024 data points over 20 ms or over 10 ms respectively.

The calculated KIrms value is the root mean square of the cylinder pressure oscillations measured over a 2 ms time interval after being triggered by a pressure increase of 0.5 bar above the high pass filtered (5 kHz) filtered mean cylinder pressure.

That is,

$$KI_{rms} = \sqrt{\sum_{i=1}^{N} (P_i - P_{mean})^2 \frac{1}{N}}$$

where N is the number of data points.

For the example shown in Figure 8:
KIrms = 5.070 bar (0.52 MPa).

APPENDIX E

Calibration of Spark Delay Unit

The spark delay unit generates a time-delayed output signal at a threshold voltage on the rising pressure profile during compression.

Coarse Delay setting = 3
Trigger level setting = 0.54 (± 0.02) V

The data for the linear regression shown in Figure 10 are as follows:-

$Y = A + BX$

A	=	-113.78362	(± 2.02917)
B	=	35.5205	(± 0.58453)

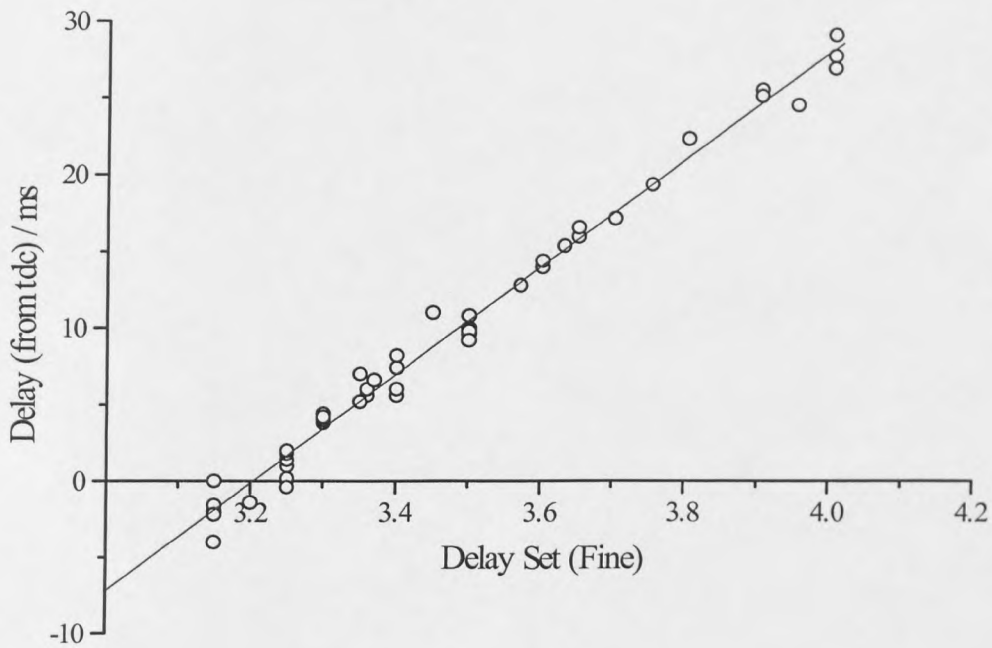

Figure 10 Calibration of the fine delay setting on the spark delay unit in terms of time-delayed output signal from the end of compression (t = 0).

REFERENCES

REFERENCES

1 Hardenberg, H. O., *Antiquity of the Internal Combustion Engine 1509-1688*, SAE SP - 977 (1993).

2 Ricardo, H.R., *The High-Speed Internal Combustion Engine*, Blackie & Son, London, (1933).

3 Cummins, C.L., *Diesels Engine*, Carnot Press, Oregon, (1993).

4 Konig, G. and Sheppard, C.G.W., SAE Paper No. 902135 (1990).

5 Heywood, J.B., *Internal Combustion Engine Fundamentals*, Wiley, New York (1988).

6 Maly, R.R., Twenty-Fifth Symposium (Int.) on Combustion, The Combustion Institute, Pittsburgh, 1994, p 111.

7 Sawyer, R.F., Twenty-Fourth Symposium (Int.) on Combustion, The Combustion Institute, Pittsburgh, 1992, p 1423.

8 Agnew, W.G., Twentieth Symposium (Int.) on Combustion, The Combustion Institute (1984), p 1.

9 *A Guide to Hazard and Operability Studies* (1977). Chemical Industries Association, London, UK.

10 Carslaw, C.D. and Fricker, N., (a) Petroleum Review, May 1995, p 227 ;
(b) Chemistry and Industry, 7 August 1995, p 593.

11 Lovell, W.G., Ind. Eng. Chem., **40**, 2388 (1948).

12 Walsh, A.D., Ninth Symposium (Int.) on Combustion, The Combustion Institute, Pittsburgh, 1963, p 1046.

13 Westbrook, C.K., Pitz, W.J. and Leppard, W.R., SAE Technical Paper 912314 (1991).

14 Saidaminov, S.S., SAE Paper No. 800046 (1980).

15 Cartlidge, J. and Tipper, C.F.H., Combust. Flame, **5**, 87 (1961).

16 Affleck, A.K. and Fish, A., Combust. Flame, **12**, 243 (1968).

17 Semenov, N.N., *Chemical Kinetics and Chain Reactions*, p. 70, The Clarendon Press, Oxford (1935).

18 Frank-Kaminetskii, D.A., Diffusion and Heat Transfer in Chemical Kinetics (Trans. J.P. Appleton), Plenum, New York (1969).

19 Yang, C.H. and Gray, B.F., J. Phys. Chem., **73**, 3395 (1969).

20 Pollard, R.T., "Gas Phase Combustion", Chapter 2 in Comp. Chem. Kin., vol. **17**, Ed. Bamford, C.H. and Tipper, C.F.H., Elsevier, (1977).

21 Walker, R.W., *A critical survey of rate constants for gas-phase hydrocarbon oxidation.* In *Specialist Periodical Report, Reaction Kinetics* (Vol. 1). The Chemical Society, London, UK (1975).

22 Salooja, K.C., Combust. Flame, **4**, 117(1962).

23 Clague, A., Hughes, K.J. and Pilling, M.J., submitted to J. Phys. Chem..

24 Déchaux, J.C., Oxidn. Combust. Rev., **6**, 75 (1973).

25 Shu, N.Wu. and Bardwell, J., Can. J. Chem., **33**, 1415 (1955).

26 Pease, R.N., (a) J. Am. Chem. Soc., **51**, 1839 (1929). (b) J. Am. Chem. Soc., **60**, 2244 (1938).

27 Griffiths, J.F. and Scott, S.K., Prog. Energy Combust. Sci., **13**, 161 (1987).

28 Perkin, W.H., J. Chem. Soc., **41**, 363 (1882).

29 Emeleus, H.J., J. Chem. Soc., 1733 (1929).

30 Sheinson R.S. and Williams, F.W., Combust. Flame, **21**, 221 (1973).

31 Gibson, C., Gray, P., Griffiths, J.F. and Hasko, S.M., Twentieth Symposium (Int.) on Combustion, The Combustion Institute, Pittsburgh, 1984, p 101.

32 Gaydon, A.G., "The Spectroscopy of Flames", 2nd edn., Chapman and Hall, London (1974).

33 Lignola, P.G., Di Maio, F.P., Marzocchella, A. and Mercogliano, R., Twenty-Second Symposium (Int.) on Combustion, The Combustion Institute, 1988, p 1625.

34 Curran, H.J., Gaffuri, P., Pitz, W.J., Westbrook, C.K., Callahan, C., Dryer, F.L. and Held, T., Central and Western States Sections and Mexican National Section, Combustion Institute, p 233 (1995).

35 Dagaut, P., Reuillon, M. and Cathonnet, M., Combust. Sci. Tech., **95**, 233, (1994).

36 Minetti, M., Carlier, M., Ribaucour, M., Therssen, E. and Sochet, L-R., Combust. Flame, **102**, 298 (1995).

37 Egolf, L.M. and Jurs, P.C., Ind. Eng. Chem., **31**, 1798 (1992).

38 Midgley, T. Jr. and Boyd, T.A., J. Soc. Auto. Eng., **15**, 659 (1920).

39 Charch, W.H., Mack, E. Jr. and Boord, C.E., Ind. Eng. Chem., **18**, 335 (1926).

40 Calingaert, G., Sci. Petroleum, **4**, 3024 (1919).

41 Halstead, M.P. and Quinn, C.P., Combust. Flame, **20**, 223 (1973).

42 Griffiths, J.F. and Mohamed, C., Chapter 5 in Comprehensive Chemical Kinetics, series ed. G. Hancock, Elsever, Amsterdam, in press.

43 Griffiths, J.F. and Phillips, C.H., J. Chem. Soc. Faraday Trans. I, **85**, 3471 (1989).

44 Griffiths, J.F., Felton, P.G. and Gray, P., Fourteenth Symposium (Int.) on Combustion, The Combustion Institute, Pittsburgh (1973), p 454.

45 Gray, P., Moule, R.J. and Griffiths, J.F., J. Chem. Soc., Faraday Symp., **9**, 103 (1974).

46 Gray, B.F., Gray, P., Griffiths, J.F., Thirteenth Symposium (Int.) on Combustion, The Combustion Institute, Pittsburgh (1971), p 239.

47 Carlier, M., Côrre, C., Minetti, R., Pauwels, J-F., Ribaucour, M. and Sochet, L-R., Twenty-Third Symposium (Int.) on Combustion , The Combustion Institute, Pittsburgh (1990), p 1753.

48 Mardles, E.W.S., J. Chem. Soc., 872 (1928).

49 Baulch, D.L., Griffiths, J.F., Pappin, A.J. and Sykes, A.F., Combust. Flame, **73**, 163 (1988).

50 Gray, P., Griffiths, J.F. and Scott, S.K., Proc. R. Soc. Lond., **A397**, 21, (1985).

51 Gray, P.,Griffiths, J.F., Hasko, S. and Lignola, P.G., Proc. R. Soc.Lond., **A374**, 313 (1981).

52 Gray, P., Griffiths, J.F., Hasko, S. and Lignola, P.G., Combust Flame, **43**, 175, (1981).

53 Déchaux, J.C., Combust. Flame, **17**, 205 (1971).

54 Gray, P., Griffiths, J.F. and Hasko, S.M., Proc. Roy. Soc. Lond., **A396**, 227, (1984).

55 Dagaut, P., Reuillon, M. and Cathonnet, M., Combust. Sci. Tech., **95**, 233, (1994).

56 Lignola, P.G., Di Maio, F.P., Marzocchella, A. and Mercogliano, R., Twenty-Second Symposium (Int.) on Combustion, The Combustion Institute, Pittsburgh (1988), p 1625.

57 Proudler, V.K., Cederbalk, P., Horowitz, A., Hughes, K.J. and Pilling, M.J., Phil. Trans. R. Soc. Lond., **A337**, 211 (1991).

58 Dryer, F.L. and Glassman, I., Fourteenth Symposium (Int.) on Combustion, The Combustion Institute, Pittsburgh (1973), p 987.

59 Venkat, C., Brezinsky, K. and Glassman, I., Nineteenth Symposium (Int.) on Combustion, The Combustion Institute, Pittsburgh (1982), p 143.

60 Brezinsky, K., Burke, E.J. and Glassman, I., Twentieth Symposium (Int.) on Combustion, The Combustion Institute, Pittsburgh (1984), p 613.

61 Dryer, F.L. and Brezinsky, K., Combust. Sci. Tech., **45**, 199 (1986).

62 Dryer, F.L. and Brezinsky, K., Combust. Sci. Tech., **45**, 225 (1986).

63 Brezinsky, K., Linteris, G.T., Litzinger, T.A. and Glassman, I., Twenty-First Symposium (Int.) on Combustion, The Combustion Institute, Pittsburgh (1986), p 833.

64 Brezinsky, K., Prog. Energy Combust. Sci., **12**, 1 (1986).

65 Emdee, J.L., Brezinsky, K. and Glassman, I., Twenty-Third Symposium (Int.) on Combustion, The Combustion Institute, Pittsburgh (1990), p 77.

66 Shaddix, C.R., Brezinsky, K. and Glassman, I., Twenty-Fourth Symposium (Int.) on Combustion, The Combustion Institute, Pittsburgh (1992), p 683.

67 Koert, D.N., Miller, D.L. and Cernansky, N.P., Combust. Flame, **96**, 34 (1994).

68 Agnew, J.T., Agnew, W. J. and Wark, K., Sixth Symposium (Int.) on Combustion, The Combustion Institute, Pittsburgh (1957), p 894.

69 Agnew, W.G. and Agnew, J.T., Tenth Symposium (Int.) on Combustion, The Combustion Institute, Pittsburgh (1965), p 123.

70 Ballinger, P.R. and Ryason, P.R., Thirteenth Symposium (Int.) on Combustion, The Combustion Institute, Pittsburgh (1971), p 271.

71 Dahm, D.B. and Voerhook, F.H., Combust. Flame, **12**, 380 (1968).

72 Fieweger, K., Blumenthal, R. and Adomeit, G., Twenty-Fifth Symposium (Int.) on Combustion, The Combustion Institute (1994), p 1579.

73 Davidson, C.F., Di Rosa, M.D., Chang, A.Y., Hanson, R.K. and Bowman, C.T., Twenty-Fourth Symposium (Int.) on Combustion, The Combustion Institute, Pittsburgh (1992), p 589.

74 Gaydon, A.G. and Hurle, I.R., "The Shock tube in high temperature chemical physics", Chapman and Hall, London (1963).

75 Burcat, A., Lifshitz, A., Scheller, K. and Skinner, G.B., Thirteenth Symposium (Int.) on Combustion, The Combustion Institute, Pittsburgh (1970). p 745.

76 Spadaccini, L.J. and Colket, M.B., Prog. Energy Combust. Sci., **20**, 431 (1994).

77 Ciezki, H.K. and Adomeit, G., Combust. Flame, **93**, 421 (1993).

78 Cadman, P., Nineteenth International Shock Wave Symposium (1993).

79 Luck C.J., Burgess, A.R., Sesty, D.H., Whitehead, D.M. and Pratley, G., Fourteenth Symposium (Int.) on Combustion, The Combustion Institute, Pittsburgh (1973), p 501.

80 Cernansky, N.P., Green, R.M., Pitz, W.J. and Westbrook, C.K., Combust. Sci. Tech., **50**, 3 (1986).

81 Blin-Simiand, N., Rigny, R. and Sahetchian, K.A., Combust. Sci. Tech., **60**, 117 (1988).

82 Sahetchian, K.A., Rigny, R. and Circan, S., Combust. Flame, **85**, 511 (1991).

83 Filipe, D.I., Li, J., Miller, D.L. and Cernansky, N.P., SAE Technical Paper, 920807 (1992).

84 Li, H., Prabhu, S.K., Miller, D.L. and Cernansky, N.P., SAE Technical Paper, 940478 (1994).

85 Leppard, W.R., SAE Trans., **96**, 934 (1987).

86 Leppard, W.R., SAE Technical Paper, 912313 (1991).

87 Lewis, B. and von Elbe, G., "Combustion, Flames and Explosions in Gases", 3rd Ed., Academic Press (1987), p 163.

88 Griffiths, J.F., Halford-Maw, P.A. and Rose, D.J., Combust. Flame, **95**, 291, (1993).

89 Griffiths, J.F., Jaio, Q., Schreiber, M., Meyer, J. and Knoche, K.F., Twenty-Fourth Symposium (Int.) on Combustion, The Combustion Institute, Pittsburgh (1992), p 1809.

90 Yang, C.H. and Gray, B.F., J. Phys. Chem., **69**, 2747 (1965).

91 Wang, X.J. and Mou, C.Y., J. Chem. Phys., **83**, 4554 (1985).

92 Bradley, D., Yeo, J., Anglo-German Meeting of the Combustion Institute, Cambridge, 1993, p 356.

93 Bradley, D., Kalghatgi, G.T., Morley, C., Snowdon, P. and Yeo, J., Twenty-Fifth Symposium (Int.) on Combustion, The Combustion Institute, Pittsburgh (1994), p125.

94 Halstead, M., Kirsch, L. J. and Quinn, C.P., Combust. Flame, **30**, 45 (1977).

95 Morley, C., Combust. Sci. Tech., **55**, 115 (1987).

96 Cox, R.A. and Cole, J.A., Combust. Flame, **60**, 109 (1985).

97 Hu, H. and Keck, J.C., SAE Technical Paper 872110 (1987).

98 Griffiths, J.F., Combust. Flame, **93**, 203 (1993).

99 Wilk, R.D., Cernansky, N.P. and Cohen, R.S., Combust. Sci. Tech., **49**, 41 (1986).

100 Westbrook, C.K., Pitz, W.J. and Warnatz, J., Twenty-Second Symposium (Int.) on Combustion, The Combustion Institute, Pittsburgh (1988), p 893.

101 Warnatz, J., Twenty-Fourth Symposium (Int.) on Combustion, The Combustion Institute, Pittsburgh (1992), p 553.

102 Chevalier, C., Pitz, W.J., Warnatz, J. and Westbrook, C.K., Twenty-Fourth Symposium (Int.) on Combustion, The Combustion Institute, Pittsburgh (1992), p 93.

103 Basevich, V.Ya., Prog. Energy Combust. Sci., **13**, 199 (1987).

104 Dagaut, P., Reuillon, M., Boettner, J-C. and Cathonnet, M., Twenty-Fifth Symposium (Int.) on Combustion, The Combustion Institute, Pittsburgh (1994), p 919.

105 Emdee, J.L., Brezinsky, K. and Glassman, I., J. Phys. Chem., **96**, 2151 (1992).

106 Pitz, W.J. and Westbrook, C.K, Combust. Flame, **63**, 113 (1986).

107 Cathonnet, M., Combust. Sci. Tech., **98**, 265 (1994).

108 Tomlin, A., Turanyi, T. and Pilling, M.J., *Chapter 4 in Comprehensive Chemical Kinetics*, series ed. G.Hancock, Elsevier, Amsterdam, in press.

109 Falk, K.G., J. Am. Chem. Soc., **28**, 1517 (1906).

110 Dixon, H.B. and Bradshaw, L., J. Chem. Soc., **105**, 2027 (1914).

111 Crofts, J.M., J. Chem. Soc., **104**, 290, 306 (1915).

112 Kondratiev, V.N., Tenth Symposium (Int.) on Combustion, The Combustion Institute (1965), p 319.

113 Tabaczynski, F.J., Hoult, D.P. and Keck, J.C., J. Fluid Mech., **42**, 249 (1970).

114 Nikanjam, M. and Grief, R., J. Heat Transfer, **100**, 527 (1978).

115 Jost, W., Third Symposium (Int.) on Combustion, The Combustion Institute (1949), p 424.

116 Sokolik, A.S., *Self-Ignition, Flame and Explosion of Gases*, Israel Program for Scientific Translations, Jerusalem (1963).

117 Martinengo, A., Oxidn. Combust. Revs., **2**, Ed. C.F.H.Tipper, Elsevier, 207 (1967).

118 Falk, K.G., J. Am. Chem. Soc., **29**, 1536 (1907).

119 Affleck, W.S. and Thomas, A., Proc. Inst. Mech. Eng., **183**, 365 (1968).

120 Beeley, P., Griffiths, J.F. and Gray, P., Combust. Flame, **39**, (1980).

121 Park, P. and Keck, J.C., SAE Technical Paper, 900027 (1990).

122 Ribaucour, M., Minetti, R., Carlier, M. and Sochet, L-R., J. Chim. Phys., **89**, 2127 (1992).

123 Kono, M., Shiga, S., Kumagai, S. and Iinuma, K., Combust. Flame, **54**, 33 (1983).

124 Hayashi, T., Taki, M., Kojima, S. and Kondo, T., Automotive Engineering, 93, **56** (1985).

125 Green, R.M. and Cloutman, L.D., SAE Paper 970823 (1997).

126 Griffiths, J.F., Jiao, Q., Kordylewski, W., Schreiber, M., Meyer, J. and Knoche, K.F., Combust. Flame, **91**, 209 (1993).

127 Lee, D. and Hochgreb, S., submitted to Combust. Flame (1997).

128 Affleck, W.S. and Fish, A., Eleventh Symposium (Int.) on Combustion, The Combustion Institute (1967), p 1003.

129 Elsworth, J.E., Haskell, W.W. and Read, I.A., Combust. Flame, **13**, 437 (1969).

130 Fish, A., Read, I.A., Affleck, W.S. and Haskell, W.W., Combust. Flame, **13**, 39 (1969).

131 Fish, A., Haskell, W.W. and Read, I.A., Proc. Roy. Soc., Lond. A **313**, 261 (1969).

132 Kirsch, L.J. and Quinn, C.P., Sixteenth Symposium (Int.) on Combustion, The Combustion Institute (1976), p 233.

133 Beeley, P., *Spontaneous ignition studies by rapid compression and shock heating*, Leeds University, PhD thesis (1973).

134 Minetti, R., Ribaucour, M., Carlier, M., Fittschen, C. and Sochet, L-R., Combust. Flame, **96**, 201 (1994).

135 Minetti, R., Ribaucour, M., Carlier, M. and Sochet, L-R., Combust. Sci. Tech., **113-114**, 170 (1995).

136 Minetti, M., Carlier, M., Ribaucour, M., Therssen, E. and Sochet, L-R., Combust. Flame, **102**, 298 (1995).

137 Griffiths, J.F., Hughes, K.J., Schreiber, M. and Poppe, C., Combust. Flame, **99**, 533 (1994).

138 Griffiths, J.F., Rose, D.J., Schreiber, M., Meyer, J. and Knoche, K.F., Proc. I. Mech. E. Symposium on Combustion in Engines, (1992), p 29.

139 Schreiber, M., Sadat Sakak, A., Poppe, C., Griffiths, J.F., Halford-Maw, P. and Rose, D.J., SAE Technical Paper, 932758, (1993).

140 Curran, H.J., Pitz, W.J. and Westbrook, C.K., Combust. Flame, *in press* (1997).

141 Cox, A., Griffiths, J.F., Mohamed, C., Curran, H.J., Pitz, W.J. and Westbrook, C.K., Twenty-Sixth Symposium (Int.) on Combustion, The Combustion Institute (1996), p 2685.

142 Martinengo, A., Melczer, J. and Schlimme, E., Tenth Symposium (Int.) on Combustion, The Combustion Institute (1965), p 323.

143 Roblee, L.H., Combust. Flame, **5**, 229 (1961).

144 Kalghatgi, G.T., Snowdon, P. and McDonald, C.R., SAE Paper 950690 (1995).

145 Curran, H.J., Gaffuri, P., Pitz, W.J., Westbrook, C.K. and Leppard, W.R., Twenty-Sixth Symposium (Int.) on Combustion, The Combustion Institute (1996), p 2669.

146 Brown, J.E., Markley, F.X. and Shapiro, H., Ind. Eng. Chem., 2141 (1955).

147 Cullis, C.F. and Waddington, D.J., Trans. Faraday Soc., **53**, p 1371 (1957).

148 Cullis, C.F., Holwill, J.M. and Pollard, R.T., Fifth Symposium (Int.) on Combustion, The Combustion Institute (1954), p 195.

149 Waddington, D.J., Seventh Symposium (Int.) on Combustion, The Combustion Institute (1959), p 165.

150 Livengood, J.C. and Wu, P.C., Fifth Symposium (Int.) on Combustion, The Combustion Institute (1954), p 347.

151 Leppard, W.R., SAE Paper 892081 (1989).

152 Curran, H.J., unpublished results (1996).

153 Hughes, K.J., Halford-Maw, P.A., Lightfoot, P.D., Turanyi, T. and Pilling, M.J., Twenty-Fourth Symposium (Int.) on Combustion, The Combustion Institute, Pittsburgh, 1992, p 645.

154 Sahetchian, K., Champoussin, J.C., Brun, M., Levy, N., Blin-Simiand, N., Aligrot, C., Jorand, F., Socoliuc, M., Heiss, A. and Guerassi, N., Combust. Flame, **103**, 207 (1995).

155 Sahetchian, K., Rigny, R. and Circan, S., Combust. Flame, **85**, 511 (1991).

156 Dagaut, P, Reuillon, M., Cathonnet, M. and Voisin, D., Combust. Sci. Tech., **103**, 349 (1994).

157 Curran, H.J., Pitz, W.J., Westbrook, C.K., Hisham, M.W.M. and Walker, R.W., Twenty-Sixth Symposium (Int.) on Combustion, The Combustion Institute (1996), p 641.

158 Cullis, J.F., Fish, A. and Gibson, Proc. Roy. Soc. Lond., A **311**, 253 (1969).

159 Pitz, W.J., SAE Paper 872107 (1987).

160 Griffiths, J.F., Prog. Energy Combust. Sci., **21**, 25 (1995).

161 Kojima, S. and Suzuoki, T., Combust. Flame, **92**, 254 (1993).

162 Griffiths, J.F., Coppersthwaite, Phillips, C.H., Westbrook, C.K. and Pitz, W.J., Twenty-Third Symposium (Int.) on Combustion, The Combustion Institute (1990), p 1745.

163 Chandraratna, M.R. and Griffiths, J.F., Combust. Flame, **99**, 626 (1994).

164 Taylor, C.F., Taylor, E.S., Livengood, J.C., Russel, W.A. and Leary, W.A., SAE Quart. Trans., **4**, 233 (1950).

165 Levedahl, W., Fifth Symposium (Int.) on Combustion, The Combustion Institute (1954), p 372.

166 Griffiths, J.F. and Hasko, S.M., Proc. Roy. Soc., London A**393**, 371 (1984).

167 Williams, A., *The Combustion of Liquid Fuel Sprays*, Butterworths, London (1989).

168 Bachalo, WD, Twenty-Fifth Symposium (Int.) on Combustion, The Combustion Institute (1994), p 333.

169 Goodger, E.M., *Hydrocarbon Fuels* (1975).

170 Goodger, E.M., J. Inst. Energy, June (1987), p 84.

171 Goodger, E.M., J. Inst. Energy, December (1987), p 199.

172 Lindsay, R.B., *Men of Physics - Lord Rayleigh- The man and his work*, Pergamon Press (1970).

173 Ritter, E., *In-line and single-plunger injection pumps*, *Diesel Fuel Injection*, ed. Robert Bosch (1994).

174 Ziemacki, M.S., I. Mech. E., **C212/85**, 343 (1985).

175 Spicher,U. and Kolmeier, H.-P., SAE Paper 861532 (1986).

176 Bone, W.A. and Fraser, R.P., Phil. Trans. Roy. Soc., A**228**, 197 (1929).

177 Bone, W.A., Fraser, R.P. and Wheeler, W.H., Phil. Trans. Roy. Soc., A**235**, 29 (1936).

178 Beatty, H.A. and Edgar, G., J. Am. Chem. Soc., **56**, 112 (1934).

179 Bollinger, L.M. and Williams, D.T., Third Symposium (Int.) on Combustion, The Combustion Institute (1949), p 176.

180 Whol, K., Kapp, N.M. and Gazley, C., Third Symposium (Int.) on Combustion, The Combustion Institute (1949), pp. 3, 288.

181 Spence, K. and Townend, D.T.A., Third Symposium on Combustion, Flame and Explosion Phenomena (1949), p 404.

182 Kumagai, S. and Isoda, H., Sixth Symposium (Int.) on Combustion, The Combustion Institute (1957), p 726.

183 Whol, K., Sixth Symposium (Int.) on Combustion, The Combustion Institute (1957), p 333.

184 Snyder, W.T., Eighth Symposium (Int.) on Combustion, The Combustion Institute (1962)m o 573.

185 Konig, G., Maly, R.R., Bradley, D, Lau, A.K.C. and Sheppard, C.G.W., SAE Paper 902136 (1990).

186 Hubner, H.J. and Klaukens, H., Ann. Phys., Leipzig, **39**, 33 (1941).

187 Schultz-Grunow, R. and Wortenberg, G., Int. J. Heat Mass Transfer, **2**, 56 (1961).

188 Melvin, A., Combust. Flame, **13**, 438 (1969).

189 Broeze, J.J., Third Symposium on Combustion, Flame and Explosion Phenomena, 146 (1949).

190 Dery, R.J., Third Symposium on Combustion, Flame and Explosion Phenomena, 235 (1949).

191 Keagy, W.R. and Ellis, H.H., Third Symposium (Int.) on Combustion, The Combustion Institute (1949), p 667.

192 Wohl, K., Shore, L., Rosenberg, H. von and Weil, C.W., Fourth Symposium (Int.) on Combustion, The Combustion Institute (1949), p 620.

193 Karlovitz, B., Dennison, D.W. and Wells, F.E., J. Chem. Phys., **19**, 541 (1951).

194 Manton, J., von Elbe, G. and Lewis, B., J. Chem. Phys., **20**, 153 (1952).

195 Egerton, Sir A.C., Saunders, A.A., Lefebvre, A.H. and Moore, N.P.W., Fifth Symposium (Int.) on Combustion, The Combustion Institute (1954), p 396.

196 Kumagai, S. and Kimura, I., Sixth Symposium (Int.) on Combustion, The Combustion Institute (1956), p 387.

197 Parker, W.G. and Wolfhard, H.G., Fuel, 35, 323 (1956).

198 Markstein, G.H., Sixth Symposium (Int.) on Combustion, The Combustion Institute (1956), p 387.

199 Mickelson, W.R. and Ernstein, N.E., Sixth Symposium (Int.) on Combustion, The Combustion Institute (1956), p 325.

200 Simon, D.M., Seventh Symposium (Int.) on Combustion, The Combustion Institute (1959), p 413.

201 Fox, M.D. and Weinberg, F.J., Proc. Roy. Soc., London A**268**, 222 (1962).

202 Herweg, R. and Maly, R.R., SAE Paper 922243 (1992).

203 Pan, J. and Sheppard, C.G.W., SAE Paper 942060 (1994).

204 Schwar, M.J.R. and Weinberg, F.J., Combust. Flame, **13**, 335 (1969).

205 Markstein, G.H., Third Symposium (Int.) on Combustion, The Combustion Institute (1949), p 162.

206 Hentschel, W., Twenty-Sixth Symposium (Int.) on Combustion, The Combustion Institute (1996), p 2503.

207 Livengood, J.C. and Leary, W.A., Ind. Eng. Chem., 2797 (1951).

208 Stiebels, B., Schreiber, M. and Sadat Sakak, A., SAE Paper 960827 (1996).

209 Zhao, R.Q., Taketomi, M., Nishida, K. and Hiroyasu, H., SAE Paper 932641 (1993).

210 Arnold, A., Dinkelacker, F., Heitzmann, T., Monkhouse, P., Schafer, M., Sick, V., Wolfrum, J., Hentschel, W. and Schindler, K.-P., Twenty-Fourth Symposium (Int.) on Combustion, The Combustion Institute (1993), p 1605.

211 Becker, H., Monkhouse, P.B., Wolfrum, J., Cant, R.S., Bray, K.N.C., Maly, R.R., Pfister, W., Stahl, G. and Warnatz, R., Twenty-Third Symposium (Int.) on Combustion, The Combustion Institute (1990), p 817.

212 Bauerle, B., Warnatz, J. and Behrendt, F., Twenty-Sixth Symposium (Int.) on Combustion, The Combustion Institute (1996), p 2619.

213 Desgroux, P., Gasnot, L. and Sochet, L.-R., App. Phys. B **61**, 69 (1995).

214 Desgroux, P., Minetti, R. and Sochet, L.-R., Combust. Sci. Tech., **113-114**, 193 (1996).

215 Eckbreth, A.C., (a) Eighteenth Symposium (Int.) on Combustion, The Combustion Institute (1981), p 1471.

(b) *Laser diagnostics for Combustion, Temperature and Species*, Abacus Press, Mass (1988).

216 Hanson, R., Twenty-First Symposium (Int.) on Combustion, The Combustion Institute (1986), p 1677.

217 Amsden, A.A., O'Rourke, P.J. and Butler, T.D., SAE Paper 872072 (1987).

218 Hildyard, C.H., unpublished report.

219 Drake, M., *The flame propagation in a spark-ignited partially oxidised fuel following rapid compression*, MSc. Thesis (1993).

220 Merdhani, S. and Sheppard, C.G.W., SAE Paper 932640 (1993).

221 Curran, H.J, Pitz, W.J., Westbrook, C.K., Griffiths, J.F. and Mohamed, C., Third Symposium on Numerical Modelling, Heidelberg (1996).

222 Chun, K.M., Heywood, H.B. and Keck, J.C., Twenty-Second Symposium (Int.) on Combustion, The Combustion Institute (1988), p 455.

223 Fernandez-Pello, A.C., Combust. Sci. Tech., **98**, 281 (1994).

224 Cowart, J.S., Keck, J.C., Heywood, J.B., Westbrook, C.K. and Pitz, W.J., Twenty-Third Symposium (Int.) on Combustion, The Combustion Institute (1990), p 1055.

225 Westbrook, C.K., Combust. Sci. Tech., **20**, 5 (1979).

226 Lund, C.M., Lawrence Livermore National Laboratory report UCRL-52504, (1978).

227 Yarlagadda, P.S., Morton, L.A., Hunter, N.R. and Gesser, H.D., Ind. Eng. Chem. Res., **27**, 252 (1988).

228 Yarlagadda, P.S., Morton, L.A., Hunter, N.R. and Gesser, H.D., Combust. Flame,

79, 216 (1990).

229 Asaba, T., Yoneda, K., Kakihara, N. and Kikita, T., Ninth Symposium (Int.) on Combustion, The Combustion Institute (1963), p 193.

230 Lifshitz, A., Scheller, K., Burcat, A. and Skinner, G.B., Combust. Flame, **16**, 311 (1971).

231 Higgin, R.M.R. and Williams, A., Twelfth Symposium (Int.) on Combustion, The Combustion Institute (1969), p 579.

232 Tan, Y., Dagaut, P., Cathonnet, M. and Boettner, J.-C., Combust. Sci. Tech., **103**, 133 (1994).

233 Tan, Y., Dagaut, P., Cathonnet, M., Boettner, J.-C., Bachman, J.S. and Carlier, P., Twenty-Fifth Symposium (Int.) on Combustion, The Combustion Institute (1994), p 1563.

234 Crossley, R.W., Dorko, E.A., Scheller, K. and Burcat, A., Combust. Flame, **19**, 373 (1972).

235 Frenklach, M. and Bornside, D.E., Combust. Flame, **56**, 1 (1984).

236 Cooke, D.F. and Williams, A., Combust. Flame, **24**, 245 (1975).

237 Kalghatgi, G., SAE Paper 952443 (1995).

238 Bradley, D., J. Chem. Soc., Faraday Trans., **92**, 2959 (1996).

239 Cadman, P. and Denning, R.J., J. Chem. Soc., Faraday Trans., **92**, 4159 (1996).

240 Haskell, W.W., SAE Paper 700059 (1970).

241 Belansky, R.H. and Wanser, K.H., Am. J. Phys., **61**, 1014 (1993).